Targeting mechanisms of the DNA damage response (DDR) to overcome acquired cisplatin resistance in tumor cells

Inaugural-Dissertation

zur Erlangung des Doktorgrades
der Mathematisch-Naturwissenschaftlichen Fakultät
der Heinrich-Heine-Universität Düsseldorf

vorgelegt von

Julia Mann
aus Gelnhausen

Düsseldorf, Oktober 2024

aus dem Institut für Toxikologie
der Heinrich-Heine-Universität Düsseldorf

Gedruckt mit der Genehmigung der
Mathematisch-Naturwissenschaftlichen Fakultät der
Heinrich-Heine-Universität Düsseldorf

Berichterstatter:

1. Prof. Dr. Gerhard Fritz

2. Prof. Dr. Lutz Schmitt

Tag der mündlichen Prüfung: 19.03.2025

Table of contents

TABLE OF CONTENTS ..... **I**

LIST OF FIGURES ..... **VI**

LIST OF TABLES ..... **XII**

LIST OF ABBREVIATIONS ..... **XIV**

1 INTRODUCTION **1**

1.1 Cancer **1**

1.1.1 Genomic instability and aneuploidy 3

1.2 Cancer treatment **3**

1.2.1 Chemotherapy 4

1.2.1.1 Cisplatin 6

1.2.2 Acquirement of cisplatin resistance 8

1.3 Cellular stress responses **9**

1.3.1 DNA damage response 9

1.3.1.1 Replicative stress response 11

1.3.1.2 DNA repair 14

1.3.1.3 Pharmacological modulation of the DDR/DNA repair for the treatment of cancer 18

1.3.2 Cell death mechanisms 19

1.4 Aims of the project **21**

2 MATERIAL AND METHODS **23**

2.1 Material **23**

2.1.1 Manufacturer's references 23

2.1.2 Consumables 25

2.1.3 Chemicals 26

2.1.4 Cytostatics & modulators of DNA damage response / DNA repair 27

2.1.5 Kits 28

2.1.6 Media and media supplements 29

2.1.7 Experimental organisms 29

2.1.7.1 Cell lines 29

2.1.7.2 Mouse strain 30

2.1.8 Enzymes 30

2.1.9 Primers 31

2.1.10 Antibodies 35

2.1.10.1 Primary antibodies 35

2.1.10.2 Secondary antibodies 35

2.1.11 Solutions and buffers 36
2.1.12 Instruments 39
2.1.13 Software 42
2.2 Methods 42
2.2.1 Cell culture 42
2.2.1.1 Authentication of cell lines 43
2.2.1.2 Cryo conservation of cells 43
2.2.1.3 Selection of cisplatin resistant cell variants 43
2.2.2 Analysis of cell viability 44
2.2.2.1 AlamarBlue assay 44
2.2.2.2 Neutral Red assay 44
2.2.2.3 Combination Index 45
2.2.3 Molecular biology 45
2.2.3.1 Isolation of genomic DNA 45
2.2.3.2 RNA isolation 46
2.2.3.3 cDNA synthesis 46
2.2.3.4 Quantitative real-time PCR 47
2.2.4 Protein biochemistry 48
2.2.4.1 Protein isolation and quantification 48
2.2.4.2 Gel electrophoretic separation of proteins (SDS-PAGE) 48
2.2.4.3 Western blot 49
2.2.5 Analysis of cell cycle distribution 50
2.2.5.1 Flow cytometry 50
2.2.5.2 S-phase activity 51
2.2.5.3 Mitotic index 51
2.2.5.4 Analysis of mitotic progression 52
2.2.6 Analysis of DNA damage 52
2.2.6.1 Alkaline Comet assay 52
2.2.6.2 Immunocytochemistry (RPA, RAD51, γH2AX + RPA) 53
2.2.6.3 DNA Fiber Spreading assay 54
2.2.7 Analysis of Cisplatin-DNA intrastrand crosslinks (Southwestern blot) 55
2.2.8 Proteome analysis 56
2.2.9 siRNA-based knockdown of RAD51 57
2.2.10 Xenograft mouse experiment 57
2.2.10.1 Study design 57
2.2.10.2 Preparation of inhibitors for injection 58
2.2.10.3 EDTA blood collection and analysis 58
2.2.10.4 Organ isolation 59
2.2.10.5 Bone marrow isolation for RNA extraction 59
2.2.10.6 Purification of total RNA from bone marrow cells 59
2.2.11 Statistical analysis 60

3 RESULTS 61

3.1 Differences between J82^{WT} and J82^{CisPt} under basal conditions and in response to cisplatin 61

3.1.1 Cytotoxicity screening with cytostatics & pharmacological inhibitors of DDR/DNA repair in J82 cell variants 61

3.1.2 mRNA expression profiles of J82 cell variants 65

3.1.3 Proteome analysis of J82 cell variants 68

3.1.4 CisPt-DNA-adduct formation in J82 cell variants 71

3.1.5 Signs for chromosomal instability in J82^{CisPt} 74

3.2 Molecular differences between J82^{WT} and J82^{CisPt} in their response to RAD51$_i$ B02 76

3.2.1 Inhibition of RAD51 foci formation by B02 after irradiation 76

3.2.2 Interplay of RAD51 inhibition and CisPt-DNA-adduct formation 77

3.2.3 mRNA expression profiles after B02 treatment 78

3.2.4 Influence of RAD51 inhibition on cell cycle and mitotic progression 80

3.2.5 Comparison of RAD51 inhibition with B02 and RAD51 knockdown via siRNA 83

3.3 Comparison of J82^{CisPt} with other cisplatin resistant cell variants 87

3.3.1 Isolation of cisplatin resistant cell variants of different tumor entities 87

3.3.1.1 Selection of cisplatin resistant A549 lung cancer cells 87

3.3.1.2 Selection of cisplatin resistant MDA-MB231 mamma carcinoma cells 88

3.3.2 mRNA expression profiles under basal conditions and after CisPt treatment 89

3.3.2.1 mRNA expression profiles of A549 lung cancer cells 89

3.3.2.2 mRNA expression profiles of SH-SY5Y neuroblastoma cells 91

3.4 Combination treatments of cytostatics and inhibitors of DDR/DNA repair to overcome CisPt resistance in J82^{CisPt} 93

3.5 Deciphering the molecular mechanism of the synergistic toxicity of the combination treatment with B02 + PF477736 97

3.5.1 Induction of apoptotic cell death by B02 + PF477736 98

3.5.2 Influence of B02 and PF47776 on the cell cycle progression 101

3.5.3 S-phase related effects triggered by B02 + PF477736 104

3.5.4 DNA damage induction and DDR activation by B02 + PF477736 111

3.6 Transferability of the findings with B02 + PF477736 in J82^{CisPt} to other tumor cell lines and other RAD51 and CHK1 inhibitors 115

3.6.1 Cytotoxicity of B02 + PF477736 in J82^{WT} and cisplatin-resistant cells of other tumor entities 116

3.6.2 Mechanistic studies in SH-SY5Y^{CisPt} 118
3.6.3 Combinations of other RAD51 and CHK1 modulators in J82^{CisPt} 119
3.7 Cytotoxicity of B02 + PF477736 in normal tissue cells *in vitro* 124
3.7.1 Cytotoxicity of B02 + PF477736 in human induced pluripotent stem cells (hiPSCs) 125
3.7.2 Cytotoxicity of B02 + PF477736 in human primary fibroblasts 126
3.8 Xenograft animal experiment with B02 + PF477736 126
3.8.1 Pre-tests for the determination of the cell number for injection 126
3.8.2 Tumor growth in the main experiment with B02 + PF477736 treatment 127
3.8.3 Animal weights over the course of the experiment with B02 + PF477736 treatment 129
3.8.4 Organ weights 129
3.8.5 EDTA blood parameters 130
3.8.6 Bone marrow RNA analysis of mice treated with B02 + PF477736 132

4 DISCUSSION 134
4.1 Potential underlying mechanisms for CisPt resistance in J82 cells 134
4.2 Comparison of different CisPt resistant cell variants 137
4.3 Distinct responses of J82^{WT} and J82^{CisPt} to RAD51 inhibition 138
4.4 Molecular mechanism of combination treatment with B02 + PF477736 in J82^{CisPt} 142
4.5 Anti-tumor efficacy of B02 + PF477736 *in vivo* 148
4.6 Effect of the combination treatment of B02 + PF477736 on non-malignant cells 150

5 CONCLUSION 154

6 OUTLOOK 155

7 SUMMARY 158

8 ZUSAMMENFASSUNG 160

9 LIST OF REFERENCES 162

10 APPENDIX 177
10.1 Supplementary material 177
10.1.1 Supplementary figures 177
10.1.2 Supplementary tables 181
10.2 Publications & congress participations 191
10.2.1 List of publications 191

10.2.2 List of congress participations 191
10.2.2.1 Poster presentations 191
10.2.2.2 Talks 192

11 ACKNOWLEDGEMENTS 193

12 EIDESSTATTLICHE ERKLÄRUNG 194

List of figures

Figure 1: Hallmarks of cancer 2

Figure 2: Bioactivation of cisplatin and schematic visualization of the resulting platinum-DNA adducts 7

Figure 3: Categorization of factors involved in the acquirement of cisplatin resistance according to Galluzzi *et al.*, 2012 8

Figure 4: Schematic diagram of the DNA damage response 11

Figure 5: Rescue mechanisms of stalled DNA replication forks 13

Figure 6: DNA repair mechanisms for various base modifications 16

Figure 7: DNA repair mechanisms for DNA double-strand breaks 18

Figure 8: Selection protocol for chemotherapeutic resistant cell variants 43

Figure 9: Functional principle of the AlamarBlue assay 44

Figure 10: Possible fluorescence patterns for the determination of replication fork stages after labelling with a pulse of Chlorodeoxyuridine (green) followed by a pulse with Iododeoxyuridine (red) 54

Figure 11: Procedure of the DNA Fiber Spreading assay 55

Figure 12: Study design of the xenograft mouse experiment for the testing of B02 + PF477736 *in vivo* 58

Figure 13: Comparison of cytotoxicity of platinum compounds in $J82^{WT}$ and $J82^{CisPt}$ ... 62

Figure 14: Comparison of cytotoxicity of other conventional cancer therapies in $J82^{WT}$ and $J82^{CisPt}$ 63

Figure 15: Comparison of cytotoxicity of oxidants in $J82^{WT}$ and $J82^{CisPt}$ 63

Figure 16: Comparison of cytotoxicity of pharmacological inhibitors against DDR factors in $J82^{WT}$ and $J82^{CisPt}$ 64

Figure 17: Comparison of cytotoxicity of RAD51 inhibitor B02 in $J82^{WT}$ and $J82^{CisPt}$ 65

Figure 18: mRNA expression of factors potentially involved in acquired cisplatin resistance compared in $J82^{WT}$ and $J82^{CisPt}$ under basal conditions 66

Figure 19: mRNA expression of factors potentially involved in acquired cisplatin resistance compared in $J82^{WT}$ and $J82^{CisPt}$ after cisplatin treatment 67

Figure 20: Proteome analysis of $J82^{CisPt}$ vs. $J82^{WT}$ under basal conditions 69

Figure 21: Proteome analysis of J82^{WT} and J82^{CisPt} cells after cisplatin treatment 71

Figure 22: Cisplatin adduct formation in J82^{WT} and J82^{CisPt} after short-term treatment with equimolar concentrations of cisplatin 72

Figure 23: Cisplatin adduct formation in J82^{WT} and J82^{CisPt} after long-term treatment with equitoxic concentrations of cisplatin 73

Figure 24: Signs of chromosomal instability in J82^{CisPt} under basal conditions 74

Figure 25: Staining of spindle apparatus markers in J82^{WT} and J82^{CisPt} under basal conditions 75

Figure 26: RAD51 foci formation in J82^{WT} and J82^{CisPt} after irradiation and RAD51 inhibition by B02 77

Figure 27: Cisplatin adduct formation in J82^{WT} and J82^{CisPt} after 24 h treatment with cisplatin and B02 78

Figure 28: mRNA expression of factors potentially involved in B02 resistance compared in J82^{WT} and J82^{CisPt} after B02 treatment 79

Figure 29: Cell cycle distribution analyses in J82^{WT} and J82^{CisPt} after treatment with RAD51$_i$ B02 80

Figure 30: Phospho histone 3 (pH3) staining of J82^{WT} and J82^{CisPt} cells treated with B02 81

Figure 31: Analysis of mitosis-specific phosphorylation of histone 3 (H3) in J82^{WT} and J82^{CisPt} cells after treatment with RAD51$_i$ B02 82

Figure 32: Staining of spindle apparatus markers in J82^{WT} and J82^{CisPt} after treatment with B02 82

Figure 33: Protein expression of RAD51 in J82^{WT} and J82^{CisPt} after treatment with RAD51 siRNA 83

Figure 34: mRNA expression of RAD51 and its paralogs in J82^{WT} and J82^{CisPt} after treatment with RAD51 siRNA 84

Figure 35: Comparison of cytotoxicity in J82^{WT} and J82^{CisPt} with RAD51 siRNA 85

Figure 36: Cell cycle distribution analyses in J82^{WT} and J82^{CisPt} after treatment with RAD51 siRNA 86

Figure 37: Phospho histone 3 (pH3) staining of J82^{WT} and J82^{CisPt} cells treated with RAD51 siRNA or B02 86

Figure 38: Cytotoxicity of cisplatin in A549 cells 87

Figure 39: Comparison of cytotoxicity of cisplatin in $A549^{WT}$ and resistance-selected $A549^{CisPt}$ 88

Figure 40: Cytotoxicity of cisplatin in MDA-MB231 cells 88

Figure 41: mRNA expression of factors potentially involved in acquired cisplatin resistance compared in $A549^{WT}$ and $A549^{CisPt}$ under basal conditions 89

Figure 42: mRNA expression of factors potentially involved in acquired cisplatin resistance compared in $A549^{WT}$ and $A549^{CisPt}$ after cisplatin treatment 90

Figure 43: mRNA expression of factors potentially involved in acquired cisplatin resistance compared in SH-SY5Y^{WT} and SH-SY5Y^{CisPt} under basal conditions 91

Figure 44: mRNA expression of factors potentially involved in acquired cisplatin resistance compared in SH-SY5Y^{WT} and SH-SY5Y^{CisPt} after cisplatin treatment 92

Figure 45: Viability of $J82^{CisPt}$ after co-treatment with cisplatin and RAD51 inhibitor B02 93

Figure 46: Viability of $J82^{CisPt}$ after co-treatment with OH-Urea and RAD51 inhibitor B02 94

Figure 47: Viability of $J82^{CisPt}$ when combining replication stress inducing anticancer therapeutics with CHK1 inhibitor PF477736 95

Figure 48: Viability of $J82^{CisPt}$ when combining PARP inhibitors with RAD51 inhibitor B02 or CHK1 inhibitor PF477736 96

Figure 49: Viability of $J82^{CisPt}$ after co-treatment with RAD51 inhibitor B02 and CHK1 inhibitor PF477736 97

Figure 50: mRNA expression of cell death factors in $J82^{CisPt}$ after treatment with $RAD51_i$ B02 and $CHK1_i$ PF477736 98

Figure 51: Protein expression of autophagy factor LC3 in $J82^{CisPt}$ after treatment with $RAD51_i$ B02 and $CHK1_i$ PF477736 99

Figure 52: Protein expression of apoptosis factors in $J82^{CisPt}$ after treatment with $RAD51_i$ B02 and $CHK1_i$ PF477736 100

Figure 53: Induction of SubG1 fraction in $J82^{CisPt}$ after co-treatment with B02 + PF477736 and pan-caspase inhibitor QVD 101

Figure 54: mRNA expression of cell cycle factors in $J82^{CisPt}$ after treatment with $RAD51_i$ B02 and $CHK1_i$ PF477736 102

Figure 55: Cell cycle distribution analyses in J82^{CisPt} after treatment with RAD51$_i$ B02 and CHK1$_i$ PF477736 103

Figure 56: Phospho histone 3 (pH3) staining of J82^{CisPt} cells treated with B02 or/and PF477736 104

Figure 57: EdU incorporation assay of J82^{CisPt} cells treated with B02 or/and PF477736 105

Figure 58: DNA fiber spreading assay of J82^{CisPt} cells treated with B02 or/and PF477736 106

Figure 59: mRNA expression of replication-related factors in J82^{CisPt} after treatment with RAD51$_i$ B02 and CHK1$_i$ PF477736 107

Figure 60: Nuclear RPA foci formation in J82^{CisPt} cells treated with B02 or/and PF477736 108

Figure 61: Protein expression of replication stress response factors in J82^{CisPt} after treatment with RAD51$_i$ B02 and CHK1$_i$ PF477736 109

Figure 62: Analysis of J82^{CisPt} cells entering mitosis with under-replicated DNA after treatment with RAD51$_i$ B02 and CHK1$_i$ PF477736 110

Figure 63: Representative pictures of mitotic catastrophe in J82^{CisPt} treated with B02 + PF477736 110

Figure 64: mRNA expression of cellular stress markers, DNA damage response and DNA repair factors in J82^{CisPt} after treatment with RAD51$_i$ B02 and CHK1$_i$ PF477736 112

Figure 65: Protein expression and activation of DNA damage response and DNA repair factors in J82^{CisPt} after treatment with RAD51$_i$ B02 and CHK1$_i$ PF477736 113

Figure 66: Alkaline comet assay of J82^{CisPt} cells treated with B02 or/and PF477736 . 114

Figure 67: Analysis of cell cycle phase-specific DNA damage signaling in J82^{CisPt} cells after treatment with RAD51$_i$ B02 and CHK1$_i$ PF477736 114

Figure 68: Immunocytochemical co-staining of γH2AX and RPA in J82^{CisPt} cells after co-treatment with B02 + PF477736 115

Figure 69: Viability of J82^{WT} after co-treatment with RAD51$_i$ B02 and CHK1$_i$ PF477736 116

Figure 70: Viability of cisplatin resistant tumor cells of different tissue types after co-treatment with RAD51$_i$ B02 and CHK1$_i$ PF477736 117

Figure 71: Protein expression of RAD51, CHK1 and PrimPol in tumor cell lines originating from different tissue types and their CisPt resistant counterparts under basal conditions 118

Figure 72: Reaction of SH-SY5Y^{CisPt} to co-treatment with RAD51$_i$ B02 and CHK1$_i$ PF477736 119

Figure 73: Viability of J82^{CisPt} after co-treatment with RAD51$_i$ B02 and CHK1$_i$ SB218078 120

Figure 74: Reaction of J82^{CisPt} to co-treatment with RAD51$_i$ B02 and CHK1$_i$ LY2603618 121

Figure 75: Viability of J82^{CisPt} after co-treatment with RAD51$_i$ B02 and pan-CHK$_i$ AZD7762 122

Figure 76: Viability of J82^{CisPt} after co-treatment with CHK1$_i$ PF477736 and RAD51$_i$ RI-1 122

Figure 77: Reaction of J82^{CisPt} to co-treatment with CHK1$_i$ PF477736 and RAD51$_i$ RI(dl)2 123

Figure 78: Viability of J82^{CisPt} after co-treatment with RAD51$_i$ B02, CHK1$_i$ PF477736 and RAD51 stimulator RS-1 124

Figure 79: Viability of Foreskin-4 human induced pluripotent stem cells (F-4 hiPSCs) after co-treatment with RAD51$_i$ B02 and CHK1$_i$ PF477736 125

Figure 80: Viability of normal human dermal fibroblasts (NHDF) after co-treatment with RAD51$_i$ B02 and CHK1$_i$ PF477736 126

Figure 81: Tumor growth of different cell numbers of J82^{CisPt} cells in a xenograft experiment 127

Figure 82: Influence of B02 or/and PF477736 treatment on tumor growth in a xenograft experiment with J82^{CisPt} cells 128

Figure 83: Monitoring of animal weight in the xenograft experiment with B02 or/and PF477736 treatment 129

Figure 84: Organ weights in the xenograft experiment with B02 or/and PF477736 treatment 130

Figure 85: Blood parameters in the xenograft experiment with B02 or/and PF477736 treatment 131

Figure 86: mRNA expression of transport, stress and cell death factors in bone marrow of NSG-(K^bD^b)^{null} mice after treatment with RAD51$_i$ B02 and CHK1$_i$ PF477736 133

Figure 87: Model of synergistic toxicity evoked by combined inhibition of CHK1 and RAD51 in cisplatin-resistant tumor cells 147

Supplementary Figure 1: Comparison of cytotoxicity in $J82^{WT}$ and $J82^{CisPt}$ with RAD51 inhibitor B02 after different treatment durations 177

Supplementary Figure 2: Comparative overview of the mRNA changes observed in different cisplatin resistant cell lines under basal conditions and after cisplatin administration 178

Supplementary Figure 3: Analysis of S-phase arrest induction after combination treatment with CHK1 + PARP inhibition in $J82^{CisPt}$ 179

Supplementary Figure 4: Comparison of the blood values measured basally in the xenograft experiment with literature values 179

Supplementary Figure 5: Additional blood parameters in the xenograft experiment with B02 or/and PF477736 treatment 180

List of tables

Table 1: Classification of selected cytostatic drugs by substance group. 5
Table 2: List of manufacturer headquarters 23
Table 3: List of consumables used 25
Table 4: List of chemicals used 26
Table 5: List of cytostatics used 27
Table 6: List of pharmacological DNA damage response & DNA repair modulators used 28
Table 7: List of commercially available assay kits used 28
Table 8: List of media used 29
Table 9: List of media supplements used 29
Table 10: List of cell lines used 29
Table 11: List of enzymes used 30
Table 12: List of human primers used for quantitative real-time PCR 31
Table 13: List of murine primers used for quantitative real-time PCR 33
Table 14: List of primary antibodies used 35
Table 15: List of Horseradish peroxidase (HRP)-coupled secondary antibodies used 35
Table 16: List of fluorescence-coupled secondary antibodies used 36
Table 17: List of solutions and buffers used 36
Table 18: List of devices and instruments used 39
Table 19: List of software used 42
Table 20: Composition of the master mix for cDNA synthesis 47
Table 21: Thermal cycler conditions used for cDNA synthesis 47
Table 22: Reaction conditions used for quantitative real-time PCR 48

Supplementary Table 1: Summary of cross-resistance analyses of J82^{CisPt} to various conventional anticancer therapeutics and DDR modifiers 181
Supplementary Table 2: List of proteins found upregulated in J82^{CisPt} when compared to J82^{WT} under basal conditions in the proteome analysis 182

Supplementary Table 3: List of proteins found down-regulated in J82^{CisPt} when compared to J82^{WT} under basal conditions in the proteome analysis 186

Supplementary Table 4: Outcomes of combination treatments with various anticancer therapeutics and inhibitors of replicative stress response in J82^{CisPt} 190

List of abbreviations

% (v/v)	Volume-volume percentage
% (w/v)	Weight-volume percentage
5-FU	5-fluorouracil
A	Adenine
AKAP1	A-kinase anchor protein 1
AKT1	AKT serine/threonine kinase 1
AKTB	β-Actin
AP site	Apurinic/apyrimidinic site
APAF1	Apoptotic protease-activating factor 1
APE1	Apurinic/apyrimidinic endonuclease 1
ApG	Crosslinking of adjacent adenine and guanine bases
APS	Ammonium peroxodisulfate
ATG3	Autophagy related 3
ATG7	Autophagy related 7
ATM	Ataxia telangiectasia mutated
ATP	Adenosine triphosphate
ATP7A	ATPase copper-transporting α
ATP7B	ATPase copper-transporting β
ATR	Ataxia telangiectasia and RAD3 related
ATRIP	ATR interacting protein
BAX	BCL2-associated protein
BBC3	BCL2 binding component 3
BCL-2	B cell lymphoma 2
BCRP	Breast Cancer Resistance Protein
BECN1	Beclin 1
BER	Base excision repair
BMFZ	*Biologisch-Medizinisches Forschungszentrum*
BRCA1	Breast cancer 1, early onset
BRCA2	Breast cancer 2, early onset
BrdU	Bromodeoxyuridine
BRIP1	BRCA1 interacting DNA helicase 1
BSA	Bovine serum albumin
BW	Body weight
CAD	Caspase-activated DNase

CALCR	Calcitonin receptor
CASP2	Caspase 2
CAT	Conventional anticancer therapeutic
CDC25a	Cell division cycle phosphatase 25a
CDC25c	Cell division cycle phosphatase 25c
CDK1	Cyclin-dependent kinase 1
CDKN1A	Cyclin-dependent kinase inhibitor 1A
cDNA	Complementary DNA
CEP55	Centrosomal protein of 55 kDa
CHK1	Checkpoint kinase 1
CHK2	Checkpoint kinase 2
CI	Combination index
CIN	Chromosomal instability
CisPt	Cisplatin
CldU	Chlorodeoxyuridine
Cq	quantification cycle
CSA	Cockayne syndrome group A
CSB	Cockayne syndrome group B
CTR1	Copper transporter 1; Solute carrier family 31, member 1
CTR2	Copper transporter 2; Solute carrier family 31, member 2
DDB2	Damage specific DNA binding protein 2
DDIT3	DNA damage inducible transcript 3
DDR	DNA damage response
DISC	Death inducing signaling complex
D-loop	Displacement loop
DMEM	Dulbecco’s Modified Eagle’s Medium
DMSO	Dimethyl sulphoxide
DNA	Deoxyribonucleic acid
DNA-PKcs	DNA-dependent protein kinase, catalytic subunit
DSB	DNA double-strand break
DSMZ	German Collection of Microorganisms and Cell Culture
e.g.	For example (*exempli gratia*)
EDTA	Ethylenediamine tetraacetic acid
EdU	5-ethynyl-2‘-deoxyuridine
ERCC1	Excision repair cross-complementation group 1
EXO1	Exonuclease 1
F-4	Foreskin-4

FADD	FAS-associated death domain protein
FANCD2	Fanconi anemia complementation group 2
FASR	Tumor necrosis factor receptor superfamily member 6
FCS	Fetal calf serum
FDA	Food and Drug Administration
FEN1	Flap endonuclease 1
G	Guanine
G-CSF	Granulocyte-colony stimulating factor
G0-phase	Gap 0 phase of the cell cycle
G1-phase	Gap 1 phase of the cell cycle
G2-phase	Gap 2 phase of the cell cycle
GADD45A	Growth arrest and DNA-damage-inducible α
GAPDH	Glycerinaldehyde-3-phosphate dehydrogenase
GG-NER	global genomic NER
GpG	Crosslinking of two adjacent guanine bases
GPX1	Glutathione peroxidase 1
GPX4	Glutathione peroxidase 4
GpXpG	Crosslinking of two non-adjacent guanine bases
GSH	Glutathione
GSTM1	Glutathione S-transferase 1
GTP	Guanosine triphosphate
H2AX	H2A histone family, member X
H3	Histone H3
HDAC	Histone deacetylase
hIPSCs	Human induced pluripotent stem cells
HMGB1	High-Mobility Group Box 1
HMOX1	Heme oxygenase 1
HR	Homologous recombination
HR23B	UV excision repair protein RAD23 homolog B
HRP	Horseradish peroxidase
HSPA1B	Heat shock protein family A member 1B
i.e.	That is (*id est*)
IC_{50}	Inhibitory concentration at 50%
IdU	Iododeoxyuridine
IGBP1	Immunoglobulin binding protein 1
IgG	Immunoglobulin G
IL-2	Interleukin 2

IL-6	Interleukin-6
IL-8	Interleukin-8
iPOND	Isolation of proteins on nascent DNA
IR	Irradiation
KAP1	KRAB-associated protein 1
KEGG	Kyoto Encyclopedia of Genes and Genomes
KRAB	Krüppel-associated box
Ku70	X-ray repair complementing defective repair in Chinese hamster cells 6 (XRCC6)
Ku80	X-ray repair complementing defective repair in Chinese hamster cells 5 (XRCC5)
LAMP1	Lysosomal-associated membrane protein 1
LC3	Microtubule-associated protein 1 light chain 3
LCMT-1	Leucine carboxyl methyltransferase 1
Lig	Ligase
LMNB1	Lamin B1
MATE1	Multidrug extrusion transporter 1; Solute carrier family 47 member 1
MCH	Mean corpuscular hemoglobin
MCHC	Mean corpuscular hemoglobin concentration
MCM	Minichromosome maintenance protein complex
MCV	Mean corpuscular volume
MDR1	Multidrug-resistance-protein 1; ATP binding cassette subfamily B member 1
MFN2	Mitofusin-2
MGMT	O^6-Methylguanine-DNA methyltransferase
MHC	Major histocompatibility complex
MLH1	mutL homolog 1
MMR	Mismatch repair
M-phase	Mitotic phase of the cell cycle
MPV	Mean platelet volume
MRE11	Meiotic recombination 11
mRNA	Messenger-RNA
MRP1	Multidrug resistance-associated protein 1; ATP binding cassette subfamily C member 1
MRP2	Multidrug resistance-associated protein 2; ATP binding cassette subfamily C member 1

MSH2	Mismatch Repair Protein 2; mutS homolog 2
MSH6	Mismatch Repair Protein 6; mutS homolog 6
n.d.	Not detectable
NBS1	Nijmegen breakage syndrome 1; nibrin
NER	Nucleotide excision repair
NHEJ	Non-homologous end-joining
NOXA	BCL2-homology 3; BH3
NP-40	Nonidet P40
NSG	NOD scid gamma
OCT2	Organic cation transporter 2; Solute carrier family 22, member 2
OH-Urea	Hydroxyurea
p	Phospho
p16	Cyclin dependent kinase inhibitor 2A
p21	Cyclin dependent kinase inhibitor 1A
p53	Cellular tumor antigen p53
PAGE	Polyacrylamide gel electrophoresis
PALB2	Partner and Localizer of BRCA2
PARP	Poly (ADP-ribose) polymerase
PBS	Phosphate-buffered saline
PCNA	Proliferating cell nuclear antigen
PCR	Polymerase chain reaction
PDTO	Patient derived tumor organoids
PDWc/PDWs	Platelet distribution width
PDX	Patient derived xenografts
PGC1a	Peroxisome proliferator-activated receptor gamma coactivator 1α
PI	Propidium iodide
PINK1	Serine/threonine-protein kinase PINK1
PMS2	PMS1 homolog 2
Pol	Polymerase
POLA1	catalytic subunit of DNA polymerase α
POLB	DNA polymerase β
POLD1	DNA polymerase δ
POLE	DNA polymerase ε
POLI	DNA polymerase ι
PPP2CA	Serine/threonine-protein phosphatase 2A catalytic subunit
PPP2R4	Serine/threonine-protein phosphatase 2A regulatory subunit

PrimPol	Primase and DNA directed polymerase
PRKN	E3 ubiquitin-protein ligase parkin
PUMA	p53 upregulated modulator of apoptosis
RAD50	RAD50 double strand break repair protein
RAD51	DNA repair protein RAD51 homolog 1
RAD51B	DNA repair protein RAD51 homolog 2
RAD51C	DNA repair protein RAD51 homolog 3
RAD51D	DNA repair protein RAD51 homolog 4
RAD52	DNA repair protein RAD52
RALBP1	RalA-binding protein 1
Rb	Retinoblastoma
RDWc/RDWs	Red cell distribution width
Rel.	Relative
REV1	DNA repair protein REV1
RIPA	Radioimmunoprecipitation assay buffer
RNA	Ribonucleic acid
RNAPII	RNA polymerase II
ROS	Reactive oxygen species
RPA	Replication protein A2
RT	Room temperature
RT-qPCR	Quantitative real-time PCR
s.c.	Subcutaneous
SD	Standard deviation
SDS	Sodium dodecyl sulfate
SEM	Standard error of the mean
SIRT4	Sirtuin 4
SLC8A3	Solute carrier family 8 member A3
SOD1	Superoxide dismutase 1
SOD2	Superoxide dismutase 2
S-phase	Synthesis phase of the cell cycle
ssDNA	Single-stranded DNA
STR	Short tandem repeat
tBOOH	Tert-butyl hydroperoxide
TBS	Tris-buffered saline
TC-NER	Transcription-coupled NER
TFIIH	Transcription factor II H
TLS	Translesion synthesis

TNF receptor 1	Tumor necrosis factor receptor 1
TOP2A	Topoisomerase II α
TOP2B	Topoisomerase II β
TOPBP1	DNA topoisomerase II binding protein 1
TP73	Tumor protein p73
ULK1	Unc-51 like autophagy activating kinase 1
UV	Ultraviolet
UVSSA	UV Stimulated Scaffold Protein A
vs.	versus
WIPI2	WD repeat domain phosphoinositide-interacting protein 2
X^{CisPt}	Cisplatin resistant cell line, whereby X is the name of the parental cell line
X_i	Inhibitor of X, whereby X is the target protein
XPA	Xeroderma pigmentosum, complementation group A
XPB	Xeroderma pigmentosum, complementation group B
XPC	Xeroderma pigmentosum, complementation group C
XPD	Xeroderma pigmentosum, complementation group D
XPF	Xeroderma pigmentosum, complementation group F
XPG	Xeroderma pigmentosum, complementation group G
XRCC2	X-ray repair cross complementing 2
XRCC3	X-ray repair cross complementing 3
ZETT	*Zentrale Einrichtung für Tierforschung und wissenschaftliche Tierschutzaufgaben*
γH2AX	H2A histone family, member X, phosphorylated at serine 139

1 Introduction

1.1 Cancer

Cancer is, alongside cardiovascular diseases, one of the most common causes of death in industrialized countries, being responsible for one fifth of all deaths. In 2020, the global incidence of cancer was estimated at 20 million cases and almost 10 million deaths were attributed to cancer (Sung *et al.*, 2021). The overall incidence keeps rising in aging populations, although improvements in prevention, diagnostics, and therapy help to curb this trend concerning mortality. Besides age, the individual cancer risk is dependent on various other factors like lifestyle (e.g. nutrition, smoking, alcohol) and environmental stressors (e.g. UV exposure), but also sex, genetic predispositions and endogenous processes (Block *et al.*, 1992; Weinstock, 1995; Sasco *et al.*, 2004; Bagnardi *et al.*, 2015; Perrino *et al.*, 2019). Endogenous processes relevant for carcinogenesis include errors in DNA replication, the formation of reactive oxygen species (ROS) during metabolic processes, and chronic inflammation.

Cancer development is a multistage process and can be divided into initiation, promotion and progression (Berenblum, 1941). During the initiation phase, a mutation event occurs in the DNA of a single cell. In the promotion phase, the cell that has undergone a mutation is multiplied by a growth stimulus. In the progression phase, the malignant transformation is completed. Mutations relevant for cancer development are often leading to the activation of proto-oncogenes, inactivation of tumor suppressor genes or inactivation of genomic stability genes. Proto-oncogenes are genes that normally positively regulate cell growth and division, or help cells stay alive. When a proto-oncogene, e.g. the small GTPase RAS, mutates and thereby becomes hyperactivated, it is called an oncogene (Bos, 1989). When this happens, the affected cell can start to grow out of control. Tumor suppressor genes are genes whose products can suppress the uncontrolled division of genomically damaged cells and thus prevent the development of tumors. A well-known tumor suppressor gene that is loss-of-function mutated in a variety of tumors is p53 (Nigro *et al.*, 1989), which in its normal state after DNA damage can trigger cell cycle arrest to gain time for DNA repair or promote apoptosis. Genomic stability is maintained by four principal mechanisms: coordinated progression through the cell cycle, accurate DNA replication during the S-phase, proper segregation of chromosomes during mitosis, and efficient repair of DNA damage (Shen, 2011). Therefore, all genes involved in these processes are considered genomic stability genes and mutations leading to their inactivation can act as drivers for the development of cancer.

Cancer can occur in a wide variety of organs and forms. In order to make statements about the most effective treatment option, their ability to metastasize or patients' survival chances, cancers are classified according to their tissue of origin, stage, grade and histology. So, for example, carcinomas arise from the epithelium, sarcomas from the mesenchyme, lymphomas from the lymphatic system and neuroendocrine tumors from the neuroectoderm. Characteristics shared by all types of cancer cells are the so-called hallmarks of cancer. Those include increased proliferation independent of external growth signals, evasion of growth suppressors, reduced execution of cell death mechanisms, replicative immortality, increased angiogenesis, capability of invasion and metastasis, deregulated cellular metabolism and avoidance of immune destruction. Genome instability and mutations as well as tumor-promoting inflammation are described as enabling processes to acquire the eight hallmarks of cancer (Hanahan, 2022) (Figure 1).

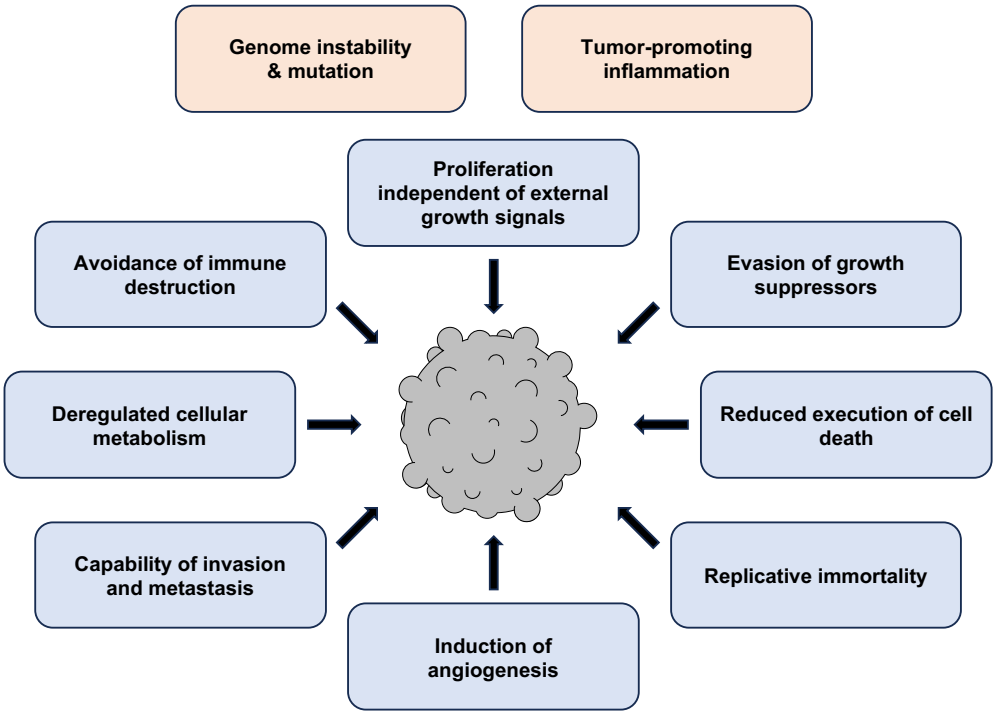

Figure 1: Hallmarks of cancer
Characteristic for malignant tumors are increased proliferation independent of external growth signals, evasion of growth suppressors, reduced execution of cell death mechanisms, replicative immortality, increased angiogenesis, capability of invasion and metastasis, deregulated cellular metabolism and avoidance of immune destruction. Genome instability and mutations as well as tumor-promoting inflammation are described as enabling processes that facilitate the acquisition of the eight hallmarks of cancer. Modified from Hanahan, 2022.

1.1.1 Genomic instability and aneuploidy

Genome instability is considered a common characteristic of cancer cells. It refers to an enhanced tendency to acquire mutations in the genome, ranging from changes in the nucleotide sequence to chromosome rearrangements, gains or losses (Aguilera and Gómez-González, 2008). It occurs when genome maintenance systems, such as DNA damage repair pathways or cell cycle checkpoints (e.g. the mitotic spindle assembly checkpoint), fail to preserve the integrity of the genome, either as a result of inherited defects or induced by exposure to environmental agents.

An increased or reduced total chromosome number compared to the normal euploid genome is termed aneuploidy. In the special case that the complete set of chromosomes is multiplied, this is referred to as polyploidy. Aneuploidy or even polyploidy is a common feature in tumor cells, which is also due to the fact that changes in ploidy can alter expression of proto-oncogenes or tumor suppressor genes (Weaver and Cleveland, 2006). If a cell is aneuploid, this does not necessarily imply that it will not pass on its exact chromosome number to its offspring. However, aneuploidy and chromosomal instability (CIN), which refers to the lack of capacity to maintain the same chromosome number from one cell generation to the next, often coexist. Cells with CIN frequently make mistakes in chromosome segregation during cell division (i.e. mitosis), about 30 times more often than stable cells, resulting after several division cycles in very complex karyotypes (Thompson and Compton, 2008).

1.2 Cancer treatment

Treatment options for cancers are, depending on the cancer type, surgery, radiation, immunotherapy, or chemotherapy. Often a combination of multiple of those is used to treat most efficiently. Surgery or radiation is the primary treatment choice for localized cancers. In contrast, drugs for chemotherapy are usually given as an infusion into the blood so that they are well distributed throughout the body and reach both the original tumor and any cancer cells that have already spread. Because of that they are the first line treatment choice for metastatic or locally advanced tumors and many soft tissue tumors.

1.2.1 Chemotherapy

Chemotherapy is the term used for cytostatic-based therapy of cancer diseases. Cytostatics prevent cells from dividing by intervening in the cell cycle progression. Cytostatic drugs can be divided into several substance groups based on their different targets in the cells, whereby not all cytostatic drugs can be assigned to just one group (Schulz, 2023) (Table 1). Some of the groups target the DNA directly and therefore affect cells in all cell cycle phases, while others have rather cell cycle phase-specific attack points.

Compounds targeting the DNA directly are for example platinum compounds like cisplatin (see chapter 1.2.1.1), that cause DNA crosslinks, or alkylating agents like cyclophosphamide, that add alkyl groups to DNA bases. Anthracyclines such as doxorubicin can intercalate into DNA, which means they reversibly bind between opposing bases located on the two different DNA strands of the double helix. Bleomycin contains a reactive group that generates hydroxyl radicals, which in turn can cause DNA strand breaks.

In order to unwind the (super)coiled DNA in preparation for replication or transcription, topoisomerases insert a single-strand break (in the case of topoisomerase I) or a double-strand break (in the case of topoisomerase II) into the DNA and, after pulling through another DNA strand, religate the break again. Topoisomerase inhibitors such as irinotecan, etoposide or the already mentioned doxorubicin bind topoisomerases after they have inserted a DNA strand break. In this state, the strand break can no longer be religated and persists. The double-strand break resulting from topoisomerase II inhibition is directly highly cytotoxic, while the single-strand break resulting from topoisomerase I inhibition is transformed into a double-strand break during the next replication and only then develops its full cytotoxic potential.

Antimetabolites and nucleoside biosynthesis inhibitors such as 5-fluorouracil (5-FU) or hydroxyurea (OH-Urea) specifically attack cells in the S-phase. Antimetabolites are incorporated into the newly synthesized DNA or RNA as dysfunctional bases and thus disrupt further strand extension. In addition, fewer nucleotides are produced due to negative feedback loop signaling to the synthesizing enzymes (Longley *et al.*, 2003). Other substances directly inhibit enzymes of the nucleoside synthesis, e.g. OH-Urea inhibits ribonucleotide reductase, and thereby lead to a shortage of DNA building blocks (Bianchi *et al.*, 1986).

Taxanes and vinca alkaloids belong to the group of microtubule-binding compounds, which either enhance (taxanes) or inhibit (vinca alkaloids) the polymerization of tubulin into microtubules. By this blockage of microtubule dynamics, they restrict intracellular

vesicle transport and cell migration and most importantly block mitosis due to defective formation of the spindle apparatus (Stanton *et al.*, 2011).
In addition to conventional cytostatics, targeted therapies with monoclonal antibodies (e.g. Cetuximab in the treatment of colorectal carcinoma), kinase inhibitors (e.g. ibrutinib in the treatment of non-Hodgkin lymphomas) or hormone antagonists (e.g. tamoxifen in the treatment of mamma carcinomas) become more common.

Table 1: Classification of selected cytostatic drugs by substance group.

Class of drugs	Examples
Directly DNA-damaging drugs	Platinum derivates (e.g. cisplatin) Alkylating agents (e.g. cyclophosphamide) Anthracyclines (e.g. doxorubicin) Bleomycin
Topoisomerase inhibitors	Topoisomerase I inhibitors (e.g. irinotecan) Topoisomerase II inhibitors (e.g. etoposide)
Antimetabolites or nucleoside biosynthesis inhibitors	Pyrimidine analogs (e.g. 5-fluorouracil) Hydroxyurea
Microtubule-binding compounds	Vinca alkaloids (e.g. vinblastine) Taxanes (e.g. paclitaxel)

Unfortunately, cytostatic drugs do not exclusively act on cancer cells but often damage and kill normal cells as well. Generally, cancer cells are more sensitive to cytostatics because of frequent defects in DNA damage response (DDR) or DNA repair and their higher proliferation rate than most healthy cells. However, there are some types of tissue with physiologically high cell turnover, like the intestinal epithelium, hematopoietic cells, hair roots and the skin. As a result, the general side effects of chemotherapy include nausea and diarrhea, anemia, hair loss and rashes (Anand *et al.*, 2023). Besides the described general adverse effects, most cytostatics additionally have drug-specific dose-limiting side effects, for instance nephrotoxicity, neurotoxicity and ototoxicity for cisplatin. A second limitation to the application of cytostatic drugs is the acquirement of resistance of cancer cells against them (see chapter 1.2.2). To prevent development of chemoresistance and minimize dose-limiting adverse effects, while at the same time enhancing the antitumor efficacy, agent combinations are often used in treatments (Schulz, 2023).

1.2.1.1 Cisplatin

Cisplatin (CisPt), together with carboplatin and oxaliplatin, belongs to the group of platinum-based anticancer drugs. Cisplatin is the most prominent compound of this group. It got its FDA (Food and Drug Administration) approval in 1978 for the treatment of testicular, advanced ovarian and bladder cancer. It is today used in the treatment of a wide range of carcinomas as crucial component in drug combinations, e.g. the PEB scheme. The PEB scheme is a polychemotherapy for the treatment of testicular germ cell tumors and combines the three cytostatics cisplatin, etoposide and bleomycin.

Cisplatin consists of a central platinum atom with two cis-directed chlorine ligands and two covalently bound ammonium groups. The uncharged cisplatin can enter the cell by passive diffusion or active transport via specific transport proteins e.g. copper transporter CTR1 (copper transporter 1; solute carrier family 31, member 1) or cation transporter OCT2 (organic cation transporter 2; solute carrier family 22, member 2) (Ishida *et al.*, 2002; Ciarimboli *et al.*, 2005, 2010; Yonezawa *et al.*, 2005; Larson *et al.*, 2009). Inside the cell the lower intracellular chloride concentration of around 4 - 20 mM in contrast to around 100 mM in the extracellular fluid, favors the aquation of cisplatin (Pinto and Lippard, 1985; Jamieson and Lippard, 1999) (Figure 2). This means that the chloride ions in the molecule are one after the other displaced by water, forming the reactive cationic di-aquo-complex $[cis\text{-}Pt(NH_3)_2(H_2O)_2]^{2+}$. This electrophilic intermediate can diffuse into the nucleus and target the DNA. The primary target of the complex is the nitrogen on position 7 of the purine bases Guanine (G) and to lesser extent Adenine (A) (Mansy *et al.*, 1978; Baik *et al.*, 2003). First, monofunctional binding of cisplatin to a base occurs, which can subsequently lead to crosslinking with a second base. These crosslinks can form between bases within one DNA strand (intrastrand crosslinks) or between both DNA strands (interstrand crosslinks). Intrastrand crosslinks between two neighboring bases are the most common, with GpG-intrastrand crosslinks accounting for about 65% and ApG-intrastrand crosslinks for about 25% of all crosslinks. The intrastrand crosslinking of two non-adjacent guanine bases (GpXpG) occurs with a significantly lower frequency of 5 - 10%. Interstrand crosslinks or residual monoadducts are even rarer, occurring at approximately 1% of cases (Eastman, 1983; Fichtinger-Schepman *et al.*, 1987). As a consequence of the CisPt-DNA crosslinks, the secondary structure of the DNA double helix is disturbed. This deformation significantly impairs / blocks the replication and transcription of DNA (Mello *et al.*, 1995; Wagner and Karnitz, 2009). The blockage of replication can cause breaks in the backbone of the DNA helix, which activate the DNA damage response to repair the existing damage (Olive and Banáth, 2009).

If the extent of the damage exceeds the cellular repair capacity, cell death by apoptosis or necrosis is triggered (see chapter 1.3.2) (Norbury and Zhivotovsky, 2004; Roos and Kaina, 2013). Cisplatin can not only interact with DNA, but also with other nucleophiles present intracellularly e.g. amino or thiol groups of proteins, which can lead to the formation of highly cytotoxic DNA-protein crosslinks. However, in the case of cisplatin binding to the thiol group of the antioxidant glutathione (GSH), this is in fact beneficial for cells, as it leads to a reduced intracellular concentration of cisplatin. This effect is mediated by the exporter multidrug resistance-associated protein 2 (MRP2), which actively transports glutathione-bound cisplatin out of the cell (Cui *et al.*, 1999). In addition, there are other transporters such as ATPase copper-transporting α (ATP7A), ATPase copper-transporting β (ATP7B) or multidrug extrusion transporter 1 (MATE1) which have been identified to cause an efflux of cisplatin out of cells, independent of glutathione (Ciarimboli, 2012).

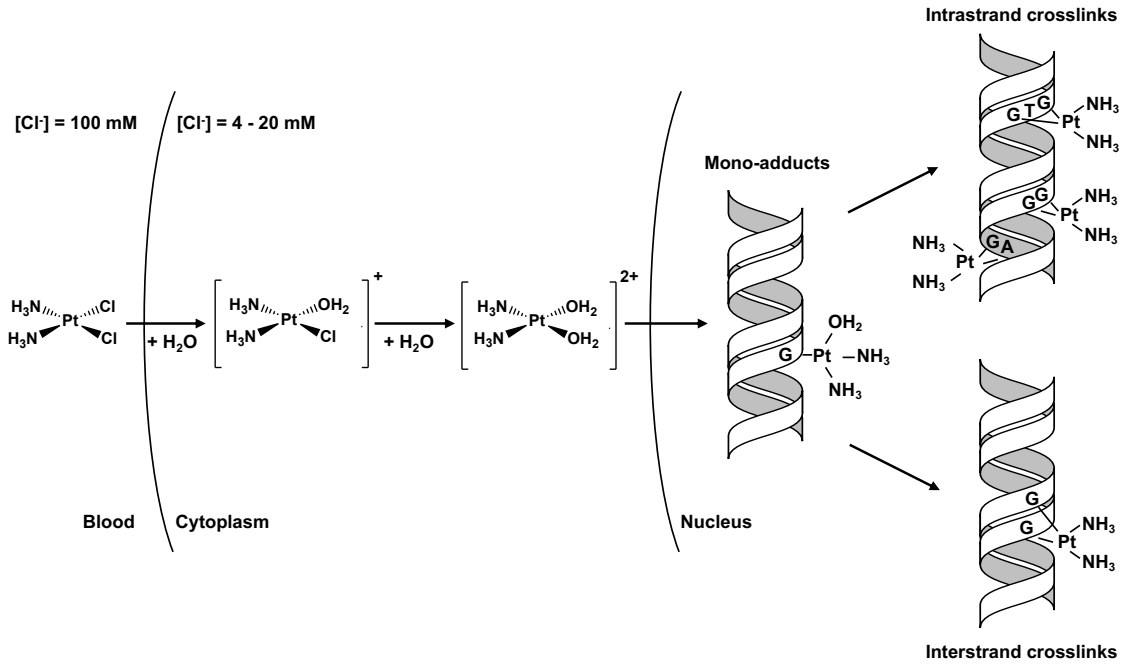

Figure 2: Bioactivation of cisplatin and schematic visualization of the resulting platinum-DNA adducts
After cisplatin has entered the cell by passive diffusion or with the help of transport proteins, it is hydrolyzed due to the lower intracellular chloride concentration ([Cl^-]). The resulting di-aquo-complex can enter the nucleus and react with the nucleotides of the DNA. This occurs preferentially at the nucleophilic N7 atom of guanine and to lesser extent at adenine. In this way, DNA mono-adducts are formed that can react further with a second nucleotide to form intra- or interstrand crosslinks. Modified from Rocha *et al.*, 2018. (This figure was created in part by using images from ChemDraw 22.2.0.)

1.2.2 Acquirement of cisplatin resistance

Chemotherapy with cisplatin often leads to an initial success defined by reduction in tumor burden or disease stabilization, but a not negligible fraction of originally sensitive tumors eventually acquires chemoresistance. The exact mechanisms leading to the development of cisplatin resistance are manifold. Nevertheless, there are general pathways that commonly play a role, and these can be classified into pre-target, on-target, post-target and off-target factors (Galluzzi *et al.*, 2012).

Pre-target factors are alterations that involve steps preceding the binding of cisplatin to DNA. These alterations could consist of reduced uptake e.g. by downregulation of CTR1, increased efflux e.g. by upregulation of MRP2, or increased inactivation of cisplatin e.g. by elevated levels of GSH or metallothioneins. On-target factors directly relate to changes in cisplatin-DNA adduct formation or processing. This often relies on increased DNA repair capacity due to increased nucleotide excision repair (NER) proficiency (see chapter 1.3.1.2) or increased by-passing capability by translesion synthesis (TLS) (see chapter 1.3.1.1). Post-target factors involve altered cell death signaling pathways, for example upregulation of antiapoptotic proteins like B cell lymphoma 2 (BCL-2) or upregulation of tumor suppressor protein p53. Molecular changes that do not present obvious links with cisplatin-evoked signals are categorized as off-target factors. These could be changes in pathways promoting pro-survival functions in response to multiple stress conditions, e.g. altered autophagy or increased levels of heatshock proteins (Galluzzi *et al.*, 2012) (Figure 3). To define which mechanism leads to the development of cisplatin resistance in a specific cell population is often complicated, because there can be several different factors involved in the mechanism of resistance in the whole population and even in one cell.

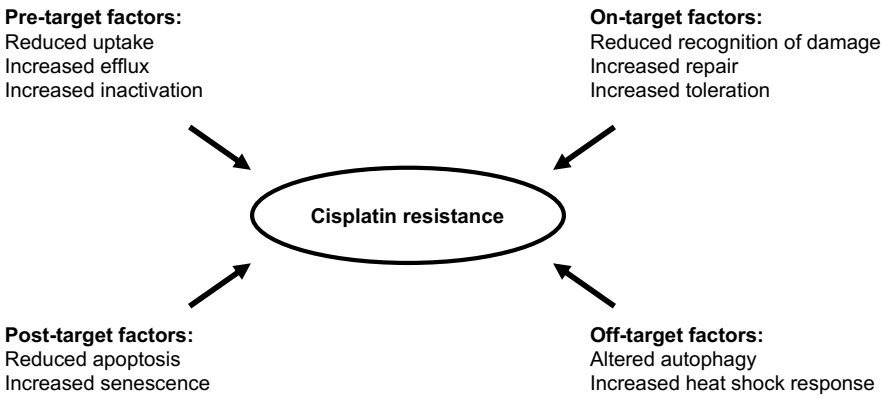

Figure 3: Categorization of factors involved in the acquirement of cisplatin resistance according to Galluzzi *et al.*, 2012
Pre-target factors are alterations that involve steps preceding the binding of cisplatin to DNA, on-target factors directly relate to changes in cisplatin-DNA adduct formation or processing and post-target factors involve altered cell death signaling pathways. Molecular changes that do not present obvious links with cisplatin-evoked signals are categorized as off-target factors.

1.3 Cellular stress responses

The term cellular stress response covers molecular changes that cells initiate in response to various stressors. Stressors can include extreme temperatures, mechanical damages or exposure to toxins damaging e.g. the DNA.

1.3.1 DNA damage response

To maintain genomic integrity, cells are equipped with the DNA damage response (DDR) network (Ciccia and Elledge, 2010). Upon detection of DNA damage via damage type-specific sensor systems, a complex signaling cascade is initiated that regulates the recruitment of repair proteins, induction of cell cycle arrest, activation of cell death or survival mechanisms. The apical serine/threonine kinases ATM (Ataxia telangiectasia mutated) and ATR (Ataxia telangiectasia and RAD3 related), as well as the DNA-dependent protein kinase DNA-PK, are considered to be key mediators between detected DNA damage and its consequences. Depending on the type of DNA damage, one of the kinases is primarily activated, in turn initiating its subsequent signaling pathway. ATM and DNA-PK are mainly activated by DNA double-strand breaks (DSBs), whereas ATR is more likely to be active in the case of DNA replication-blocking lesions. However, since the damage-free transfer of DNA to daughter cells is highly important for a healthy cell population, there are strong redundancies in most mechanisms of the DDR to enable compensation in the event of a proteins' loss of function (Ciccia and Elledge, 2010).

For DNA double-strand breaks, a damage sensor is the MRN complex consisting of MRE11 (meiotic recombination 11), RAD50 (RAD50 double strand break repair protein) and NBS1 (Nijmegen breakage syndrome 1; nibrin) (Figure 4). The MRN complex recruits ATM to the DNA damage (Lee and Paull, 2005). ATM is a homo-dimer in its inactive state, but is monomerized when binding to the double-strand break, autophosphorylated and thereby activated (Bakkenist and Kastan, 2003). Alternatively, DNA double-strand breaks can be recognized via the heterodimer of Ku70 (X-ray repair complementing defective repair in Chinese hamster cells 6; XRCC6) and Ku80 (X-ray repair complementing defective repair in Chinese hamster cells 5; XRCC5), whereby DNA-PKcs (DNA-dependent protein kinase, catalytic subunit) is recruited to the DNA damage (Davis *et al.*, 2014). The protein RPA (replication protein A2), on the other hand, binds to free single-stranded DNA and recruits ATR together with ATRIP (ATR interacting protein) to the lesion (Zou and Elledge, 2003; Ball *et al.*, 2005). ATM, DNA-PKcs, as well as ATR phosphorylate histone 2AX (H2A histone family, member X; H2AX) at serine 139 (γH2AX), which regulates chromatin organization

and serves as a signal that marks the damage site for DNA repair proteins (Rogakou *et al.*, 1998; Ward and Chen, 2001; Stiff *et al.*, 2004). Therefore, γH2AX is considered as surrogate marker for DNA damage (Mah *et al.*, 2010). ATM also phosphorylates the KRAB (Krüppel-associated box) corepressor KAP1 (KRAB-associated protein 1), mediating chromatin decondensation important for DNA repair (Cann and Dellaire, 2011).

In order to provide cells with sufficient time for repair of DNA damage, the continuation of the cell cycle can be temporarily suspended at various so-called cell cycle checkpoints. Such checkpoints exist at the transition of cells from G1- to S-phase (G1/S checkpoint), in S-phase (intra-S-phase checkpoint) and at the transition from G2-phase to mitosis (G2/M checkpoint). For cell cycle arrest initiation, the cell cycle checkpoint kinases CHK1 and CHK2 are activated by ATR and ATM respectively (Guo *et al.*, 2000; Matsuoka *et al.*, 2000). CHK1 or CHK2 in turn inactivate members of the cell division cycle phosphatase 25 (CDC25) family. The inactivation of CDC25a (cell division cycle phosphatase 25a) arrests the cell cycle at the G1/S checkpoint or the intra-S-phase checkpoint, whereas the inactivation of CDC25c (cell division cycle phosphatase 25c) leads to arrest at the G2/M checkpoint (Matsuoka, 1998; Xiao *et al.*, 2003). Another way to initiate cell cycle arrest during the transition from G1- to S-phase is via the phosphorylation of tumor suppressor p53 at serine 15 leading to stabilization of p53 and upregulated transcription of p21 (protein 21; cyclin dependent kinase inhibitor 1) (el-Deiry *et al.*, 1994; Shieh *et al.*, 1997; Lambert *et al.*, 1998). The phosphorylation of p53 at a different phosphorylation site (serine 46) can also lead to the induction of apoptosis if DNA damage is too severe for repair (Oda *et al.*, 2000).

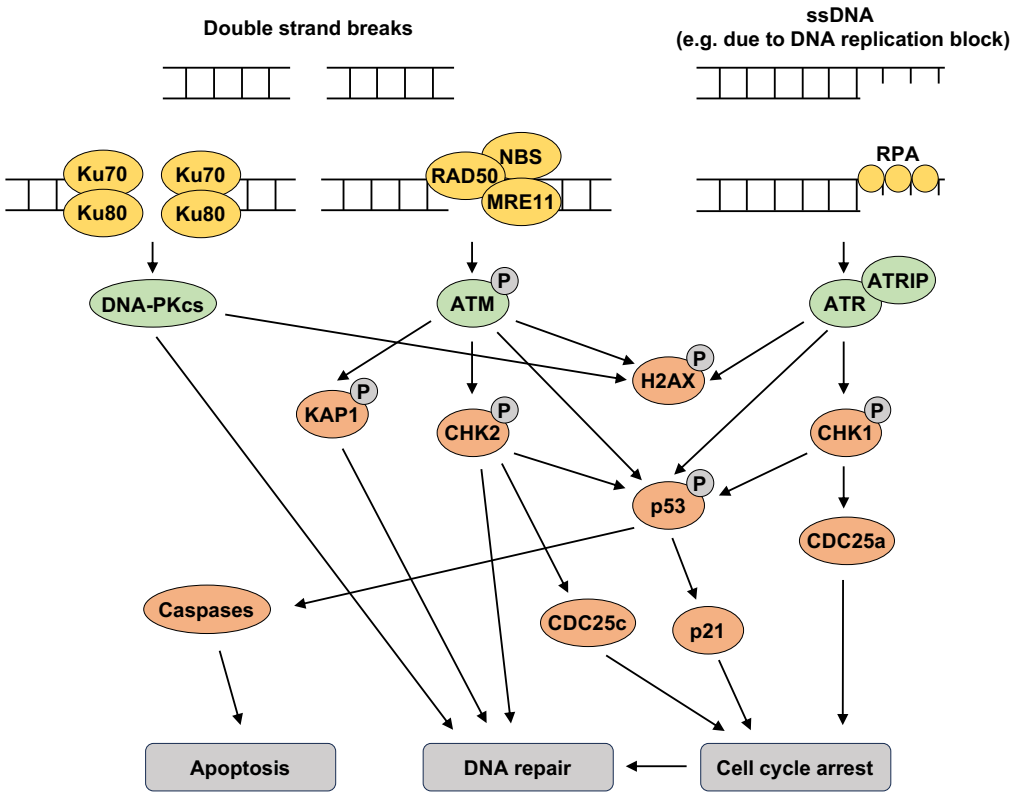

Figure 4: Schematic diagram of the DNA damage response
The DNA damage response is triggered by DNA double-strand breaks or replication-blocking lesions / single-stranded DNA (ssDNA). Double-strand breaks are detected by Ku70 (X-ray repair complementing defective repair in Chinese hamster cells 6; XRCC6) and Ku80 (X-ray repair complementing defective repair in Chinese hamster cells 5; XRCC5) or by the MRN complex, consisting of the proteins MRE11 (meiotic recombination 11), RAD50 (RAD50 double strand break repair protein) and NBS1 (Nijmegen breakage syndrome 1; nibrin). After recognition by Ku70/Ku80, the DNA-PKcs (DNA-dependent protein kinase) is activated. If the DNA damage is detected by the MRN complex, ATM (ataxia telangiectasia mutated) can bind to the double-strand break and is activated. DNA single strand regions (ssDNA) are recognized by RPA (replication protein A2) and as a result ATR (ataxia telangiectasia and RAD3 related) together with ATRIP (ATR interacting protein) is recruited to the lesion and activated. Subsequently, DNA-PKcs, ATM and ATR activate several specific substrates involved in cell cycle control, DNA repair and apoptosis. Substrates include H2AX (H2A histone family, member X), KAP1 (KRAB-associated protein 1), CHK1 (Checkpoint kinase 1), CHK2 (Checkpoint kinase 2), CDC25a (cell division cycle phosphatase 25a), CDC25c (cell division cycle phosphatase 25c), p53 and p21 (cyclin dependent kinase inhibitor 1A; CDKN1A).

1.3.1.1 Replicative stress response

The replicative stress response is a subcategory of the DNA damage response that acts with DNA damage in S-phase cells. Replicative stress refers to the slowing down or blockage of the replication fork during DNA synthesis. Obstacles for the replisome can amongst others be imbalances of factors involved in replication or modifications of the DNA, e.g. DNA crosslinks or secondary DNA structures like R-loops (Zeman and Cimprich, 2014).

Interstrand crosslinks, e.g. caused by cisplatin, simultaneously block DNA synthesis on both leading and lagging strand, whereas other types of replication barriers only affect one of the strands. Lagging strand obstacles are normally well tolerated because of the physiological discontinuous nature of Okazaki fragments (Pasero and Vindigni, 2017).

In case of the leading strand, replication blockage leads to the formation of long stretches of single-stranded DNA (ssDNA) as the helicase continues to unwind the DNA strands while the DNA polymerase is halted (Figure 5) (Byun *et al.*, 2005). ssDNA is very unstable and therefore requires protection. The protein RPA binds to single-stranded DNA regions, thereby protecting them from nuclease-dependent degradation and preventing the formation of secondary structures (Kim *et al.*, 1994). The RPA-covered ssDNA then triggers a signaling cascade mediated by a complex of ATR and ATRIP with further activation of CHK1 (Liu *et al.*, 2000; Cortez *et al.*, 2001; Zou and Elledge, 2003). Activated ATR and CHK1 both phosphorylate a wide range of substrates, thereby inhibiting cell cycle progression and suppressing replication origin firing in a cell-wide manner, providing time for repair (Saldivar *et al.*, 2017). Concurrently with checkpoint activation, RPA is replaced by DNA repair protein RAD51 homolog 1 (RAD51) at the ssDNA. This mediates replication fork reversal, forming the so-called chicken foot structure, facilitating fork repair (Zellweger *et al.*, 2015). At this stage, RAD51, together with other fork protectors e.g. BRCA2 (breast cancer 2, early onset) protects the nascent DNA from degradation by nucleases (Rickman and Smogorzewska, 2019). Once the damage has been removed, the replication fork must be restarted. This can either occur in an homologous recombination (HR)-dependent manner (see Figure 7) or via branch migration (Liao *et al.*, 2018). If blockage of replication forks cannot be resolved or due to insufficient protection of replication intermediates, the replication fork collapses, this results in DNA double-strand breaks and the dissociation of the entire replisome (Zeman and Cimprich, 2014). If this happens genome-wide, this phenomenon is termed replication catastrophe.

In addition to the option of DNA repair, there are various damage tolerance mechanisms to overcome replication stress. One of them is translesion synthesis (TLS). In this process, special polymerases e.g. polymerase η can bypass DNA lesions and then continue to synthesize DNA as usual, but they are more prone to errors than the classical DNA polymerases (Powers and Washington, 2018). Other specialized polymerases such as PrimPol (Primase and DNA directed polymerase), an RNA/DNA primase-polymerase, can perform a process called repriming. In this case, DNA synthesis is simply reinitiated behind a replication-blocking DNA lesion (Tirman *et al.*, 2021a). Thereby fork stalling is prevented, but a ssDNA gap is left behind (Mourón *et al.*, 2013). These gaps are then filled by other TLS pathways in S- and G2-phase (Taglialatela *et al.*, 2021; Tirman *et al.*, 2021b). The activity of PrimPol is promoted by CHK1-mediated phosphorylation (Mehta *et al.*, 2022) (Figure 5).

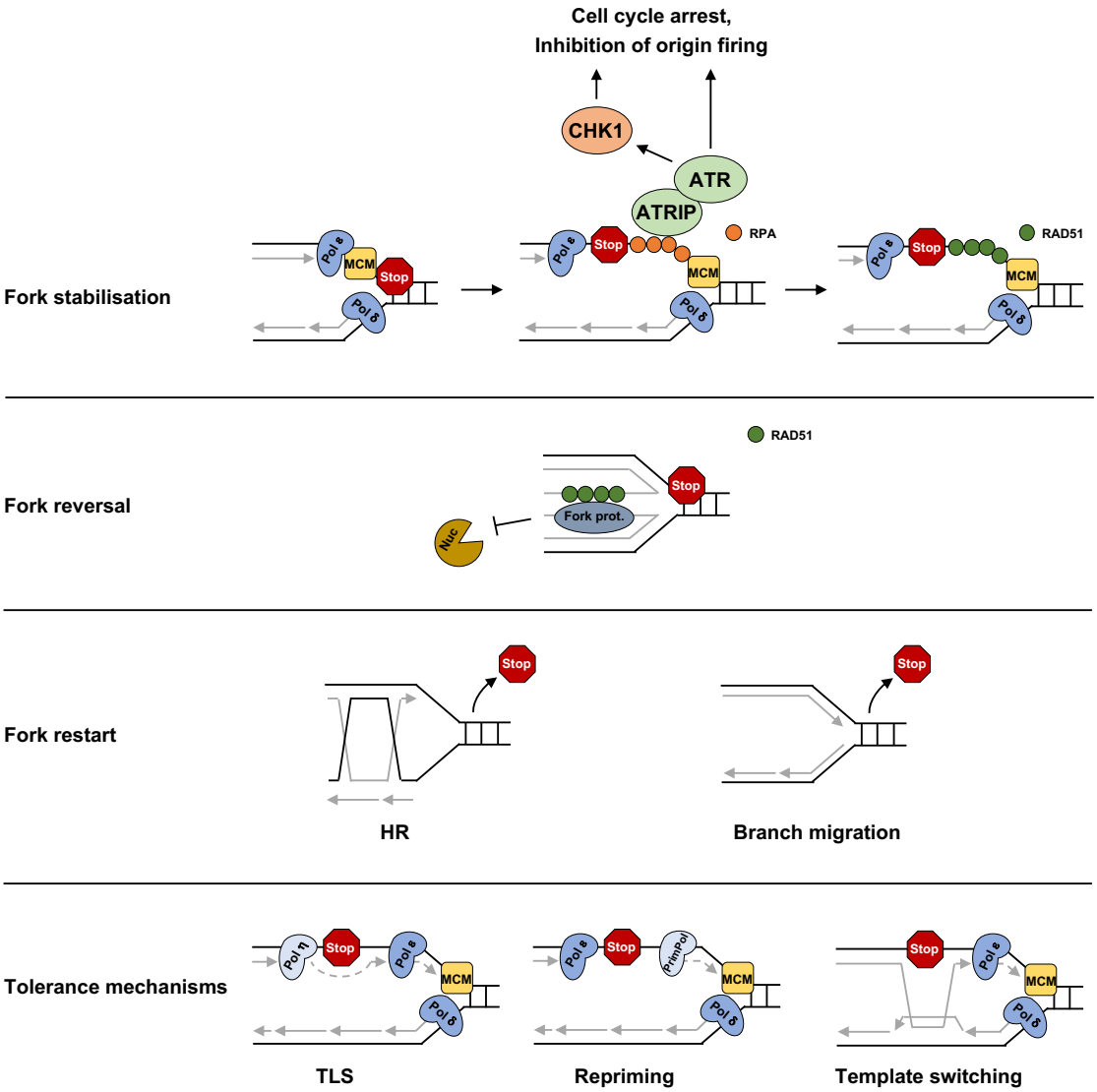

Figure 5: Rescue mechanisms of stalled DNA replication forks
After fork stalling, single-stranded DNA (ssDNA) generated by uncoupling of the helicase (MCM) from the polymerase (Pol ε) is coated by RPA (Replication protein A2) to prevent secondary structure formation. The ssDNA-RPA complex induces activation of the replication checkpoint via ATR (Ataxia telangiectasia and RAD3 related) and CHK1 (Checkpoint kinase 1), which will regulate a wide range of cellular events to promote fork recovery, e.g. cell cycle arrest and global inhibition of origin firing. RAD51 (DNA repair protein RAD51 homolog 1) soon replaces RPA and mediates replication fork reversal to facilitate fork repair. The reversed forks are protected by various fork protectors (Fork prot.) from degradation by nucleases (Nuc). After removal of replication stress, stalled replication forks can be restarted in an homologous recombination (HR)-mediated manner or through branch migration. There are also various tolerance mechanisms for overcoming replication barriers. In translesion synthesis (TLS) special polymerases like polymerase η (Pol η) can simply bypass DNA lesions and then continue to synthesize DNA as usual. After a few nucleotides, the role is taken over again by a classical DNA polymerase. In another process called repriming, different specialized polymerases like PrimPol (Primase and DNA directed polymerase) can reinitiate replication behind the polymerase-blocking DNA lesion. Modified from Liao *et al.*, 2018; Conti and Smogorzewska, 2020.

1.3.1.2 DNA repair

Various DNA repair mechanisms have developed to ensure the preservation of the genetic information after DNA damage caused by endogenous or exogenous influences. Different repair pathways are responsible for specific types of damage, for example, small base modifications, e.g. oxidative base damage, are repaired via base excision repair (BER), while bulky lesions or crosslinks distorting the DNA helix structure, e.g. cisplatin-DNA-crosslinks, are mainly removed via nucleotide excision repair (NER). Methylations on the O^6 position of guanine are eliminated by direct reversion repair and base mismatches by mismatch repair (MMR) (Figure 6). There are two repair pathways for the repair of DNA double-strand breaks, namely non-homologous end-joining (NHEJ) and homologous recombination (HR) (Hoeijmakers, 2001; Chatterjee and Walker, 2017) (Figure 7).

In BER, damage-specific glycosylases recognize DNA modifications and excise it, creating an apurinic or apyrimidinic site (AP site). Some glycosylases also have an endonuclease activity to cut the DNA backbone, in others this function is taken over by specific endonucleases, e.g. APE1 (apurinic/apyrimidinic endonuclease 1). Depending on the number of newly inserted nucleotides required for repair, distinction is made between two pathways, short patch BER and long patch BER. In short patch BER, a single AP site is filled by DNA polymerase β (Pol β), then DNA ligase III, in cooperation with XRCC1, Pol β and PARP1, links the inserted nucleotide to the existing DNA strand (Kubota *et al.*, 1996). In long patch BER, the first nucleotide is also inserted by Pol β, but then further DNA synthesis is carried out by polymerase δ (Pol δ) or polymerase ε (Pol ε) together with PCNA (proliferating cell nuclear antigen) (Stucki *et al.*, 1998; Podlutsky *et al.*, 2001). The generated DNA overhang is removed by flap endonuclease FEN1 and the DNA strand is ligated by ligase I together with PCNA and Pol β (Klungland, 1997; Robertson *et al.*, 2009) (Figure 6A).

The NER can be categorized into two distinct pathways termed global genomic NER (GG-NER) and transcription-coupled NER (TC-NER). GG-NER is used to remove damage in non-transcribed areas of the genome and on the non-transcribed strand of transcribed regions, while TC-NER becomes active in transcribed regions. Damage detection in GG-NER is carried out by the protein complexes XPC-HR23B (Xeroderma pigmentosum, complementation group C; UV excision repair protein RAD23 homolog B) and RPA-XPA (Replication protein A2; Xeroderma pigmentosum, complementation group A) (Sugasawa *et al.*, 1998). Through this the transcription factor TFIIH (transcription factor II H) is recruited. Among its components are the proteins XPB (Xeroderma pigmentosum, complementation group B) and XPD (Xeroderma

pigmentosum, complementation group D), which have helicase activity and unwind the DNA in close vicinity of the damage. The initiation of TC-NER occurs when RNA polymerase II (RNAPII) encounters DNA damage during transcription and is blocked (Donahue *et al.*, 1994; Lainé and Egly, 2006). The proteins CSA (Cockayne syndrome group A) and CSB (Cockayne syndrome group B) are involved to remove RNAPII from the site of damage and thereby allow the attachment of repair factors (Duan *et al.*, 2021). UVSSA (UV Stimulated Scaffold Protein A) then recruits TFIIH to the damage to unwind the surrounding DNA (Van Der Weegen *et al.*, 2020). In both types of NER, the endonuclease XPG (Xeroderma pigmentosum, complementation group G) and the endonuclease complex XPF-ERCC1 (Xeroderma pigmentosum, complementation group F; Excision repair cross-complementation group 1) are recruited to excise the existing damage bilaterally at a distance of a few bases (Fagbemi *et al.*, 2011). The resulting gap in the DNA is filled by Pol δ and Pol ε based on the sequence of the complementary DNA strand and ligated by DNA ligase I (Mu *et al.*, 1995; Marteijn *et al.*, 2014) (Figure 6B).

Direct reversion repair is based on an enzymatic reaction in which alkyl residues are transferred directly from the DNA to an enzyme, which is thereby irreversibly inactivated (Gutierrez and O'Connor, 2021). The enzyme responsible for direct reversion repair is O^6-Methylguanine-DNA methyltransferase (MGMT), which possesses the ability to remove methyl groups from the O^6 position of guanine and, to a lesser extent, the O^4 position of thymine (Paalman *et al.*, 1997) (Figure 6C).

In MMR, base mismatches are recognized by MutSα, consisting of MSH2 (mutS homolog 2) and MSH6 (mutS homolog 6). Then the MutLα complex, which consists of MLH1 (mutL homolog 1) and PMS2 (PMS1 homolog 2) is recruited. This complex has endonuclease activity and cuts the DNA strand in proximity of the mismatch. The exonuclease Exo1 (Exonuclease 1) is recruited and removes the incorrect DNA segment. The DNA strand is resynthesized by polymerases δ and the last gap is closed by ligase I (Longley *et al.*, 1997; Genschel *et al.*, 2002; Christmann *et al.*, 2003; Zhang *et al.*, 2005; Kadyrov *et al.*, 2006; Li, 2008) (Figure 6D).

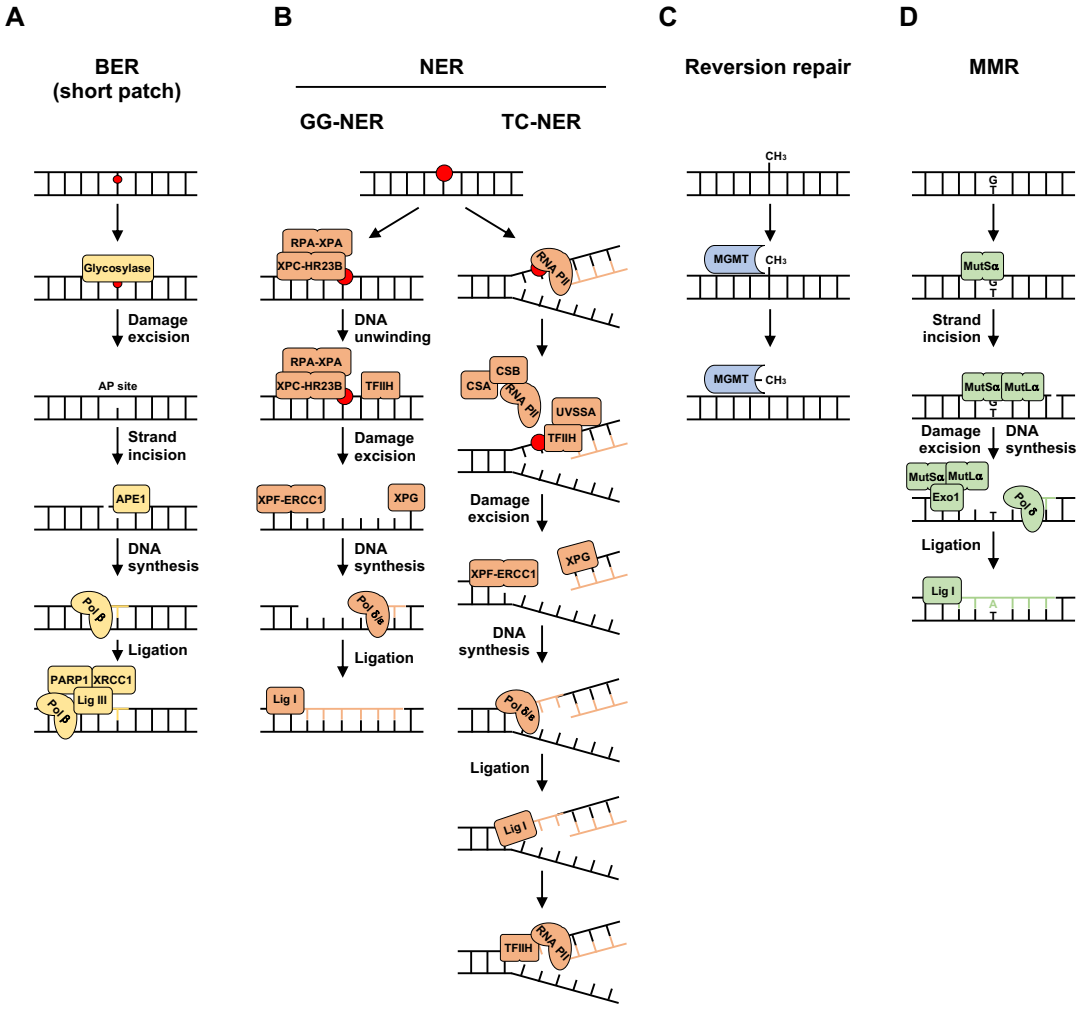

Figure 6: DNA repair mechanisms for various base modifications
A: Base excision repair (BER) removes smaller base modifications from the DNA. BER is initiated by DNA glycosylases, which also excise the damaged base, generating an apurinic/apyrimidinic site (AP site). Subsequently, the phosphodiester bond in the backbone of the DNA is cleaved by apurinic endonuclease-1 (APE1). The missing base at the AP site is refilled by the DNA polymerase β (Pol β) and the DNA strand is religated by ligase II (Lig II) together with PARP1 and XRCC1.
B: Nucleotide excision repair (NER) is used to remove bulky adducts and crosslinks. One distinguishes between global genomic (GG)-NER and transcription-coupled (TC)-NER. Damage detection in GG-NER is carried out by the protein complexes XPC-HR23B (Xeroderma pigmentosum, complementation group C; UV excision repair protein RAD23 homolog B) and RPA-XPA (Xeroderma pigmentosum, complementation group A). Through this, transcription factor TFIIH is recruited. Among its components are the proteins XPB (Xeroderma pigmentosum, complementation group B) and XPD (Xeroderma pigmentosum, complementation group D), which have helicase activity and unwind the DNA around the damage. TC-NER is initiated when RNA polymerase II (RNA PII) encounters DNA damage during transcription and is blocked. The proteins CSA (Cockayne syndrome group A) and CSB (Cockayne syndrome group B) remove RNA PII from the site of damage and thereby allow the attachment of repair factors. UVSSA (UV Stimulated Scaffold Protein A) then recruits TFIIH to the damage. In both types of NER, the endonuclease XPG (Xeroderma pigmentosum, complementation group G) and the endonuclease complex XPF-ERCC1 (Xeroderma pigmentosum, complementation group F; Excision repair cross-complementation group 1) excise the existing damage bilaterally at a distance of a few bases. The resulting gap in the DNA is then filled by Pol δ or ε (Pol δ/ε) based on the sequence of the complementary DNA strand and ligated by DNA ligase I (Lig I).
C: Direct reversion repair refers to the repair of the O6-alkyl guanine by the O6-methylguanine-DNA methyltransferase (MGMT). The alkyl residue is irreversibly transferred to the enzyme, thereby inactivating the enzyme.
D: Mismatch repair (MMR) is responsible for the removal of base mismatches. The mismatch is recognized by the heterodimer MutSα and the heterodimer MutLα is recruited. The endonuclease activity of this complex cuts the strand in proximity to the mismatch. The exonuclease Exo1 is recruited and removes the incorrect segment. The strand is resynthesized by the polymerases δ and ligated by Lig I.
Modified from Christmann *et al.*, 2003.

A further type of DNA damage is DNA double-strand breaks (DSBs). DSBs result from the simultaneous rupture of both complementary strands of the DNA double helix at sites that are closely situated. DNA double-strand breaks may be caused by ionizing radiation or cytostatic drugs, but also during replication secondary from DNA strand linkages or DNA single-strand breaks. As this type of damage is extremely cytotoxic for cells, there are two ways to repair it. HR is a very precise process as it uses the sequence homologous region on the corresponding sister chromatid of the damaged site as a template to repair the DNA double-strand break. Due to the dependence on the presence of sister chromatids, however, the pathway can only be used in the S- and G2-phase. The more error-prone NHEJ is preferentially used in the G0- and G1-phase (Thompson and Schild, 2001; Lieber, 2008).

In NHEJ, the broken DNA ends are rejoined regardless of their sequence, which can result in the loss of nucleotides. The heterodimer of Ku70 and Ku80 serves as a damage sensor in this repair pathway. This factor also ensures that the free DNA ends remain in close proximity to each other and are not degraded by nucleases (Weterings, 2003). DNA-PKcs is recruited to Ku-bound DNA ends in complex with the nuclease Artemis. DNA ends can either be ligated directly or, if the ends are incompatible, processed to a ligatable configuration. When DNA resection is required, DNA-PKcs undergoes autophosphorylation and activates Artemis by phosphorylation. This gives Artemis the ability to cut DNA at single strand–double strand boundaries, which includes all overhangs (Ma *et al.*, 2002). Ligation of the DNA ends is then carried out exclusively by the complex of ligase IV and XRCC4 (Pannunzio *et al.*, 2018) (Figure 7A).

In HR, the double-strand break is recognized by the MRN complex and the DNA ends are processed by the nuclease MRE11, which is part of the MRN complex, to create 3' overhangs (Trujillo *et al.*, 1998). The resulting single-stranded DNA regions are bound by RPA and thus protected from the formation of secondary structures. With the help of BRCA1 (breast cancer 1, early onset), BRCA2, PALB2 (Partner and Localizer of BRCA2) and RAD52 (DNA repair protein RAD52), RPA is replaced by RAD51, which polymerizes and forms filamentous structures (Zelensky *et al.*, 2014). RAD51 with the help of RAD52 searches for the homologous sequence on the sister chromatid and mediates strand invasion, forming the so-called displacement loop (D-loop) (Baumann and West, 1998). Using the homologous sister strand, the required DNA sequence at the 3' end of the overhangs is newly synthesized by DNA polymerases. The emerging crossed structure is also called Holliday structure. After complete synthesis of the missing regions, the crossover is resolved and the DNA backbone is religated (Christmann *et al.*, 2003) (Figure 7B).

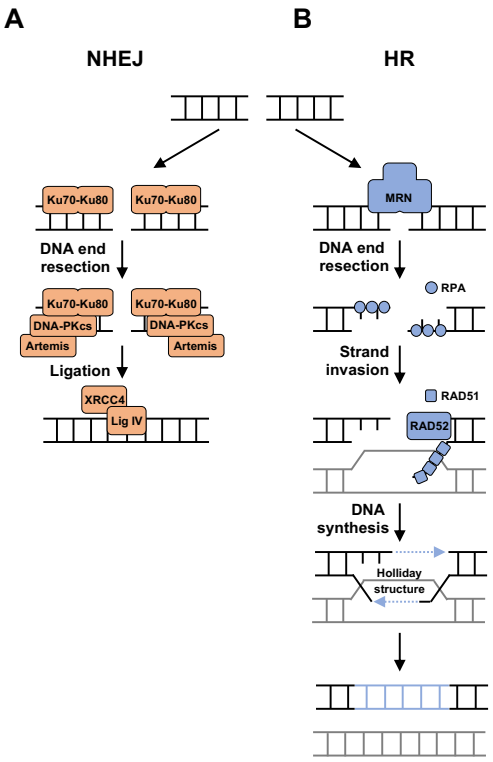

Figure 7: DNA repair mechanisms for DNA double-strand breaks
Double-strand breaks are repaired either by non-homologous end joining (NHEJ) or homologous recombination (HR). In the more error-prone NHEJ (A), the breakage is detected by the heterodimer of Ku70 (X-ray repair complementing defective repair in Chinese hamster cells 6; XRCC6) and Ku80 (X-ray repair complementing defective repair in Chinese hamster cells 5; XRCC5). This recruits the complex of DNA-PKcs and Artemis to the DNA damage. If there are suitable overhangs, the double-strand break can be ligated directly by ligase IV (Lig IV) with the help of XRCC4. Otherwise, the ends are processed by the nuclease Artemis before ligation. In error-free HR (B), the break is detected and processed by the MRN complex, resulting in 3' single-strand overhangs. These are protected by RPA (Replication protein A2) and RAD51 is recruited to the DNA double-strand break. RAD51 with the help of RAD52 is responsible for the search for the matching sequence and for the strand invasion of the single strand into the sister chromatid. The sister strand serves as a template for DNA synthesis, after which the crossed DNA strands (Holliday structure) are separated again and re-ligated. Modified from Christmann *et al.*, 2003.

1.3.1.3 Pharmacological modulation of the DDR/DNA repair for the treatment of cancer

Since the DDR is such an important network that regulates whether cells survive or die, its components may be targeted to induce cell death in tumor cells. A clinically applied therapeutic strategy where the DDR is targeted to treat cancer is the inhibition of histone deacetylases (HDACs). HDACs are enzymes that remove acetyl groups from lysines of both histones and non-histone proteins. With this function, they play a role in a multitude of biological processes, including epigenetic regulation of gene expression, transcription factor activity modulation, protein–protein interactions and protein stability (West and Johnstone, 2014; Roos and Krumm, 2016). Among the stress-imposing consequences of HDAC inhibition in tumor cells are alterations in DNA damage signaling, cell cycle arrest, DNA repair and apoptosis. For example, the inhibition of HDACs disturbs the transcription patterns of DNA repair factors RAD50, MRE11 or RAD51 (Groselj *et al.*,

2013). Approved HDAC inhibitors, e.g. Vorinostat, are mainly used for the treatment of hematologic cancers (Bian *et al.*, 2015).

Inhibitors against the DNA repair factor PARP (poly (ADP-ribose) polymerase), e.g. Olaparib or Niraparib, are used in the clinic to treat cancers with defects in HR, frequently found in mamma carcinoma or ovarian carcinoma. This HR deficiency is often based on mutations in BRCA1 or BRCA2 but can also result from mutations in other essential HR factors, which is then termed BRCAness (Moynahan *et al.*, 1999; Murai and Pommier, 2023). These mutations make the tumor cells highly sensitive to PARP inhibitors (Bryant *et al.*, 2005; McCabe *et al.*, 2006). PARPs are involved in the recognition and repair initiation of DNA single-strand breaks. Inhibition of PARP prevents its dissociation from the DNA after signal transduction. PARP-DNA adducts then result in DNA double-strand breaks, which, in cells with HR deficiency, must be repaired via the more error-prone NHEJ. As a result, the tumor cells accumulate mutations and undergo cell death if there is too much damage. The interplay between BRCAness and PARP inhibition perfectly exemplifies the principle of synthetic lethality. This term describes the connection of two genes, whereby the deficiency in the expression of either gene alone is tolerated by cells, but simultaneous perturbation of both genes gives rise to cell death (Helleday, 2011).

1.3.2 Cell death mechanisms

There are numerous different cell death mechanisms which can be activated in cells in response to different triggers, with the best-known and most relevant being apoptosis and necrosis. In response to extensive and/or irreparable DNA damage, the programmed cell death of apoptosis is usually initiated as a protective mechanism for the whole organism. Phenotypic characteristics of apoptosis are shrinkage of the affected cells, together with a process called membrane blebbing, where vesicular bulges are formed on the cell surface. In addition, nuclear condensation, endonuclease-dependent DNA fragmentation and sequestration of apoptotic bodies, which subsequently undergo phagocytosis, takes place. Since the cell membrane remains intact during the entire process, there is no inflammatory reaction (Elmore, 2007).

Caspases, which are cysteine-dependent proteases, play an important role in the course of apoptosis. These enzymes are normally present in cells as inactive pro-caspases and must first be activated by proteolytic cleavage. Caspases are divided into initiator- and effector-caspases. The first category includes caspases 2, 8, 9 and 10, while the second includes caspases 3, 6 and 7. Effector caspases have enzymatic activity and lead to cleavage of a variety of proteins but are dependent on activation by initiator caspases in order to do so (Cohen, 1997; Elmore, 2007). Effector caspases also activate

the Caspase-activated DNase (CAD), which then degrades the chromosomal DNA (Sakahira *et al.*, 1998; Roos *et al.*, 2016).
The initiation of apoptosis can occur via an extrinsic or intrinsic pathway. The extrinsic pathway is stimulated by the binding of extracellular ligands to "death receptors" such as TNF receptor 1 (tumor necrosis factor receptor 1) or the Fas receptor. The adaptor protein FADD (FAS-associated death domain protein) and pro-caspase 8 are then recruited, resulting in the formation of the DISC (death inducing signaling complex). Within this complex, caspase 8 is activated and serves as an initiator caspase, which in turn activates effector caspases (Kischkel *et al.*, 1995; Grimm *et al.*, 1996; Wajant, 2002). The intrinsic, mitochondria-mediated pathway is activated in response to internal cellular factors, for example DNA damage. Activation of the tumor suppressor protein p53 leads to an accumulation of pro-apoptotic protein members of the BCL2 family on the mitochondrial membrane. These include BAX (BCL2-associated protein), PUMA (BCL2-binding component 3) and NOXA (BCL2-homology 3; BH3) (Cory and Adams, 2002). This leads to a permeabilization of the mitochondrial membrane and to an efflux of death-promoting factors, including cytochrome c, from the intermembrane compartment of the mitochondria (Saelens *et al.*, 2004). In the cytosol, cytochrome c interacts with the adapter protein APAF 1 (apoptotic protease-activating factor-1) and pro-caspase 9 to form the apoptosome. This complex formation activates caspase 9 which in turn begins to activate the effector caspases (Zou *et al.*, 1999; Hill *et al.*, 2004).

In contrast to apoptosis, necrosis is not actively executed by cells. It happens when the cells are too severely damaged for controlled apoptosis. Necrosis involves an influx of sodium and calcium ions, which disrupts ion homeostasis, leading to water entering the cell to compensate for this imbalance. This causes the cell to swell, its membrane is lysed and the cell contents are released into the extracellular compartment (D'Arcy, 2019). The cytoplasmic components released during this process attract phagocytes and an inflammatory reaction occurs (Rock and Kono, 2008).

1.4 Aims of the project

Although cisplatin plays a pivotal role as chemotherapeutic drug for the therapy of various types of cancer for decades, acquired drug resistance of malignant cells is still a major clinical impediment. The main mode of action of cisplatin is forming crosslinks in the genomic DNA and thereby inducing replication stress. In consequence, the DNA damage response (DDR), a complex network regulating cell cycle arrest, DNA repair and cell death, gets activated. Alterations in these signaling pathways can contribute to the acquirement of cisplatin resistance. For this reason, we hypothesize that pharmacological modulation of the DDR or DNA repair mechanisms may be utilized to overcome acquired cisplatin resistance in malignant cells.

The objective of this thesis therefore is to evaluate the usefulness of novel combination treatments employing pre-selected DDR and DNA repair inhibitors to overcome acquired cisplatin resistance. The optimal outcome would thereby be to identify a compound combination, that shows antitumorigenic efficacy in a variety of cisplatin-resistant malignant cell lines originating from different tissue types. At the same time, the selected treatment regimen ideally should not demonstrate any adverse effects on non-malignant cells. Additionally, this work aims to identify superior candidate mechanisms contributing to acquired tumor cell resistance to cisplatin.

To address this research question, cisplatin-resistant cell variants of different tumor entities, especially bladder carcinoma cells J82, are used as *in vitro* models. For the identification of potential mechanisms contributing to acquired cisplatin resistance in J82 cells, a cytotoxicity screening with conventional anticancer therapeutics and pharmacological DDR/DNA repair inhibitors, as well as comparative mRNA and protein expression analyses under basal conditions and after CisPt treatment are conducted in parental $J82^{WT}$ cells and CisPt resistant $J82^{CisPt}$ cells. Various combination treatments of cisplatin with a selected DDR inhibitor or two DDR inhibitors together are then examined concerning their potential to induce additive or synergistic cytotoxicity in $J82^{CisPt}$ and cisplatin resistant cell lines originating from other tumor entities. The mode of action of a selected combination treatment, that evokes cytotoxicity in synergistic manner, is then examined in more detail. To this end, the emphasis lays on investigations of the cell cycle, proliferation, DNA damage and DDR activation.

To address the important issue of potential adverse effects on normal tissue cells, the influence of the most promising combination treatment on the viability of non-malignant human cells is being investigated. Moreover, a xenograft model in mice is employed to assess the anticancer efficacy, as well as adverse effects of the selected compounds as combination and mono treatments *in vivo*.

Overall, this study aims to contribute to a deeper understanding of the potential mechanisms underlying acquired anticancer therapy resistance and provide the experimental basis for the development of new therapeutic strategies to overcome acquired cisplatin resistance by using non-genotoxic inhibitors of the DDR and DNA repair.

2 Material and Methods

2.1 Material

2.1.1 Manufacturer's references

Table 2: List of manufacturer headquarters

Manufacturer	Headquarter
Abcam	Cambridge, United Kingdom
Active Motif	Carlsbad, CA, USA
APExBIO Technology	Houston, TX, USA
Applied Biosystems	Waltham, MA, USA
baseclick GmbH	Neuried, Germany
Bayer AG	Leverkusen, Germany
B. Braun Melsungen AG	Melsungen, Germany
Becton Dickinson GmbH	Heidelberg, Germany
Bemis Company Inc.	Neenah, WI, USA
Bethyl Laboratories Inc.	Montgomery, TX, USA
Binder GmbH	Tuttlingen, Germany
Bioline	London, United Kingdom
Bio-Rad	Hercules, CA, USA
Biozym Scientific GmbH	Hessisch Oldendorf, Germany
Brand GmbH & Co. KG	Wertheim, Germany
Calbiochem	Darmstadt, Germany
Carl Roth GmbH & Co. KG	Karlsruhe, Germany
Carl Zeiss Microscopy GmbH	Oberkochen, Germany
Cell Signaling Technology	Danvers, MA, USA
ComboSyn, Inc.	Paramus, NJ, USA
Corning, Inc.	Corning, NY, USA
Cytiva	Marlborough, MA, USA
Engelbrecht Medizin- & Labortechnik GmbH	Edermünde, Germany
Eurofins Genomics	Luxembourg, Luxembourg
Eppendorf AG	Hamburg, Germany
Exelitas Technologies Corp.	Waltham, MA, USA
Fluka BioChemika	Charlotte, NC, USA
Fresenius Kabi Deutschland GmbH	Bad Homburg, Germany
German Collection of Microorganisms and Cell Culture (DSMZ)	Braunschweig, Germany
GraphPad Software	Boston, MA, USA

Manufacturer	Headquarter
Hanna Instruments	Woonsocket, RI, USA
Ingenieurbüro CAT, M. Zipperer GmbH	Ballrechten-Dottingen, Germany
Invitrogen	Waltham, MA, USA
Kartell S.p.A.	Noviglio, Italy
Leica Biosystems Nussloch GmbH	Wetzlar, Germany
Memmert GmbH & Co. KG	Schwabach, Germany
Merck KGaA	Darmstadt, Germany
Mettler Toledo International Inc.	Columbus, OH, USA
Millipore	Billerica, MA, USA
Morphisto GmbH	Offenbach am Main, Germany
National Institutes of Health	Bethesda, MD, USA
Nordwest Handel AG	Dortmund, Germany
Olympus	Shinjuku, Japan
PAA Laboratories	Cölbe, Germany
Paul Marienfeld GmbH & Co. KG	Lauda-Königshofen, Germany
Qiagen GmbH	Hilden, Germany
Roche	Basel, Suisse
Rockland Immunochemicals, Inc.	Limerick, PA, USA
Santa Cruz	Santa Cruz, CA, USA
Sarstedt AG & Co. KG	Nümbrecht, Germany
Scil animal care company GmbH	Gurnee, IL, USA
Serva Elecrophoresis GmbH	Heidelberg, Germany
Sigma-Aldrich	Steinheim, Germany
Starlab International GmbH	Hamburg, Germany
StemCell Technologies	Vancouver, BC, Canada
Stuart scientific	Nottingham, UK
Tecan Group Ltd.	Männedorf, Suisse
Thermo Fisher Scientific Inc.	Waltham, MA, USA
TPP Techno Plastic Products AG	Trasadingen, Suisse
TriTek Corp.	Sumerduck, VA, USA
Vector Laboratories	Burlingame, CA, USA
VWR International	Radnor, PA, USA
WiCell Stem Cell Bank	Madison, WI, USA
Zoetis	Parsippany, NJ, USA

2.1.2 Consumables

Table 3: List of consumables used

Name	Manufacturer
6 well plates	Sarstedt AG & Co. KG
12 well plates	Sarstedt AG & Co. KG
96 well plates	Greiner Bio-One International AG
Cannulas Sterican® 26 G x 12 mm	B. Braun Melsungen AG
Cell culture dishes ∅ 3.5 cm	Greiner Bio-One International AG
Cell culture dishes ∅ 6 cm	Greiner Bio-One International AG
Cell spatula	TPP Techno Plastic Products AG
Cover glasses ∅ 18 mm	VWR International
Cryo containers (Cryo.s™)	Greiner Bio-One International AG
Filter tips 1000 µl for use with the QIAcube®	Qiagen GmbH
Glass pasteur pipettes	Brand GmbH & Co. KG
Microscope slides	Engelbrecht Medizin- & Labortechnik GmbH
Microvette® 100 EDTA K3E	Sarstedt AG & Co. KG
Multi dispenser pipette tips (Combitips® advanced) 5 ml	Eppendorf AG
Nitrocellulose blotting membrane (Amersham™ Protran™ 0.2 µm)	Cytiva
Parafilm	Bemis Company Inc.
Pipette tips 10 µl	Biozym Scientific GmbH
Pipette tips 200 µl	Starlab International GmbH
Pipette tips 1000 µl	Starlab International GmbH
Pipette tips 2500 µl	Eppendorf AG
Safe-lock tubes 0.5 ml	Eppendorf AG
Safe-lock tubes 1.5 ml	Sarstedt AG & Co. KG
Safe-lock tubes 2 ml	Eppendorf AG
Sterile syringe filters 0.2 µm	VWR International
Syringes Injekt®-F Luer Solo 1 ml	B. Braun Melsungen AG
T25 Cell culture flasks	Greiner Bio-One International AG
T75 cell culture flasks	Greiner Bio-One International AG
Tissue embedding cassettes	Kartell S.p.A.
Tubes 15 ml	Greiner Bio-One International AG
Tubes 50 ml	Greiner Bio-One International AG
Whatman chromatography paper	Cytiva

2.1.3 Chemicals

Table 4: List of chemicals used

Chemical	Supplier
Acetic acid	Carl Roth GmbH & Co. KG
Agarose	Carl Roth GmbH & Co. KG
Agarose low gelling temperature	Sigma-Aldrich
Ammonium peroxodisulfate (APS)	Merck
Ammoniumacetate	Merck
Bovine Serum Albumin (BSA)	Carl Roth GmbH & Co. KG
$CaCl_2$*$2H_2O$	Merck
Chlorodeoxyuridine (CldU)	Sigma-Aldrich
Corn oil	Sigma-Aldrich
Dimethyl sulphoxide (DMSO)	Carl Roth GmbH & Co. KG
Dimethylformamide	Sigma-Aldrich
Erylysis buffer	Morphisto
Ethanol	VWR International
Ethylenediamine tetraacetic acid (EDTA)	Carl Roth GmbH & Co. KG
Fluoroshield	Sigma-Aldrich
Formaldehyde (37%)	Carl Roth GmbH & Co. KG
Goat serum	Sigma-Aldrich
H_2O_2 (30%)	Sigma-Aldrich
HCl	Carl Roth GmbH & Co. KG
HEPES	Carl Roth GmbH & Co. KG
IMMOIL-F30CC Immersion oil	Olympus
Iododeoxyuridine (IdU)	Sigma-Aldrich
Isotonic NaCl solution	Fresenius Kabi Deutschland GmbH
Ketamin	Zoetis
KH_2PO4	Millipore
Lipofectamine® RNAiMAX	Invitrogen
Methanol	VWR International
Methylene blue	Sigma-Aldrich
$MgCl_2$*$6H_2O$	Merck
Milk powder	Carl Roth GmbH & Co. KG
Na_2HPO_4*$2H_2O$	Millipore
NaCl	VWR International
NaOH pellets	Millipore
Nonidet P40 (NP-40)	Fluka BioChemika

Chemical	Supplier
PageRuler™ Plus Prestained Protein Ladder	Thermo Fisher Scientific Inc.
Phenylmethylsulfonylfluoride (PMSF)	Sigma-Aldrich
Ponceau S	Carl Roth GmbH & Co. KG
Prolong Gold DAPI	Invitrogen
Propidium iodide	Sigma-Aldrich
Protease inhibitor cocktail	Millipore
Resazurin	Sigma-Aldrich
Roti®-Load 1	Carl Roth GmbH & Co. KG
Roti®Histofix 4.5%	Carl Roth GmbH & Co. KG
Rotiphorese® Gel 30	Carl Roth GmbH & Co. KG
siRNA set GeneSolution Hs_RAD51_7	Qiagen GmbH
Sodium acide	Fluka BioChemika
Sodium citrate	Merck
Sodium desoxycholate	Sigma-Aldrich
Sodium dodecyl sulfate (SDS)	Carl Roth GmbH & Co. KG
Sodium fluoride	Merck
Sodium laurylsarcosinate	Sigma-Aldrich
Sodium orthovanadate	Sigma-Aldrich
TEMED	Carl Roth GmbH & Co. KG
Tert-butyl hydroperoxide (tBOOH)	Sigma-Aldrich
Tris Base	Sigma-Aldrich
Tris HCl	Carl Roth GmbH & Co. KG
Triton X-100	Sigma-Aldrich
Tween 20	Sigma-Aldrich
Vectashield DAPI	Vector Laboratories
Xylazin (Rompun 2%)	Bayer AG

2.1.4 Cytostatics & modulators of DNA damage response / DNA repair

Table 5: List of cytostatics used

Name	Supplier
5-fluorouracil	Medac
Carboplatin	TEVA
Cisplatin	TEVA
Doxorubicin	Cellpharm
Hydroxyurea	Sigma-Aldrich
Oxaliplatin	Accord Healthcare

Table 6: List of pharmacological DNA damage response & DNA repair modulators used

Name	Substance group	Supplier
AZD7762	Pan CHK inhibitor	Sigma-Aldrich
B02	RAD51 inhibitor	Tocris Bioscience
Entinostat	HDAC inhibitor	Selleckchem
LY2603618	CHK1 inhibitor	APExBIO Technology
Mirin	MRE11 inhibitor	Abcam
Niraparib	PARP inhibitor	MedChemExpress
Olaparib	PARP inhibitor	APExBIO Technology
PF477736	CHK1 inhibitor	Sigma-Aldrich
RI-1	RAD51 inhibitor	Calbiochem
RI(dl)2	RAD51 inhibitor	Tocris Bioscience
RS-1	RAD51 stimulator	Selleckchem
SB218078	CHK1 inhibitor	Tocris Bioscience
Vorinostat	HDAC inhibitor	Sigma-Aldrich

2.1.5 Kits

Table 7: List of commercially available assay kits used

Name	Manufacturer
BM Chemiluminescence Blotting Substrate (POD)	Roche
Click-iT™ RNA Alexa Fluor 488™ Imaging	Invitrogen
DC™ Protein assay	Bio-Rad
DNeasy Blood & Tissue	Qiagen GmbH
EdU Click-488 Cell Proliferation assay	baseclick GmbH
High-Capacity cDNA Reverse Transcription	Applied Biosystems
RNase-free DNase Set	Qiagen GmbH
RNeasy® Mini	Qiagen GmbH
SensiMix SYBR® Hi-ROX	Bioline

2.1.6 Media and media supplements

Table 8: List of media used

Name	Manufacturer
Dulbecco's Modified Eagle's Medium (DMEM) – high glucose	Sigma-Aldrich
DMEM without phenol red	Sigma-Aldrich
mTeSR™1	StemCell Technologies
RPMI-1640	Sigma-Aldrich

Table 9: List of media supplements used

Name	Manufacturer
Fetal calf serum (FCS)	PAA Laboratories
Glutamine	Sigma-Aldrich
Human embryonic stem cell qualified matrigel	Corning, Inc.
Penicillin/Streptomycin	Sigma-Aldrich
Y-27632 dihydrochloride (ROCK inhibitor)	Sigma-Aldrich

2.1.7 Experimental organisms

2.1.7.1 Cell lines

Table 10: List of cell lines used

Name	Description	Supplier
A2780	Human ovarian carcinoma cell line	Sigma-Aldrich
$A2780^{CisPt}$	Cisplatin-resistant human ovarian carcinoma cell line	Sigma-Aldrich
A549	Human lung carcinoma cell line	DSMZ
Foreskin-4 (F-4)	human induced pluripotent stem cells (hIPSCs)	WiCell Stem Cell Bank
J82	Human bladder carcinoma cell line	DSMZ
MDA-MB231	Human breast carcinoma cell line	DSMZ
NHDF	Normal Human Dermal Fibroblasts	PromoCell
SH-SY5Y	Human neuroblastoma cell line	DSMZ

The used cisplatin resistant cell variants $J82^{CisPt}$, $A549^{CisPt}$ and $SH\text{-}SY5Y^{CisPt}$ were previously by others or personally isolated from their respective parental cell line as described in chapter 2.2.1.3.

2.1.7.2 Mouse strain

For the xenograft experiment in mice (see chapter 2.2.10), animals of strain number 9270 obtained from the "Zentrale Einrichtung für Tierforschung und wissenschaftliche Tierschutzaufgaben" (ZETT) Düsseldorf (corresponds to Jackson Laboratory Strain #023848) were used. The official name of these animals is NOD.Cg-Prkdc^{scid} H2-K1$^{b\text{-}tm1Bpe}$ H2-D1$^{b\text{-}tm1Bpe}$ Il2rg^{tm1Wjl}/SzJ and their common name is NSG-(K^{b}D^{b})^{null}.

NOD scid gamma (NSG) mice are non-obese diabetic animals (NOD/ShiLtJ) harboring a spontaneous severe combined immunodeficiency mutation (Prkdc^{scid}) and a complete null allele of the Interleukin 2 (IL-2) receptor common gamma chain Il2rg^{tm1Wjl} mutation. The scid mutation in the DNA repair complex protein Prkdc renders the mice B- and T-cell deficient and the *IL2rg*^{tm1Wjl} mutation prevents cytokine signaling through multiple receptors, leading to a lack in functional NK cells. NSG-(K^{b}D^{b})^{null} mice are NSG animals additionally genetically modified with the H2-K1$^{b\text{-}tm1Bpe}$ knockout allele (K^{b} null) and H2-D1$^{b\text{-}tm1Bpe}$ knockout allele (D^{b} null) replacing their endogenous major histocompatibility complex (MHC) class I K^{d} and D^{d} loci. As a consequence, these mice lack murine MHC class I and exhibit reduced xenogeneic graft-versus-host disease response. In summary, all these mutations contribute to the fact that the mice are highly immunodeficient and are therefore well suited for engrafting human material without provoking an immune response.

2.1.8 Enzymes

Table 11: List of enzymes used

Name	Supplier
DNase-free RNase	Qiagen GmbH
RNase A	Serva Elecrophoresis GmbH
Trypsin/EDTA solution (10 x)	Sigma-Aldrich

2.1.9 Primers

Table 12: List of human primers used for quantitative real-time PCR

Target	Primer sequence	
	forward	**reverse**
ACTB	TGGCATCCACGAAACTACC	GTGTTGGCGTACAGGTCTT
AKAP1	TAGTCGGTCGGCTAATTG	ATGTTGAGAGCCTTCTATGT
AKT1	ATTGTGAAGGAGGGTTGG	TGAAGGTGCCATCATTCT
ATG3	AGGACAATATAAGGCTTCAA	TTCCAACAATCCACTCTC
ATG7	GAACCTCAGTGAATGTATG	AACCTTGTCCAAGTCTAA
ATP7A	AGGCAGAAGTAAGGTATAATCC	CTCACAACAAGTTCCAAAAC
ATP7B	AAAGAGCAAAACCTCAGAAG	CCCTGATGATTAAATTGTCCTC
BAX	TTTGCTTCAGGGTTTCATC	CTCAGCTTCTTGGTGGAC
BBC3	CTCATCATGGGACTCCTG	GCTACATGGTGCAGAGAA
BCL2	CGACTCCTGATTCATTGG	TCTACTTCCTCTGTGATGT
BCRP (ABCG2)	AAAGCCACAGAGATCATAGAG	GATCTTCTTCTTCTTCTCACC
BECN1	GGATGGAAGGGTCTAAGA	CTGTGGTAAGTAATGGAG
BRCA1 (FANCS)	AAGACTTCTACAGAGTGAA	CAGTTCCAAGGTTAGAGA
BRCA2 (FANCD1)	AACAACAATTACGAACCAA	AACATTCCTTCCTAAGTCTA
BRIP1	GAAACTACACAGCAGATTAGAA	ACAACAGCACCTAGAACA
CASP2	GAGAGAAAGAACTGGAATT	TCTGGTCACATAGAACAT
CDC25a	GTGAAGAACAACAGTAATC	TGAGGTAGGGAATGTATT
CDC25C	ATGACAATGGAAACTTGGTG	CATCTGAAATCTCTTCTGCC
CDKN1A (p21)	TACATCTTCTGCCTTAGT	TCTTAGGAACCTCTCATT
CDKN2A (p16)	AGGTCCCTCAGACATCC	AATGAAAACTACGAAAGCGG
CHK1	CCACCTCTTCATAACAACAA	TAAATCACAATCGCCACTC
CHK2	GCACTGTCACTAAGCAGAAAT	AGGCACCACTTCCAAGAG
CTR1 (SLC31A1)	TGATGCCTATGACCTTCTAC	GAATGCTGACTTGTGACTTAC
CTR2 (SLC31A2)	CTGTACTGTATGAAGGCATC	AAAGTGACACAAATACCACC
DDB2 (XPE)	TTTAACCCTCTCAATACCA	CTACTAGCAGACACATCC
DDIT3	ACTGAGCGTATCATGTTAA	CAGGTGTGGTGATGTATG
ERCC1	AGGAAGAAATTTGTGATAC	TGTGTAGATCGGAATAAG
EXO1	GAAAAGACCAAGAAGTGCAGAGC	CCAGGTCAGGCACAAACACT
FANCD2	CTCAGTGACCTACTGATAGAG	TAGGAAGTTTGGGTCAAGTC
FASR	TTATCTGATGTTGACTTGAGTAA	GGCTTCATTGACACCATT
GADD45A	ATCCACATTCATCTCAAT	GTAACTACAAAGGTATTTCA

Target	Primer sequence	
	forward	reverse
GAPDH	CATGAGAAGTATGACAACAG	ATGAGTCCTTCCACGATA
GPX1	GCCAAGAACGAAGAGATT	TCGAAGAGCATGAAGTTG
GPX4	AATTCGATATGTTCAGCAAGAT	GTCCTTCTCTATCACCAGG
GSTM1	ACTATCCTTCGTGAACATC	AGACACAACCACTAACAG
HMGB1	CTAGAGCCCATCTTCGAGGC	TAGTCAGAACGGGTCGTGGA
HMOX1	CAACAAAGTGCAAGATTC	AGAAAGCTGAGTGTAAGG
HSPA1B	GGACTTTGACAACAGGCT	GCTTGTTCTGGCTGATGT
IGBP1	CAGAGGAATTCAGAAAAGCAG	TGGAGTGTTTGTTCATCATC
IL-6	CCAATCTGGATTCAATGA	GTTCCTCACTACTCTCAA
IL-8	TGCGCCAACACAGAAATTATTGTAA	TGAATTCTCAGCCCTCTTCAAAAAC
LAMP1	TTTGGAAGAGGACATACACT	CACAGTCTTGATTTCTTTGGA
LCMT-1	GATGGACACATACTGGATTC	CTTTAGCTTCTCTTCCAGTTC
LMNB1	GACCAGCTGCTCCTCAACTATG	GACCAGCTGCTCCTCAACTATG
MATE1 (SLC47A1)	GAGACATCATTAATCTGGTGG	CAACCTTCTGATTTCCACTC
MDR1 (ABCB1)	AGTCGGAGTATCTTCTTC	TTGAATAGCGAAACATTGA
MFN2	GGAGTATTTTGTCCGCCTGC	GCAGAATCCCAATCTTCATCCAG
MRE11	GCCTGTCCAGTTTGAAAT	GGTTGCCATCTTGATAGTT
MRP1 (ABCC1)	AGCAGAAAAATGTGTTAGGG	TACCCACTGGTAATACTTGG
MSH2	CTTCTTCTGGTTCGTCAGTATAGA	ATCATTCTCCTTGGATGCCTTAT
NBS1	CAGGATTAAAGACAACAACTCC	GTATCTGCTTGCTCTGATTC
OCT2 (SLC22A2)	GAAGCCGAAAATATGCAAAG	TGCAGGGATTTCTACTTTTG
PALB2 (FANCN)	ATAAACATTCCGTCGAACAG	ACTCTGAAACCAATTGTAGG
PGc1a	TGAACGGTACTTTTCTGCCCC	ATGCTGCTTGCACAAACTGG
PINK1	CAGGAGATCCAGGCAATT	ATGGTGGCTTCATACACA
POLB	AAGTTCATGGGTGTTTGC	ATGGTGTACTCATTGATTGTG
POLD1	TCTGGGATGATGATGATGC	GTGTTCTGCCTCCATCTC
POLE	TTTGGCATTTGACATTGAG	AATCATCATAATCTGGTCTGT
POLI	AACAGAAATGGTTGAGAAGAG	CAAGCAGGTTTATAGACTGATTA
PPP2CA	ATGGAGGGATATAACTGGTG	CTTGGTTACCACAACGATAAC
PPP2R4	TAGTCGCTCTTCTCAACA	TTCTGCTTCCTCATCAAG
PRKN	TTGTCAGGTTCAACTCCA	CACAGTCCAGTCATTCCT
RAD50	CTGAACGTGAGTTAAGCAAG	GTATGATGGTTTAACTGCTCC

Target	Primer sequence	
	forward	reverse
RAD51	AATTAGTTCCAATGGGTTT	TGAAGTAGTTTGTCAAGC
RAD51B	CTTGATTCAGAGAGAAGACAG	GATGGTGTAGACAAATGAGG
RAD51C	AGGTTCGACTAGTGATAGTG	TAATAACCGAGTACGAAGAGAC
RAD51D	CTCAGGTATGTCTCTGTATGG	ATCTGGAAGATGTCAAATGC
RAD52	GCTGAAGGATGGTTCATATC	CTTTGTCCAGAATACAGTTTCC
RALBP1	AAAAGACAGGAGTGTGAAAC	GTTCAGTCAGGATCTCATTC
REV1	AACACATATTATTGCCACAA	GAATGTAGGAGAGGAGTC
SIRT4	TGTGCTTGGATTGTGGGGAA	GGACTTGGAAACGCTCTTGC
SLC8A3	TGAGAGTATTGGTGTTATGGA	TGTGAATTGTTTTGACAGTTTC
SOD1	TCTGTTTCAATGACCTGTATT	GCCTCATAATAAGTGCCATA
SOD2	CAAGCCTGGTACATACTGA	CTTTGATGGTTGACAGATTCT
TOP2A	ACGGTGTTGGATATTCTAAG	AAGCGAGCCTGATTATTC
TOP2B	ATAACATTCCAACCAGAT	GGCAATTTCTTTCCATTA
TOPBP1	GCTCCAACGAGTTCAGAA	CCTTTATCTTCAATGCCTCTTC
TP53	AGCACTAAGCGAGCACTG	ACGGATCTGAAGGGTGAAA
TP73	CACTTTGAGGTCACTTTC	ATCTGGCAGTAGAGTTTC
ULK1	CACAGCAAAGGCATCATC	CGAAGTCAGCGATCTTGA
XRCC2	ATGTGTAGTGCCTTCCATAG	TCAAGAATATCACCATGCAC
XRCC3	CATTGTTCTGTCTTTCCT	CTCCTTTACCGATTTCAG

Table 13: List of murine primers used for quantitative real-time PCR

Target	Primer sequence	
	forward	reverse
Actb	GCATTGCTGACAGGATGCAG	CCTGCTTGCTGATCCACATC
Akap1	CCACATAGAAGGCTCTCA	TGACTTCCACAGTGATACC
Akt1	AGAAGAGACTCTGAGCATCA	AAGGTGCCATCGTTCTTG
Atg3	ACCACCTCCTATGTGTTCA	TGTGTAGTCATATTCTATTGTTGGA
Atg7	GCACAACACCAACACACT	CGAAGGTCAGGAGCAGAA
Bax	CTGGACACTGGACTTCCT	GCCACAAAGATGGTCACT
Bbc3	TTTTCTGCACCATGTAGC	CAGTCACCATGAGTCCTT
Bcl2	GTGTGGTTGCCTTATGTAT	GTATATCCGCTACAAGTTACA
Bcrp	GAATCACACCATCCAACAG	GATTTATGCCTTTCAACATCAG
Becn1	GATGGGAACTCTGGAGGT	GGCTGTGGTAAGTAATGGA
Calcr	ACCAATCTCACTGACTCC	GTACAGACCTTCTCCTTCATA

Target	Primer sequence	
	forward	**reverse**
Casp2	TACTGCTCACAACCCTCTC	GGACCATCACCATTATCTAAGG
Fasr	AGAACCTCCAGTCGTGAA	ATCTATCTTGCCCTCCTTGA
Gapdh	TCTCCTGCGACTTCAACA	TCTCTTGCTCAGTGTCCTT
Gpx1	TTGGTGATTACTGGCTGC	TGATATTCAGCACTTTATTCTTAGTAG
Gpx4	CTGGGAAATGCCATCAAAT	GTCCTTCTCTATCACCTGG
Gstm1	ACACAGCCTTCATTCTCC	AATTCTAGGAAGCGTGAGTT
Hmox1	CCAGAGTCCCTCACAGAT	CCCAAGAGAAGAGAGCCA
Hspa1b	AGACGCTGACAGCTACTC	CTCGCTTCTGGAAGGCT
Lamp1	CAGAGCGTTCAACATCAG	CTGGCATTCATCCCAAAC
Mdr1	TGGAACTTGAAGAGGACC	GCATAACGAAACATTGTAAGC
Oct2	TCGTCACTGAGTTTAACCT	AGAGATAGCATTGATGAGGAT
Pgc1a	CCGAGAATTCATGGAGCAAT	TTTCTGTGGGTTTGGTGTGA
Pink1	TGTGTATGAAGCCACCAT	AACCTGCCGAGATATTCC
Prkn	CCATGATAGTGTTTGTCAGG	TTGTTCCAGGTCACAGTT
Slc8a3	CTATGAGTTCAAGAGTACAGTG	CTCTCCTCTCCAGATTCG
Sod1	ACCAGTTGTGTTGTCAGG	TTTCTTAGAGTGAGGATTAAAATGAG
Sod2	GAATGTAATCAACTGGGAGAAT	CATAGAATTATCAGGTATGTGGAA
Top2a	CTTCAGGAGCCGTCACCAT	GAGCAGTATATGTTCCAGTTGT
Top2b	TGGGTGAACAATGCTACAAA	TGTATGTATCAGGACGAAGGA
Topbp1	GCTGTCGGATATATCTTTGTG	CTCCCACAATTACATGAGTTAC
Ulk1	AAATCAAAATCCTGAAGGAACTA	AGGTCTCCACCATTACAAT

All primers were synthesized by Eurofins Genomics and diluted to 3 µM before use. Newly designed primers were tested concerning their specificity and accuracy before their first use. For this purpose, a RT-qPCR run with cDNA dilutions (1:2, 1:4, 1:8 and 1:16) was performed. In the case of high specificity, the melting curves should only show one peak. In the case of high accuracy, the Cq-values of the different cDNAs should reflect the dilution factor of two.

2.1.10 Antibodies

2.1.10.1 Primary antibodies

Table 14: List of primary antibodies used

Target	Species	Supplier	Dilution
BrdU	Mouse	BD	1:70
BrdU	Rat	Abcam	1:140
Caspase 7	Rabbit	Cell signaling	1:1000
CHK1	Mouse	Cell signaling	1:1000
Cisplatin modified DNA	Rat	Abcam	1:5000
Cleaved caspase 7	Rabbit	Cell signaling	1:1000
LC3-B	Rabbit	Cell signaling	1:1000
PARP	Rabbit	Cell signaling	1:1000
Pericentrin	Rabbit	Abcam	1:1000
Phospho CHK1 (Ser345)	Rabbit	Cell signaling	1:500
Phospho histone H3 (Ser10)	Rabbit	Thermo Fisher	1:30 – 1:500
Phospho KAP1 (Ser824)	Rabbit	Bethyl Laboratories	1:5000
Phospho p53 (Ser15)	Rabbit	Cell signaling	1:1000
Phospho RPA32 (Ser33)	Rabbit	Abcam	1:5000
Phospho RPA32 (Ser4/8)	Rabbit	Bethyl Laboratories	1:2000
PrimPol	Rabbit	Proteintech	1:1000
RAD51	Rabbit	Abcam	1:500
RPA32	Mouse	Millipore	1:500
α-Tubulin	Rat	Santa Cruz	1:500
β-Actin	Mouse	Santa Cruz	1:50000
γH2AX (Ser139)	Mouse	Millipore	1:100 – 1:1000

2.1.10.2 Secondary antibodies

Table 15: List of Horseradish peroxidase (HRP)-coupled secondary antibodies used

Name	Supplier	Dilution
Goat anti mouse IgG HRP	Rockland Immunochemicals	1:2000
Goat anti rabbit IgG HRP	Rockland Immunochemicals	1:2000
Goat anti rat IgG HRP	Rockland Immunochemicals	1:2000

Table 16: List of fluorescence-coupled secondary antibodies used

Name	Supplier	Dilution
Alexa Fluor® 488 Goat anti mouse	Invitrogen	1:200 – 1:500
Alexa Fluor® 488 Goat anti rabbit	Invitrogen	1:200 - 1:500
Alexa Fluor® 488 Goat anti rat	Invitrogen	1:400 – 1:1000
Alexa Fluor® 555 Goat anti mouse	Invitrogen	1:250 – 1:500
Alexa Fluor® 555 Goat anti rabbit	Invitrogen	1:1000

2.1.11 Solutions and buffers

Table 17: List of solutions and buffers used

Name	Composition
Blotting buffer	25 mM Tris Base 192 mM Glycin 20% (v/v) Ethanol
Collecting gel (5%)	1 ml 1.5 M Tris Base (pH 6.8) 1.3 ml Acrylamide (30%) (Rotiphorese® Gel 30) 5.4 ml dH_2O 80 µl TEMED (10%) 160 µl SDS (10%) 80 µl APS (100 g/l)
DNase-free RNase	1 mg/ml RNase A 10 mM Tris HCl (pH 7.4)
Electrophoresis buffer (pH > 13)	300 mM NaOH 1 mM Na_2EDTA
Hypotonic PI solution	50 µg/ml Propidium iodide 0.1% Sodium citrate 0.1% Triton X-100
Lysis buffer for DNA Fiber Spreading assay	0.5% (w/v) SDS 200 mM Tris HCl (pH 7.4) 50 mM EDTA (pH 8)

Name	Composition
Lysis buffer (pH 10) for alkaline Comet assay	2.5 M NaCl 100 mM EDTA 10 mM Tris Base 1% Sodium laurylsarcosinate Directly before use: 89 ml Lysis buffer + 10 ml DMSO + 1 ml Triton X-100
Methylene blue	0.5 M Sodium acetate 0.4 g/l Methylene blue
NaCl/P_i buffer	1.06 mM KH_2PO_4 154 mM NaCl 3.77 mM Na_2HPO_4
Neutral red extraction solution	50% Ethanol 1% Acetic acid
Neutral red fixation solution	1% Formaldehyde 1% $CaCl_2$
Neutral red incubation solution	0.01% Neutral red 0.1 M HEPES In cell culture medium
Neutral red stock solution	0.1% Neutral red 2 drops of glacial acetic acid
Neutralisation buffer (pH 7.5)	400 mM Tris Base
PBS (pH 7.4)	137 mM NaCl 2.7 mM KCl 10 mM $Na_2HPO_4*2H_2O$ 1.76 mM KH_2PO_4
$PBS^{+Ca/+Mg}$	0.1 mg/ml $MgCl_2*6H_2O$ 0.13 mg/ml $CaCl_2*2H_2O$ In PBS

Name	Composition
PBS high salt (pH 7.4)	400 mM NaCl 2.7 mM KCl 10 mM Na_2HPO_4*$2H_2O$ 1.76 mM KH_2PO_4
PBS-Triton X-100	PBS + 0.3% (v/v) Triton X-100
PBS-Tween 20	PBS + 0.05% (v/v) Tween 20
PI solution	50 µg/ml Propidium iodide in PBS
Ponceau-S solution	1.5 g/l Ponceau-S 5 ml/l Acetic acid
Resazurin-NaCl/P_i solution	1 ml Resazurin stock solution 999 ml NaCl/P_i buffer
Resazurin stock solution	440 mM Na-Resazurin In Dimethylformamide
RIPA buffer	50 mM Tris HCl (pH 8) 150 mM NaCl 2 mM EDTA (pH 8) 1% (v/v) NP-40 0.1% (w/v) SDS 1% (v/v) Sodium deoxycholate 1 mM Sodium orthovanadate 1 mM PMSF 50 mM Sodium fluoride 1 x Protease inhibitor cocktail
SDS running buffer	1 g/l SDS 25 mM Tris Base 192 mM Glycin

Name	Composition
Separating gel (15%)	5 ml 1.5 M Tris Base (pH 8.8) 10 ml Acrylamide (30%) (Rotiphorese® Gel 30) 4.5 ml dH_2O 80 µl TEMED (10%) 200 µl SDS (10%) 200 µl APS (100 g/l)
SSC (10 x) (pH 7.0)	1.5 M NaCl 150 mM Sodium citrate
TBS	150 mM NaCl 50 mM Tris Base (pH 7.4)
TBST	TBS + 0.1% (v/v) Tween 20
TE buffer	10 mM Tris HCl 1 mM EDTA (pH 8)

2.1.12 Instruments

Table 18: List of devices and instruments used

Type of device / instrument	Model	Manufacturer
Absorbance microplate reader	Sunrise	Tecan Group Ltd.
Bench centrifuge	myFUGE™ Mini	Benchmark
Blotting system	Mini Trans-Blot® Cell	Bio-Rad
Caliper	Promat	Nordwest Handel AG
Cell freezing container	CoolCell®	Corning, Inc.
Centrifuge	Centrifuge 5702	Eppendorf AG
Centrifuge	Heraeus PICO 17	Thermo Fisher Scientific Inc.
Clipper	Aesculap® Exacta GT416	B. Braun Melsungen AG
CO_2 incubator	C 150	Binder GmbH
Cooling centrifuge	Heraeus Megafuge 16R	Thermo Fisher Scientific Inc.
Cooling centrifuge	Heraeus Fresco 17	Thermo Fisher Scientific Inc.

Type of device / instrument	Model	Manufacturer
Cooling plate	EG1150C	Leica Biosystems Nussloch GmbH
Counting chamber	Neubauer improved	Paul Marienfeld GmbH & Co. KG
Electrophoresis chamber	DNA Sub Cell™	Bio-Rad
Electrophoresis system	Mini-PROTEAN Tetra Cell	Bio-Rad
Flow cytometer	BD Accuri™ C6 Plus	Becton Dickinson GmbH
Flow cytometer	LSRFortessa™ Cell Analyzer	Becton Dickinson GmbH
Fluorescence lamp	HBO50	Carl Zeiss AG
Fluorescence lamp	x-Cite Series 120Q	Exelitas Technologies Corp.
Fluorescence microscope	BX43	Olympus
Fluorescence microscope	Axiolab	Carl Zeiss AG
Gel imaging system	ChemiDoc™ Touch	Bio-Rad
Glass bottles	-	Schott AG
Glass cuvettes	-	Sarstedt AG & Co. KG
Glass pipettes	-	Brand GmbH & Co. KG
Heating / drying oven	-	Memmert GmbH & Co. KG
Heating block	Thermomixer compact	Eppendorf SE
Hematology analyzer	scil Vet ABC™	Scil animal care company GmbH
Ice machine	SPR-80	NordCap®
Irradiation system	Gammacell® 1000 Elite	Best Theratronics Ltd.
Magnetic stirrer	HI 190M	Hanna Instruments
Manual Counter	-	Carl Roth GmbH & Co. KG
Multi-dispenser pipette	Multipette® M4	Eppendorf AG
Multimode microplate reader	Infinite F200	Tecan Group Ltd.
Paraffin dispensing station	EG1150H	Leica Biosystems Nussloch GmbH
pH meter	FiveEasy	Mettler Toledo International Inc.

Type of device / instrument	Model	Manufacturer
Pipette 10 µl	Research®	Eppendorf SE
Pipettes 100 µl; 1000 µl; 2500 µl	Reference®	Eppendorf SE
Pipettes 10 µl; 100 µl; 1000 µl	Pipetman classic	Gilson
Pipette controller	Easypet® 3	Eppendorf SE
Power supply	PowerPac™ Basic	Bio-Rad
Power supply	PowerPac™ HC	Bio-Rad
Precision scale	ABS	Kern & Sohn GmbH
Real-Time PCR system	CFX96™	Bio-Rad
Robotic workstation	QIAcube®	Qiagen GmbH
Rocking shaker	ST5	Ingenieurbüro CAT, M. Zipperer GmbH
Rotator	SB3	Stuart scientific
Scale	EMB 500-1BE	Kern & Sohn GmbH
Scale	PCB	Kern & Sohn GmbH
Sonicator	EpiShear™ Probe	Active Motif
Spectrophotometer	NanoVue™ Plus	GE Healthcare
Sterile workbench	Safe 2020	Thermo Fisher Scientific Inc.
Suction pump	Mini-Vac eco	Peqlab Biotechnologie GmbH
Thermocycler	Tpersonal	Biometra®
Transmitted light microscope	Axiovert 40 CFL	Carl Zeiss AG
Transmitted light microscope	CKX41	Olympus
Vortexer	Bio Vortex V1	Peqlab Biotechnologie GmbH
Water bath	WNB22	Memmert GmbH & Co. KG
Water purification system	Milli-Q® Advantage A10	Merck Millipore

2.1.13 Software

Table 19: List of software used

Name	Supplier
BD Accuri™ C6	Becton Dickinson GmbH
BD FACSDiva version 6.2	Becton Dickinson GmbH
CellSens Dimension	Olympus
CFX Manager 3.1	Bio-Rad
ChemDraw 22.2.0	Revvity Signals Software
CompuSyn version 1.0	ComboSyn, Inc.
FlowJo X 10.0.7r2	Becton Dickinson GmbH
GraphPad Prism 6.0c	GraphPad Software
Image Lab™ Touch version 2.3.0.07	Bio-Rad
ImageJ 2.9.0/1.53t	National Institutes of Health
TriTek Comet Score™ Freeware v1.5	TriTek Corp.
Zen 2012	Carl Zeiss Microscopy GmbH

2.2 Methods

2.2.1 Cell culture

J82^{WT} and thereof derived J82^{CisPt} cells (Höhn *et al.*, 2016) as well as SH-SY5Y^{WT}, SH-SY5Y^{CisPt}, A549^{WT}, A549^{CisPt}, MDA-MB231 and NHDF were grown in DMEM containing 10% FCS and 1% penicillin/streptomycin. A2780^{WT} and their corresponding cisplatin-resistant variant A2780^{CisPt} were grown in RPMI-1640 with 10% FCS, 1% penicillin/streptomycin and 1% glutamine. Foreskin-4 hIPSCs were grown in cell culture plates coated with human embryonic stem cell qualified Matrigel in mTeSR1 medium containing 10 mM Y-27632 dihydrochloride to prevent differentiation (Mboni-Johnston *et al.*, 2023). All mentioned cell lines were grown in CO_2 incubators with a temperature of 37 °C and CO_2 content of 5%.

The cells were passaged at a confluence of 80 – 90%. For this purpose, they were detached from the bottom of the cell culture flask by incubation with trypsin/EDTA at 37 °C, separated and seeded with fresh medium in the desired number in a new culture flask and/or for experiments in different well formats. If not stated otherwise, treatments of logarithmically growing cells were performed 24 h after seeding. To ensure that all experiments were performed with mycoplasma free cells, cells were regularly tested for contamination by PCR-based method.

2.2.1.1 Authentication of cell lines

The cell lines used were authenticated at Eurofins Genomics by means of short tandem repeat (STR) profiling and comparison of the obtained profiles with databases of human cell lines (DMSZ, Cellosaurus). Besides this, during the experiments, attention was paid to the cell lines characteristic morphology and cisplatin resistant cells were regularly tested to confirm their CisPt resistant phenotype.

2.2.1.2 Cryo conservation of cells

In order to store cells for a later date, they were cryopreserved. For this purpose, the cells were detached from a T75 cell culture flask, pelleted (1300 rpm, 3 min, RT) and resuspended in 3 ml cell culture medium. One ml of cell suspension was mixed with 1 ml of freezing medium, consisting of 80% FCS and 20% DMSO, in each cryovial. The cryovials were frozen at -80 °C for 48 hours with the aid of the CoolCell® cell freezing container, which ensures a constant freezing rate of -1 °C per minute. For permanent storage, the cryovials were then transferred to a tank containing liquid nitrogen.

If required, a cryovial was taken from the nitrogen tank, the cell solution was diluted with culture medium and centrifuged (800 rpm, 5 min, RT) directly after. The supernatant was discarded, the cell pellet was resuspended in fresh cell culture medium and cells were cultivated as described in chapter 2.2.1.

2.2.1.3 Selection of cisplatin resistant cell variants

To determine an appropriate concentration for selection of CisPt resistant cell variants, human tumor cell lines (A549 lung carcinoma cells, MDA-MB231 mamma carcinoma cells) were pulse-treated with cisplatin for 4 h and their viability was measured 72 h after. From the obtained values, the IC_{50} was identified and used as concentration for selection. Selection followed the same protocol as previously used for isolating CisPt resistant J82 bladder carcinoma cells (Höhn *et al.*, 2016). The tumor cells were treated two times per week at intervals of 48 hours with the defined concentration for 4 h. A week of treatments was always followed by a one-week intermission. This procedure was repeated for five rounds, so that the entire selection took ten weeks in total (Figure 8).

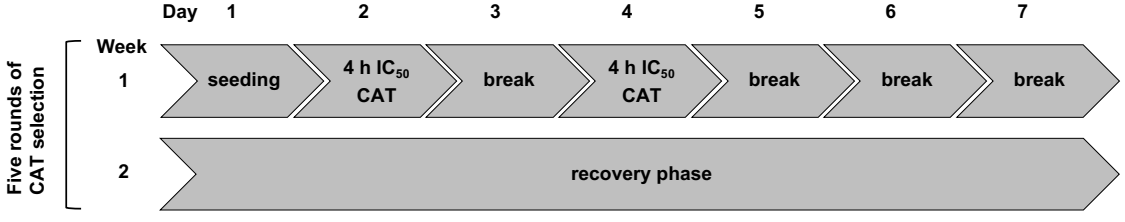

Figure 8: Selection protocol for chemotherapeutic resistant cell variants
Cells were treated two times per week at intervals of 48 hours with the IC_{50} of a CAT for 4 h. A week of treatments was always followed by one-week of recovery. This procedure was repeated five times.

2.2.2 Analysis of cell viability

2.2.2.1 AlamarBlue assay

Cell viability was determined using the AlamarBlue assay (O'Brien *et al.*, 2000). In this assay, viable cells are detectable by their ability to effectively metabolize the non-fluorescent, blue dye resazurin to fluorescent, pink resorufin (Figure 9). Hence, the detected fluorescence is regarded as a measure of cell viability.

Cells were incubated with resazurin working solution (final concentration 44 µM) in DMEM without phenol red for a fixed duration defined at first experiment (1.5 - 3 h depending on the cell line; 37 °C; 5% CO_2). After incubation fluorescence was measured (excitation: 535 nm, emission: 590 nm, 5 flashes, integration time: 20 µs) using the Infinite F200 multimode plate reader. Background fluorescence was subtracted from the measured values using blank wells containing only the resazurin solution but no cells. Relative viability in the untreated control was set to 100%. If not stated otherwise, data are shown as the mean ± standard deviation (SD) of three independent experiments each performed in biological quadruplicate.

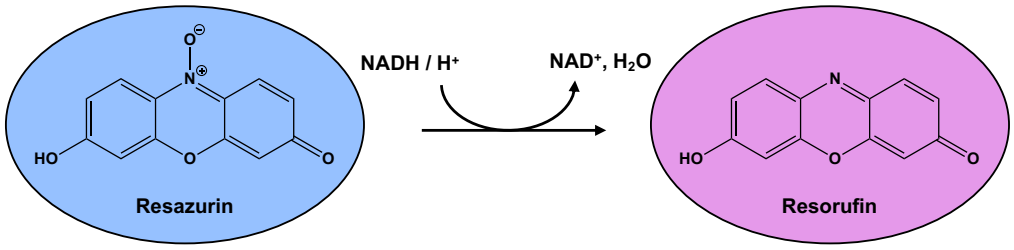

Figure 9: Functional principle of the AlamarBlue assay
The blue, non-fluorescent dye resazurin is metabolized to pink, fluorescent resorufin in viable cells. This reaction consumes NADH / H^+ and produces NAD^+ and H_2O.

2.2.2.2 Neutral Red assay

Additionally, cell viability was examined with the Neutral Red assay (Repetto *et al.*, 2008). This test is based on the uptake of the dye Neutral Red into the lysosomes of viable cells. The slightly cationic dye enters the cells by endocytosis and diffusion, where it is bound to anionic residues of the lysosomal membrane. In the acidic environment of the lysosomes, Neutral Red turns red and gets ionized, which prevents the dye from migrating out of the lysosomes again. In damaged or dead cells, due to changes in the cell membrane or a disruption in the lysosomal membrane, the ability to absorb and bind Neutral Red is reduced. Cytotoxicity is therefore reflected by a reduction in red staining.

Cells were incubated with Neutral Red incubation solution in an atmosphere containing 5% CO_2 for 90 min. After aspirating the incubation solution, fixation was performed by shortly adding the Neutral Red fixation solution. After washing with PBS,

the Neutral Red that was taken up by the cells was extracted by adding Neutral Red extraction solution (shaking 15 min at room temperature (RT)). Absorbance was then measured using the Sunrise absorbance microplate reader at 540 nm wavelength. Background absorbance was subtracted from the measured values using blank wells containing no cells. Relative viability in the untreated control was set to 100%. If not stated otherwise, data are shown as the mean ± standard deviation (SD) of three independent experiments each performed in biological quadruplicate.

2.2.2.3 Combination Index

To determine whether a combination treatment had additive, synergistic or antagonistic effects on cell viability, the combination index (CI) was calculated using the cytotoxicity data obtained from AlamarBlue assays (see chapter 2.2.2.1). The Compusyn software, which is based on the Chou–Talalay method, was used for calculation of CI (Chou, 2010). A CI < 0.9 was considered as synergistic, 0.9 ≤ CI ≤ 1.2 as additive and CI > 1.2 as antagonistic effect.

2.2.3 Molecular biology

2.2.3.1 Isolation of genomic DNA

Genomic DNA isolation was performed semi-automatically with the DNeasy Blood & Tissue Kit and the QIAcube® according to the protocol “Purification of total DNA from animal blood or cells V2”. DNA isolation is based on binding of the DNA to a silica membrane in a specialized high-salt buffer system, purification by several washing steps and, in a final step, elution of the DNA from the membrane.

After treatment, the cells were washed with PBS, detached from the culture dish with trypsin, separated and pelleted by centrifugation (300 x g, 5 min, RT). The resulting pellet was resuspended in 100 µl PBS and the genomic DNA was isolated using the aforementioned protocol according to the manufacturer's instructions (elution volume 1 & 2 set to 50 µl). The concentration and purity of the isolated DNA was determined photometrically using the NanoVue™ Plus spectrophotometer. The purity of the DNA can be assessed from the quotients of absorbances, whereby the absorbance ratios of 2.0 to 2.2 for 260 nm/230 nm and 1.8 for 260 nm/280 nm correspond to pure DNA. The isolated DNA was then stored at -20 °C until further use.

2.2.3.2 RNA isolation

Isolation of RNA was performed semi-automatically with the RNeasy Mini Kit using the QiaCube® according to the protocol “Purification of total RNA from animal tissues and cells including DNase digestion”. The RNA isolation is based on the binding of RNA to a silica membrane in a specialized high-salt buffer system, purification by several washing steps and the final elution of the RNA from the membrane. This procedure purifies all RNA molecules > 200 nucleotides and thereby enables an enrichment of mRNA since other RNAs, such as rRNAs and tRNAs, are mostly excluded by their size.

After treatment, the cells were put on ice, scraped from the culture dish with a cell spatula, separated and pelleted by centrifugation (300 x g, 5 min, 4 °C). The resulting pellet was resuspended in 350 µl RLT buffer for lysis and RNA isolation was performed using the aforementioned protocol according to the manufacturer's instructions (elution volume set to 30 µl). The concentration and purity of the isolated RNA was determined photometrically using the NanoVue™ Plus spectrophotometer. The purity of the RNA can be assessed from the quotients of absorbances, whereby the absorbance ratios of 2.0 to 2.2 for 260 nm/230 nm and 2.0 for 260 nm/280 nm are indicative of pure RNA. The isolated RNA was snap-frozen in liquid nitrogen and then stored at -80 °C until further use.

2.2.3.3 cDNA synthesis

The cDNA (meaning complementary DNA) is a DNA that is synthesized as a complementary copy of an RNA using the enzyme reverse transcriptase, an RNA-dependent DNA polymerase. The cDNA is then used as template for the quantitative real-time PCR reaction.

cDNA synthesis was performed with the High-Capacity cDNA Reverse Transcription Kit according to the manufacturer's instructions. Unless otherwise described 2000 ng of the previously isolated RNA was used for cDNA synthesis. RNA was mixed 1:1 with a master mix described in Table 20, so that the total volume of the reaction mix per tube was 20 µl. The reaction tubes were loaded into the Tpersonal thermal cycler and cDNA synthesis was performed using the conditions listed in Table 21. The cDNA was then stored at ‑20 °C until further use.

Table 20: Composition of the master mix for cDNA synthesis

Reagent	Volume
10x Buffer RT	2.0 µl
25x dNTP mix (100 mM)	0.8 µl
10x Random primers	2.0 µl
Ribolock RNase inhibitor (40 u/µl)	0.5 µl
MultiScribe™ reverse transcriptase	1.0 µl
RNase free dH_2O	3.7 µl

Table 21: Thermal cycler conditions used for cDNA synthesis

Step	Temperature	Time
Primer annealing	25 °C	10 min
cDNA synthesis	37 °C	120 min
Enzyme deactivation	85 °C	5 min
Storage of the cDNA	8 °C	indefinite

2.2.3.4 Quantitative real-time PCR

For quantitative analysis of mRNA expression, quantitative real-time PCR was performed with the CFX Real-time PCR Detection System and using the SensiMix SYBR® Hi-ROX Kit. In PCR, specific regions of DNA are amplified with the aid of selective primers. The special aspect about real-time PCR is that it uses a fluorescent dye like SYBR Green that intercalates into double-stranded DNA and thereby allows a quantification of the amount of DNA present. The quantification is based on calculation of the fluorescence threshold, the so-called Cq-value (quantification cycle value). This corresponds to the value, where the SYBR Green fluorescence signal significantly exceeds the background fluorescence.

For quantitative real-time PCR, the previously synthesized cDNA was amplified using the listed primers (Table 12, Table 13). 20 ng of cDNA and 0.25 µM of primer were used per well. The conditions used for real-time PCR runs are stated in Table 22. The elongation step was followed by a plate read, where the SYBR Green fluorescence, that is proportional to the DNA amount, was detected. Denaturation, primer hybridization, elongation and plate read were repeated for 45 cycles. The normalized mRNA expression ($\Delta\Delta$Cq) was calculated by the CFX Manager 3.1 software by relating all Cq-values to the ones of the housekeepers β-actin and GAPDH. For further analysis, the relative mRNA expression of untreated cells, or wildtype cells for comparison of basal differences between two cell variants, were set to 1.0. Only changes in the mRNA expression of ≥ 2.0 and ≤ 0.5 were considered as biologically relevant.

Table 22: Reaction conditions used for quantitative real-time PCR

Step	Temperature	Time
Polymerase activation	95 °C	10 min
Denaturation	95 °C	15 sec
Primer hybridization	55 °C	15 sec
Elongation	72 °C	17 sec

2.2.4 Protein biochemistry

2.2.4.1 Protein isolation and quantification

At the desired time point, the cell culture dishes were put on ice, cells were washed with PBS, scraped from the dish with a cell spatula, separated and pelleted by centrifugation (300 x g, 5 min, 4 °C). The cell pellets were taken up in 200 µl RIPA buffer, incubated for 20 min, and sonicated (30% amplitude, 2 s pulse, 1 s pause, 5x). The cells are thereby disrupted by high-frequency sound waves. The resulting cell debris was then pelleted by centrifugation (10000 x g, 10 min, 4 °C) and the protein-containing supernatant was transferred to a new reaction tube. The protein concentration of the solution was determined using the DC™ Protein assay according to the manufacturer's instructions. The measurement of absorbance at 595 nm was carried out with the Sunrise absorbance microplate reader. The protein concentration of all samples was adjusted to the same value with RIPA buffer and mixed with 1/4 volume Roti®-Load 1. The SDS present in the buffer enables the denaturation and solubilization of the proteins and superimposes their intrinsic charge through the negative charge of the resulting SDS-protein complex. In addition, the secondary structure of the proteins is neutralized by the β-mercaptoethanol present in the buffer. This means that the mobility of the proteins in the subsequent electrophoresis depends exclusively on their molecular weight. The protein lysates were snap-frozen with liquid nitrogen and stored at -80 °C until further use.

2.2.4.2 Gel electrophoretic separation of proteins (SDS-PAGE)

The proteins were separated according to their molecular weight using discontinuous sodium dodecyl sulfate-polyacrylamide gel electrophoresis (SDS-PAGE). In this method, the negatively charged proteins migrate to the anode of an electric field and are separated by the pores in the acrylamide gel according to their molecular weight. The proteins first migrate into a collecting gel with neutral pH, in which they are concentrated at the border to the separating gel to achieve higher definition of the protein bands. Then the proteins migrate into a separating gel

with a basic pH, in which the actual separation according to their size takes place. The running distance is thereby inversely proportional to the molecular weight.
The protein lysates were prior to the electrophoresis denatured by heating (95 °C, 5 min). For SDS-PAGE 5% collecting gels and 15% separating gels were used. The electrophoresis was performed using the Mini-PROTEAN Tetra Cell electrophoresis system. The proteins were separated in SDS running buffer with a current of 10 to 30 mA per gel until the desired separation. As objective size indicator, the PageRuler™ Plus Prestained Protein Ladder was utilized.

2.2.4.3 Western blot

Western blot is a technique for transferring proteins to a membrane, where they can then be detected using immunological reactions employing protein-specific antibodies.
The proteins separated by SDS-PAGE were transferred to a nitrocellulose membrane using the Mini Trans-Blot® Cell System (300 mA, 90 min). The successful transfer of the proteins was confirmed by temporary staining of all proteins with Ponceau-S solution (1 min, RT). All the steps described below were performed under constant slow shaking of the membrane. To prevent unspecific binding of antigens to the used antibodies, the membrane was blocked with 5% milk in TBST (2 h, RT). Afterwards the membrane was washed with TBST (3 x 5 min, RT) and incubated with the desired primary antibody specific for the target protein overnight at 4 °C. For dilutions of the used antibodies see Table 14. The antibodies were diluted either in 5% milk in TBST or 5% BSA in TBST according to manufacturer's information. On the next day, unbound primary antibodies were removed by washing of the membrane with TBST (3 x 5 min, RT). The membrane was then incubated with a horseradish peroxidase-coupled secondary antibody directed against the species of the primary antibody used (2 h, RT). The dilution of the secondary antibody was always 1:2000 and prepared in 5% milk in TBST. After washing again with TBST (3 x 5 min, RT), the membrane was incubated with the luminol-containing chemiluminescence solution of the BM Chemiluminescence Blotting Substrate (POD) Kit to detect protein-antibody binding (1 min, RT). The signals were then visualized using the ChemiDoc™ Touch gel imaging system.

2.2.5 Analysis of cell cycle distribution

2.2.5.1 Flow cytometry

Cell cycle distribution was analyzed by flow cytometry using the Nicoletti protocol. This method makes use of the fact that the DNA content in the different cell cycle phases varies from single DNA content in G0/G1-phase to double DNA content in G2/M-phase. Since DNA replication is ongoing during S-phase, the DNA content of cells in the S-phase is between single and doubled. Apoptotic cells are defined as cells with a lower DNA content than cells in the G0/G1-phase (SubG1 fraction), as enzymatic fragmentation of the DNA takes place during cell death. The differences in DNA content can be observed using the fluorescent dye propidium iodide (PI), as this intercalates into the DNA and thus triggers a fluorescence signal of varying intensity depending on the amount of DNA present.

Adherent cells were trypsinized and combined with the medium that contained floating i.e. dead cells. After centrifugation (300 x g, 5 min, 4 °C, reduced brake), the supernatant was discarded. Cell pellets were resuspended in 1.5 ml hypotonic PI solution. After incubation for 20 min at RT samples were subjected to flow cytometric analysis using the BD Accuri™ C6. Duplets were excluded from final analysis by gating and 10000 events per sample were measured.

To identify in which cell cycle phase specific markers are expressed, antibody-based staining of those markers was combined with cell cycle analysis by PI staining. To this end, cells were harvested, fixed with 1% formaldehyde in PBS (15 min, 4 °C), permeabilized in ice-cold 80% ethanol (2 h, -20 °C) and blocked with 1% BSA in PBS-Triton X-100 (5 min, RT). After centrifugation (300 x g, 5 min, 4 °C, reduced brake), the cell pellet was resuspended in blocking solution containing the considered primary antibody (pH3 1:30 / γH2AX 1:100, overnight, 4 °C). On the next day fluorescence-labelled secondary antibody incubation was performed in blocking solution (1:200, 1 h, RT). For co-staining with PI, cells were then incubated with PBS containing 10 µg/ml PI and 100 µg/ml DNase-free RNase (1 h, RT). Samples were right after subjected to flow cytometric analysis using the LSRFortessa™ Cell Analyzer. Dead cells and duplets were excluded from final analysis by gating and 10000 events per sample were measured. Further analysis of the results was carried out with FlowJo software or floreada.io web application.

2.2.5.2 S-phase activity

For analysis of S-phase activity, EdU incorporation was analyzed using the EdU-Click 488 Cell Proliferation assay. EdU (5-Ethynyl-deoxyuridine) is a nucleoside analog to thymidine and is incorporated into DNA during active DNA synthesis. For visualization, the kit uses a chemical reaction with the fluorescent dye 6-FAM azide, so that cells that have incorporated EdU into their DNA emit a fluorescent signal at 488 nm.

Cells were seeded onto coverslips, treated, and at the considered time point incubated with 10 µM EdU (2 h, 37 °C, atmosphere containing 5% CO_2). Afterwards, cells were fixed with 4% formaldehyde in PBS (15 min, RT), permeabilized with 0.5% PBS-Triton X-100 (20 min, RT) and incubated with the reaction cocktail included in the assay Kit (30 min, RT, in the dark) according to the manufacturer's protocol. In between the steps, washing was conducted with 3% BSA in PBS. Ultimately, the cells were mounted in Vectashield containing DAPI. Microscopic analysis was performed with an Olympus BX43 fluorescence microscope (20x objective). The percentage of EdU positive nuclei as well as their fluorescence intensity were assessed using ImageJ.

2.2.5.3 Mitotic index

The phosphorylation of histone H3 as a marker for the mitotic index was analyzed via immunocytochemical staining.

Cells were seeded onto coverslips. After treatment, cells were fixed with 4% formaldehyde in PBS (15 min, RT) and permeabilized with ice-cold ethanol (20 min, -20 °C). Following blocking with 5% BSA in PBS-Triton X-100 (1 h, RT), incubation with phospho histone H3 (Ser10) (pH3) antibody was performed (1:500 in blocking solution, overnight, 4°C). On the next day, washing with PBS-Triton X-100, PBS high salt and again PBS-Triton X-100 was done. Incubation with the secondary fluorescence-labelled antibody was conducted (1:500 in blocking solution, 2 h, RT, in the dark) and after further washing with PBS, cells were mounted in Vectashield containing DAPI. Microscopic analysis was performed with an Olympus BX43 fluorescence microscope (20x objective). The percentage of pH3 positive nuclei was assessed using ImageJ.

2.2.5.4 Analysis of mitotic progression

An immunocytochemical co-staining of α-tubulin, as marker for the mitotic spindles, and pericentrin, as marker for the centrosomes, was applied (Bergmann *et al.*, 2020) to classify different mitotic stages and identify defects in mitotic progression as described (Baudoin and Cimini, 2018).

Cells were seeded onto coverslips and at the analysis time point fixed with 4% formaldehyde in PBS (20 min, RT), washed with $PBS^{+Ca/+Mg}$, permeabilized with 0.25% Triton X-100 in PBS (5 min, RT) and blocked with 3% BSA in PBS (2 h, RT). Incubation with the α-tubulin antibody (1:500 in 1% BSA in PBS) was done overnight at 4 °C. On the next day the samples were incubated with the pericentrin antibody (1:1000 in 1% BSA in PBS, 2.5 h, RT). Fluorescence-labeled secondary antibodies (1:1000 in 1% BSA in PBS) were incubated for 2 h at RT and cells were mounted with Prolong Gold DAPI. Microscopic analysis was performed with an Olympus BX43 fluorescence microscope (100x objective), where z-stack images were taken. The chromatin structure, number and location of centrosomes and arrangement of spindles were considered for classification of different mitotic phases and abnormalities. Relative abundances were calculated from at least 50 mitotic cells.

2.2.6 Analysis of DNA damage

2.2.6.1 Alkaline Comet assay

The formation of DNA strand breaks and apurinic/apyrimidinic sites was monitored via the alkaline Comet assay (Olive and Banáth, 2006). The concept of the Comet assay is a single cell gel electrophoresis, in which the migration speed of the DNA is size-dependent. Chromosomal DNA as a whole is too large to migrate out of the nucleus in the electric field. Only damaged, fragmented DNA is able to migrate out of the compact nuclear DNA network. The smaller the DNA fragments are, the faster they migrate in the gel and form a so-called comet tail, which gives the assay its name. The proportion of DNA in the comet tail thus indirectly allows a statement to be made about the amount of DNA strand breaks in the individual cell. The alkaline Comet assay is a special variant of the Comet assay in which the DNA is denatured using an alkaline buffer, which allows the detection of alkali-labile sites and DNA single-strand breaks together with DNA double-strand breaks. Directly after cell harvesting, 10 µl of a cell suspension ($2x10^6$ cells/ml) were mixed with 120 µl of warm 0.5% low melting point agarose, transferred onto agarose-coated (1.5%) glass slides and cooled for 5 min. After incubation in alkaline lysis buffer (1 h, 4 °C) and denaturation of the DNA in precooled electrophoresis buffer with pH > 13 (25 min, 4 °C, protected from light), electrophoresis was performed at 4 °C (25 min,

electric current: 300 mA constant, 25 V). Slides were then washed with neutralization buffer and dried. Directly before fluorescence microscopic analysis, slides were stained with propidium iodide solution to stain the DNA. Comets were evaluated with a Zeiss Axiolab fluorescence microscope and quantification of migrated DNA was performed with TriTek Comet Score™ software, evaluating 50 cells per condition.

2.2.6.2 Immunocytochemistry (RPA, RAD51, γH2AX + RPA)

In response to genotoxic stress some proteins involved in DDR, like RAD51, RPA or γH2AX, bind to DNA in large numbers. These protein accumulations can be made microscopically visible as nuclear foci by immunocytochemical staining.

To this end, cells were seeded onto coverslips and after treatment fixed with an ice-cold mixture of methanol and acetone (7:3) (10 min, -20 °C). After blocking with 1% goat serum in PBS (3 x 10 min, RT), incubation with RPA2 antibody and/or RAD51 antibody was performed overnight (1:500, 4 °C). The day after, washing with goat serum in PBS was performed (3 x 10 min, RT) and samples were incubated with fluorescence-labelled secondary antibodies diluted in the blocking solution (1:500, 2 h, RT). After further washing with goat serum in PBS (3 x 10 min, RT), the cells were mounted in Vectashield containing DAPI and nuclear foci were counted by microscopic analysis using an Olympus BX43 fluorescence microscope (100x objective).

For RPA + γH2AX co-staining, cells were fixed with 4% formaldehyde in PBS (15 min, RT) and permeabilized with ice-cold ethanol (20 min, -20 °C). After blocking with 5% BSA in PBS-Triton X-100 (1 h, RT), incubation with primary antibodies was performed overnight (RPA2 1:500, γH2AX 1:1000, 4°C). On the next day, samples were washed with PBS high salt (2 min, RT) and PBS-Triton X-100 (5 min, RT) followed by incubation with fluorescence-labelled secondary antibodies (1:500, 2 h, RT). After further washing with PBS and PBS-Triton X-100, the cells were mounted in Vectashield containing DAPI and nuclei were analyzed microscopically using an Olympus BX43 fluorescence microscope (100x objective). For γH2AX the nuclear fluorescence intensity was measured and for RPA2 nuclear foci were counted using ImageJ.

2.2.6.3 DNA Fiber Spreading assay

For analysis of DNA replication dynamics, the DNA Fiber Spreading assay was applied (Biber and Wiesmüller, 2021). With this technique the progress of individual DNA replication forks can be visualized by incorporation of two different nucleotide analogs (Chlorodeoxyuridine (CldU) and Iododeoxyuridine (IdU)) into the newly synthetized DNA and their staining with fluorescently labelled antibodies. With the here used labelling strategy of one pulse with CldU, followed by one pulse with IdU, there are five distinguishable patterns of red and green fluorescence that can be produced. These indicate sites where replication is initiating (origins), elongating, or where replication is merging between two adjacent replicons (terminations) (Figure 10). By comparing different treatment groups regarding their track lengths of elongating forks or asymmetry at first pulse origins, replication fork slow-down and replication fork stalling can be detected. Evaluating the relative prevalence of the different types of labelling patterns, allows an assessment on shifts in the composition of replication stages e.g. towards more origin firing.

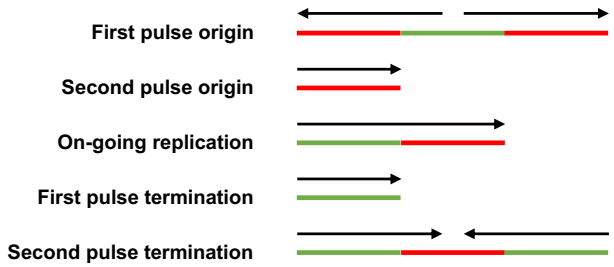

Figure 10: Possible fluorescence patterns for the determination of replication fork stages after labelling with a pulse of Chlorodeoxyuridine (green) followed by a pulse with Iododeoxyuridine (red)

Cells were incubated with 20 µM CldU (20 min, 37 °C in an atmosphere containing 5% CO_2) and right afterwards incubated with 200 µM IdU (20 min, 37 °C in an atmosphere containing 5% CO_2) (Figure 11). The cells were harvested using trypsin, counted and diluted to a cell number of 1250 cells/µl in PBS. 2 µl of this cell suspension were transferred onto a glass slide and mixed with 6 µl of lysis buffer. After 6 min incubation, slides were tilted upwards to stretch the fibers, dried for 6 min lying horizontally flat, fixed (5 min, RT, fixing solution: methanol:acetic acid 3:1), dried again for 7 min lying horizontally flat and stored overnight in 70% ethanol at 4 °C. The next day, slides were incubated with 100% methanol (5 min, RT), denatured with 2.5 M HCl (1 h, RT) and blocked with 5% BSA in PBS (1 h, 37 °C). The fibers were stained with rat anti-BrdU (1:140) for CldU detection and mouse anti-BrdU (1:70) for IdU detection (1 h, RT, antibodies in 0.5% BSA-PBS). After washing with PBS-Tween20 and PBS, incubation with secondary antibodies anti-rat 488 (1:400) and

anti-mouse 555 (1:250) was performed (1 h, RT, antibodies in 0.5% BSA-PBS). Following washing with PBS-Tween20 and PBS, the slides were mounted with Fluoroshield and fibers were analysed using an Olympus BX43 fluorescence microscope (40x objective). 200 fibers of ongoing replication were analyzed per sample for track length measurements. For evaluation of asymmetry at replication origins at least 10 fibers per sample were measured.

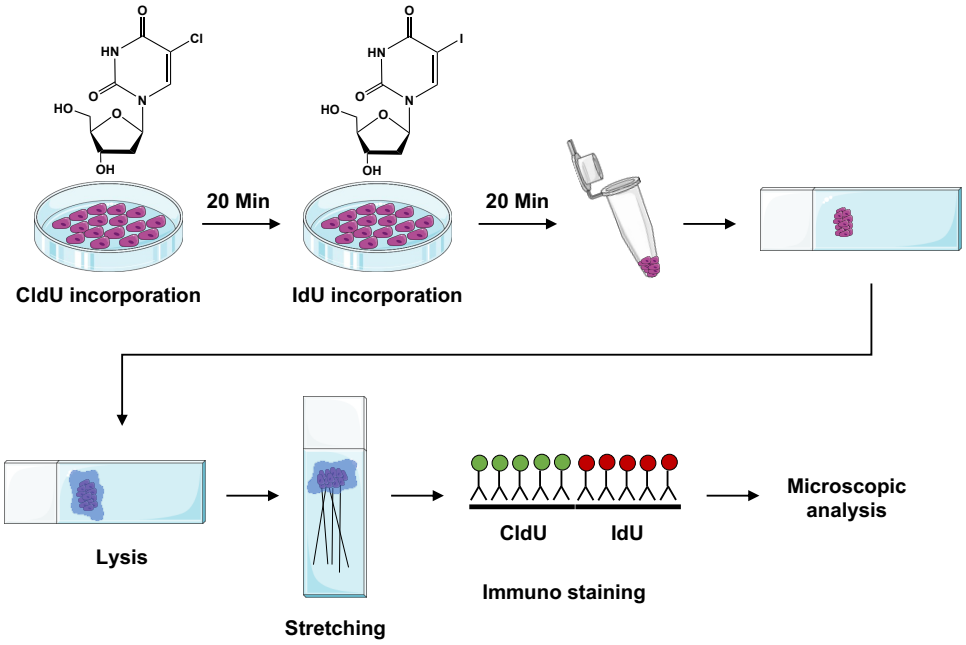

Figure 11: Procedure of the DNA Fiber Spreading assay
Cells were incubated for 20 minutes with CldU (Chlorodeoxyuridine) and right afterwards for 20 minutes with IdU (Iododeoxyuridine). Cells were harvested, the cell suspension given onto a glass slide and mixed with lysis buffer. Slides were tilted upwards to stretch the DNA fibers and fibers were stained immunocytochemically with two different antibodies detecting CldU and IdU. (This figure was created in part by using images from Servier Medical Art, licensed under Creative Commons Attribution 4.0 Unported License.)

2.2.7 Analysis of Cisplatin-DNA intrastrand crosslinks (Southwestern blot)

The amount of platinum-DNA intrastrand crosslinks induced by CisPt treatment was quantified via Southwestern blot analysis. This method is based on loading equivalent amounts of DNA to a nitrocellulose membrane and detecting the Cisplatin-DNA intrastrand crosslinks directly with an DNA adduct-specific antibody. The here used antibody recognizes only the intrastrand crosslinks formed by Cisplatin between adjacent guanines.

Isolated genomic DNA was diluted to 1 µg/100 µl in TE buffer. DNA was denatured by heating to 95 °C for 10 minutes and then cooled off on ice. Cold DNA solution was diluted 1:1 with 2 M ice-cold ammonium acetate. A nitrocellulose membrane was soaked in 1 M ammonium acetate and then inserted into an in-house built dot blot apparatus. The dot blot apparatus was sealed with parafilm, and a vacuum was generated by

sucking out air with a pump. 200 µl of the DNA solution, correlating to 1 µg DNA, was given into the respective slots and empty slots were filled with 200 µl TE buffer. After all liquid was sucked through the membrane, the membrane was washed with 1 M ammonium acetate followed by dH_2O and incubated for 5 minutes with 5x SSC. The DNA on the membrane was fixed by heating to 80 °C for 2 h. Blocking was performed with 5% milk powder in TBST (1 h, RT) followed by incubation with the primary antibody detecting cisplatin modified DNA (1:5000 in 5% milk powder in TBST; overnight; 4 °C). On the next day, the membrane was washed extensively with TBST, incubated with the corresponding secondary antibody (Goat anti rat IgG HRP; 1:2000 in 5% milk powder in TBST; 2 h; RT) and washed again with TBST. Detection of the bound antibodies was conducted via electro chemiluminescence reaction. Staining with DNA-binding dye methylene blue was used as a loading control. To this end the membrane was incubated for 5 minutes with methylene blue solution and shortly washed with dH_2O. The intensity of the different signals was determined densitometrically using ImageJ.

2.2.8 Proteome analysis

The proteome is the totality of all proteins in an organism under defined conditions and at a specific point in time. Proteome analyses are large-scale studies, where the complete spectrum of proteins in cell samples are identified and quantified. The content of the proteome is constantly changing according to the current needs of a cell. Conclusions from protein expression profiles can thus be drawn e.g. about whether cells are stressed or trying to counteract a certain type of damage.

At the desired time point for analysis, the cell culture dishes were put on ice, cells were washed with PBS and scraped from the dish with a cell spatula. The harvested cells were pelleted by centrifugation (800 x g, 3 min, 4 °C), resuspended in PBS and once again pelleted by centrifugation (800 x g, 3 min, 4 °C). The pellets were snap-frozen with liquid nitrogen and stored at -80 °C. Further procedure, i.e. isolation of whole cell protein lysate and mass spectrometry-based proteome analysis, was performed in the Molecular Proteomics Laboratory of the “Biologisch-Medizinisches Forschungszentrum”. Data was obtained from three independent samples per condition. In the evaluation, cut-off values of a twofold/halving of the protein content and a p-value ≤ 0.05 were defined for the assessment of relevant effects. Additionally, KEGG pathway analyses were performed for the regulated proteins in order to define interacting signaling networks.

2.2.9 siRNA-based knockdown of RAD51

Knockdown of RAD51 was performed with the GeneSolution siRNA set Hs_RAD51_7 and the transfection reagent Lipofectamine® RNAiMAX. To this end, Lipofectamine® RNAiMAX was diluted 1:50 in cell culture medium without supplements and mixed by pipetting up and down three times. siRNA stock solution (1 µM) was diluted 1:33 in cell culture medium without supplements and mixed by pipetting up and down three times. Both components were mixed gently by pipetting up and down three times and incubated for 20 min at room temperature. Normal cell culture medium of the cells was replaced by medium containing FCS but no penicillin/streptomycin. The transfection mixture of Lipofectamine® RNAiMAX and siRNA was then added to the cells drop by drop. Knock-down efficacy was tested after incubation of the cells with siRNA for 24 h, 48 h and 72 h. Analysis of RAD51 knock-down effects was carried out, depending on the endpoint considered, after 24 h or 72 h incubation with siRNA.

2.2.10 Xenograft mouse experiment

The described xenograft mouse experiment was approved by the „Landesamt für Natur, Umwelt und Verbraucherschutz Nordrhein-Westfalen“ (LANUV) under file number 81-02.04.2019.A240(/01). The corresponding internal study number of the ZETT Düsseldorf is G240/19.

2.2.10.1 Study design

For the xenograft mouse experiment, NSG-$(K^bD^b)^{null}$ animals were used (see chapter 2.1.7.2). The animals were weighed at least every second day throughout the whole experiment to check their body weight (BW). At the beginning of the experiment, mice were partly shaved and a defined number of $J82^{CisPt}$ cells were injected subcutaneously into both flanks of the animals. The growth of the subcutaneous tumors was monitored regularly, at least three times per week, by size measurement with a caliper. The tumor volume was calculated from the measured values with the formula $V = 0.5 \times (\text{length} \times \text{width}^2)$. When the tumors of the mice reached an average tumor volume of 0.2 cm^3 or after a maximum of 27 days, the planned treatment was started. The animals were divided into four treatment groups (solvent control (corn oil), PF477736, B02, PF477736 + B02) of four to five animals. The pharmacological inhibitors (PF477736 10 mg/kg BW; B02 10 mg/kg BW) or solvent were applied by intraperitoneal injection, twice a week at intervals of 48 hours and over a period of 3 weeks. On the individual injection days, PF477736 was administered in the morning and B02 in the afternoon.

Planned termination of the experiment was five days after the last injection of the inhibitors (Figure 12). If before that, tumor volume reached 1 cm^3 or animals showed clear signs of suffering (significant weight loss, altered habitus, wounds in the area of the tumor) the experiment was terminated earlier. At termination of the experiment, organ extraction was performed as described in chapter 2.2.10.4. In order to record possible adverse effects of the mono- and combination treatments, blood samples of all mice were taken at the beginning and end of the experiment as described in chapter 2.2.10.3.

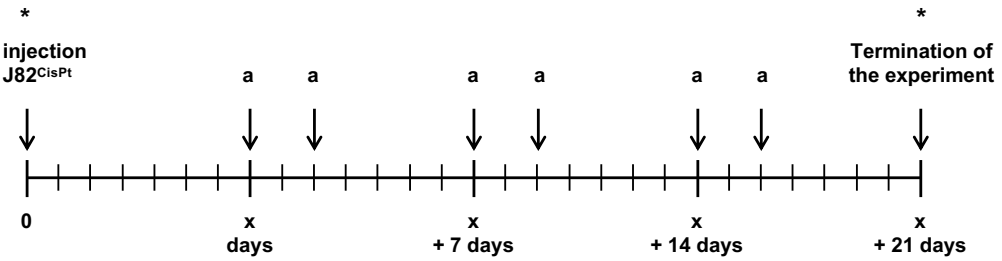

Figure 12: Study design of the xenograft mouse experiment for the testing of B02 + PF477736 *in vivo*
$J82^{CisPt}$ cells were injected subcutaneously (s.c.) into both flanks of the animals. The treatment with the inhibitors was started when the averaged tumor volume reached 0.2 cm^3 or after a maximum of 27 days (x). The inhibitors were administered twice a week at intervals of 48 h and over a period of 3 weeks (a). Planned termination of the experiment was 21 days after the first injection of the inhibitors. Blood was taken from the animals at the beginning and the end of the experiment (*).

2.2.10.2 Preparation of inhibitors for injection

The inhibitors B02 and PF477736 were aliquoted at 1 mg and stored at 4 °C. On the day of injection, the needed number of aliquots were each dissolved in 1 ml corn oil. For homogenization the solutions were shaken on a vortexer at maximum speed, then sonicated (35% amplitude, 2 s pulse, 1 s pause, 5x), heated in a heating block (37 °C, 15 min, 500 rpm) and again shaken on a vortexer at maximum speed.

2.2.10.3 EDTA blood collection and analysis

About 100 µl blood was taken from the tail vein of the mice at the beginning of the experiment and on the day of organ isolation. The blood was collected directly into EDTA tubes and continuously rotated at low speed until the blood count parameters were measured later the same day. The measurement was carried out with the scil Vet ABC™ hematology analyzer at the ZETT Düsseldorf.

2.2.10.4 Organ isolation

On the day of organ isolation, the mice were weighted and given a high dose of anesthetics according to their weight (0.2 mg/g Ketamine + 0.02 mg/g Xylazin) by intraperitoneal injection. Mice were killed by cervical dislocation. The chest, abdomen and skull of the animals were opened and desired organs (intestine, kidneys, liver, lung, heart and brain) were isolated. In addition to that, the tibia of a hind leg was isolated, and its length was determined. The organs were weighted with a precision scale and photos were taken next to a scale bar. The extracted organs were sectioned, and parts were placed into safe-lock tubes for subsequent RNA and protein isolation while other parts were placed into tissue embedding cassettes for further processing into histological sections. The safe-lock tubes containing organ parts were directly snap-frozen in liquid nitrogen and then stored at -80 °C. The tissue embedding cassettes were stored overnight in Roti®Histofix 4.5%, rinsed with tap water for 15 min the next morning and then stored in PBS at 4 °C until dehydration.

2.2.10.5 Bone marrow isolation for RNA extraction

During organ extraction, the femurs of the mice were isolated and the thick ends of the bones were cut off on both sides. A syringe filled with 500 µl sodium chloride solution was inserted at one end, the solution was flushed through the bone and collected in a safe-lock tube. The collected solution was reinserted into the syringe and flushing was repeated 2 – 3 times. The resulting solution containing bone marrow cells was mixed with 1 ml Erylysis buffer and transferred to a 15 ml tube. After incubation for 5 min, the reaction was stopped by adding 5 ml PBS. The cells were pelleted by centrifugation (1200 rpm, 5 min, 4 °C), washed with PBS and centrifuged once more (1200 rpm, 5 min, 4 °C). The resulting cell pellet was resuspended in 350 µl RTL buffer included in the RNeasy® Mini Kit and stored at -80 °C until RNA isolation.

2.2.10.6 Purification of total RNA from bone marrow cells

Isolation of RNA was performed using the RNeasy® Mini Kit (see chapter 2.2.3.2). The frozen cell RTL buffer suspension (see chapter 2.2.10.5) was thawed and homogenized by shaking on a vortexer. The samples were mixed with 350 µl 70% ethanol, transferred into a RNeasy spin column with a collection container and centrifuged (8000 x g, 15 sec). The flow through was discarded, 350 µl RW1 buffer was given onto the spin column and centrifuged (8000 x g, 15 sec). The flow through was discarded, 80 µl DNase from the RNase-free DNase Set was given onto the spin column and incubated for 15 min at RT. 350 µl RW1 buffer were given onto

the spin column, centrifuged (8000 x g, 15 sec) and flow through was discarded. 500 µl RPE buffer were given onto the spin column, centrifuged (8000 x g, 15 sec) and flow through was discarded. Again, 500 µl RPE buffer were given onto the spin column, centrifuged (8000 x g, 2 min) and flow through was discarded. The spin columns were then centrifuged (17000 x g, 1 min) to remove any remaining liquid and flow through was discarded. The RNA was then eluted from the spin column by adding 30 µl RNase-free water and centrifugation (8000 x g, 1 min). The NanoVue™ Plus spectrophotometer was used to photometrically determine the concentration and purity of the isolated RNA. The purity of the RNA can be assessed from the quotients of absorbances, where absorbance ratios of 2.0 to 2.2 for 260 nm/230 nm and 2.0 for 260 nm/280 nm are indicative of pure RNA. The isolated RNA was snap-frozen with liquid nitrogen and then stored at -80 °C until further use.

2.2.11 Statistical analysis

For statistical analysis the unpaired two-tailed Student's t-test or one-way ANOVA were applied using GraphPad Prism 6 software. p-values ≤ 0.05 were considered as significant and were marked with an asterisk (*), plus (+) or hashtag (#) as specified in the figure legends.

3 Results

3.1 Differences between $J82^{WT}$ and $J82^{CisPt}$ under basal conditions and in response to cisplatin

3.1.1 Cytotoxicity screening with cytostatics & pharmacological inhibitors of DDR/DNA repair in J82 cell variants

The formerly isolated cisplatin-resistant bladder cancer cell variant ($J82^{CisPt}$) was mainly used as *in vitro* model of acquired CisPt resistance (Höhn *et al.*, 2016). Compared to parental $J82^{WT}$ cells, $J82^{CisPt}$ cells are characterized by an about four-times higher IC_{50} in response to CisPt after long-term treatment and even six-times higher IC_{50} after short-term treatment (Figure 13A, B, E). In an initial cytotoxicity screening, $J82^{CisPt}$ cells were analyzed regarding cross-sensitivities/-resistances to various conventional anticancer therapeutics (CATs) and pharmacological inhibitors of the DDR and DNA repair by measuring cell viability applying the AlamarBlue assay. These extensive cytotoxicity analyses were conducted to get hints towards the putative molecular mechanism(s) contributing to acquired cisplatin-resistance in this cell model. Moreover, it was used to identify DDR-modulatory compounds that could effectively re-sensitize $J82^{CisPt}$ cells to cisplatin treatment or induce cell death in the CisPt resistant cell variant in a resistance-independent way.

$J82^{CisPt}$ were cross-resistant to other platinum-based drugs i.e. carboplatin and oxaliplatin (Figure 13C, D, E) while showing comparable sensitivity to prototypical inducers of DSBs, i.e. topoisomerase II inhibitor doxorubicin and ionizing radiation (Figure 14A, B). Remarkably, $J82^{CisPt}$ showed stronger decrease in viability than $J82^{WT}$ with the ribonucleotide reductase inhibitor OH-Urea and the antimetabolite 5-Fluorouracil (5-FU) (Figure 14C, D), which both are well-known inducers of replicative stress (Longley *et al.*, 2003; Musiałek and Rybaczek, 2021). The two oxidants tBOOH and H_2O_2 induced weaker cytotoxicity in $J82^{CisPt}$ than in $J82^{WT}$ (Figure 15).

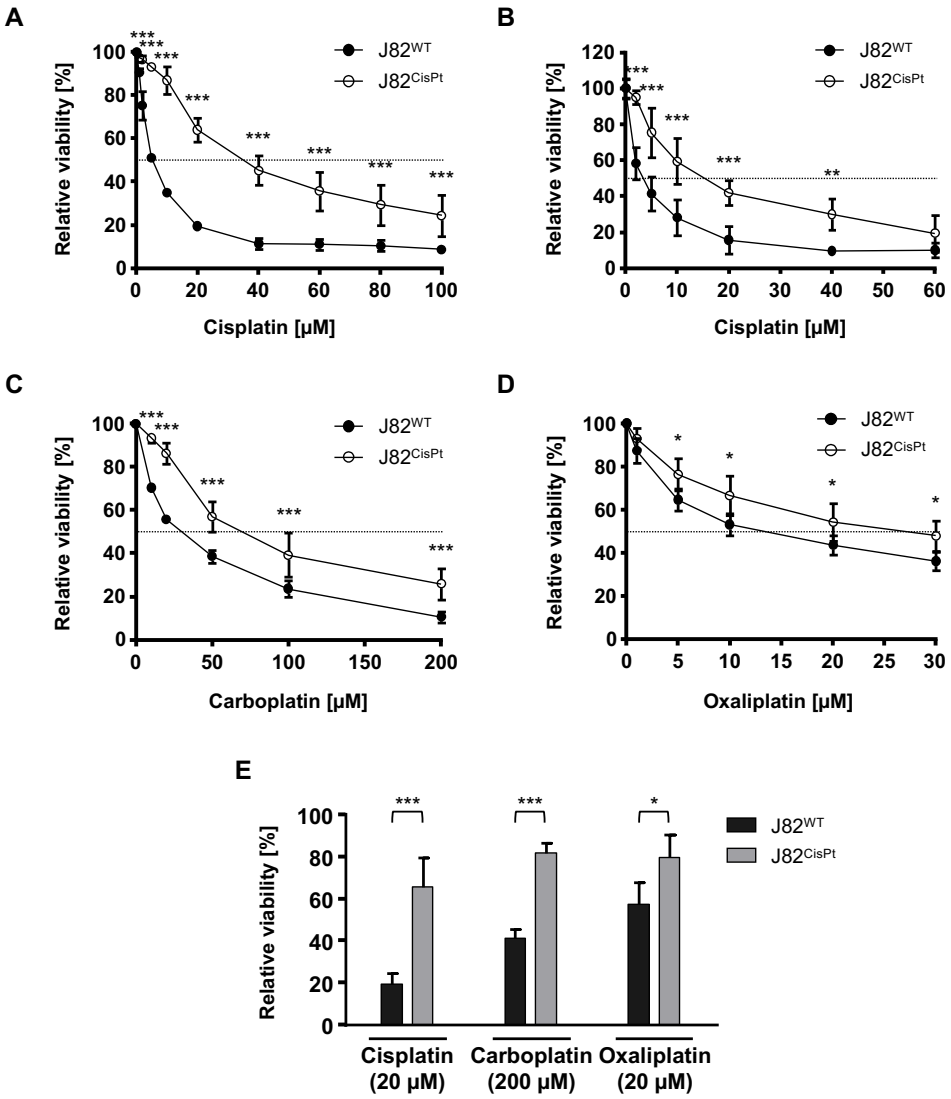

Figure 13: Comparison of cytotoxicity of platinum compounds in J82^{WT} and J82^{CisPt}
J82^{WT} and J82^{CisPt} cells were treated with different concentrations of cisplatin (A, B, E), carboplatin (C, E) or oxaliplatin (D, E) for 4 h + 72 h post-incubation (A, E) or 72 h (B, C, D) and cell viability was determined through the AlamarBlue assay. The viability of the untreated control for each cell variant was set at 100%, and all associated treatments were related to this value. The dotted line at 50% relative viability (A, B, C, D) facilitates the reading of the IC_{50} value, which represents the concentration of a substance that results in a 50% loss of cell viability compared to the untreated control. Data presented are the mean ± SD from three independent experiments, each performed in biological quadruplicates. *$p \leq 0.05$; **$p \leq 0.01$; ***$p \leq 0.001$; significant difference compared to J82^{WT}.

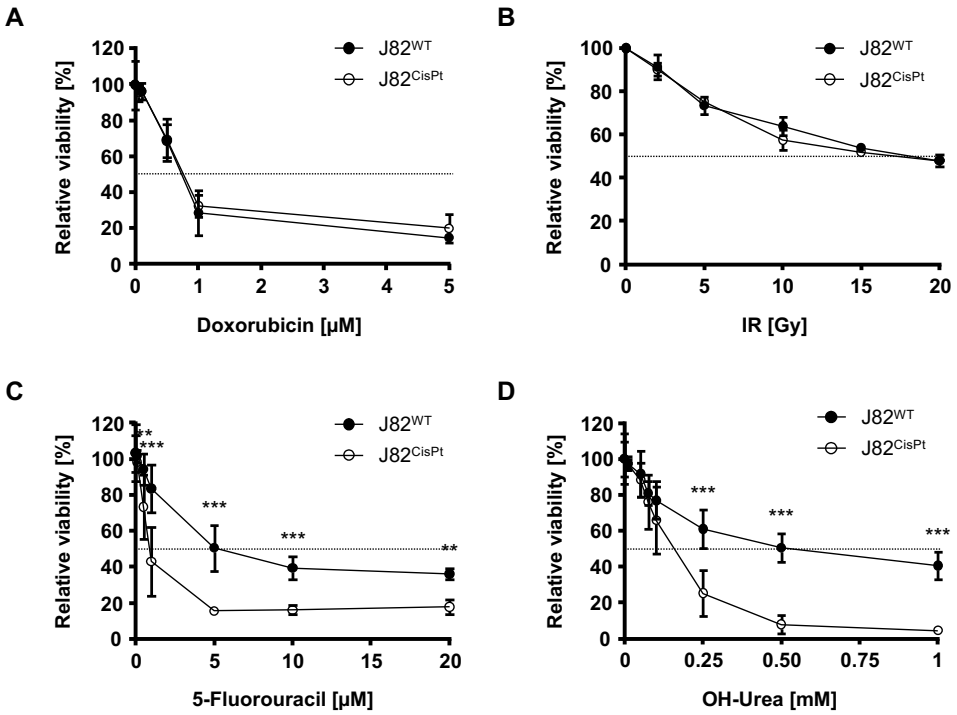

Figure 14: Comparison of cytotoxicity of other conventional cancer therapies in J82^{WT} and J82^{CisPt}
J82^{WT} and J82^{CisPt} cells were treated with different concentrations of doxorubicin (A), 5-Fluorouracil (C) or OH-Urea (D) for 72 h and viability was measured via the AlamarBlue assay. J82^{WT} and J82^{CisPt} cells were irradiated with different doses by a radioactive source (IR) before seeding and viability was measured 72 h after via the AlamarBlue assay (B). The untreated control of each cell variant was set to 100% viability and all associated treatments were related to this. The dotted line at 50% relative viability facilitates the reading of the IC_{50} value. This value indicates the concentration of a substance at which there is a 50% loss of viability among the cells in a given population, when compared to an untreated control. Data presented are the mean ± SD from three to four independent experiments, each performed in biological quadruplicates. **p ≤ 0.01; ***p ≤ 0.001; significant difference compared to J82^{WT}.

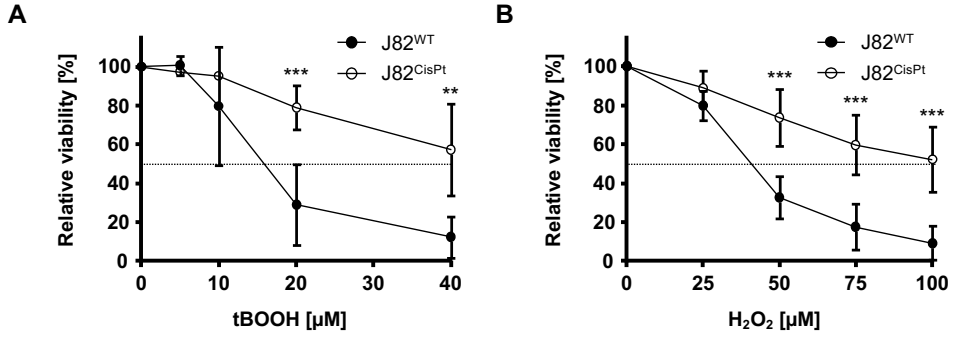

Figure 15: Comparison of cytotoxicity of oxidants in J82^{WT} and J82^{CisPt}
J82^{WT} and J82^{CisPt} cells were subjected to treatment with varying concentrations of tert-butyl hydroperoxide (tBOOH) (A) or H_2O_2 (B) over a 72-hour period and cell viability was subsequently measured via the AlamarBlue assay. The untreated control of each cell variant was set to 100% viability and all associated treatments were related to this. The dotted line at 50% relative viability allows for the convenient reading of the IC_{50} value, which indicates the concentration of a substance at which 50% viability loss of the cell population occurs in comparison to the untreated control. Data presented are the mean ± SD from three to four independent experiments, each performed in biological quadruplicates. **p ≤ 0.01; ***p ≤ 0.001; significant difference compared to J82^{WT}.

Regarding pharmacological inhibitors of DNA repair and DDR, we observed cross-resistance of J82^{CisPt} cells to the RAD51 inhibitor B02 after various treatment durations (Figure 16A, Supplementary Figure 1). This result was additionally demonstrated when employing the Neutral Red assay (Figure 17). In contrast, J82^{CisPt} cells revealed no cross-resistance to the CHK1 inhibitor PF477736, the MRE11 inhibitor Mirin and the PARP inhibitor Niraparib (Figure 16B, C, D). J82^{CisPt} cells were found to be more sensitive than J82^{WT} to treatment with the pan-HDAC inhibitor Vorinostat and class I inhibitor Entinostat (Figure 16E, F).

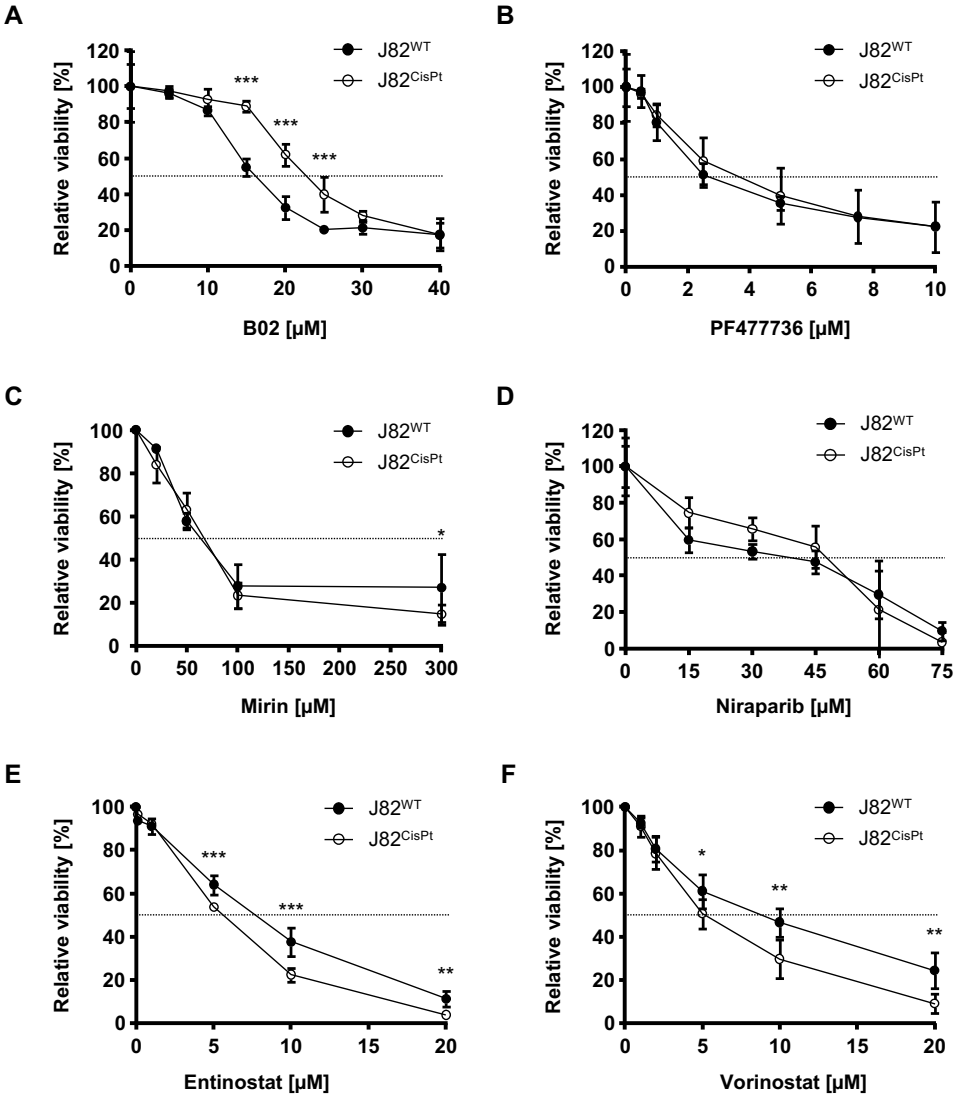

Figure 16: Comparison of cytotoxicity of pharmacological inhibitors against DDR factors in J82^{WT} and J82^{CisPt}

J82^{WT} and J82^{CisPt} cells were treated with different concentrations of RAD51 inhibitor B02 (A), CHK1 inhibitor PF477736 (B), MRE11 inhibitor Mirin (C), PARP inhibitor Niraparib (D) or HDAC inhibitors Entinostat and Vorinostat (E, F) over a 72-hour period, and viability was subsequently measured via the AlamarBlue assay. The viability of the untreated control for each cell variant was set at 100%, and all associated treatments were related to this value. The dotted line at 50% relative viability facilitates the reading of the IC_{50} value, which represents the concentration of a substance that results in a 50% loss of cell viability compared to the untreated control. Data presented are the mean ± SD from three independent experiments, each performed in biological quadruplicates. *$p \leq 0.05$; **$p \leq 0.01$; ***$p \leq 0.001$; significant difference compared to J82^{WT}.

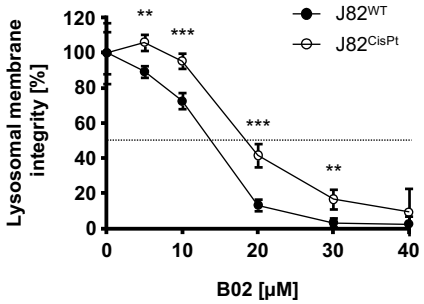

Figure 17: Comparison of cytotoxicity of RAD51 inhibitor B02 in J82^{WT} and J82^{CisPt}
J82^{WT} and J82^{CisPt} cells were treated with varying concentrations of RAD51 inhibitor B02 for 72 h and viability was assessed using the Neutral Red assay. The untreated control of each cell variant was set to 100 % viability and all associated treatments were related to this. The dotted line at 50% relative viability facilitates the reading of the IC_{50} value. This value indicates the concentration of a substance at which there is a 50% loss of viability among the cells in a given population, when compared to an untreated control. Data presented are the mean ± SD from three independent experiments, each performed in biological quadruplicates. **$p \leq 0.01$; ***$p \leq 0.001$; significant difference compared to J82^{WT}.

A summarized overview of all tested substances and the IC_{50} values of the two J82 cell variants can be found in Supplementary Table 1. To conclude, the resistance profile of J82^{CisPt} cells offers insights into the potential mechanisms underlying their acquired resistance to CisPt. The cross-resistance of J82^{CisPt} to platinum-based drugs suggests that the underlying mechanism of their CisPt resistance may be attributed to alterations in platinum-DNA-crosslink formation. In addition, the cross-resistance of J82^{CisPt} to oxidants provides evidence of the presence of enhanced detoxification mechanisms. Furthermore, the cross-resistance of the cells to the RAD51 inhibitor B02 may be indicative of an enhanced DNA damage repair capacity. For this reason, among the pharmacological inhibitors under consideration, the RAD51 inhibitor B02 is a particularly promising candidate for resensitizing the cells to cisplatin treatment. As an alternative strategy, the sensitivity of the cisplatin resistant J82 cells to replication stress-inducing substances or HDAC inhibitors may be exploited as a means of circumventing cisplatin resistance.

3.1.2 mRNA expression profiles of J82 cell variants

In order to gain an impression of the molecular changes in J82^{CisPt} that may contribute to its characteristic resistance profile observed in the cytotoxicity screening, the RNA expression of various transporters, repair factors, replication stress-associated factors, mitochondrial damage markers and senescence markers was analyzed using RT-qPCR. The factors analyzed were selected on the basis of known resistance-inducing mechanisms as well as in view of the question why J82^{CisPt} react more sensitive to replication stress-inducing substances. The aim was to investigate basal differences between the two J82 cell variants and the influence of cisplatin treatment on their mRNA expression profiles.

Under basal conditions the mRNA expression of various transport proteins was different in J82^{CisPt} cells in comparison to J82^{WT} cells (Figure 18). Namely, ATP7A and BCRP showed increased expression, while ATP7B, MATE1, MDR1 and OCT2 were expressed less. Looking at DNA repair factors, J82^{CisPt} showed an upregulation of the RAD51 paralogs RAD51B and RAD51D on the mRNA level, while RAD51 itself was not differently expressed between both cell variants. Other factors of the homologous recombination repair pathway e.g. MRE11, RAD50 or RAD52 also did not show any differences in mRNA levels. All analyzed factors important for replicative stress response and cell cycle arrest like CHK1/2 and CDC25a/c did not show altered mRNA expression in J82^{CisPt}. Also, factors involved in mitochondrial damage response were not differentially expressed. Furthermore, J82^{CisPt} showed about 3.5-fold higher mRNA expression of senescence-related cytokines IL-6 and IL-8 than J82^{WT}, but not of other senescence-related factors analyzed.

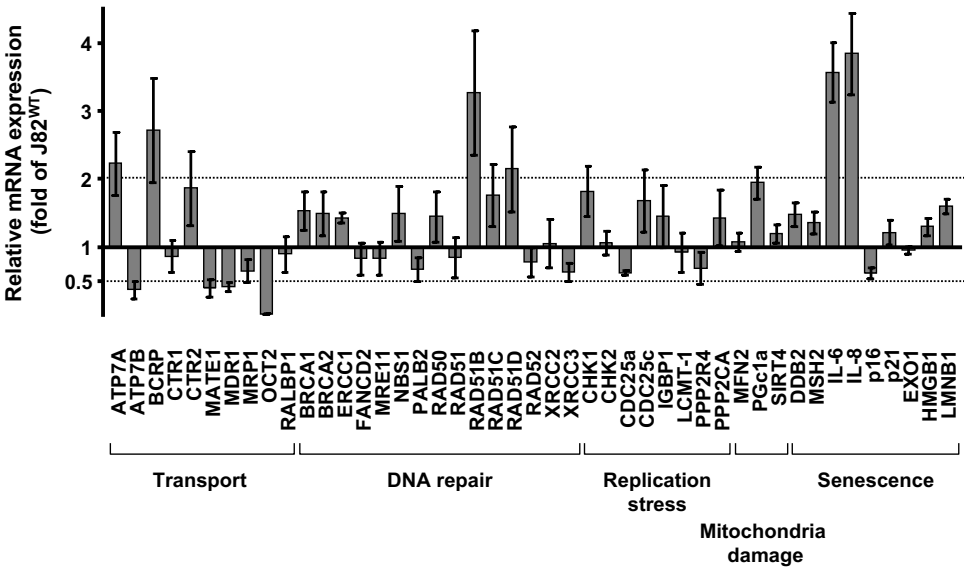

Figure 18: mRNA expression of factors potentially involved in acquired cisplatin resistance compared in J82^{WT} and J82^{CisPt} under basal conditions
RNA from three independent experiments was pooled before cDNA synthesis. Thresholds for increased/decreased mRNA expression were set at 2-fold difference between J82^{CisPt} vs. J82^{WT} (dotted lines). Data presented are the mean ± SD from technical triplicates.

After 24 h treatment with 10 µM cisplatin, the mRNA expression of various transporters was altered in J82^{WT} cells with ATP7A, ATP7B and MRP1 being downregulated and CTR2 upregulated, while in J82^{CisPt} there was no altered mRNA expression of the analyzed transporters (Figure 19). Concerning repair factors, both cell variants showed downregulation of RAD51B mRNA. J82^{CisPt} slightly upregulated RAD51 mRNA in response to CisPt treatment, although with high standard deviation, while J82^{WT} upregulated repair factors BRCA1, XRCC2 and XRCC3. In J82^{WT} CisPt treatment induced the mRNA upregulation of cell cycle regulator CHK1, while in J82^{CisPt} there was

a weak upregulation of CHK2. Both cell variants had upregulated mRNA expression of CDC25a, this effect being stronger in J82^{WT} than in J82^{CisPt}. In J82^{WT} additionally weak upregulation of CDC25c, IGBP1 and PPP2CA mRNA was detected. Looking at mitochondria damage markers, J82^{WT} had upregulated mRNA levels of MFN2, and both cell variants showed an upregulation of SIRT4, which was stronger in J82^{WT}. J82^{WT} also upregulated a variety of senescence-related markers to different extent, namely DDB2, IL-6, IL-8, p21, EXO1 and HMGB1. p21 and EXO1 were also found upregulated in J82^{CisPt}, but not as strong as in J82^{WT}.

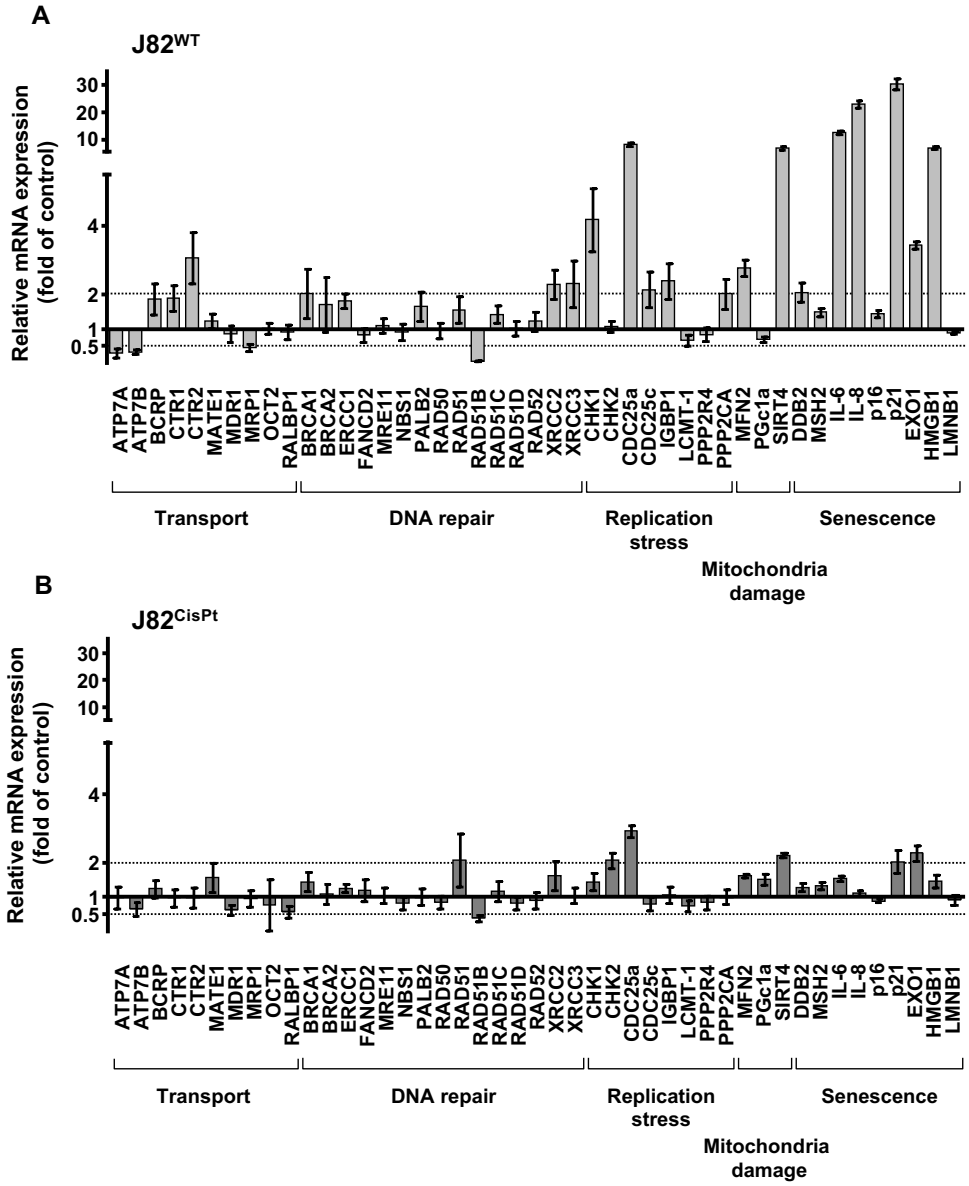

Figure 19: mRNA expression of factors potentially involved in acquired cisplatin resistance compared in J82^{WT} and J82^{CisPt} after cisplatin treatment

Cells were treated for 24 h with 10 µM cisplatin before mRNA expression analysis of selected factors by RT-qPCR. The respective untreated control was set to 1.0 and the cisplatin response of J82^{WT} (A) or J82^{CisPt} (B) was related to this. Thresholds for increased/decreased mRNA expression were set at 2-fold difference between CisPt treated vs. respective untreated (dotted lines). cDNA used for mRNA expression analyses was generated from pooled samples of three independent experiments and data presented are the mean ± SD from technical triplicates.

In summary, the results of the mRNA analysis suggest that altered expression of drug transport proteins, RAD51 paralogs involved in DNA repair, or senescence-associated interleukins in untreated $J82^{CisPt}$ may be associated with the mechanism of cisplatin resistance in these cells. In response to CisPt treatment, $J82^{WT}$ exhibited alterations in mRNA expression of a plethora of factors involved in transport, DNA repair, cell cycle arrest, mitochondrial damage response and senescence. In contrast, $J82^{CisPt}$ demonstrated a relatively stable mRNA expression profile, which may be attributed to their reduced sensitivity to cisplatin.

3.1.3 Proteome analysis of J82 cell variants

Next, it should be investigated whether the differences observed on the mRNA level are reflected at the protein level or whether other changes in the expression pattern of proteins can provide an indication of the cisplatin resistance mechanism in $J82^{CisPt}$. To this end, a broad-based screening was carried out using proteome analysis, which was conducted at the BMFZ Düsseldorf. A basal comparison of the proteome of the two J82 cell variants was performed and their altered expression pattern after administration of an equimolar concentration of cisplatin was analyzed.

In total 4324 proteins were detected in the cells under basal conditions. Thereof, the majority was not differentially regulated, still 75 proteins were upregulated and 82 proteins were downregulated in $J82^{CisPt}$ when comparing them to $J82^{WT}$ (Figure 20A, B). Among the upregulated proteins were e.g. the catalytic subunit of DNA polymerase α (POLA1), which is essential for initiation of DNA synthesis, or centrosomal protein of 55 kDa (CEP55), which is important for successful cytokinesis. All differentially expressed proteins were subjected to a KEGG pathway analysis clustering proteins into groups for biological relatedness. One protein can thereby also be assigned to several distinct groups. The most highly represented KEGG pathway upregulated in $J82^{CisPt}$ was “endocytosis” with six proteins, namely ADP ribosylation factor guanine nucleotide exchange factor 1, RAD11 family interacting protein 5, ADP ribosylation factor GTPase activating protein 3, amphiphysin, major histocompatibility complex class I and SMAD family member 3 (Figure 20C, Supplementary Table 2). The KEGG pathway with the most proteins downregulated in $J82^{CisPt}$ was “metabolic pathways” with 15 members (aldehyde dehydrogenase 1 family member L1, 5'-aminolevulinate synthase 1, ferrochelatase, monoamine oxidase A, quinolinate phosphoribosyltransferase, glutaryl-CoA dehydrogenase, aldehyde dehydrogenase 6 family member A1, asparagine synthetase, dehydrogenase E1 and transketolase domain containing 1, aldehyde dehydrogenase 5 family member A1, L-2-hydroxyglutarate dehydrogenase, acetylserotonin O-methyltransferase like,

nicotinate phosphoribosyltransferase, palmitoyl-protein thioesterase 2 and serine palmitoyltransferase long chain base subunit 2. In contrast, four proteins of the "metabolic pathways" cluster were also upregulated, namely fumarylacetoacetate hydrolase, acyl-CoA synthetase long chain family member 5, lysophosphatidylcholine acyltransferase 2 and glycerol-3-phosphate acyltransferase 3 (Supplementary Table 3). The KEGG pathway called "pathways in cancer" was also represented in both directions with some proteins upregulated in J82^{CisPt} and others downregulated. Upregulated members of this pathway were SMAD3, nuclear factor kappa B subunit 2, platelet derived growth factor receptor beta and Rac family small GTPase 2, while fibroblast growth factor 2, laminin subunit beta 2 and transforming growth factor beta 2 showed lower protein occurrence in J82^{CisPt} than in J82^{WT}. A list of all under basal conditions differentially regulated proteins and if applicable their classification in the KEGG pathways can be seen in Supplementary Table 2 and Supplementary Table 3.

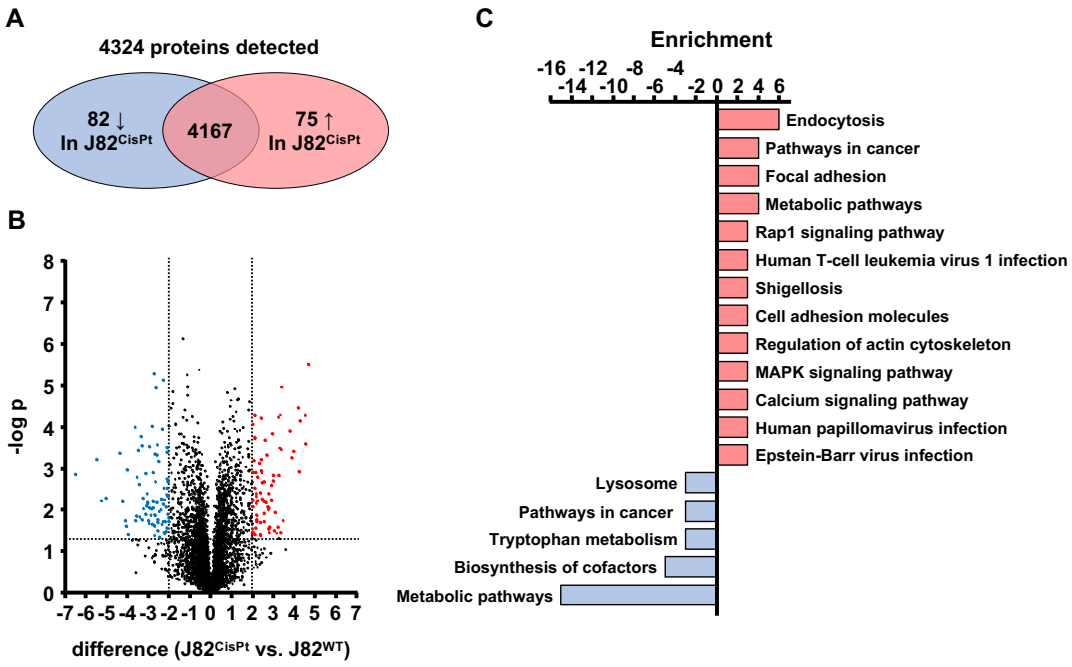

Figure 20: Proteome analysis of J82^{CisPt} vs. J82^{WT} under basal conditions
Data is presented as Venn diagram (A) and as Volcano plot (B), with proteins upregulated in J82^{CisPt} indicated in red and proteins downregulated in J82^{CisPt} indicated in blue. Thresholds for increased/decreased protein expression were set at 2-fold difference between J82^{CisPt} vs. J82^{WT} and -log p ≥ 1.3 (corresponding to p ≤ 0.05). Differentially regulated proteins were clustered into KEGG pathways and enrichment of pathways with three or more representatives are shown (C). Proteome data was generated from biological triplicates.

After treatment of the two cell variants with 10 µM cisplatin for 24 h, not many proteins showed an altered expression compared to the basal state. In J82^{WT} only two proteins were found upregulated after cisplatin treatment, namely the actin cytoskeleton organizer Cdc42 effector protein 4 and glutamine synthetase, which converts glutamate and

ammonia to glutamine (Figure 21A, B). Downregulated were several proteins required for ribosome biogenesis, like ATP-dependent helicase DDX52, ribosome biogenesis protein BMS1, ribosome production factor 1 and ribosome biogenesis protein NSA2 homolog. Through their importance in ribosome biogenesis these factors indirectly influence the process of translation needed for protein biosynthesis. Other downregulated proteins play a role in cell adhesion and organization of the cytoskeleton. Those include transforming growth factor-beta-induced protein ig-h3, laminin subunit beta-2, collagen alpha-1(V) chain and collagen alpha-1(XII) chain. Besides this, downregulated proteins were involved in transcriptional regulation (polycomb group protein ASXL1), neural development (teneurin-3), organogenesis in general (neuropilin-1) as well as endocytosis and phagocytosis of apoptotic cells (prolow-density lipoprotein receptor-related protein 1).
In $J82^{CisPt}$ four proteins were upregulated after CisPt treatment, of which two are involved in cell cycle processes (Figure 21C, D). Those two were sororin, which is a regulator of sister chromatid cohesion in mitosis, and cell division cycle protein 16 homolog as component of an E3 ubiquitin ligase that controls progression through mitosis and the G1-phase. In addition, AP-1 complex subunit sigma-2, that plays a role in protein sorting in the late-Golgi/trans-Golgi network and endosomes, and the mitochondrial protein glutathione s-transferase 3, important for cellular detoxification, showed increased occurrence. Interestingly, only one protein was found to be downregulated in $J82^{CisPt}$ after incubation with CisPt and that was DDB1- and CUL4-associated factor 13, which is part of a precursor of the small eukaryotic ribosomal subunit.

In summary the differences between $J82^{WT}$ and $J82^{CisPt}$ found on the mRNA level (see chapter 3.1.2) were not reflected on the protein level in the proteome analysis. As indicated by the KEGG pathway analysis, $J82^{CisPt}$ exhibit the most pronounced expression alterations compared to $J82^{WT}$ in proteins associated with endocytosis and metabolic signaling, as well as proteins already identified as being frequently mutated in cancer. Accordingly, alterations in these processes may potentially contribute to the cisplatin resistant phenotype of $J82^{CisPt}$. Moreover, elevated expression of proteins involved in DNA synthesis and mitotic cell division may provide an indication of the cisplatin resistance mechanism of in $J82^{CisPt}$. In addition, the proteome analysis demonstrated that cisplatin treatment altered the protein expression of completely disparate factors in $J82^{WT}$ and $J82^{CisPt}$, suggesting that divergent mechanisms are initiated by the drug in the two cell variants.

A

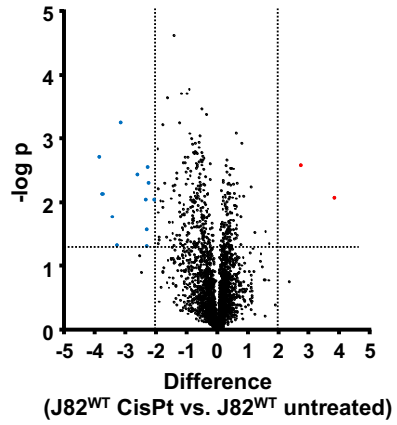

B

Protein	Diff	-log p
Cdc42 effector protein 4	3.85	2.08
Glutamine synthetase	2.73	2.58
ATP-dependend helicase DDX52	-2.06	2.04
Ribosome biogenesis protein BMS1	-2.25	2.30
Transforming growth factor-beta-induced protein ig-h3	-2.28	2.56
Polycomb group protein ASXL1	-2.31	1.31
Teneurin-3	-2.31	1.58
Prolow-density lipoprotein receptor-related protein 1	-2.34	2.05
Laminin subunit beta-2	-2.59	2.44
Ribosome production factor 1	-3.15	3.25
Neuropilin-1	-3.28	1.32
Collagen alpha-1(V) chain	-3.41	1.77
Collagen alpha-1(XII) chain	-3.75	2.13
Ribosome biogenesis protein NSA2 homolog	-3.85	2.71

C

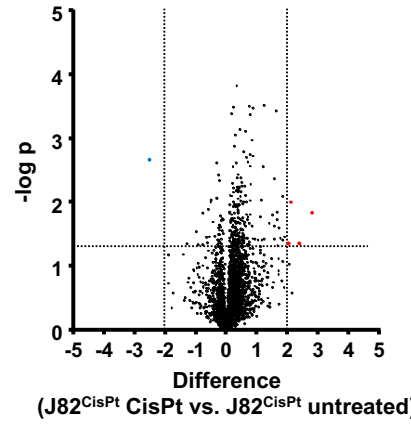

D

Protein	Diff	-log p
Sororin	2.80	1.84
AP-1 complex subunit sigma-2	2.39	1.35
Glutathione S-transferase 3	2.11	2.00
Cell division cycle protein 16 homolog	2.03	1.36
DDB1- and CUL4-associated factor 13	-2.51	2.66

Figure 21: Proteome analysis of J82^{WT} and J82^{CisPt} cells after cisplatin treatment
Cells were treated for 24 h with 10 µM cisplatin prior to proteome analyses. Data is presented as volcano plot in (A) for J82^{WT} and in (C) for J82^{CisPt}, with proteins upregulated after CisPt treatment indicated in red and proteins downregulated in their expression after CisPt treatment indicated in blue. Thresholds for increased/decreased expression were set at 2-fold difference between CisPt treated vs. respective untreated and -log p ≥ 1.3 (corresponding to p ≤ 0.05). Differentially regulated proteins are listed in (B) for J82^{WT} and in (D) for J82^{CisPt}. Proteome data was generated from biological triplicates.

3.1.4 CisPt-DNA-adduct formation in J82 cell variants

To examine if the cisplatin resistance in J82^{CisPt} cells might be due to altered drug uptake, DNA accessibility or monoadduct to crosslink conversion, the formation of CisPt-DNA intrastrand crosslinks after CisPt treatment was compared in J82^{WT} and J82^{CisPt} by Southwestern blot analyses. A short-term treatment with CisPt of 4 h thereby depicts the initial formation of Pt(GpG) adducts, while a 24 h continuous treatment reflects a steady state between monoadduct formation and their conversion into crosslinks.

When treating J82^{WT} and J82^{CisPt} cells with various equimolar concentrations of CisPt for 4 h, J82^{CisPt} showed a significantly lower level of Pt(GpG) adducts (Figure 22).

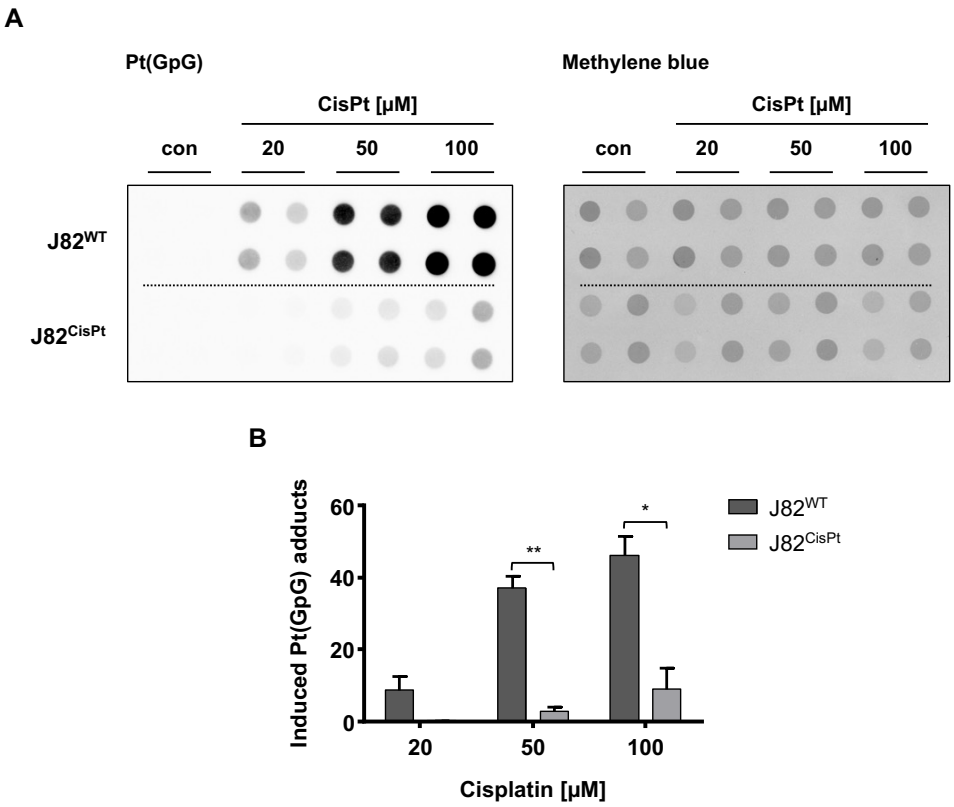

Figure 22: Cisplatin adduct formation in J82^{WT} and J82^{CisPt} after short-term treatment with equimolar concentrations of cisplatin
J82^{WT} and J82^{CisPt} cells were treated for 4 h with different equimolar concentrations of cisplatin before cisplatin adduct (Pt(GpG)) formation was measured by Southwestern blot analysis.
A: Pt(GpG) signal of the performed Southwestern blot (left). Methylene blue was used as a loading control (right). Biological duplicates were applied in a horizontal arrangement, with a technical duplicate positioned vertically alongside each sample.
B: Quantification of the Southwestern blot shown in (A). Pt(GpG) signals were related to the respective methylene blue signals to normalize on DNA content. The resulting normalized values were related to the untreated control (con) of the respective cell variant to obtain induced Pt(GpG) adducts. Data shown are the mean + SD. *$p \leq 0.05$; **$p \leq 0.01$; significant difference between J82^{CisPt} vs. J82^{WT}.

For a second Southwestern blot analysis not only an equimolar CisPt concentration, but also equitoxic CisPt concentrations, meaning concentrations evoking comparable amounts of cytotoxicity, were chosen based on the results of the cytotoxicity measurements after 72 h treatment (Figure 13B). Chosen concentrations were around the IC_{40} (2 µM in J82^{WT} vs. 10 µM in J82^{CisPt}), IC_{60} (5 µM in J82^{WT} vs. 20 µM in J82^{CisPt}) and IC_{80} (10 µM in J82^{WT} vs. 50 µM in J82^{CisPt}). This time cells were treated for 24 h prior to analysis. Again, J82^{CisPt} showed less formation of Pt(GpG) adducts comparing to J82^{WT} with the equimolar concentration of 10 µM CisPt. At the same time both cell variants showed induction of Pt(GpG) adduct formation to similar extent with all equitoxic concentrations of CisPt (Figure 23A, B). The induced CisPt adducts correlate negatively with the measured viability after 72 h in both cell variants without differing significantly (Figure 23C).

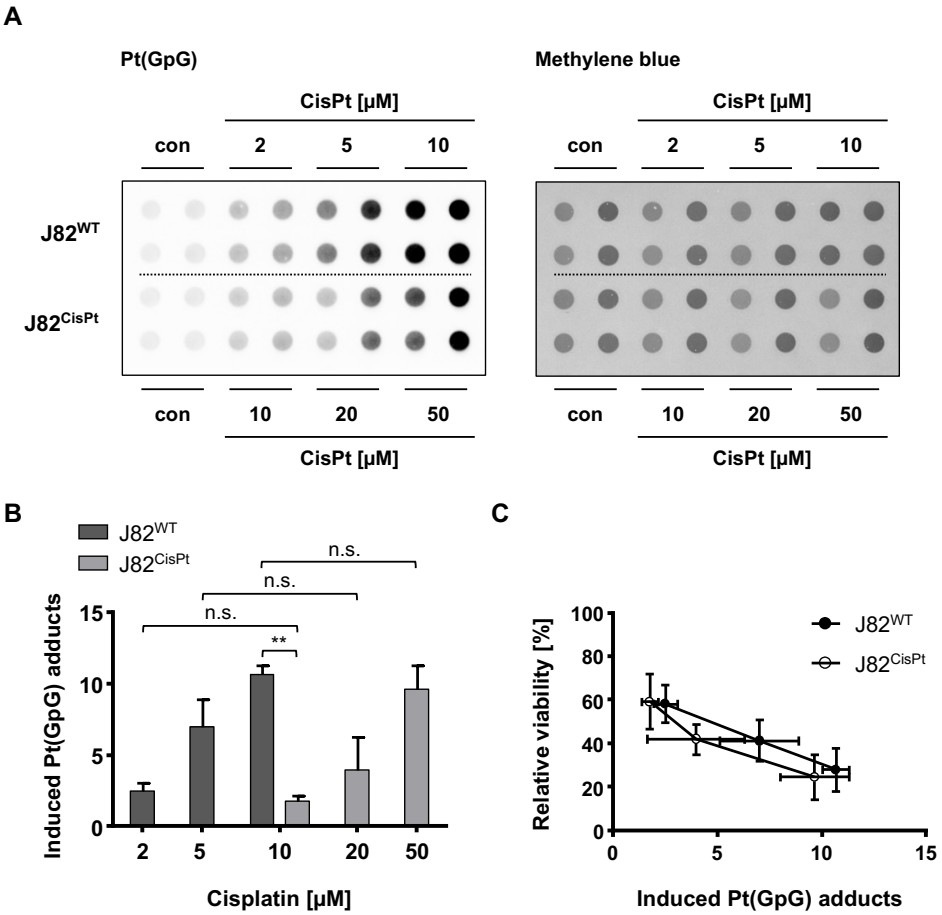

Figure 23: Cisplatin adduct formation in J82^{WT} and J82^{CisPt} after long-term treatment with equitoxic concentrations of cisplatin
J82^{WT} and J82^{CisPt} cells were treated for 24 h with different equitoxic concentrations of cisplatin before cisplatin adduct (Pt(GpG)) formation was measured by Southwestern blot analysis.
A: Pt(GpG) signal of the performed Southwestern blot (left). Methylene blue was used as a loading control (right). Biological duplicates were applied in a horizontal arrangement, with a technical duplicate positioned vertically alongside each sample.
B: Quantification of the Southwestern blot shown (A). Pt(GpG) signals were related to the respective methylene blue signals to normalize on DNA content. The resulting normalized values were related to the untreated control (con) of the respective cell variant to obtain induced Pt(GpG) adducts. Data shown are the mean + SD. n.s.: not significant different; **$p \leq 0.01$; significant difference between J82^{CisPt} vs. J82^{WT}.
C: The numbers of induced Pt(GpG) adducts from (B) were plotted against the previously measured viability of the respective cells after 72 h CisPt treatment (n = 3). Data shown are the mean ± SD.

In conclusion, the significantly reduced formation of CisPt-DNA adducts in J82^{CisPt} cells when compared to J82^{WT} cells following treatment with equimolar concentrations of CisPt may represent a component of the cisplatin resistance mechanism in J82^{CisPt} cells. It is a plausible hypothesis that the reduced adduct formation may be the consequence of decreased drug uptake, reduced DNA accessibility or a time delay in the conversion of monoadducts to crosslinks.

3.1.5 Signs for chromosomal instability in J82^{CisPt}

It was noticed during immunocytochemical staining that nuclei of non-mitotic J82^{CisPt} cells show abnormalities associated with chromosomal instability, such as chromatin bridges, mis-shaped nuclei or small round chromatin-containing structures attached to cell nuclei (Figure 24).

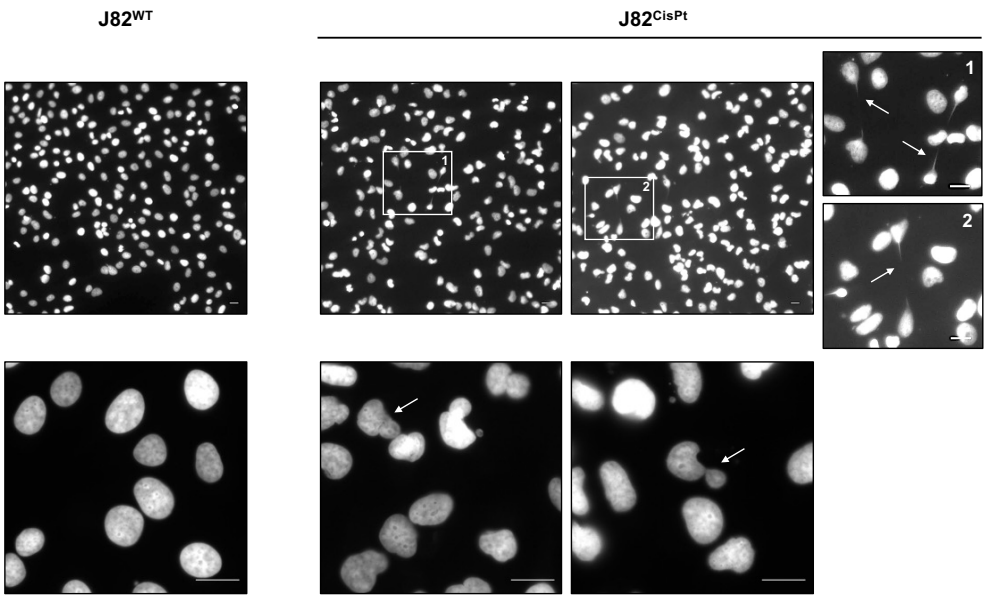

Figure 24: Signs of chromosomal instability in J82^{CisPt} under basal conditions
Representative microscopic images (DAPI staining) of nuclei of untreated J82^{WT} and J82^{CisPt} cells. Chromatin bridges and mis-shaped nuclei with chromatin-containing attachments, which were frequently observed in J82^{CisPt} cells, are highlighted by white arrows. The scale bars correspond to 20 µm.

Such malformations and chromosomal instability can occur due to the inefficient distribution of chromatin in mitosis. The formation of a functional spindle apparatus is an essential step for preventing this. Mitosis is made up of prophase, metaphase, anaphase and telophase. In prophase, the chromosomes are condensed, the nuclear envelope breaks down and the mitotic spindles begin to form and bind to chromosomes at their centromeres. In metaphase, the chromosomes line up at the middle of the cell. In anaphase, the sister chromatids are pulled apart by the spindles towards opposite ends of the cell. In telophase, the mitotic spindles are disassembled, the chromosomes decondense and the nuclear membrane re-forms. These different phases can be distinguished from one another by applying an immunocytochemical staining for centrosome marker pericentrin and spindle marker α-tubulin together with chromatin staining by DAPI. When comparing mitotic J82^{WT} and J82^{CisPt} cells under basal conditions, it is noticeable that J82^{CisPt} showed a high percentage of cells in pro-metaphase, a stage in the conversion from prophase to metaphase, and at the same time less cells in metaphase and anaphase (Figure 25). J82^{CisPt} also showed an almost 2-fold higher proportion of abnormal mitotic cells than J82^{WT}. These mitotic

malformations include monopolar or apolar cells that have formed only one centrosome or none at all. More than two centrosomes per cell also represent an abnormality. In addition, both centrosomes must be located on opposite sides of the chromatin in order to divide it properly.

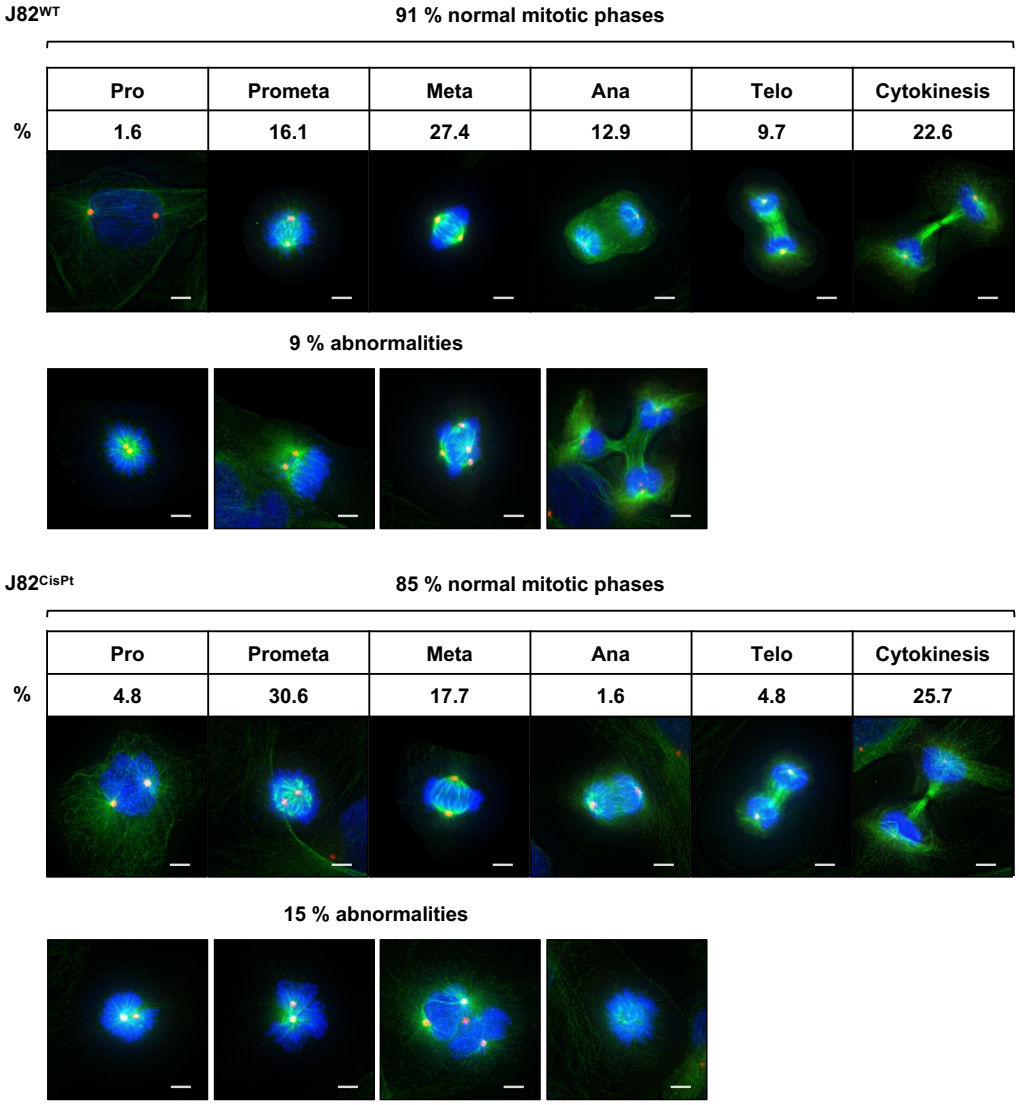

Figure 25: Staining of spindle apparatus markers in J82^{WT} and J82^{CisPt} under basal conditions
Spindle marker α-tubulin (green), centrosome marker pericentrin (red) and chromatin dye DAPI (blue) were co-stained in J82^{WT} and J82^{CisPt} cells. Fifty mitotic J82^{WT} and J82^{CisPt} cells were analyzed for quantification of different mitotic stages (pro-, prometa-, meta-, ana-, telophase and cytokinesis) and abnormalities. The scale bars correspond to 5 µm.

Overall, the alteration in the ratio of cells in the different mitotic phases suggests that J82^{CisPt} cells spend a longer period of time in the early stages of mitosis than J82^{WT} cells. The additional observation of a high proportion of mitotic spindle malformations in J82^{CisPt} may be the underlying cause of the presence of malformed nuclei and chromatin bridges in these cells.

3.2 Molecular differences between J82^{WT} and J82^{CisPt} in their response to RAD51$_i$ B02

Compared to J82^{WT}, J82^{CisPt} cells showed resistance to the RAD51 inhibitor B02 in terms of cytotoxicity (Figure 16A). Based on this, it was hypothesized that the DNA repair factor RAD51 might play a role in their CisPt resistance and further comparative studies were performed on the response of the two cell variants after treatment with B02.

3.2.1 Inhibition of RAD51 foci formation by B02 after irradiation

To rule out the possibility that resistance to the inhibitor is due to mutations/conformational changes in the RAD51 protein and thus the inability of the inhibitor to bind its target, the capability of B02 to inhibit of RAD51 foci formation was evaluated comparatively in J82^{WT} and J82^{CisPt}. Irradiation, known to induce RAD51 foci formation, was used in this context as response enhancer to see the inhibitory effect more clearly (Haaf *et al.*, 1995; Sak *et al.*, 2005). The basal number of RAD51 foci per nucleus were on the same level in J82^{WT} and J82^{CisPt} (Figure 26). After irradiation there was a significant increase of RAD51 foci in both cell variants. This increase was slightly stronger in J82^{CisPt} cells, but not statistically different to J82^{WT}. When treating cells with B02 before irradiation, the number of RAD51 foci was significantly lower than after irradiation alone, with foci numbers per nucleus approximately at basal levels in both cell variants. This effect was shown for two concentrations of B02. The comparable reduction in the formation of RAD51 foci following irradiation in J82^{WT} cells and J82^{CisPt} cells treated with B02 demonstrates that the RAD51 inhibitor can bind to its target protein equally in both cell variants.

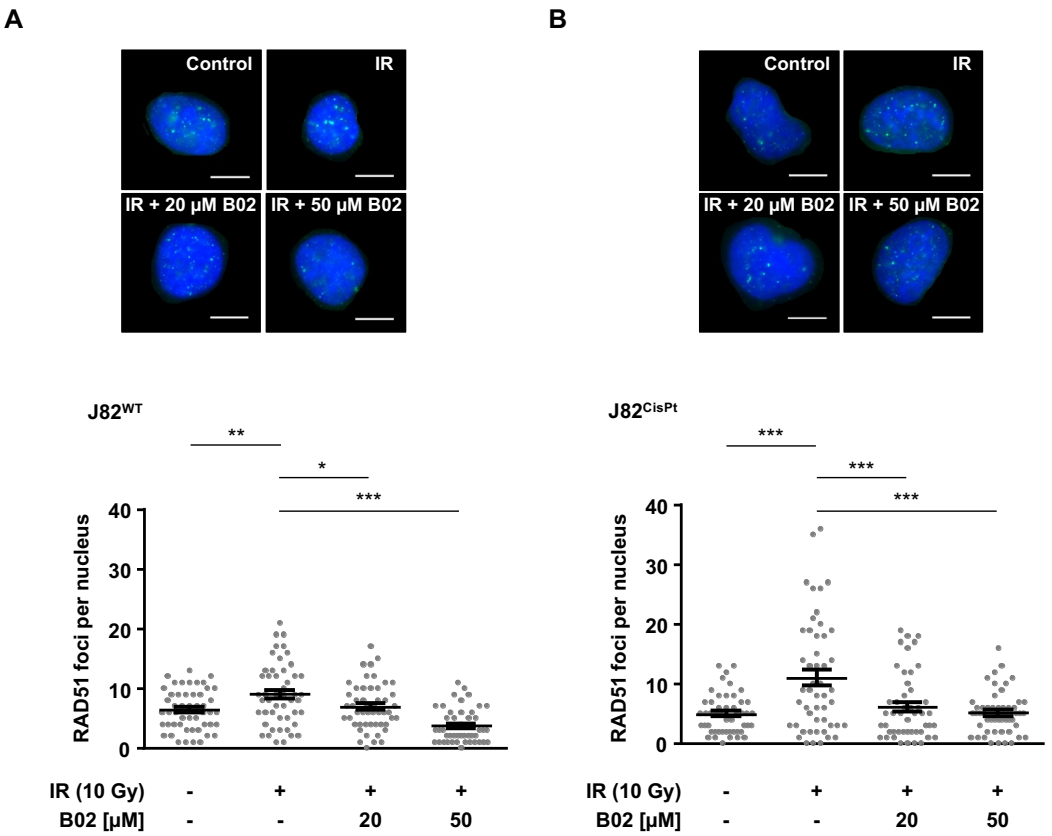

Figure 26: RAD51 foci formation in J82^{WT} and J82^{CisPt} after irradiation and RAD51 inhibition by B02
The formation of RAD51 foci in the nuclei of J82^{WT} cells (A) and J82^{CisPt} cells (B) was analyzed via immunocytochemical staining 3 h after irradiation (IR) with 10 Gy. For some groups, the RAD51 inhibitor B02 was added 30 minutes before IR. Data are shown with each dot representing one analyzed nucleus and the black lines showing the mean ± SEM from 50 nuclei. The scale bars in the representative pictures correspond to 10 µm. *$p \leq 0.05$; **$p \leq 0.01$; ***$p \leq 0.001$

3.2.2 Interplay of RAD51 inhibition and CisPt-DNA-adduct formation

To investigate whether there is an interplay between RAD51 inhibition and the formation of CisPt-DNA adducts, Southwestern blot analysis was used. J82^{WT} and J82^{CisPt} cells were treated with equimolar concentrations of CisPt or/and RAD51$_i$ B02 for 24 h. As expected, no adducts were detected with B02 alone in both cell variants (Figure 27). The previous result that more DNA adducts were measured in J82^{WT} than in J82^{CisPt} at the same concentration of CisPt was again confirmed. It was found that RAD51 inhibition by B02 did not alter the induction of CisPt-DNA adducts significantly at the concentrations tested. This result demonstrates that the DNA repair factor RAD51 exerts no notable influence on the formation of CisPt-DNA adducts.

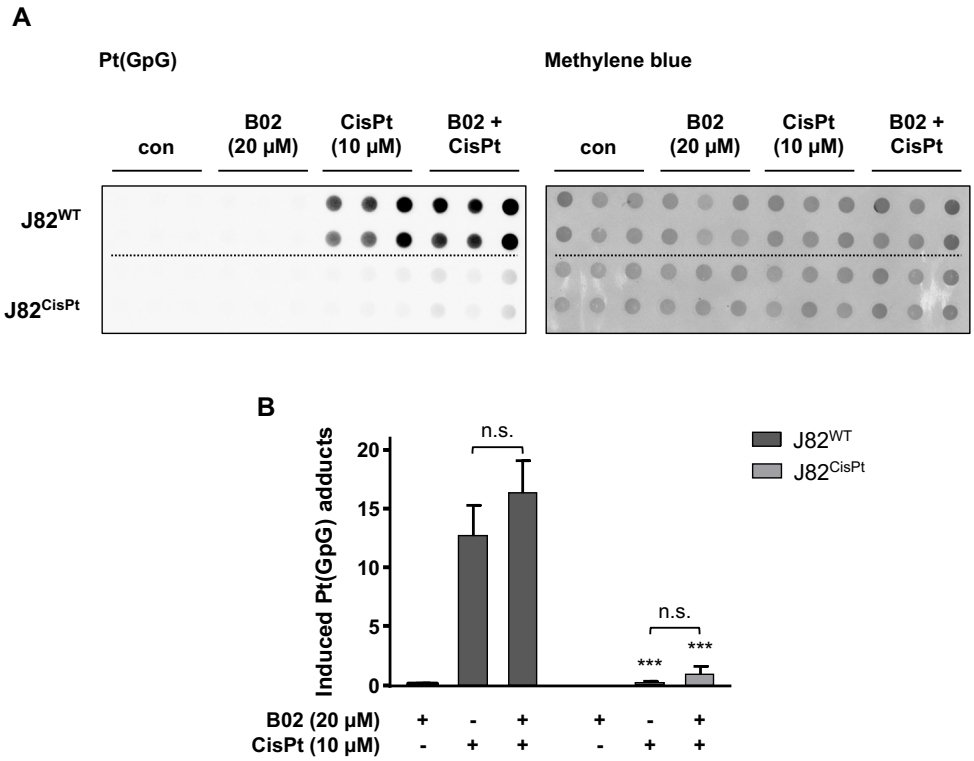

Figure 27: Cisplatin adduct formation in J82^{WT} and J82^{CisPt} after 24 h treatment with cisplatin and B02
J82^{WT} and J82^{CisPt} cells were treated for 24 h with the indicated concentrations of cisplatin or/and B02 before cisplatin adduct (Pt(GpG)) formation was measured by Southwestern blot analysis.
A: Pt(GpG) signal of the performed Southwestern blot (left). Methylene blue was used as a loading control (right). Biological triplicates were applied in a horizontal arrangement, with a technical duplicate positioned vertically alongside each sample.
B: Quantification of the southwestern blot shown (A). Pt(GpG) signals were related to the respective methylene blue signals to normalize on DNA content. The resulting normalized values were related to the untreated control (con) of the respective cell variant to obtain induced Pt(GpG) adducts. Data shown are the mean + SD. ***$p \leq 0.001$; significant difference compared to J82^{WT} (*). No significant differences (n.s.) were obtained when comparing the respective CisPt + B02 combination-treatment vs. CisPt mono-treatment.

3.2.3 mRNA expression profiles after B02 treatment

mRNA expression profiles of selected factors were analyzed in J82^{WT} and J82^{CisPt} by qRT-PCR after 24 h treatment with 20 µM B02 (Figure 28). Concerning transporters, both

cell variants showed an upregulation of ATP7A and CTR1 mRNA after treatment. In addition to that, J82^{WT} had an increased mRNA expression of CTR2 and MDR1. B02 treatment upregulated the mRNA expression of DNA repair factors BRCA1, BRCA2 and XRCC2 in J82^{WT} as well as in J82^{CisPt}. In J82^{WT} cells additionally RAD51B was found to be upregulated. RAD51 itself did not show altered mRNA expression levels in any cell variant. mRNA expression of CHK2 and CDC25a was increased in both cell variants, whereas mRNA expression of CHK1 and CDC25c was increased only in J82^{WT}. Furthermore, only J82^{WT} showed upregulated mRNA expression of MFN2 and SIRT4, two factors involved in mitochondrial damage response. Among the senescence-related factors analyzed, both cell variants showed a downregulation in mRNA of IL-6 and

an upregulation in mRNA of p21 and HMGB1. J82^{CisPt} additionally had an increased level of IL-8 mRNA.

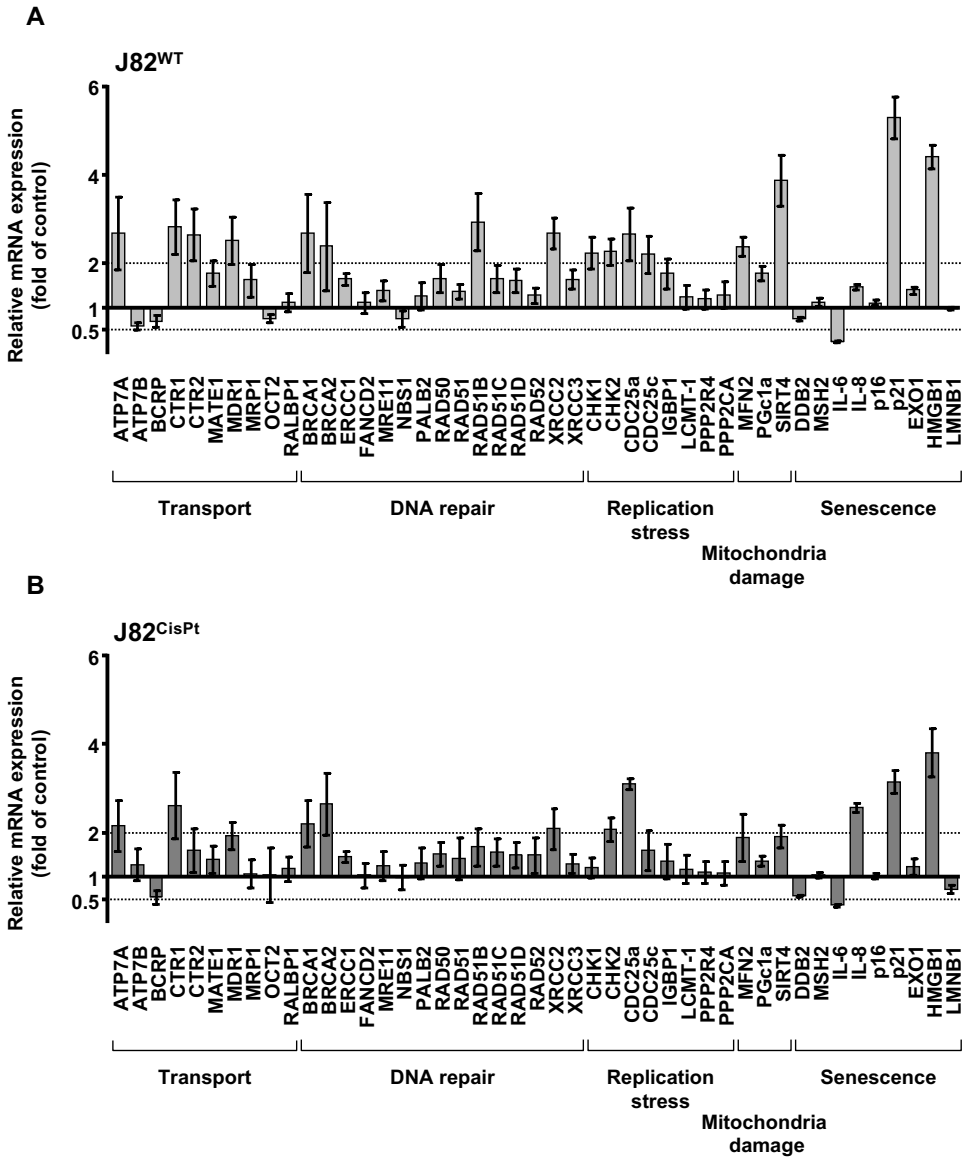

Figure 28: mRNA expression of factors potentially involved in B02 resistance compared in J82^{WT} and J82^{CisPt} after B02 treatment

Cells were treated for 24 h with 20 µM B02 before mRNA expression analysis of selected factors by RT-qPCR. The respective untreated control was set to 1.0 and B02 treatment of J82^{WT} (A) or J82^{CisPt} (B) was related to this. Thresholds for increased/decreased mRNA expression were set at 2-fold difference between B02 treated vs. respective untreated (dotted lines). cDNA used for mRNA expression analyses was generated from pooled samples of three independent experiments and data presented are the mean ± SD from technical triplicates.

In summary, B02 generally induced comparable alterations in the mRNA expression in both J82 cell variants. Still, J82^{CisPt} demonstrated a relatively weaker response, as anticipated, due to its resistance to the inhibitor. The increased mRNA expression of CHK1/2 and CDC25a/c provide evidence that B02 may induce cell cycle arrest in both J82 cell variants. Moreover, the results of the mRNA analysis suggest that B02

potentially triggers senescence. The increased mRNA expression of mitochondria damage response factors in J82^{WT} cells may be indicative of mitochondrial damage induction by B02 specifically in this cell variant.

3.2.4 Influence of RAD51 inhibition on cell cycle and mitotic progression

Cell cycle analyses in the flow cytometer showed that a G2/M-phase arrest occurred in J82^{WT} after 24 h treatment with 20 µM B02, which was not present in J82^{CisPt} (Figure 29). In both cell variants, however, a slight increase in the SubG1 fraction was already visible to the same extent at this time. After 72 h of treatment, a similar picture was seen with 10 µM B02, although this time the induction of SubG1 was more pronounced in J82^{WT} than in J82^{CisPt}. Interestingly, both cell variants showed a similarly strong induction of SubG1 after 72 h treatment with 20 µM B02.

The data on cell cycle progression demonstrate that B02 is capable of inducing G2/M cell cycle arrest in J82^{WT} cells, but not in J82^{CisPt}. Given the comparable degree of induction of the SubG1 fraction by 72 h treatment with 20 µM B02 in J82^{WT} and J82^{CisPt}, which does not align with the dissimilarity in viability reduction, it is plausible that the loss of viability is not solely attributable to cell death mechanisms.

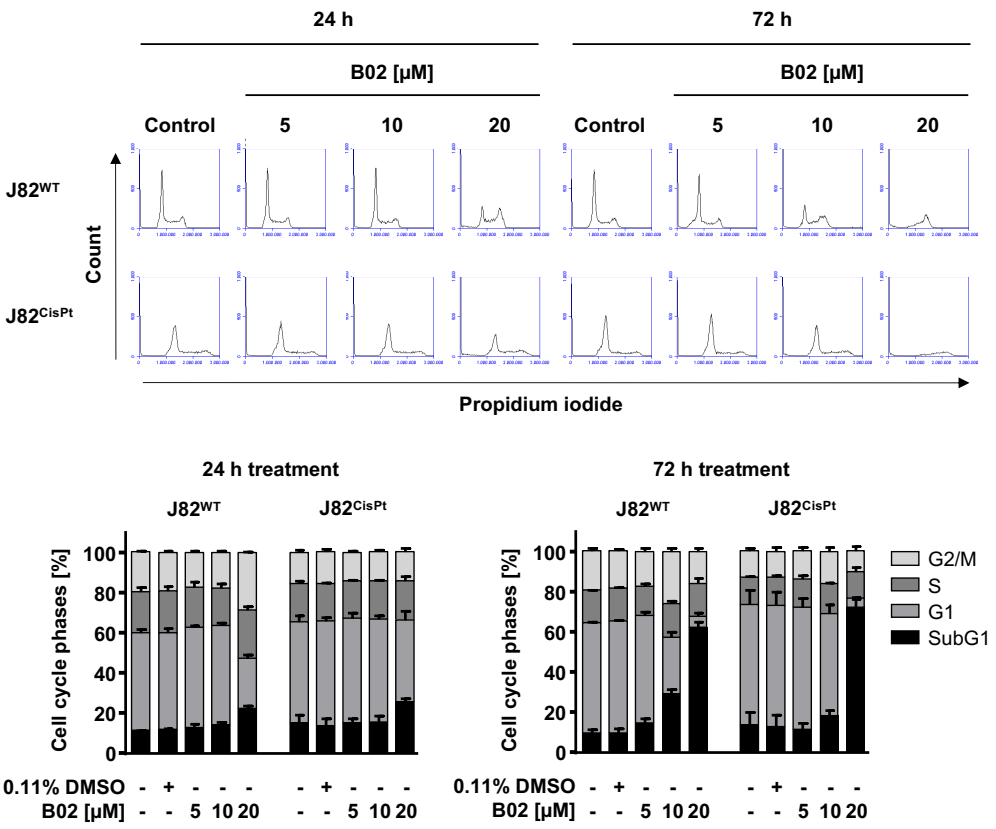

Figure 29: Cell cycle distribution analyses in J82^{WT} and J82^{CisPt} after treatment with RAD51$_i$ B02
Cells were treated for 24 h or 72 h with the indicated concentrations of B02 before cell cycle distribution was analyzed by flow cytometric analysis employing propidium iodide staining. DMSO was included in the study as solvent control. Data are presented as mean + SD from n = 3 independent experiments.

Normally, as cytotoxicity increases with higher concentrations of a substance, the percentage of dividing cells in a cell population decreases. Remarkably, immunocytochemical staining of phosphorylated histone 3 at Serine 10 (pH3) as marker for mitotic cells showed an increase in the number of pH3 positive cells after 24 h treatment with 20 µM B02. This effect was in the mean stronger in $J82^{WT}$ cells than in $J82^{CisPt}$ cells, yet no statistically significant difference was noted between the two cell variants (Figure 30).

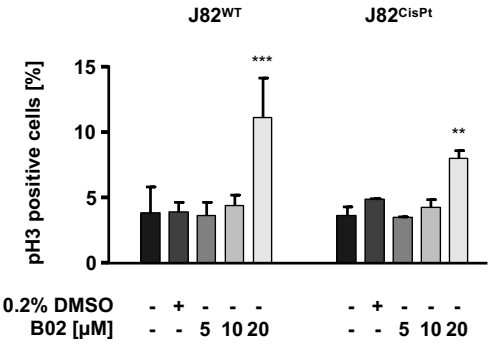

Figure 30: Phospho histone 3 (pH3) staining of $J82^{WT}$ and $J82^{CisPt}$ cells treated with B02
Cells were incubated with different concentrations of B02 as indicated for 24 h before immunocytochemical staining for pH3. DMSO was included in the study as solvent control. Data are presented as mean + SD and were derived from two to five independent experiments, where in each case 1000 – 2000 nuclei per sample were analyzed. **p ≤ 0.01; ***p ≤ 0.001; significant compared to control of the respective cell variant.

To examine whether histone 3 was phosphorylated independently of mitosis in response to RAD51 inhibition, flow cytometric analysis of cell cycle distribution was conducted in combination with pH3 staining. This revealed that pH3 signal was still exclusively emitted by cells with doubled chromosome content after B02 treatment (Figure 31). Further, this read-out confirmed the former finding that the number of pH3 positive cells increased with 20 µM B02 treatment and this effect appeared to be stronger in $J82^{WT}$ than in $J82^{CisPt}$. As a control, CisPt was also included in the study. As expected, CisPt treatment caused a reduction in the pH3 signal, which was more pronounced in $J82^{WT}$ than in $J82^{CisPt}$.

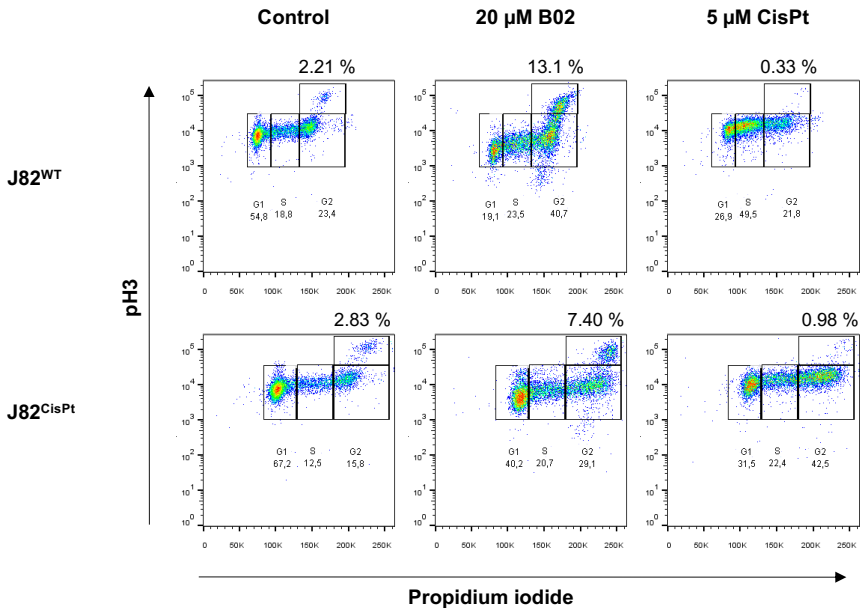

Figure 31: Analysis of mitosis-specific phosphorylation of histone 3 (H3) in J82^{WT} and J82^{CisPt} cells after treatment with RAD51$_i$ B02
Cells were treated with RAD51 inhibitor B02 (20 µM) or cisplatin (5 µM) for 24 h. To analyze the DNA content of pH3 (Ser10) positive cells, co-staining of pH3 with propidium iodide was applied and examined by flow cytometry. Displayed representative images and gating of the flow cytometric analyses were generated using FlowJo software.

Another possibility to explain the increase of the pH3 signal seen after B02 treatment in J82^{WT} cells and J82^{CisPt} cells would be that the cells get stuck in mitosis. Evaluation of the spindle apparatus in mitotic cells after 24 h treatment with 20 µM B02 revealed a high number of monopolar cells in J82^{WT} as well as J82^{CisPt}, with the percentage being higher in J82^{WT} (Figure 32). In both cell variants there were sporadically still some mitotic cells in prometaphase found and, in the case of J82^{CisPt}, also in meta- and anaphase. However, on closer inspection, these cells also showed abnormal spindle formations with crossed spindles.

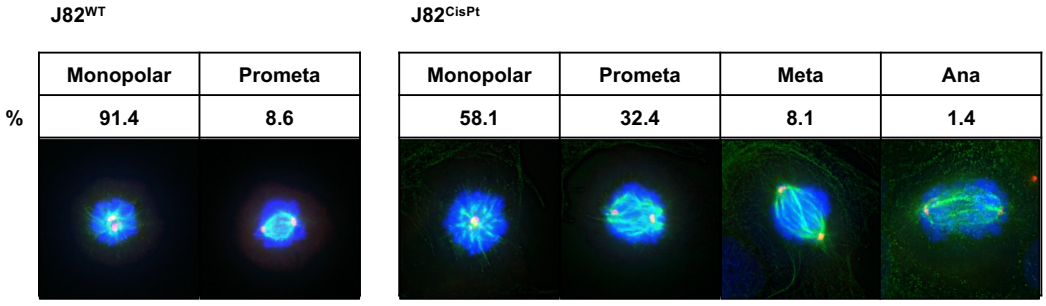

Figure 32: Staining of spindle apparatus markers in J82^{WT} and J82^{CisPt} after treatment with B02
J82^{WT} and J82^{CisPt} cells were treated with 20 µM B02 for 24 h before co-staining with spindle marker α-tubulin (green), centrosome marker pericentrin (red) and chromatin dye DAPI (blue). Seventy mitotic J82^{WT} and J82^{CisPt} cells were analyzed for quantification of different mitotic stages (pro-, prometa-, meta-, ana-, telophase and cytokinesis) and abnormalities (e.g. monopolarity).

From these data, we can infer that the observed increase in pH3 signal in the presence of B02 does not result from mitosis-unspecific phosphorylation of the histone. It is more probable that the stronger pH3 signal is a consequence of the cells remaining arrested in the initial stages of mitosis as a result of aberrant spindle formation. As the observed effects were less pronounced in $J82^{CisPt}$ than in $J82^{WT}$, this may provide a potential explanation for the reduced cytotoxic effect of the inhibitor in $J82^{CisPt}$.

3.2.5 Comparison of RAD51 inhibition with B02 and RAD51 knockdown via siRNA

In order to verify whether the reported effects with B02 are indeed due to the inhibition of RAD51 or whether the inhibitor may trigger RAD51 non-specific effects that cause the observed phenotype, some relevant endpoints were compared following RAD51 inhibition by B02 and RAD51 knockdown using siRNA.

First, the knockout efficiency of the RAD51 siRNA at the protein level was tested using Western blotting. Three different concentrations of siRNA (1 nM, 5 nM and 10 nM) and three incubation periods were tested in $J82^{WT}$ and $J82^{CisPt}$ (Figure 33). After 24 hours of incubation with the siRNA, it can be seen that the RAD51 protein content was already lower than in the untreated controls. This effect was stronger in the $J82^{WT}$ cells than in $J82^{CisPt}$. With longer incubation over 48 or 72 h, the expression decreased further, so that RAD51 was hardly detectable in both cell variants. There was no difference in knockdown efficiency with different concentrations of siRNA tested. Thus, the lowest concentration of 1 nM was chosen for further experiments.

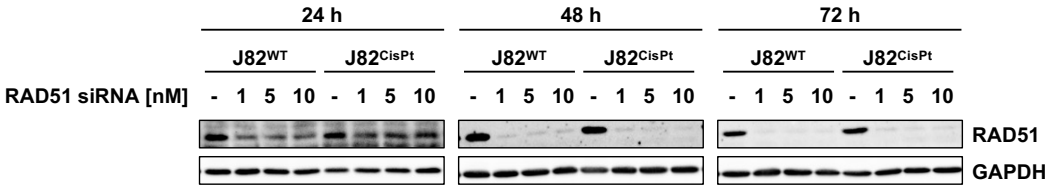

Figure 33: Protein expression of RAD51 in $J82^{WT}$ and $J82^{CisPt}$ after treatment with RAD51 siRNA
Cells were treated for 24 h, 48 h or 72 h with the indicated concentrations of RAD51 siRNA before protein expression of RAD51 was examined via Western blot analyses. The protein expression on GAPDH was used as loading control.

The next step was to examine whether 1 nM of the RAD51 siRNA specifically reduced the mRNA expression of RAD51. This was assessed using RT-qPCR for two time points. The RAD51 siRNA reduced RAD51 mRNA by 80 - 90% with the short treatment duration (24 h) and also over a longer period of time (72 h) in both J82 cell variants (Figure 34). At the same time the RAD51 paralogs RAD51B, RAD51C, RAD51D, XRCC2 and XRCC3 showed no changes in mRNA expression due to the siRNA, suggesting that the siRNA used acts specifically for RAD51. Furthermore, this means that no compensatory upregulation of the RAD51 paralogs is triggered by the knockdown of RAD51 at the mRNA level.

Scrambled siRNA is an siRNA not binding to any mRNA present in cells and therefore serves as a vehicle control of the used transfection media. As expected, no downregulation of mRNA was observed for any of the analyzed factors with scrambled siRNA.

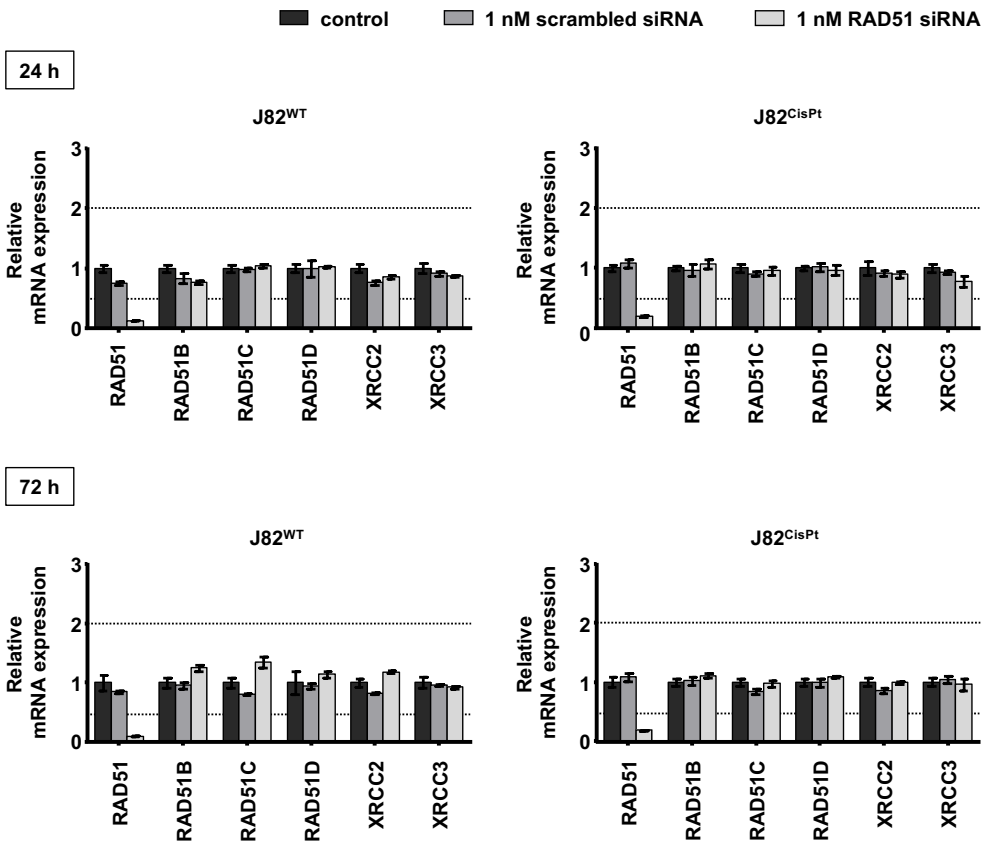

Figure 34: mRNA expression of RAD51 and its paralogs in J82^{WT} and J82^{CisPt} after treatment with RAD51 siRNA

The mRNA expression of untreated cells was set to 1.0 and expression of scrambled siRNA (vehicle control) and RAD51 siRNA treated cells was related to this. Thresholds for increased/decreased mRNA expression were set at 2-fold difference between treated vs. respective control (dotted lines). Data presented are the mean ± SD from technical triplicates.

Since reduced cytotoxicity of J82^{CisPt} was observed with RAD51 inhibitor B02 compared to J82^{WT}, an AlamarBlue assay was performed after 72 h of treatment with the RAD51 siRNA. Both cell variants showed no significant reduction in viability with RAD51 siRNA compared to the respective control (scrambled siRNA) and no significant difference in viability was observed between the two cell variants (Figure 35). The knockdown of RAD51 by siRNA thus did not result in any observable metabolic decline in either J82 cell variant over a period of 72 hours.

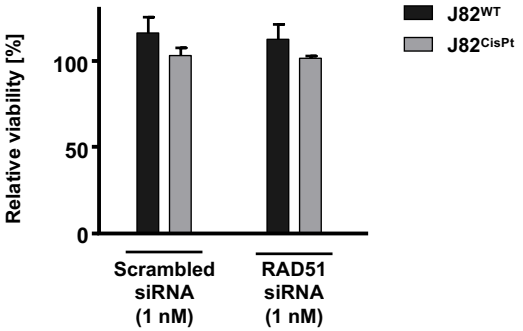

Figure 35: Comparison of cytotoxicity in J82^{WT} and J82^{CisPt} with RAD51 siRNA
J82^{WT} and J82^{CisPt} cells were treated with the indicated concentrations of scrambled siRNA (vehicle control) or RAD51 siRNA for 72 h and viability was measured via AlamarBlue assay. The untreated control of each cell variant was set to 100% viability and all respective treatments were related to this. Data presented are the mean + SD from biological quadruplicates.

With 20 µM B02, a G2/M arrest in J82^{WT} and no cell cycle changes in J82^{CisPt} were observed after 24 h, as in previous experiments (Figure 29, Figure 36). With the RAD51 siRNA, no such arrest was observed in J82^{WT} at the same time of analysis and there were also no other changes in the cell cycle profiles. In contrast to the B02 treatment, no increased SubG1 fraction was observed when the cells were treated with siRNA for 72 hours. This is consistent with the result of the AlamarBlue assay that no cytotoxicity was triggered by the siRNA over this period (Figure 35). There was, however, a slight G2/M arrest in J82^{WT} cells after 72 h siRNA incubation.

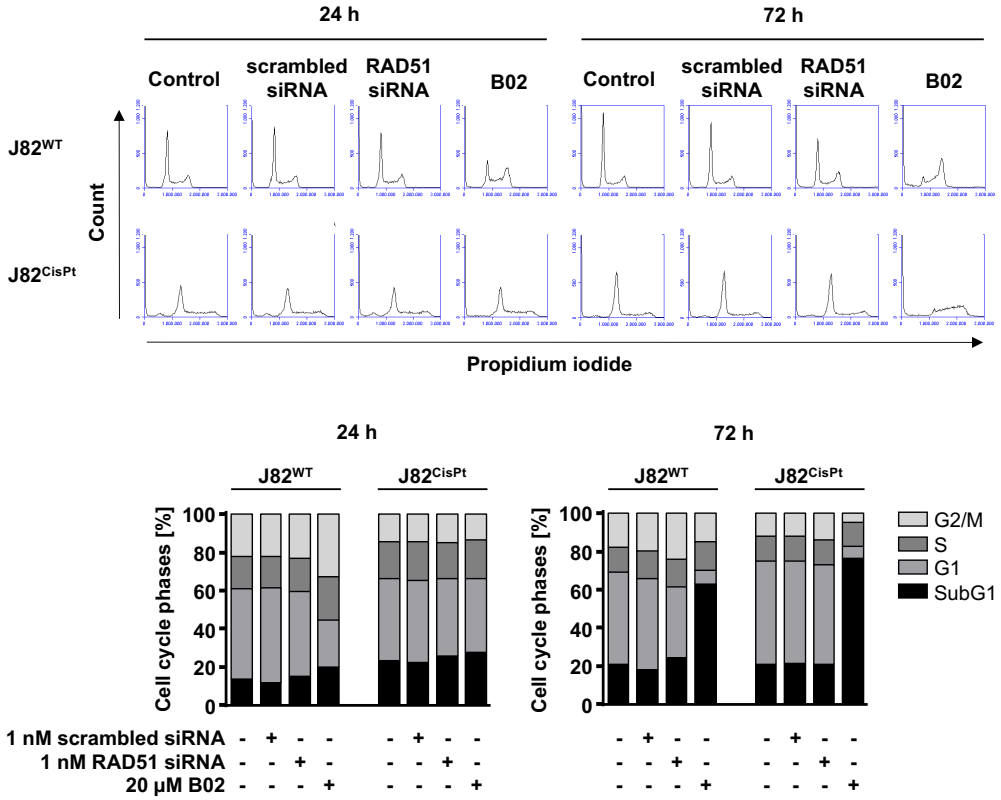

Figure 36: Cell cycle distribution analyses in J82^{WT} and J82^{CisPt} after treatment with RAD51 siRNA
Cells were treated for 24 h or 72 h with RAD51 siRNA or B02 before cell cycle distribution was analyzed by flow cytometric analysis employing propidium iodide staining. Scrambled siRNA was included in the study as vehicle control. A total of 10000 counts per sample were measured for quantification. Displayed representative histograms and gating of the flow cytometric analyses were generated using BD Accuri C6 software.

With 20 µM B02, as before, an increase in pH3 positive cells was observed in both J82 cell variants, with a trend to be more pronounced in J82^{WT} (Figure 30, Figure 37). However, when the cells were treated with RAD51 siRNA for 24 h, this characteristic increase in the pH3 signal was not observed.

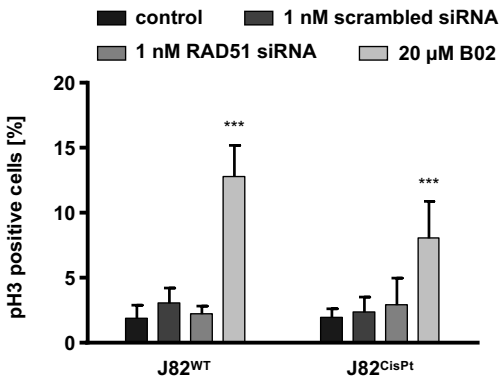

Figure 37: Phospho histone 3 (pH3) staining of J82^{WT} and J82^{CisPt} cells treated with RAD51 siRNA or B02
Cells were incubated with the indicated treatments for 24 h before immunocytochemical staining for pH3. Data are presented as mean + SD and were derived from 1000 – 2000 nuclei per sample. ***p ≤ 0.001; significant compared to control of the respective cell variant.

In summary, the results obtained by RAD51 inhibition with B02 could not be reproduced by knockdown of RAD51 using siRNA. This finding suggests two potential interpretations: firstly, that B02 induces effects in cells that are independent of RAD51, or alternatively, that the mechanisms triggered by the inhibition of RAD51 differ from that initiated by RAD51 knockdown.

3.3 Comparison of J82^{CisPt} with other cisplatin resistant cell variants

3.3.1 Isolation of cisplatin resistant cell variants of different tumor entities

In addition to the cisplatin resistant cell models already available in the laboratory (J82 bladder carcinoma and SH-SY5Y neuroblastoma), further resistant cell lines of other tumor entities (A549 lung carcinoma and MDA-MB231 mamma carcinoma) should be generated by applying the same selection process as previously used (Höhn *et al.*, 2016) (see chapter 2.2.1.3).

3.3.1.1 Selection of cisplatin resistant A549 lung cancer cells

As dose-finding for selection of cisplatin resistant cell variants, an IC_{50} determination for CisPt after 4 h treatment with 72 h post-incubation period was carried out in A549 cells. The IC_{50} determination using the AlamarBlue assay resulted in a value of 30 µM cisplatin (Figure 38) and this concentration was used for selection of CisPt resistant cells.

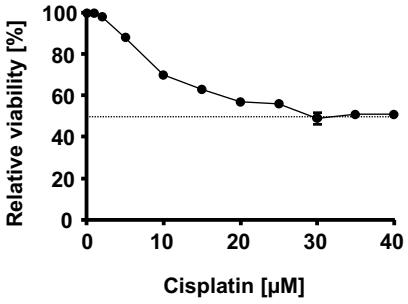

Figure 38: Cytotoxicity of cisplatin in A549 cells
A549 cells were subjected to treatment with different concentrations of cisplatin for 4 h followed by a post-incubation period of 72 h. Subsequently, cell viability was measured via the AlamarBlue assay. The untreated control was set to 100% viability and all treatments were related to this. The dotted line at 50% relative viability facilitates the reading of the IC_{50} value, which represents the concentration of a substance that results in a 50% loss of cell viability compared to the untreated control. Data were generated in one to two independent experiments, each performed in biological quadruplicates. Data are presented as the mean (± SD if applicable).

After completion of the selection process, the cytotoxicity of cisplatin in A549^{CisPt} cells was compared with that in the parental A549^{WT} cells. The IC_{50} value of CisPt after 72 h treatment was almost doubled in A549^{CisPt} compared to A549^{WT} (45 µM in A549^{CisPt} vs. 25 µM in A549^{WT}) (Figure 39).

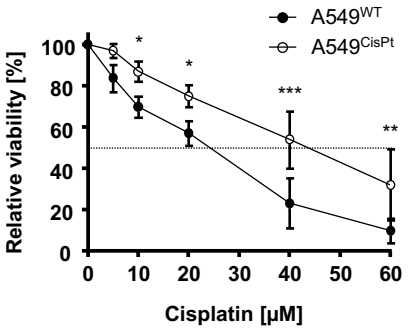

Figure 39: Comparison of cytotoxicity of cisplatin in A549^{WT} and resistance-selected A549^{CisPt}
A549^{WT} and A549^{CisPt} cells were treated with different concentrations of cisplatin for 72 h. Cell viability was determined through the AlamarBlue assay. The viability of the untreated control for each cell variant was set at 100%, and all associated treatments were related to this value. The dotted line at 50% relative viability facilitates the reading of the IC_{50} value. This value indicates the concentration of a substance at which there is a 50% loss of viability among the cells in a given population, when compared to an untreated control. Data presented are the mean ± SD from three independent experiments, each performed in biological quadruplicates. *p ≤ 0.05; **p ≤ 0.01; ***p ≤ 0.001; significant difference compared to A549^{WT}.

3.3.1.2 Selection of cisplatin resistant MDA-MB231 mamma carcinoma cells

In preparation for selection, the IC_{50} value for CisPt after 4 h treatment followed by 72 h post-incubation period was determined in MDA-MB231 cells applying the AlamarBlue assay. The determined IC_{50} value and subsequently used concentration for selection was 40 µM CisPt (Figure 40). Unfortunately, the selection for cisplatin resistant MDA-MB231 cells could not be completed successfully since the cells died during the selection process.

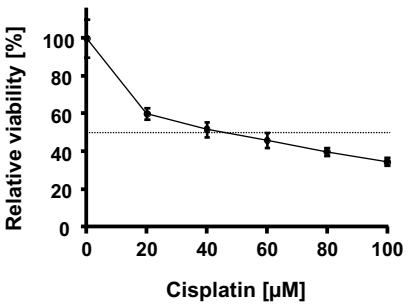

Figure 40: Cytotoxicity of cisplatin in MDA-MB231 cells
MDA-MB231 cells were treated with different concentrations of cisplatin for 4 h followed by a post-incubation period of 72 h. Viability was assessed using the AlamarBlue assay. The untreated control was set to 100% viability and all treatments were related to this. The dotted line at 50% relative viability allows for the convenient reading of the IC_{50} value, which indicates the concentration of a substance at which 50% viability loss of the cell population occurs in comparison to the untreated control. Data are presented as the mean ± SD from biological quadruplicates.

3.3.2 mRNA expression profiles under basal conditions and after CisPt treatment

3.3.2.1 mRNA expression profiles of A549 lung cancer cells

The self-selected cisplatin resistant A549^{CisPt} cells were compared to their parental cell line A549^{WT} concerning the mRNA expression of selected factors potentially involved in acquired drug resistance. Under basal conditions, the two cell variants differed in the mRNA expression of the two transporters MDR1 and MRP1, which were upregulated in the resistant cell line, as well as the mRNA of the transporter MATE1 and the DNA repair factor RAD51C, which were downregulated in the resistant cells (Figure 41).

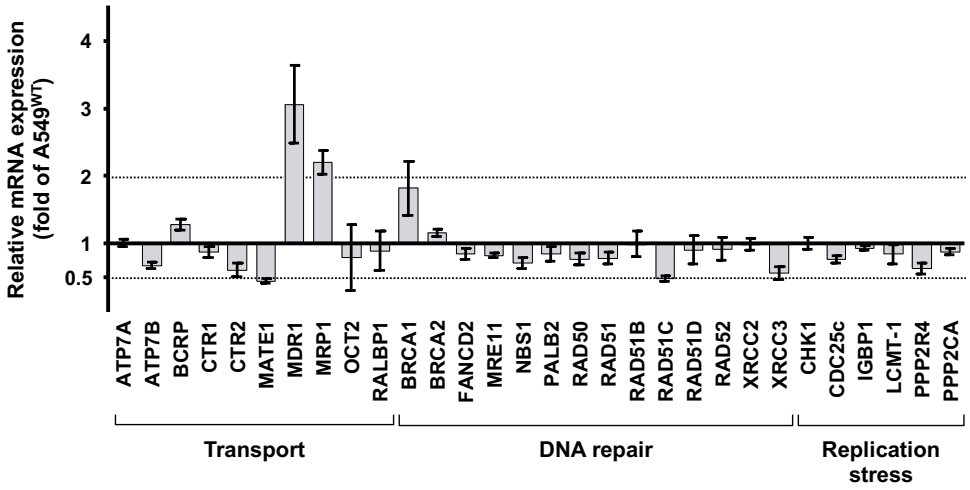

Figure 41: mRNA expression of factors potentially involved in acquired cisplatin resistance compared in A549^{WT} and A549^{CisPt} under basal conditions
RNA from three independent experiments was pooled before cDNA synthesis. The mRNA expression of A549^{WT} cells was set to 1.0 and expression of A549^{CisPt} cells was related to this. Thresholds for increased/decreased mRNA expression were set at 2-fold difference between A549^{CisPt} vs. A549^{WT} (dotted lines). Data presented are the mean ± SD from technical triplicates.

After treatment with 30 µM cisplatin for 24 h, both cell variants showed similar responses by upregulating the mRNA of transporter CTR2 and downregulating the mRNA of RAD51 paralog RAD51B (Figure 42). In the case of CTR2 the response of A549^{WT} was ~2-fold stronger, while for RAD51B the extent of the downregulation was comparable in A549^{WT} and A549^{CisPt}. In addition to the mentioned factors, A549^{WT} showed increased mRNA expression of transporter ATP7A and DNA repair factor RAD52, as well as decreased expression of DNA repair factors FANCD2, RAD51 and XRCC2. A549^{CisPt}, in turn, were found to have upregulated expression of RAD51C.

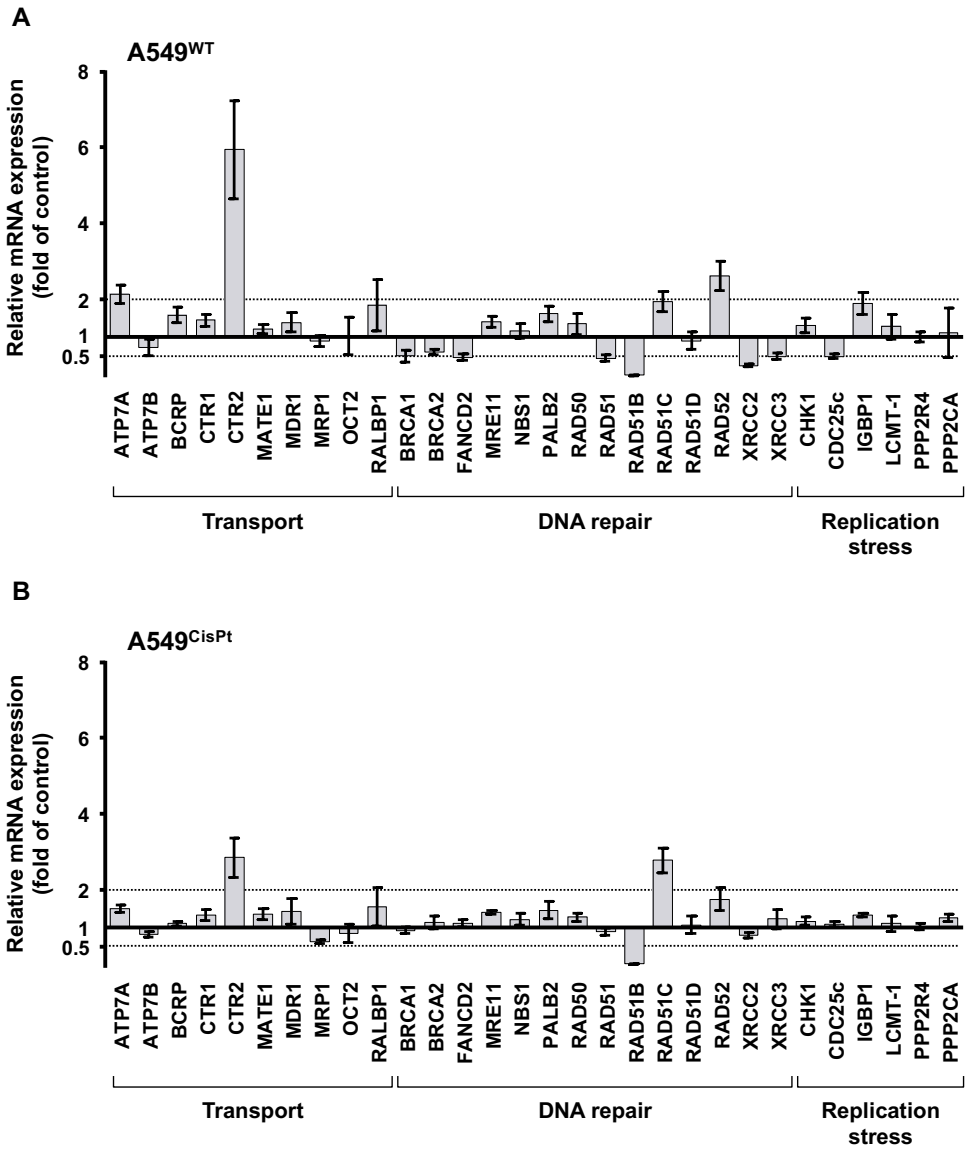

Figure 42: mRNA expression of factors potentially involved in acquired cisplatin resistance compared in A549^{WT} and A549^{CisPt} after cisplatin treatment
Cells were treated for 24 h with the 30 µM cisplatin before mRNA expression analysis of selected factors by RT-qPCR. The respective untreated control was set to 1.0 and cisplatin treatment of A549^{WT} (A) or A549^{CisPt} (B) was related to this. Thresholds for increased/decreased mRNA expression were set at 2-fold difference between CisPt treated vs. respective untreated (dotted lines). cDNA used for mRNA expression analyses was generated from pooled samples of three independent experiments and data presented are the mean ± SD from technical triplicates.

The mRNA analyses demonstrated that, under both basal conditions and in response to cisplatin treatment, the mRNA expression of several drug transporters differed between the two A549 cell variants. This may indicate that transport processes are involved in the cisplatin resistance mechanism of A549^{CisPt} cells.

3.3.2.2 mRNA expression profiles of SH-SY5Y neuroblastoma cells

In addition to the self-selected resistant A549^{CisPt} cells, the mRNA expression profile of a cisplatin resistant neuroblastoma cell line SH-SY5Y^{CisPt}, formerly isolated at the institute, was examined in comparison to its parental cells SH-SY5Y^{WT}. Under basal conditions none of the analyzed factors showed different mRNA expression between both cell variants, besides the transporter OCT2, that was not detectable in SH-SY5Y^{CisPt} (Figure 43).

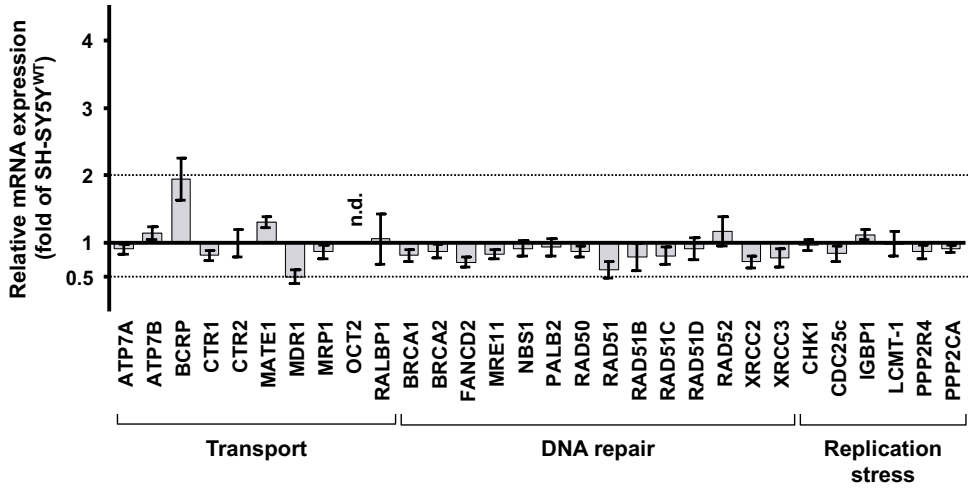

Figure 43: mRNA expression of factors potentially involved in acquired cisplatin resistance compared in SH-SY5Y^{WT} and SH-SY5Y^{CisPt} under basal conditions
RNA from three independent experiments was pooled before cDNA synthesis. The mRNA expression of SH-SY5Y^{WT} cells was set to 1.0 and expression of SH-SY5Y^{CisPt} cells was related to this. Thresholds for increased/decreased mRNA expression were set at 2-fold difference between SH-SY5Y^{CisPt} vs. SH-SY5Y^{WT} (dotted lines). Data presented are the mean ± SD from technical triplicates. (n.d. = not detectable)

After treatment with 3 µM CisPt for 24 h, OCT2 expression was downregulated in SH-SY5Y^{WT} and still not detectable in SH-SY5Y^{CisPt}. All other analyzed factors were not differentially expressed in the CisPt treated vs. untreated cells (Figure 44).

The presented findings indicate that the resistance of SH-SY5Y^{CisPt} cells to cisplatin may be associated with the downregulation of transporter OCT2. It seems that all other factors investigated are not fundamental to the mechanism of cisplatin resistance in SH-SY5Y^{CisPt} cells.

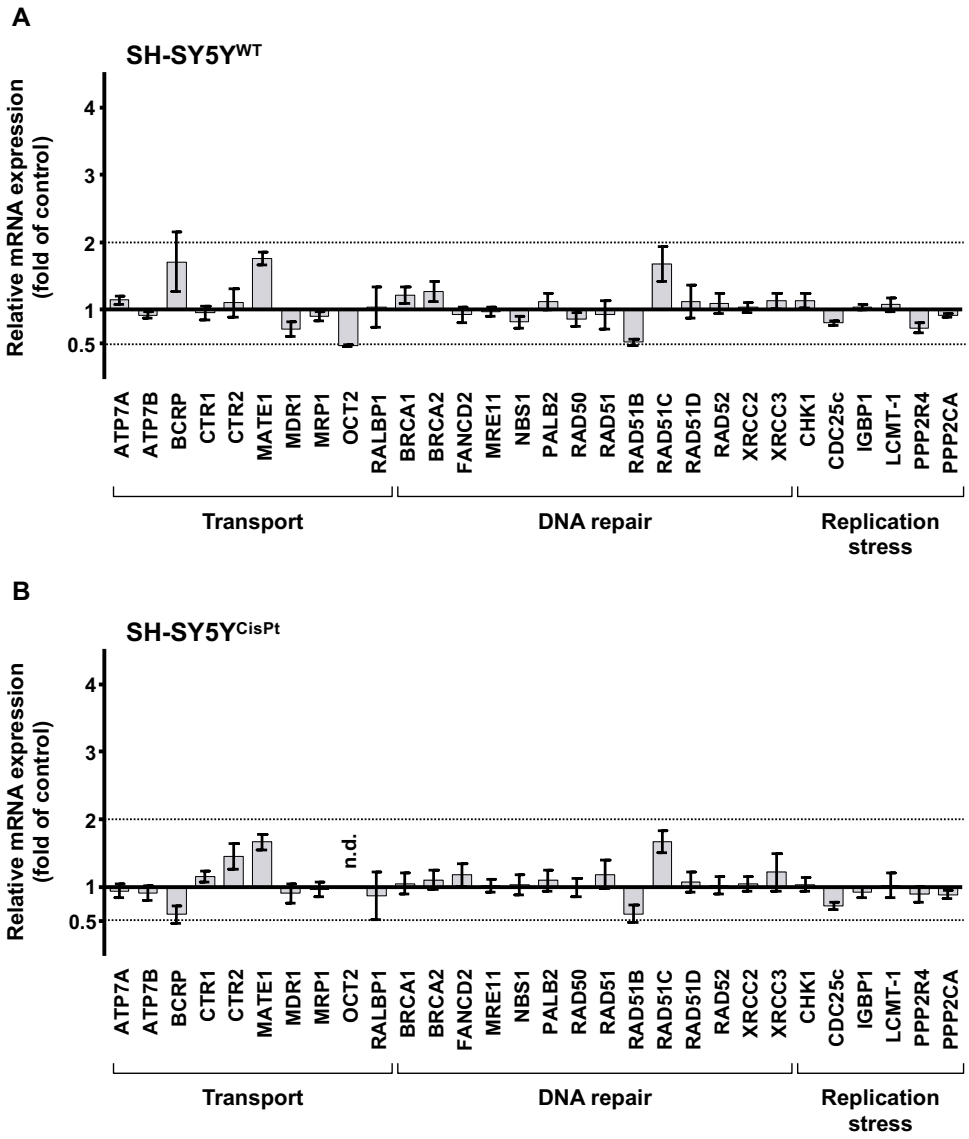

Figure 44: mRNA expression of factors potentially involved in acquired cisplatin resistance compared in SH-SY5Y^{WT} and SH-SY5Y^{CisPt} after cisplatin treatment
Cells were treated for 24 h with the 3 µM cisplatin before mRNA expression analysis of selected factors by RT-qPCR. The respective untreated control was set to 1.0 and cisplatin treatment of SH-SY5Y^{WT} (A) or SH-SY5Y^{CisPt} (B) was related to this. Thresholds for increased/decreased mRNA expression were set at 2-fold difference between CisPt treated vs. respective untreated (dotted lines). cDNA used for the mRNA expression analyses was generated from pooled samples of three independent experiments and data presented are the mean ± SD from technical triplicates. (n.d. = not detectable)

A comparative overview of the mRNA changes observed in the different cisplatin-resistant cell lines compared to their parental cells under basal conditions and a summary of the alterations after cisplatin administration in wildtype and resistant cells can be found in Supplementary Figure 2. Overall, the results of the mRNA expression analyses in the different cell lines did not exhibit any major similarities. This may suggest that distinct molecular processes are triggered in response to cisplatin in the different cell lines and that their cisplatin resistance is based on dissimilar molecular mechanisms.

3.4 Combination treatments of cytostatics and inhibitors of DDR/DNA repair to overcome CisPt resistance in J82^{CisPt}

The primary objective of this work was to investigate whether cells that have acquired resistance to cisplatin can be rendered susceptible to therapeutic intervention again through the use of pharmacological inhibitors of DDR and DNA repair. The initial cytotoxicity screening already showed differences in the responses of J82^{CisPt} and J82^{WT} to mono-treatments with some cytostatic drugs or DDR inhibitors (Supplementary Table 1). Some substances were selected based on these results and tested in J82^{CisPt} in combination treatments to determine whether they cause synergistic cytotoxicity, meaning greater toxicity in combination than would be expected from their mono-treatments.

Since J82^{CisPt} had shown a cross resistance against the RAD51 inhibitor B02 in the cytotoxicity screening, one idea was to re-sensitize the cells to cisplatin by simultaneous targeting of RAD51 by B02. Combining different low to moderate toxic concentrations of both compounds resulted in combination indices around 1, indicating an additive cytotoxic effect (Figure 45).

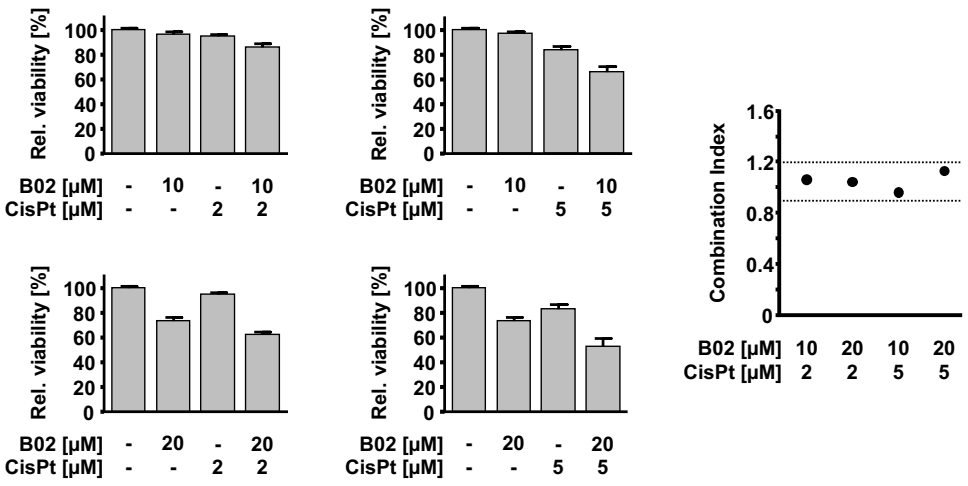

Figure 45: Viability of J82^{CisPt} after co-treatment with cisplatin and RAD51 inhibitor B02
J82^{CisPt} cells were treated with different low to moderate cytotoxic concentrations of cisplatin (2 µM, 5 µM) or/and B02 (10 µM, 20 µM) for 72 h and viability was measured via the AlamarBlue assay. The viability of the untreated control was set at 100%, and all other groups were related to this. Data presented are the mean + SD from biological quadruplicates. From the obtained viability data, combination indices (CI) were calculated using CompuSyn software (CI > 1.2 antagonistic; 0.9 ≤ CI ≤ 1.2 additive; CI < 0.9 synergistic).

J82^{CisPt} reacted sensitive to replication stress inducing substances in the cytotoxicity screening. This sensitivity should be enhanced by combining conventional replication stress inducing anticancer therapeutics (OH-Urea or 5-FU) with inhibitors of factors of the replicative stress response (RAD51 or CHK1). Interestingly, combining different concentrations of OH-Urea and B02 led to antagonistic effects with combination indices above 1.2 (Figure 46). In contrast, strong synergistic cytotoxic effects were achieved using the combination of OH-Urea or 5-FU with PF477736 (Figure 47).

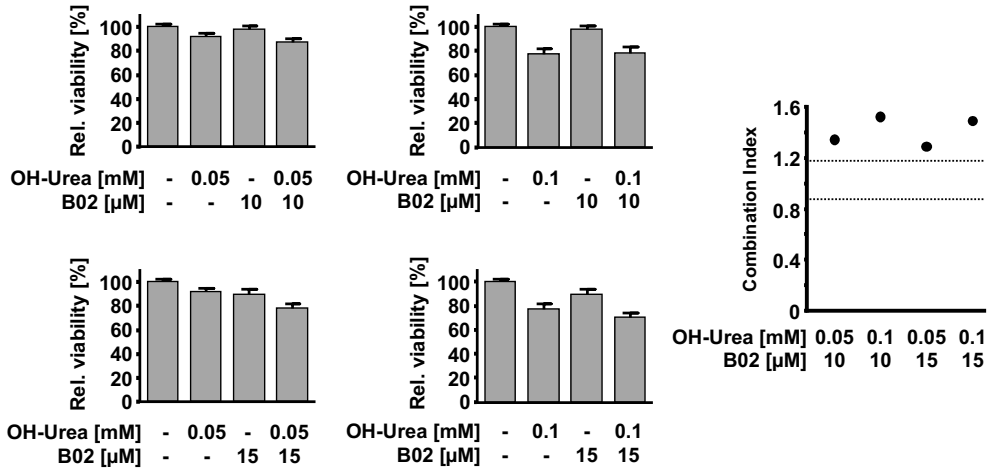

Figure 46: Viability of J82^{CisPt} after co-treatment with OH-Urea and RAD51 inhibitor B02
J82^{CisPt} cells were treated with different low to moderate cytotoxic concentrations of OH-Urea (0.05 mM, 0.1 mM) or/and B02 (10 µM, 15 µM) for 72 h and cell viability was assessed through the AlamarBlue assay. The untreated control was set to 100% viability and all other groups were related to this. Data presented are the mean + SD from biological quadruplicates. The viability data were used to calculate combination indices (CI) with the use of the CompuSyn software (CI > 1.2 antagonistic; $0.9 \leq CI \leq 1.2$ additive; CI < 0.9 synergistic).

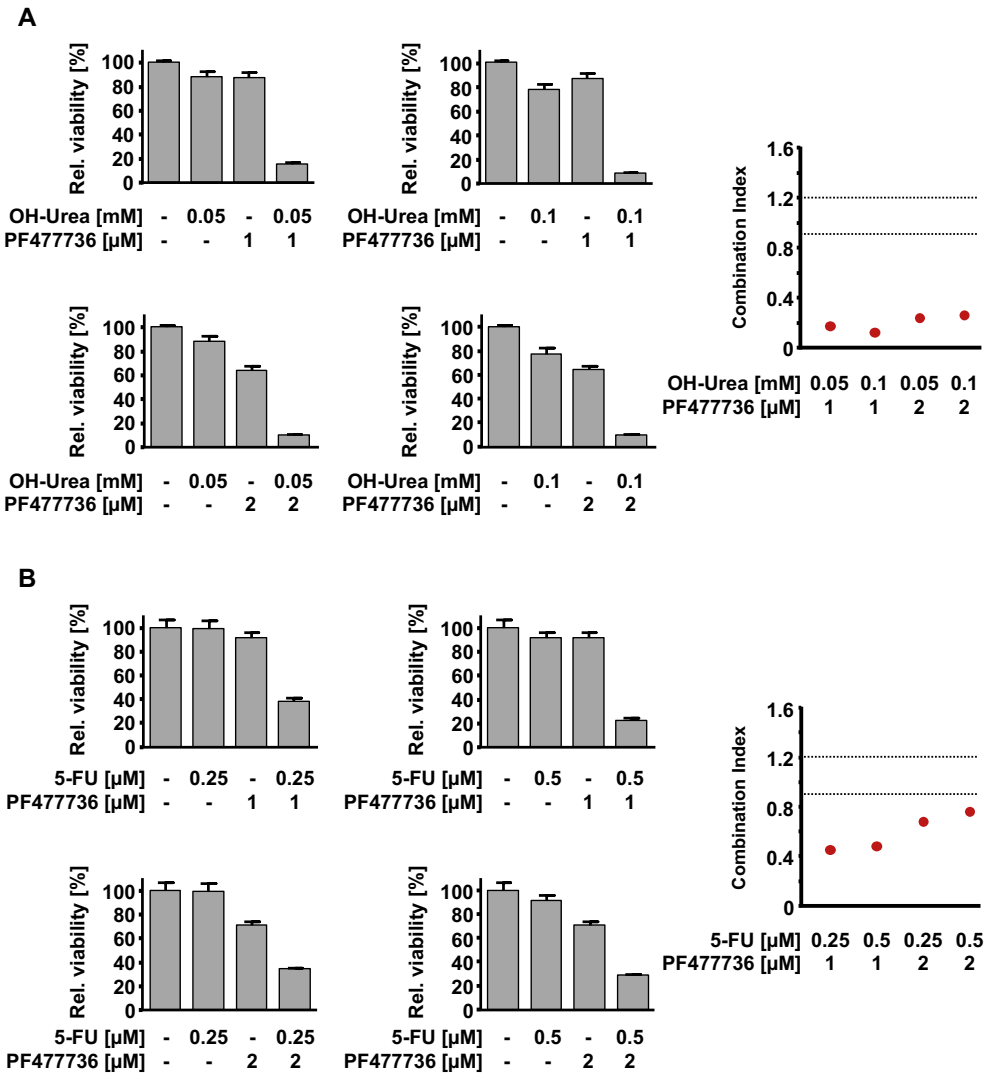

Figure 47: Viability of J82^{CisPt} when combining replication stress inducing anticancer therapeutics with CHK1 inhibitor PF477736
J82^{CisPt} cells were treated with different low to moderate cytotoxic concentrations of OH-Urea (0.05 mM, 0.1 mM) or/and PF477736 (1 µM, 2 µM) (A) or 5-FU (0.25 µM, 0.5 µM) or/and PF477736 (1 µM, 2 µM) (B) for 72 h. Subsequently, cell viability was determined via the AlamarBlue assay. The untreated control was set to 100% viability and all other groups were related to this. Data presented are the mean + SD from biological quadruplicates. From the obtained viability data, combination indices (CI) were calculated using CompuSyn software (CI > 1.2 antagonistic; 0.9 ≤ CI ≤ 1.2 additive; CI < 0.9 synergistic).

Another idea was targeting two different factors of replicative stress response by pharmacological modulators, thereby combining two non-genotoxic compounds. When various concentrations of RAD51 inhibitor B02 and PARP inhibitor Niraparib were combined, only antagonistic cytotoxic effects were obtained (Figure 48A). The combination of CHK1 inhibitor PF477736 with PARP inhibitor Niraparib or Olaparib also reduced viability in a rather antagonistic, at best additive, manner (Figure 48B).

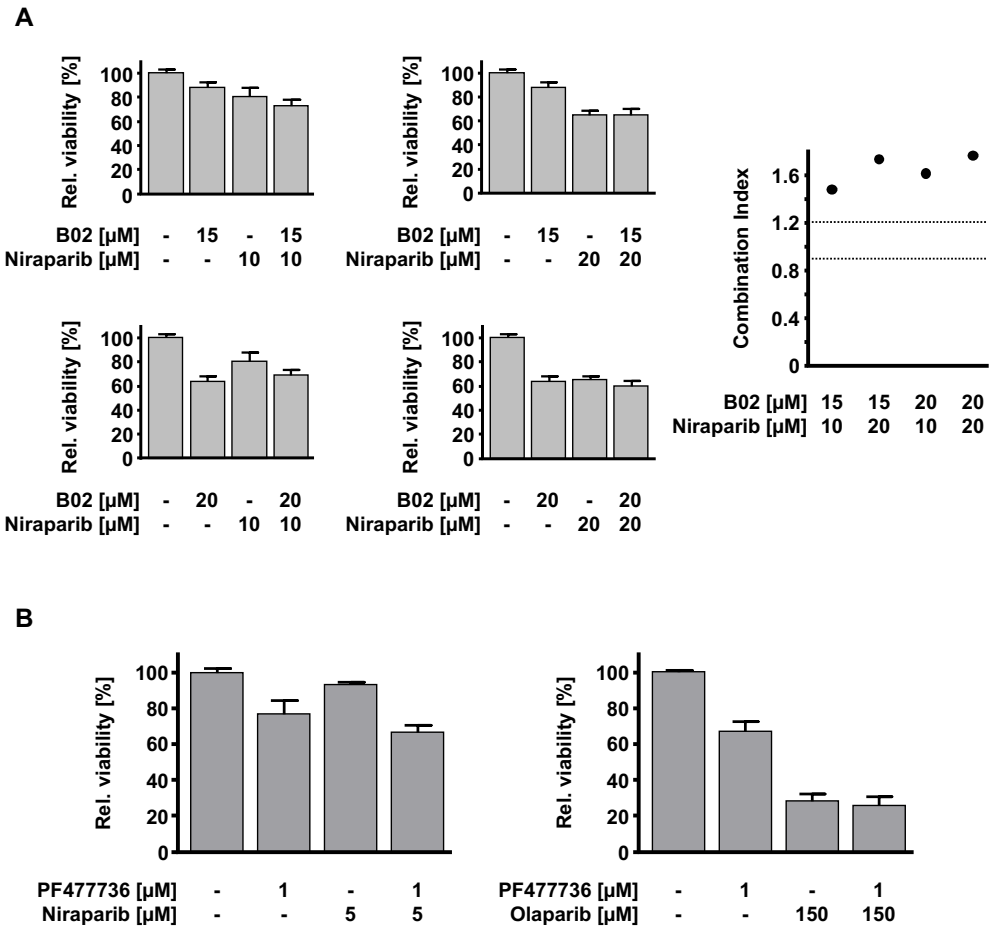

Figure 48: Viability of J82^{CisPt} when combining PARP inhibitors with RAD51 inhibitor B02 or CHK1 inhibitor PF477736
J82^{CisPt} cells were treated with different low to moderate cytotoxic concentrations of B02 (15 µM, 20 µM) or/and PARP$_i$ Niraparib (10 µM, 20 µM) (A) or PF477736 (1 µM) or/and PARP$_i$ 5 µM Niraparib/ 150 µM Olaparib (B) for 72 h and viability was measured via the AlamarBlue assay. The viability of the untreated control was set at 100%, and all other groups were related to this. Data presented are the mean + SD from biological quadruplicates. From the obtained viability data of B02 + Niraparib, combination indices (CI) were calculated using CompuSyn software (CI > 1.2 antagonistic; 0.9 ≤ CI ≤ 1.2 additive; CI < 0.9 synergistic).

Combining low to moderate toxic concentrations of the CHK1 inhibitor PF477736 with RAD51 inhibitor B02, on the contrary, caused additive to synergistic cytotoxicity in J82^{CisPt} cells (Figure 49).

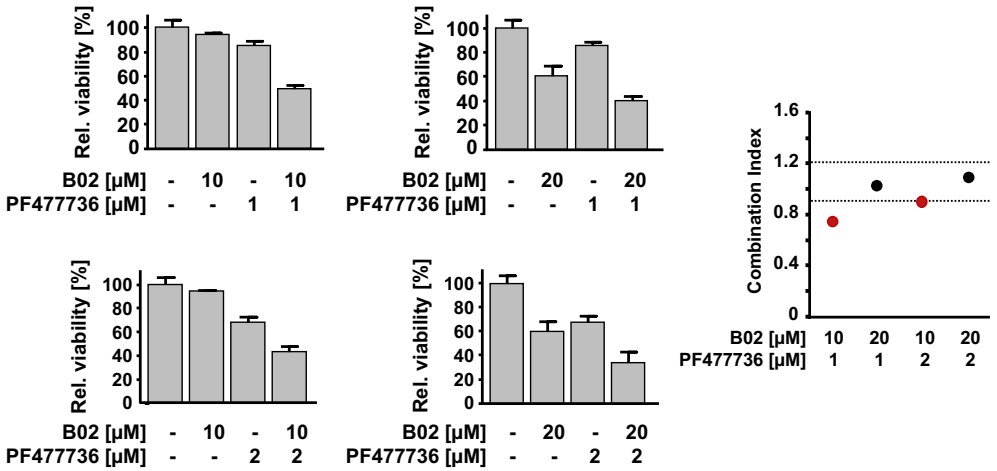

Figure 49: Viability of J82^{CisPt} after co-treatment with RAD51 inhibitor B02 and CHK1 inhibitor PF477736

J82^{CisPt} cells were subjected to treatment with different low to moderate cytotoxic concentrations of B02 (10 µM, 20 µM) or/and PF477736 (1 µM, 2 µM) for 72 h and subsequently cell viability was measured via the AlamarBlue assay. The untreated control was set to 100% viability and all other groups were related to this. Data presented are the mean + SD from three independent experiments, each performed in biological quadruplicates. The viability data were used to calculate combination indices (CI) with the use of the CompuSyn software (CI > 1.2 antagonistic; 0.9 ≤ CI ≤ 1.2 additive; CI < 0.9 synergistic).

A tabular overview of all combination treatments tested, and their outcome can be found in Supplementary Table 4. Overall, these extensive studies showed that exploiting the sensitivity of J82^{CisPt} to replication stress-inducing substances may be an effective strategy for circumventing their CisPt resistance. Especially the combination of the two non-genotoxic pharmacological inhibitors B02 and PF477736 appeared promising and should undergo further investigation.

3.5 Deciphering the molecular mechanism of the synergistic toxicity of the combination treatment with B02 + PF477736

Since the combination treatment of RAD51 inhibitor (RAD51$_i$) B02 + CHK1 inhibitor (CHK1$_i$) PF477736 had shown a synergistic cytotoxic effect in the cisplatin-resistant bladder carcinoma cells J82^{CisPt}, the molecular mechanism of the additive to synergistic cytotoxicity combination of the two non-genotoxic compounds should be examined more closely. For all investigations concerning the molecular mechanism, the combination of 10 µM B02 and 1 µM PF477736 was used, since the strongest synergistic response was observed with these concentrations.

3.5.1 Induction of apoptotic cell death by B02 + PF477736

In order to find out whether synergistic cytotoxicity is cell death-dependent or whether other factors play a role, the induction of cell death-related mechanisms was investigated in more detail.

As a screening approach, a RT-qPCR was conducted looking at factors of various common cell death pathways (Figure 50). As expected, the solvent control (0.11% DMSO) did not induce differential mRNA expression of any of the examined factors. No relevant changes in the mRNA expression of the factors under consideration were found in the B02 treatment either. In contrast, the mRNA of pro-apoptotic factor BBC3 was upregulated and parkin (PRKN), which is involved in mitophagy, was downregulated following the PF477736 mono-treatment. In the combination treatment with both inhibitors, the anti-apoptotic marker B-cell lymphoma 2 (BCL2) and the autophagy marker lysosomal associated membrane protein 1 (LAMP1) were both increased in mRNA expression. Another marker for autophagy, unc-51 like autophagy activating kinase 1 (ULK1), showed a trend towards upregulation just below the threshold value. All three factors upregulated by the combination treatment reflect the synergistic effect of the two inhibitors, as mRNA expression of the corresponding factors was not altered in the mono-treatments. The ferroptosis factors included in the analysis were not altered in expression at the RNA level with any of the treatments applied.

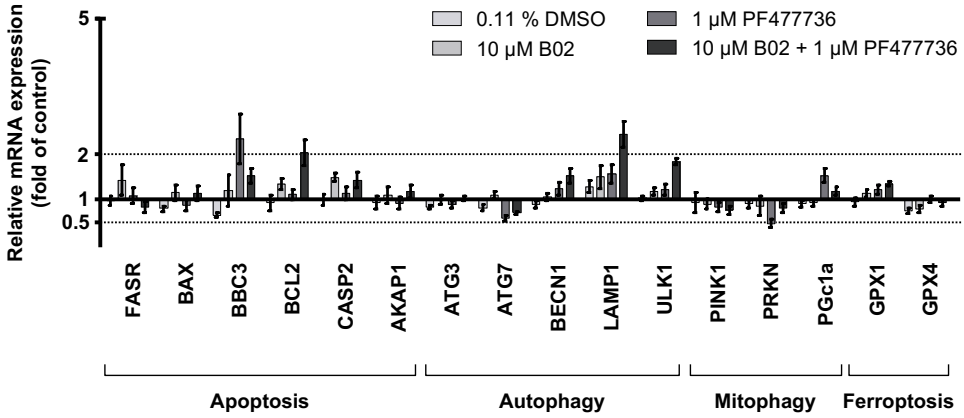

Figure 50: mRNA expression of cell death factors in J82^{CisPt} after treatment with RAD51$_i$ B02 and CHK1$_i$ PF477736

Cells were treated for 24 h with the indicated substance(s) before mRNA expression analysis of selected factors by RT-qPCR. DMSO was included in the study as solvent control. The untreated control was set to 1.0 and all other treatments were related to this. Thresholds for increased/decreased mRNA expression were set at 2-fold difference between treated vs. untreated (dotted lines). cDNA used for mRNA expression analyses was generated from pooled samples of three independent experiments and data presented are the mean ± SD from technical triplicates.

According to the obtained RT-qPCR data, autophagy might be involved in the execution of cell death after B02 + PF477736 treatment. A further investigation was therefore conducted to ascertain whether autophagy induction can also be detected on the protein level. An important step in autophagy is the formation of autophagosomes, which take up cellular material such as misfolded proteins or entire organelles to be degraded. The protein microtubule-associated protein 1 light chain 3 (LC3) has a crucial function in the formation of autophagosomes (Tanida *et al.*, 2008). Upon autophagy activation, the cytosolic form of LC3, LC3-I, conjugates with phosphatidylethanolamine. The conjugate, called LC3-II, is then incorporated into the membrane of autophagosomes. The conversion of LC3-I to LC3-II also changes the migration behavior of the protein in SDS-PAGE, allowing indirect detection of autophagy activation via Western blot analyses.

The Western blot analysis of LC3 indicated a conversion of LC3-I to LC3-II following treatment with B02, PF477736, and the combination of both inhibitors (Figure 51). This finding suggests that autophagy is activated when RAD51, CHK1 or both factors are inhibited. A clear synergistic effect resulting from the simultaneous inhibition of both factors was not discernible in the Western Blot analysis conducted.

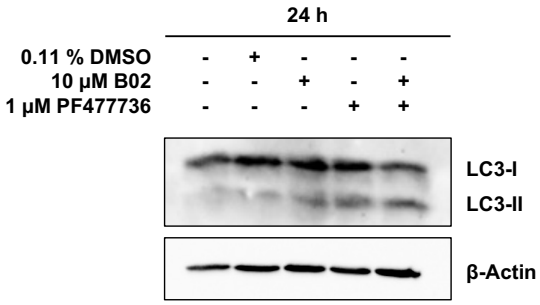

Figure 51: Protein expression of autophagy factor LC3 in J82^{CisPt} after treatment with RAD51$_i$ B02 and CHK1$_i$ PF477736
Cells were treated for 24 h with the indicated substance(s) before protein expression was examined via Western blot analysis. In the study, DMSO was utilized as solvent control. In order to normalize the protein expression levels across samples, β-Actin was employed as loading control.

The mRNA analysis of apoptosis markers did not show a consistent profile; therefore, some markers were analyzed on protein level via Western blot analyses. As described in chapter 1.3.2, caspases need to be cleaved to get activated, hence cleaved effector caspase 7 serves as a marker of activated apoptosis. Activated caspases in turn cleave different proteins during apoptosis. Among the substrates cleaved by effector caspases is PARP, thus PARP cleavage is seen as an indirect marker of apoptosis.

Cleaved caspase 7 and cleaved PARP could be detected in the B02 + PF477736 co-treated group already at an early timepoint of 6 h treatment (Figure 52). These signals got stronger after 24 h treatment. After 24 h treatment, both markers could also be detected in the PF477736-treated group, with the signals being weaker than in the combination treatment. B02 alone and the solvent control did not induce cleavage of caspase 7 or PARP at any timepoint. Uncleaved caspase 7 and uncleaved PARP were measured as controls and could be detected in all samples equally, meaning levels of the source proteins were unchanged by the respective treatments.

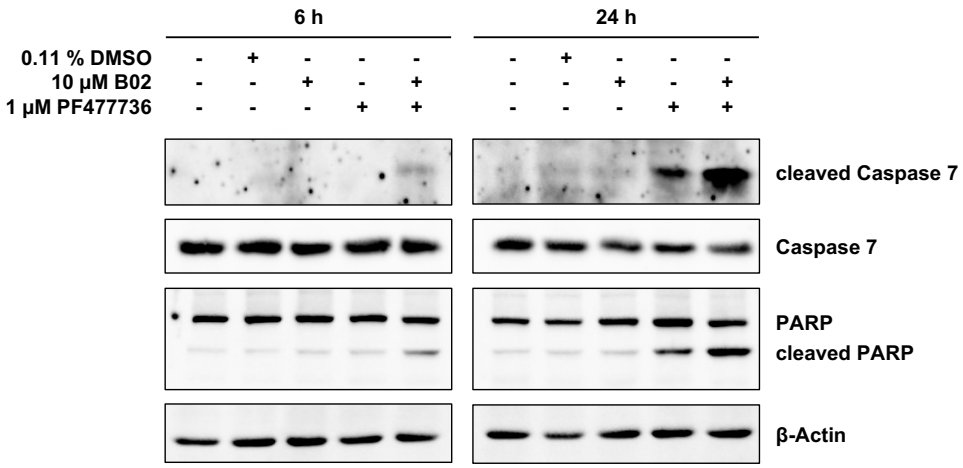

Figure 52: Protein expression of apoptosis factors in J82^{CisPt} after treatment with RAD51$_i$ B02 and CHK1$_i$ PF477736
Cells were treated for 6 h or 24 h with the indicated substance(s) before protein expression was examined via Western blot analysis. DMSO was included in the study as solvent control. The protein expression of β-Actin was used as loading control.

Since apoptosis is mediated by caspases, the pan-caspase inhibitor QVD should abrogate the execution of this cell death pathway. So, to test whether the observed cell death is apoptosis-related in a functional assay, the dual treatment of B02 and PF477736 was applied together with 10 µM pan-caspase inhibitor QVD and the induction of SubG1 fraction measured by flow cytometry was compared to only B02 + PF477736. If cell death is apoptosis-dependent, then the SubG1 fraction should be reduced by co-treatment with QVD.

After 24 h treatment, there was already a trend visible that co-treatment with QVD reduced the induction of SubG1 fraction. This effect was more pronounced at later timepoints (48 h and 72 h treatment), where the induction in SubG1 fraction was significantly lower in co-treatment with QVD than with B02 + PF477736 alone (Figure 53).

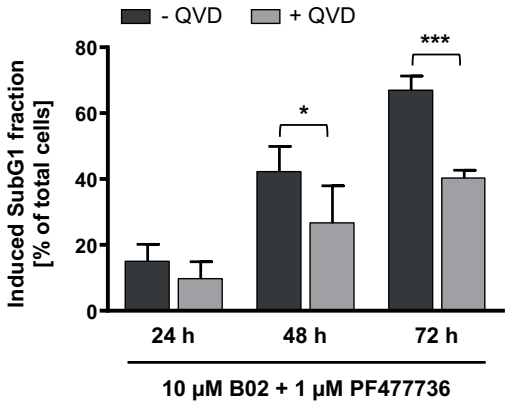

Figure 53: Induction of SubG1 fraction in J82^{CisPt} after co-treatment with B02 + PF477736 and pan-caspase inhibitor QVD
J82^{CisPt} cells were treated for 24 h, 48 h or 72 h with 10 µM B02 + 1 µM PF477736 ± 10 µM QVD before cell cycle distribution with emphasis on the proportion of SubG1 fraction was analyzed by flow cytometric analysis employing propidium iodide staining. Data are presented as mean + SD from three independent experiments. *p ≤ 0.05; ***p ≤ 0.001

Taken together, these findings show that the synergistic cell death evoked by simultaneous treatment with B02 + PF477736 is at least partly dependent on apoptosis. According to the RT-qPCR data and an initial Western blot analysis, autophagy might also play a role. In contrast, there is no evidence to suggest that mitophagy or ferroptosis are involved.

3.5.2 Influence of B02 and PF47776 on the cell cycle progression

To gain a better understanding of the molecular mechanisms triggering the synergistic induction of cell death by combined treatment with CHK1$_i$ and RAD51$_i$, selected proliferation- and cell cycle-related endpoints were investigated after the co-treatment of J82^{CisPt} cells.

In view of the fact that CHK1 and RAD51 play a pivotal role in ensuring the accuracy of DNA duplication in S-phase, we selected several factors i.e. topoisomerase II α (TOP2A), topoisomerase II β (TOP2B) and DNA topoisomerase II binding protein 1 (TOPBP1) for the mRNA expression analysis, as they also play central roles in the replication process. In addition, the two factors Cdc25a and Cdc25c were selected for mRNA expression analysis, as these are crucial for triggering cell cycle arrest and, in this process, act as targets of CHK1.

The two isoforms of DNA topoisomerase II, TOP2A and TOP2B, which are nuclear enzymes involved in chromosome condensation and the relief of torsional stress during DNA transcription and replication, were not altered in their mRNA expression by the applied treatments (Figure 54). Also, TOPBP1, that interacts with topoisomerase II β and thereby supports its induction of transient breakages of DNA strands, was not differentially expressed by treatment with the inhibitors. The two cell cycle regulating phosphatases CDC25a and CDC25c showed altered mRNA expression profiles. CDC25a, required for progression from G1- to S-phase, was upregulated by the combined treatment with B02 + PF477736. In contrast to that, CDC25c, that triggers entry into mitosis, was upregulated with PF477736 mono-treatment and just below the set threshold in the combi-treatment group.

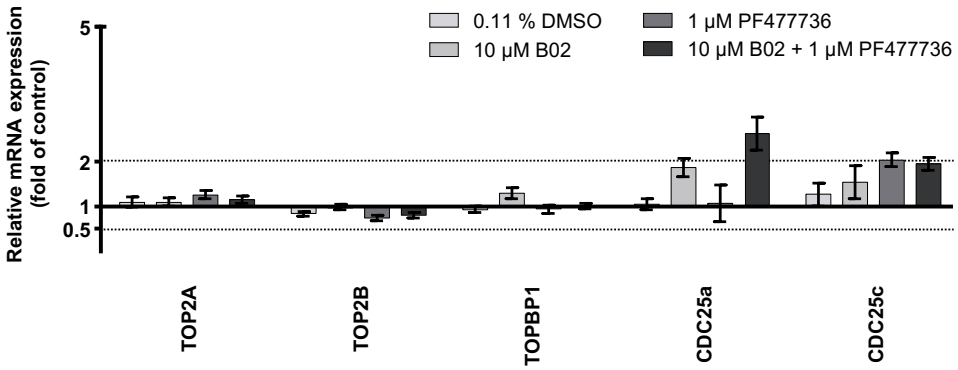

Figure 54: mRNA expression of cell cycle factors in J82^{CisPt} after treatment with RAD51$_i$ B02 and CHK1$_i$ PF477736
Cells were treated for 24 h with the indicated substance(s) before mRNA expression analysis of selected factors by RT-qPCR. DMSO was included in the study as solvent control. The untreated control was set to 1.0 and all other treatments were related to this. Thresholds for increased/decreased mRNA expression were set at 2-fold difference between treated vs. untreated (dotted lines). cDNA used for mRNA expression analyses was generated from pooled samples of three independent experiments and data presented are the mean ± SD from technical triplicates.

Flow cytometry-based cell cycle analyses revealed reduced percentage of cells in G1-phase following PF477736 mono-treatment and in combination with B02 and, in the case of B02 + PF477736 co-treatment, also a reduction in the percentage of G2/M-phase cells (Figure 55). At the same time, both PF477736 alone and in combination with B02 resulted in S-phase arrest, accompanied by an accumulation of dead cells as reflected by an increase in the subG1 fraction. The S-phase arrest at 24 h was not significantly different between these two groups. However, at both the early (24 h) and late (72 h) time point, the combined treatment caused a higher proportion of cells in the subG1 fraction.

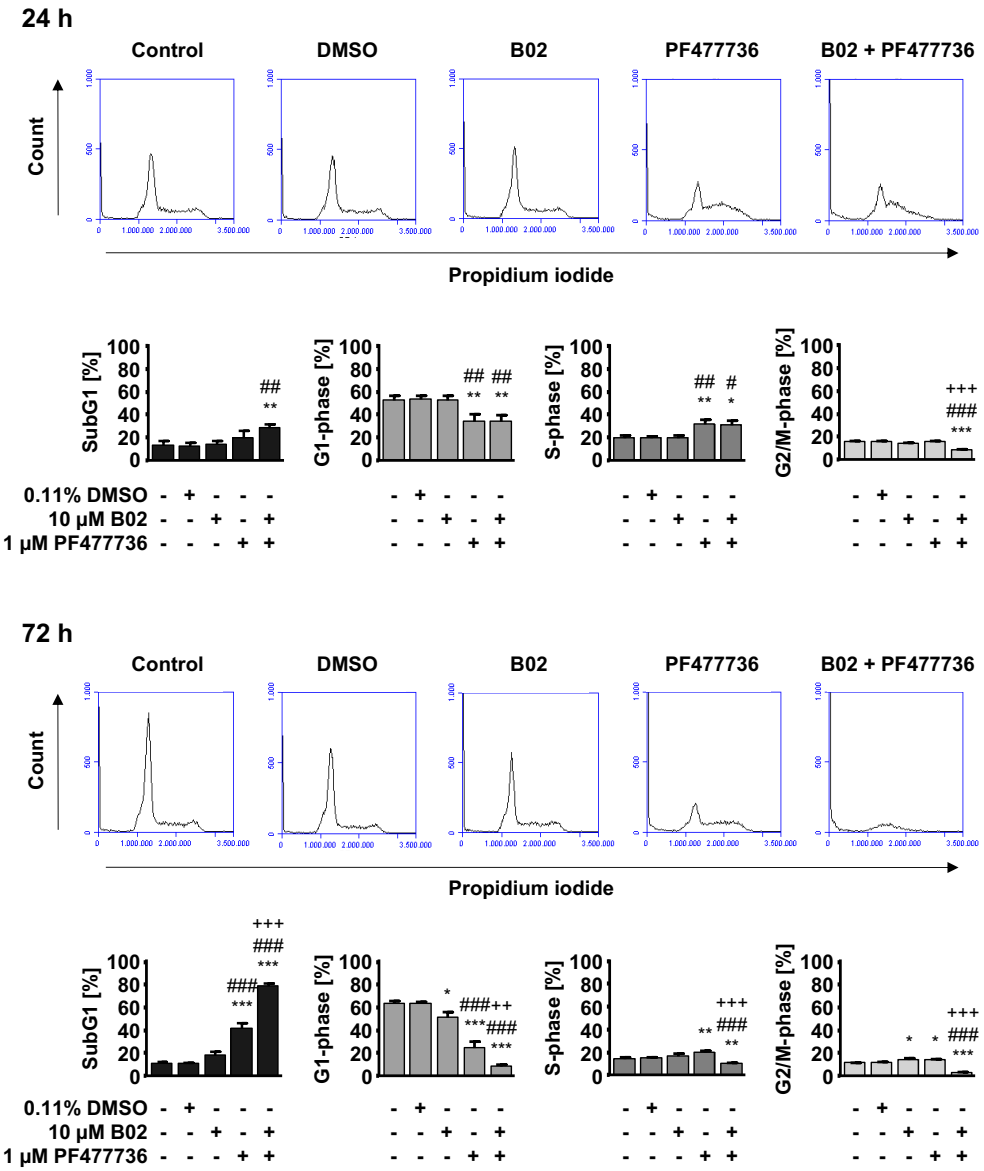

Figure 55: Cell cycle distribution analyses in J82^{CisPt} after treatment with RAD51$_i$ B02 and CHK1$_i$ PF477736

Cells were treated for 24 h or 72 h with 10 µM B02 ± 1 µM PF477736 before cell cycle distribution was analyzed by flow cytometric analysis employing propidium iodide staining. DMSO was included in the study as solvent control. Data are presented as mean + SD from n = 3 independent experiments. Displayed representative histograms and gating of the flow cytometric analyses were generated using BD Accuri C6 software. *p ≤ 0.05; **p ≤ 0.01; ***p ≤ 0.001; significant compared to control (*), to B02 mono-treatment (#) and to PF477736 mono-treatment (+).

Staining for mitosis marker pH3 revealed a reduction of the percentage of mitotic cells after 24 h both in the combination treatment and the PF4777736 mono-treatment (Figure 56).

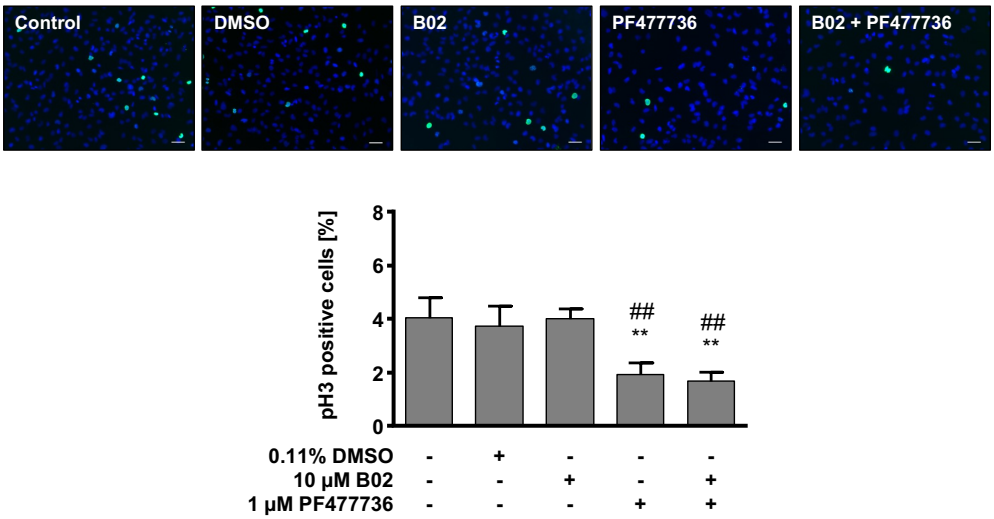

Figure 56: Phospho histone 3 (pH3) staining of J82^{CisPt} cells treated with B02 or/and PF477736
J82^{CisPt} cells were incubated with the indicated treatments for 24 h. DMSO was included in the study as solvent control. Data are presented as mean + SD and were derived from three independent experiments, where in each case 1000 – 2000 nuclei were analyzed per sample. The representative images show nuclei in blue and pH3 signal in green. The scale bar in the representative images corresponds to 50 µm. **p ≤ 0.01; significant compared to control (*) and to B02 mono-treatment (#).

In conclusion, the combination of B02 and PF477736 results in a cell cycle arrest in the S-phase, while simultaneously reducing the number of cells undergoing mitosis. It is likely that the cell cycle arrest is initiated by PF477736, as the CHK1$_i$ elicits comparable effects when administered as a monotherapy. The simultaneous inhibition of CHK1 and RAD51 still results in a higher rate of cell death, as reflected by the SubG1 fraction in the flow cytometric analysis, compared to that observed in the CHK1$_i$ mono-treated group.

3.5.3 S-phase related effects triggered by B02 + PF477736

Since RAD51 and CHK1, besides their importance in the DDR, both also play central roles in the replication stress response and a S-phase arrest was observed in the flow cytometry-based analyses, it was assumed that the synergistic cytotoxicity has its origin in the S-phase. Therefore, further investigations on replication-based effects were performed.

EdU incorporation was monitored to assess replication activity. J82^{CisPt} cells treated with the combination of RAD51$_i$ and CHK1$_i$ revealed significantly less EdU incorporating cells after 24 h of treatment than the mono-treatments with either compound, which did not show any significant changes compared to the controls (Figure 57). It can thus be stated that the simultaneous administration of both inhibitors reduces the replication activity of J82^{CisPt} cells in synergistic manner.

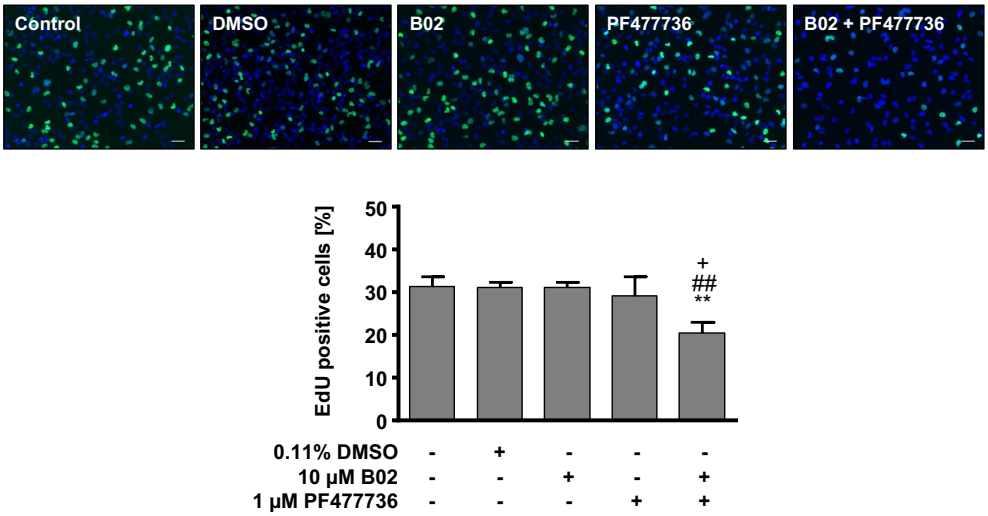

Figure 57: EdU incorporation assay of J82^{CisPt} cells treated with B02 or/and PF477736
J82^{CisPt} cells were incubated with the indicated treatments for 24 h followed by an EdU pulse of 2 h. DMSO was included in the study as solvent control. Data are presented as mean + SD and were derived from three independent experiments, where in each case 1000 – 2000 nuclei were analyzed per sample. The representative images show nuclei in blue and EdU signal in green. The scale bar in the representative images corresponds to 50 µm. *p ≤ 0.05; **p ≤ 0.01; significant compared to control (*), to B02 mono-treatment (#) and to PF477736 mono-treatment (+).

In order to analyze the effect of co-treatment with B02 + PF477736 on the level of DNA replication forks, a DNA fiber spreading assay was performed. Analysis of J82^{CisPt} cells treated for 6 h with the combination of CHK1$_i$ + RAD51$_i$ revealed shorter chlorodeoxyuridine (CldU) and iododeoxyuridine (IdU) tracks in double-labelled DNA fibers compared to the untreated control and the mono-treatments, indicating slowed replication fork progression (Figure 58A). The shorter DNA fibers are unlikely to be a consequence of excessive origin firing, as the percentage of origins, indicated by tricolored fibers with the arrangement red-green-red, did not show major differences between the groups, particularly between PF477736 treatment (20%) and B02 + PF77736 treatment (18%) (Figure 58B). The two red tracks in these fibers should normally have the same length, as the replication forks should run at the same speed in both directions. However, comparing the length of the two red tracks on each tricolored fiber revealed a statistically significant increase in asymmetry after combination treatment as compared to all other groups (Figure 58C). This indicates severe replication fork stalling. In conclusion, B02 + PF77736-treated J82^{CisPt} cells show a strong disruption of DNA replication dynamics due to replication fork stalling that is not seen after either drug alone.

A

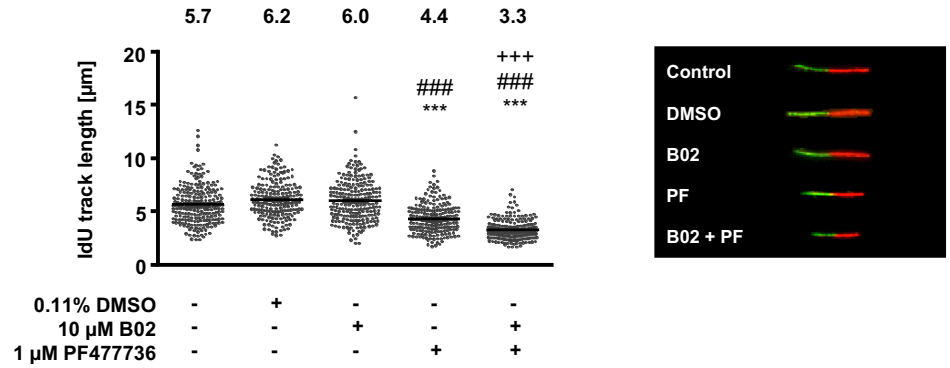

B

% (mean ± SD)	Control	DMSO	B02	PF477736	B02 + PF477736
Origins	13.1 ± 1.7	8.1 ± 2.1 ns	12.6 ± 7.8 ns	19.9 ± 2.2 ns	17.8 ± 11.9 ns
Terminations	32.2 ± 6.8	35.4 ± 6.7 ns	26.1 ± 2.1 ns	28.4 ± 1.6 ns	12.4 ± 3.0 *

C

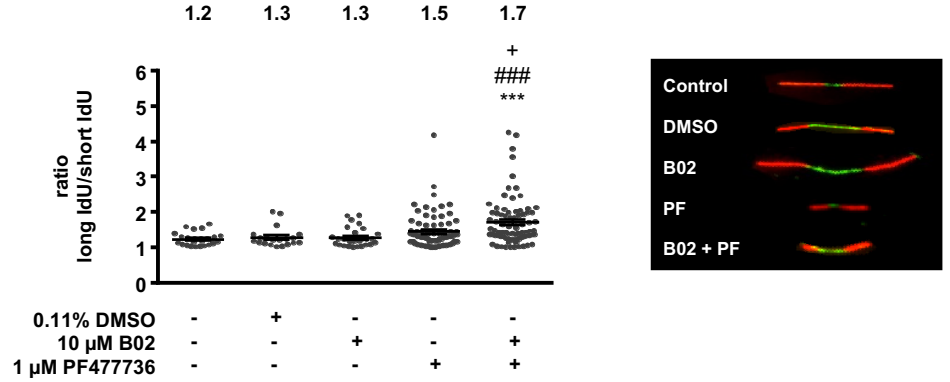

Figure 58: DNA fiber spreading assay of J82^{CisPt} cells treated with B02 or/and PF477736
Cells were treated with 10 µM B02, 1 µM PF477736 or the combination of both for 6 h. DMSO was included in the study as solvent control. Directly after, cells were pulse-treated with two different BrdU analogs (CldU and IdU) for 20 minutes each. Following immunofluorescence staining, DNA fibers were analyzed microscopically, and fiber lengths were measured using ImageJ. Data presented were obtained from two independent experiments, where in each case 200 fibers were measured per sample. Each dot represents one analyzed fiber, and the black lines show the mean ± SEM. The mean values are also given above the graphs.
A: For the evaluation of nascent DNA elongation, the IdU and CldU track lengths of bi-colored DNA fibers was measured. Graphically displayed here is the IdU track length.
B: Table summarizing the evaluation of proportions of origins and terminations in the total fiber population (ns: not significant).
C: As measure of DNA replication fork stalling, fork asymmetry was determined from three-colored replication origins as the ratio of the longer red IdU fiber track length versus the shorter red IdU fiber track length departing from the same green CldU track.
*p ≤ 0.05; **p ≤ 0.01; ***p ≤ 0.001; significant compared to control (*), to B02 mono-treatment (#) and to PF477736 mono-treatment (+).

As a mediator of the intra-S-phase checkpoint and as target of one of the compounds used, the mRNA expression of CHK1 was measured and revealed no compensatory effects for CHK1 at the mRNA level (Figure 59). PPP2R4 encodes for the regulatory subunit and PPP2CA for the catalytic subunit alpha isoform of protein phosphatase 2A

(PP2A), which dephosphorylates the cell cycle regulator retinoblastoma protein (Rb) after DNA damage in S-phase. By this, DNA synthesis is suppressed and cell cycle arrest is initiated (Tong *et al.*, 2015). The mRNA expression of the catalytic subunit of PP2A was moderately upregulated by the CHK1 inhibitor treatment (PF477736) to slightly below the set threshold. However, with the simultaneous inhibition of CHK1 and RAD51, which presumably induces more DNA damage than CHK1 inhibitor treatment alone, mRNA expression tended to return to control levels. IGBP1 is a positive regulator of PP2A that protects the catalytic subunit from degradation (Kong *et al.*, 2009). Likewise, LCMT-1 is a positive regulator of PP2A that performs methylation of the catalytic subunit required for holoenzyme assembly (Stanevich *et al.*, 2011). Both regulators showed no differential mRNA expression after treatment with the inhibitors.

Of the DNA polymerases investigated, only the mRNA of polymerase ι (POLI), an error-prone polymerase involved in translesion synthesis, was slightly below 2-fold upregulated after combination treatment with B02 + PF477736. The catalytic subunits of the replicative polymerases δ (POLD1) and ε (POLE) showed no change in mRNA expression after treatment with the inhibitors. Polymerase beta (POLB), which is involved in base excision repair, and the repriming polymerase PrimPol were also not affected in their expression by the treatment.

In conclusion, the mRNA expression data provide no evidence to suggest enhanced direct or indirect stimulation of PP2A, which would facilitate DNA damage-induced cell cycle arrest in S-phase after combined treatment with B02 and PF477736. The missing transcriptional upregulation of polymerases indicates that there is no increase in DNA synthesis or bypass of replication barriers.

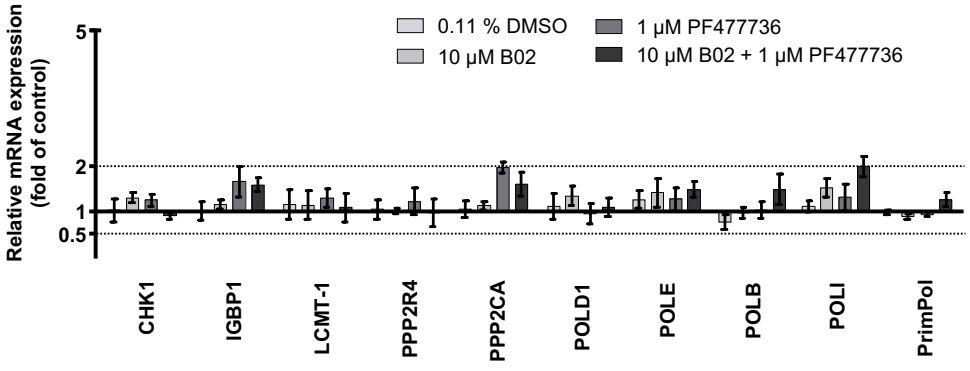

Figure 59: mRNA expression of replication-related factors in J82^{CisPt} after treatment with RAD51$_i$ B02 and CHK1$_i$ PF477736

Cells were treated for 24 h with the indicated substance(s) before mRNA expression analysis of selected factors by RT-qPCR. DMSO was included in the study as solvent control. The untreated control was set to 1.0 and all other treatments were related to this. Thresholds for increased/decreased mRNA expression were set at 2-fold difference between treated vs. untreated (dotted lines). cDNA used for mRNA expression analyses was generated from pooled samples of three independent experiments and data presented are the mean ± SD from technical triplicates.

It is known that due to uncoupling of the minichromosome maintenance protein complex (MCM) helicase from the replication complex, excessive DNA unwinding occurs at stalled replication forks. This results in high levels of ssDNA (Byun *et al.*, 2005). Such ssDNA will be protected from degradation by coating with RPA. RPA-coated ssDNA generates analyzable foci in the nuclei, thus serving as a surrogate marker for the cellular level of ssDNA. The number of RPA foci per nucleus was increased significantly after $CHK1_i$ treatment for 6 h and 24 h (Figure 60). With the combinatory treatment of B02 and PF477736, the number of RPA foci was also increased already after 6 h of treatment and rose even further after 24 h treatment. This accumulation of RPA foci was found to be significantly elevated not only in comparison to the untreated control, but also in comparison to the mono-treatment with either inhibitor.

These findings indicate that the use of the $RAD51_i$ as a mono-treatment does not result in the formation of single-stranded DNA, whereas the $CHK1_i$ is found to be capable of doing so. Still, treatment with $RAD51_i$ and $CHK1_i$ results in the more pronounced formation of single-stranded DNA compared to mono-treatment with the $CHK1_i$ at an early and late time point. This finding is consistent with the previous observations concerning the induction of arrested replication forks (Figure 58), which are postulated to be a significant source of ssDNA.

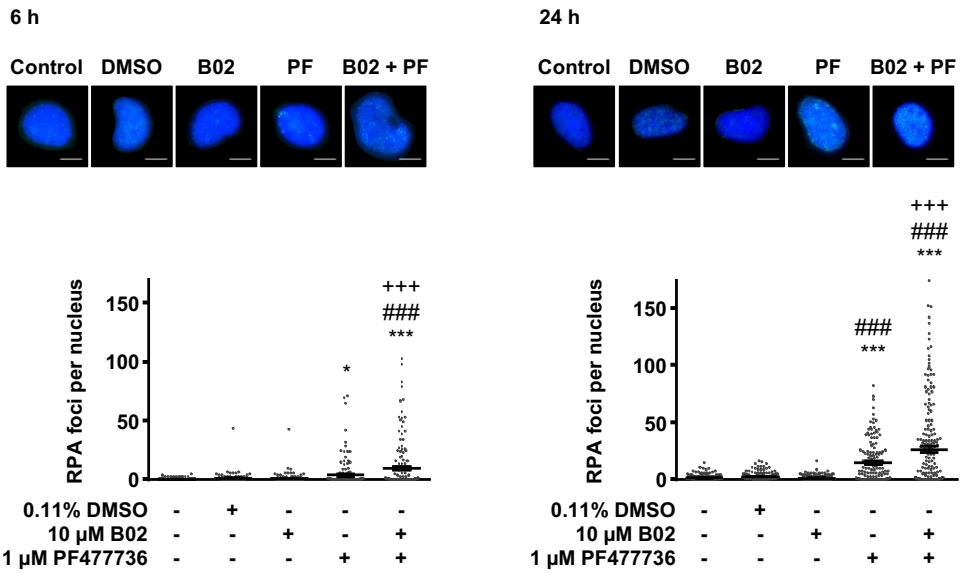

Figure 60: Nuclear RPA foci formation in J82^{CisPt} cells treated with B02 or/and PF477736
Cells were treated for 6 h or 24 h with 10 µM B02 or/and 1 µM PF477736 before immunocytochemical staining of RPA. DMSO was included in the study as solvent control. Data are shown with each dot representing one analyzed nucleus and the black lines showing the mean ± SEM from three independent experiments, where in each case foci in 50 nuclei were counted. The scale bar in the representative pictures correspond to 10 µm. * $p \leq 0.05$; ** $p \leq 0.01$; *** $p \leq 0.001$; significant compared to control (*), to B02 mono-treatment (#) and to PF477736 mono-treatment (+).

Furthermore, after 24 h monotherapy with $CHK1_i$ and already after 6 h concurrent treatment with $RAD51_i$, high protein levels of the ATR-catalyzed Ser33-phosphorylated RPA subunit RPA32 and the DNA-PK- and ATM-mediated Ser4/Ser8-phosphorylated RPA32 were detected (Figure 61). These RPA phosphorylations are catalyzed by the aforementioned members of the phosphatidylinositol 3-kinase-related kinase family in response to replication stress for the recruitment of DNA repair proteins (Lai *et al.*, 2019). The amount of Ser345-phosphorylated CHK1 was equally high after PF477736 and the combination treatment with B02 at both time points. This activating phosphorylation of CHK1 is catalyzed by ATR in response to blocked DNA replication (Zhao and Piwnica-Worms, 2001). Paradoxically, the accumulation of Ser345-phosphorylated CHK1 is also regarded as measure of CHK1 inhibition (Leung-Pineda *et al.*, 2006). Since the same concentration of PF477736 was used in the mono- and combination-treatment group, it was reasonable that phosphorylation occurred to a similar extent with both treatments. The protein expression of the repriming polymerase PrimPol remained unchanged by the applied treatments (Western Blot analysis of PrimPol was conducted by Lena Abbey (Institute of Toxicology, Heinrich Heine University, Düsseldorf)). In conclusion, the combined inhibition of RAD51 and CHK1 exhibited a more pronounced activation of RPA at an early time point than the two inhibitors individually.

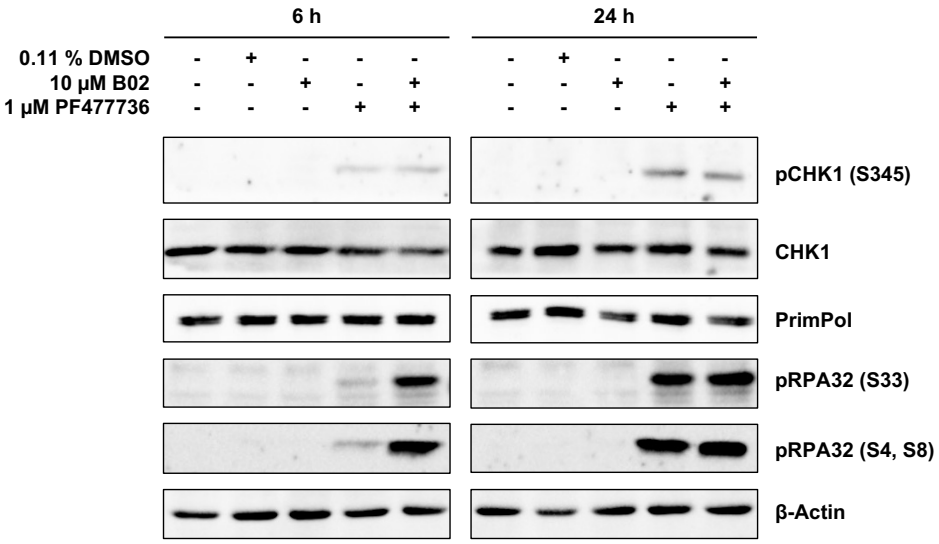

Figure 61: Protein expression of replication stress response factors in $J82^{CisPt}$ after treatment with $RAD51_i$ B02 and $CHK1_i$ PF477736
Cells were treated for 6 h or 24 h with the indicated substance(s) before protein expression was examined via Western blot analyses. DMSO was included in the study as solvent control. The protein expression of β-Actin was used as loading control. Western Blot analysis of PrimPol was conducted by Lena Abbey (Institute of Toxicology, Heinrich Heine University Düsseldorf).

Errors that occur during S-phase can be carried over into mitosis and interfere with the proper separation of cells. More precisely, errors in S-phase can lead to the transition of premature cells with under-replicated DNA into mitosis. Indeed, double staining with the pH3 antibody and propidium iodide sporadically showed pH3 positive cells with a DNA content of S-phase cells (2.77%), indicating a premature entry of some co-treated J82^{CisPt} cells into mitosis (Figure 62). Moreover, when DAPI-stained nuclei were examined by fluorescence microscopy, some of the nuclei of the co-treated cells showed morphological features of mitotic catastrophe, such as multiple nucleus fragments (Figure 63) (Sazonova *et al.*, 2021).

These data suggests that some cells, following treatment with B02 + PF477736, are able to progress from the S-phase to mitosis despite having under-replicated DNA. Nevertheless, mitosis is then most likely severely disrupted - to the extent that the cells are forced to undergo a mitotic catastrophe. Of note, only a small proportion of the total cell population exhibited the described phenotype.

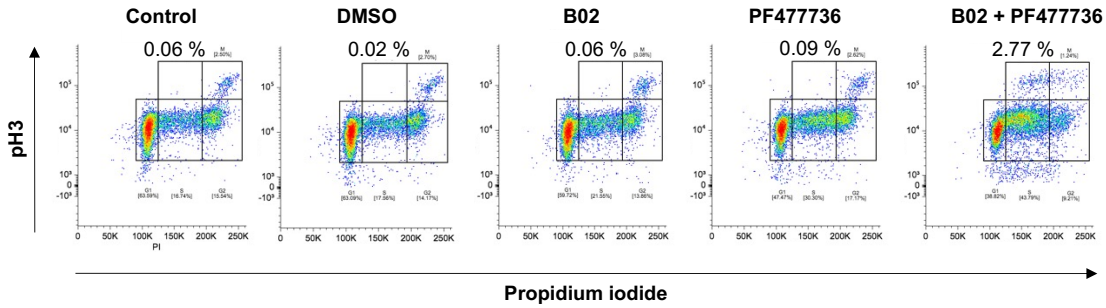

Figure 62: Analysis of J82^{CisPt} cells entering mitosis with under-replicated DNA after treatment with RAD51$_i$ B02 and CHK1$_i$ PF477736
Cells were treated with RAD51 inhibitor B02 (10 µM), CHK1 inhibitor PF477736 (1 µM) or both for 24 h. DMSO was included in the study as solvent control. To analyze the DNA content of cells undergoing mitosis, a co-staining of pH3 (Ser10) and propidium iodide was applied and examined by flow cytometry with emphasis on pH3-positive cells containing DNA content of S-phase cells. Displayed representative images and gating of the flow cytometric analyses were generated using Floreada.io web application.

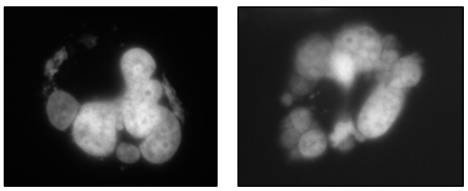

Figure 63: Representative pictures of mitotic catastrophe in J82^{CisPt} treated with B02 + PF477736
Displayed representative images were taken after DAPI staining of J82^{CisPt} cells treated for 24 h with a combination of RAD51 inhibitor B02 (10 µM) and CHK1 inhibitor PF477736 (1 µM).

3.5.4 DNA damage induction and DDR activation by B02 + PF477736

Since the replication stress induced by B02 + PF477736 did not appear to lead to cell death via mitotic catastrophe for the most part, the question remained as to how the replication stress ultimately triggers cell death. It should therefore be investigated whether the observed replicative stress leads to DNA damage and activation of the DDR and, if so, which mechanisms are involved exactly.

To this end, the expression of some general stress markers and detoxifying enzymes, as well as DDR and DNA repair factors were analyzed on the mRNA level. Among general stress markers and detoxification enzymes, heme oxygenase 1 (HMOX1) and heat shock protein family A member 1B (HSPA1B) mRNA levels were similarly upregulated by B02 alone and in combination with PF477736, while AKT serine/threonine kinase 1 (AKT1), glutathione S-transferase 1 (GSTM1), superoxide dismutase 1 and 2 (SOD1, SOD2) were unaffected by the treatments used (Figure 64A).

The mRNA expression of RAD51 itself and its paralogs were not altered by the applied treatments. Both with B02 alone and in combination with PF477736, BRCA1 was just below the limit to be considered upregulated (Figure 64B). The mRNA expression of BRCA2, on the other hand, was increased with the PF477736 mono treatment just above the defined threshold and slightly more in combination with B02. RAD52 mRNA was also slightly upregulated after treatment with the CHK1 inhibitor, but in combination with B02 close to control level again. Growth arrest and DNA-damage-inducible alpha (GADD45A) mRNA was upregulated about 12-fold after PF477736 mono-treatment and a bit weaker at 8-fold in the combination treatment. The mRNA expression of DNA damage inducible transcript 3 (DDIT3) was slightly upregulated after B02 treatment (2.6-fold), more strongly with PF477736 treatment (6.7-fold) and even more in the combination of both inhibitors (13.4-fold). CDKN1A (p21) behaves similarly with a 2.3-fold increased mRNA expression after B02, a 3.7-fold increased mRNA expression after PF477736 and a 7-fold increased mRNA expression after the combination of both inhibitors. CDKN1A and DDIT3 thus showed synergistic mRNA expression through the combination of both compounds, which may be indicative of cell cycle arrest induction in synergistic manner by the simultaneous inhibition of RAD51 and CHK1. Moreover, the elevated mRNA expression of DDIT3 may indicate pro-apoptotic processes.

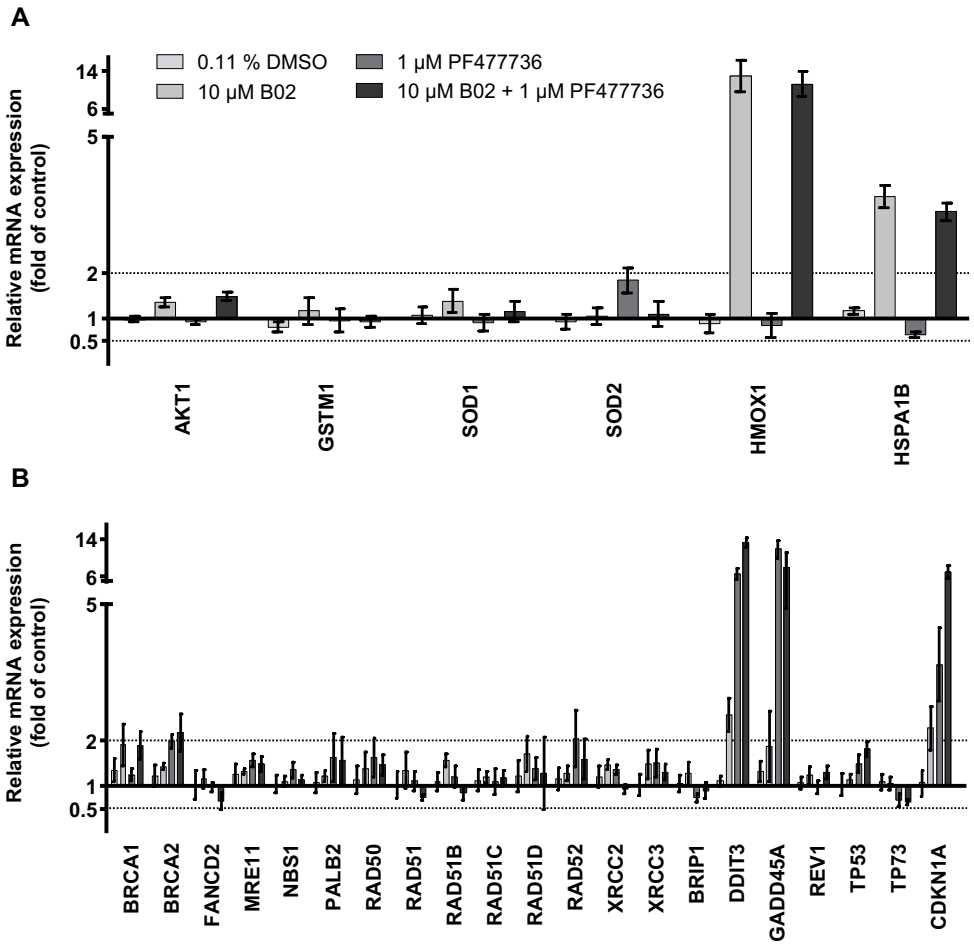

Figure 64: mRNA expression of cellular stress markers, DNA damage response and DNA repair factors in J82^{CisPt} after treatment with RAD51$_i$ B02 and CHK1$_i$ PF477736
Cells were treated for 24 h with the indicated substance(s) before mRNA expression analysis of selected cellular stress markers (A) and DNA damage response and DNA repair factors (B) by RT-qPCR. DMSO was included in the study as solvent control. The untreated control was set to 1.0 and all other treatments were related to this. Thresholds for increased/decreased mRNA expression were set at 2-fold difference between treated vs. untreated (dotted lines). cDNA used for the mRNA expression analyses was generated from pooled samples of three independent experiments and data presented are the mean ± SD from technical triplicates.

Phosphorylated Histone 2AX at Ser139 (γH2AX), a known marker of DNA damage and replication fork collapse (Fragkos *et al.*, 2023), was detected in Western blot samples already after 6 h of RAD51$_i$ + CHK1$_i$ co-treatment, while RAD51$_i$ or CHK1$_i$ treatment alone did not or not yet induce such a signal (Figure 65). KAP1 is phosphorylated on Ser824 by ATM in response to genotoxic stress and is thought to be essential for chromatin relaxation, which is in turn important for transcription of various DDR factors and DNA repair (Ziv *et al.*, 2006). KAP1 phosphorylated at this phosphorylation site could be detected via Western blot analysis after 6 h and 24 h with PF477736 mono treatment and in combination with B02 in the same extent. p53 is a key player in the DDR and can initiate different response pathways through phosphorylation at different sites. The phosphorylation site Ser15 investigated here is known to trigger cell cycle arrest. Like pKAP1, pP53 was detected at a comparable level in the CHK1$_i$ mono treatment

and the combination treatment with RAD51$_i$. This phosphorylation, however, visibly increased with longer treatment duration. The protein expression of RAD51 as a DNA repair protein and as target of one of the inhibitors used was also investigated. It was found that the RAD51 protein level decreased after 24 hours of treatment with the combination of B02 and PF477736. However, the protein expression was not visibly changed with the RAD51 inhibitor B02 alone or at the earlier time point analyzed (Western Blot analysis of RAD51 was conducted by Lena Abbey (Institute of Toxicology, Heinrich Heine University, Düsseldorf)). In summary, these data demonstrate that the phosphorylation of H2AX at an early time point is specifically synergistically triggered by the inhibition of RAD51 and CHK1, whereas the activation of other DDR factors examined does not reflect the synergistic interplay.

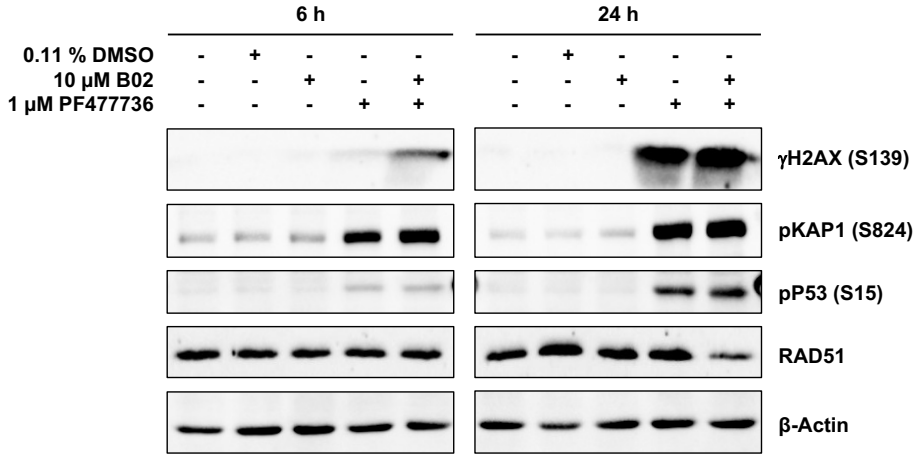

Figure 65: Protein expression and activation of DNA damage response and DNA repair factors in J82^{CisPt} after treatment with RAD51$_i$ B02 and CHK1$_i$ PF477736
Cells were treated for 6 h or 24 h with the indicated substance(s) prior protein expression analysis via Western blot. DMSO was included in the study as solvent control. The protein expression of β-Actin was used as loading control. Western Blot analysis of RAD51 was conducted by Lena Abbey (Institute of Toxicology, Heinrich Heine University Düsseldorf).

The synergistic induction of DNA damage seen in the γH2AX signal in the Western blot analysis was confirmed using the alkaline comet assay, which specifically detects DNA strand breaks. Accordingly, cells treated with B02 + PF477736 showed a significantly higher comet tail intensity than PF477736 mono-treated cells after 24 h treatment (Figure 66).

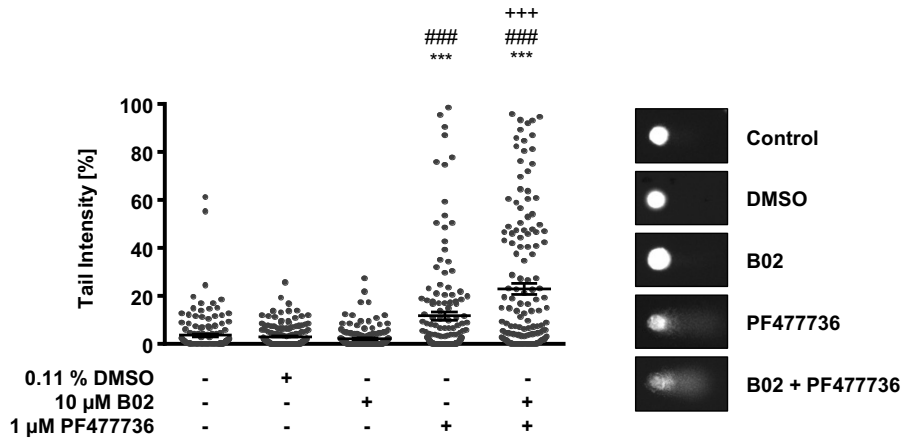

Figure 66: Alkaline comet assay of J82^{CisPt} cells treated with B02 or/and PF477736
J82^{CisPt} cells were incubated with the indicated treatments for 24 h. DMSO was included in the study as solvent control. Data presented were derived from three independent experiments, where in each case the tail intensity of 50 cells per sample were analyzed. Each dot represents one analyzed cell and the black lines show the mean ± SEM. ***p ≤ 0.001; significant compared to control (*), to B02 mono-treatment (#) and to PF477736 mono-treatment (+).

Analyzing the number of γH2AX positive cells in different phases of the cell cycle revealed that DNA damage is mainly generated in S-phase cells (Figure 67). A clear increase in γH2AX positive S-phase cells was detected already after 6 h of RAD51$_i$ + CHK1$_i$ treatment. This was not observed in the mono-treated groups. Consistent with the Western blot analysis, the PF477736-treated group showed a marked but slightly less pronounced γH2AX signal compared to the co-treated group after 24 h of incubation, while B02 mono-treatment did not cause any increase in the γH2AX signal.

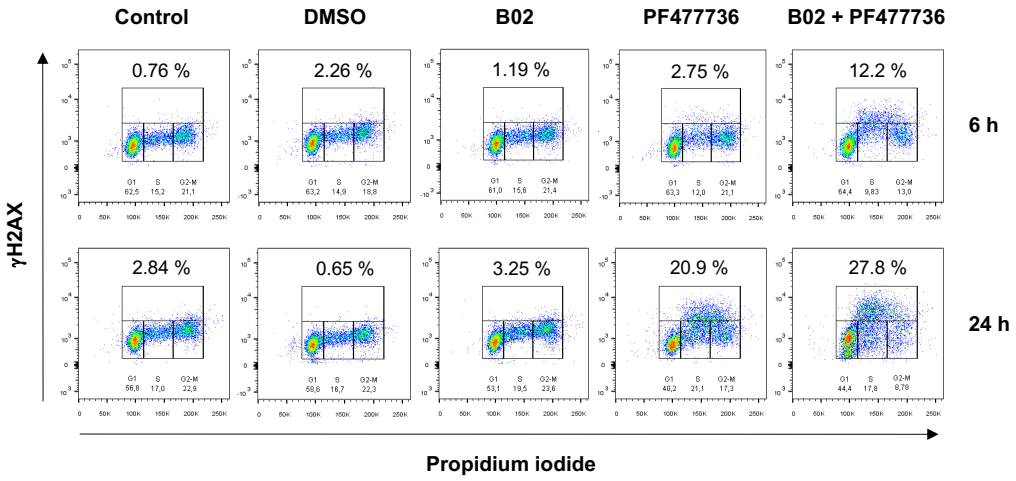

Figure 67: Analysis of cell cycle phase-specific DNA damage signaling in J82^{CisPt} cells after treatment with RAD51$_i$ B02 and CHK1$_i$ PF477736
Cells were treated with CHK1 inhibitor PF477736 (1 µM), RAD51 inhibitor B02 (10 µM) or both for 6 h or 24 h. DMSO was included in the study as solvent control. To analyze the DNA content of cells showing DNA damage signaling, a co-staining of γH2AX and propidium iodide was applied and examined by flow cytometry. A total of 10000 counts per sample were measured for quantification. Displayed representative images and gating of the flow cytometric analyses were generated using FlowJo software.

To check whether the γH2AX positive cells are the same cells that have a large number of RPA foci, i.e. strong replication stress, co-staining was applied. This staining indicated that cells with a high number of RPA foci in their nuclei were indeed the primary source of the γH2AX signal, since nuclei with more than 10 RPA foci showed significantly stronger γH2AX signal than nuclei with less than 10 RPA foci (Figure 68).

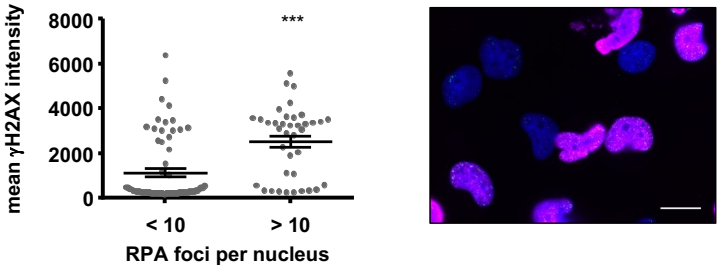

Figure 68: Immunocytochemical co-staining of γH2AX and RPA in J82^{CisPt} cells after co-treatment with B02 + PF477736
J82^{CisPt} cells were treated with 10 µM B02 + 1 µM PF477736 for 24 h before immunocytochemical co-staining of γH2AX and RPA to test for correlation of both markers. For γH2AX the mean fluorescence intensity of nuclei was measured and for RPA foci per nucleus were counted. Data are shown with each dot representing one analyzed nucleus and the black lines showing the mean ± SEM from two independent experiments, where in each case 50 nuclei were analyzed. The representative image shows nuclei in blue, γH2AX signal in magenta and RPA foci in green. The scalebar in the representative image corresponds to 20 µm. ***$p \leq 0.001$; significant compared to nuclei with < 10 RPA foci.

Taken together, the combined treatment with B02 and PF477736 demonstrated a synergistic effect on the induction of DNA strand breaks and S-phase-specific DNA damage signaling, particularly after a short treatment period. In addition, this DNA damage signaling is predominantly attributed to cells that exhibit elevated levels of ssDNA.

3.6 Transferability of the findings with B02 + PF477736 in J82^{CisPt} to other tumor cell lines and other RAD51 and CHK1 inhibitors

Since the investigations have so far only been carried out in one cell line (J82^{CisPt}), the transferability of the results to other cisplatin-resistant cell lines of different tumor entities, as well as the parental J82 cells, should be assessed. In addition, further modulators of RAD51 and CHK1 were combined to see whether the synergistic effect and underlying mechanism of B02 and PF477736 is compound group-uniform. Some of these modulators have a slightly different specificity or mode of action than B02 or PF477736, hence, comparing the results with each other may provide further insight into the exact molecular mechanism of the concurrent treatment with CHK1$_i$ and RAD51$_i$.

3.6.1 Cytotoxicity of B02 + PF477736 in J82^{WT} and cisplatin-resistant cells of other tumor entities

J82^{WT} cells were treated with four different concentration combinations of B02 + PF477736 and viability was measured after 72 h incubation. Calculation of the combination indices from the measured viability data revealed slightly synergistic cytotoxic effects for one combination and additive effects for the other three (Figure 69).

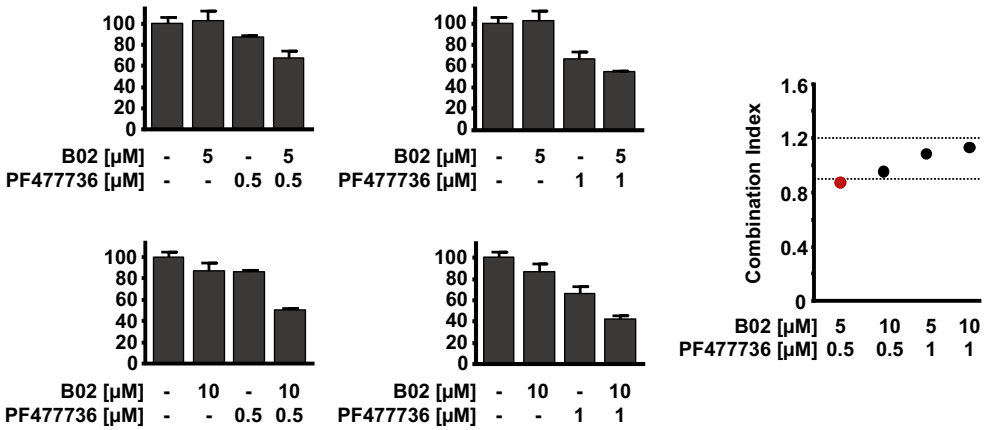

Figure 69: Viability of J82^{WT} after co-treatment with RAD51$_i$ B02 and CHK1$_i$ PF477736
J82^{WT} cells were treated with different low to moderate cytotoxic concentrations of B02 (5 µM, 10 µM) or/and PF477736 (0.5 µM, 1 µM) over a 72-hour period. Subsequently, cell viability was measured via the AlamarBlue assay. The untreated control was set to 100% viability and all other groups were related to this. Data presented are the mean + SD from biological quadruplicates. From the obtained viability data, combination indices (CI) were calculated using CompuSyn software (CI > 1.2 antagonistic; 0.9 ≤ CI ≤ 1.2 additive; CI < 0.9 synergistic).

The same experimental approach was used for the cisplatin-resistant cell lines SH-SY5Y^{CisPt}, A549^{CisPt} and A2780^{CisPt}. The neuroblastoma cells SH-SY5Y^{CisPt} and the lung carcinoma cells A549^{CisPt} showed a synergistic reduction in viability with three of the four tested concentration combinations of B02 + PF477736 (Figure 70A, B). In contrast, only additive cytotoxic effects were observed with the ovarian cancer cells A2780^{CisPt} (Figure 70C).

In conclusion, the simultaneous inhibition of RAD51 and CHK1 has been demonstrated to induce a synergistic cytotoxic response not only in J82 bladder carcinoma cells, but also in cisplatin-resistant cell lines derived from other tumor entities. Nevertheless, this outcome does not appear to be universally valid for all cisplatin-resistant cell lines.

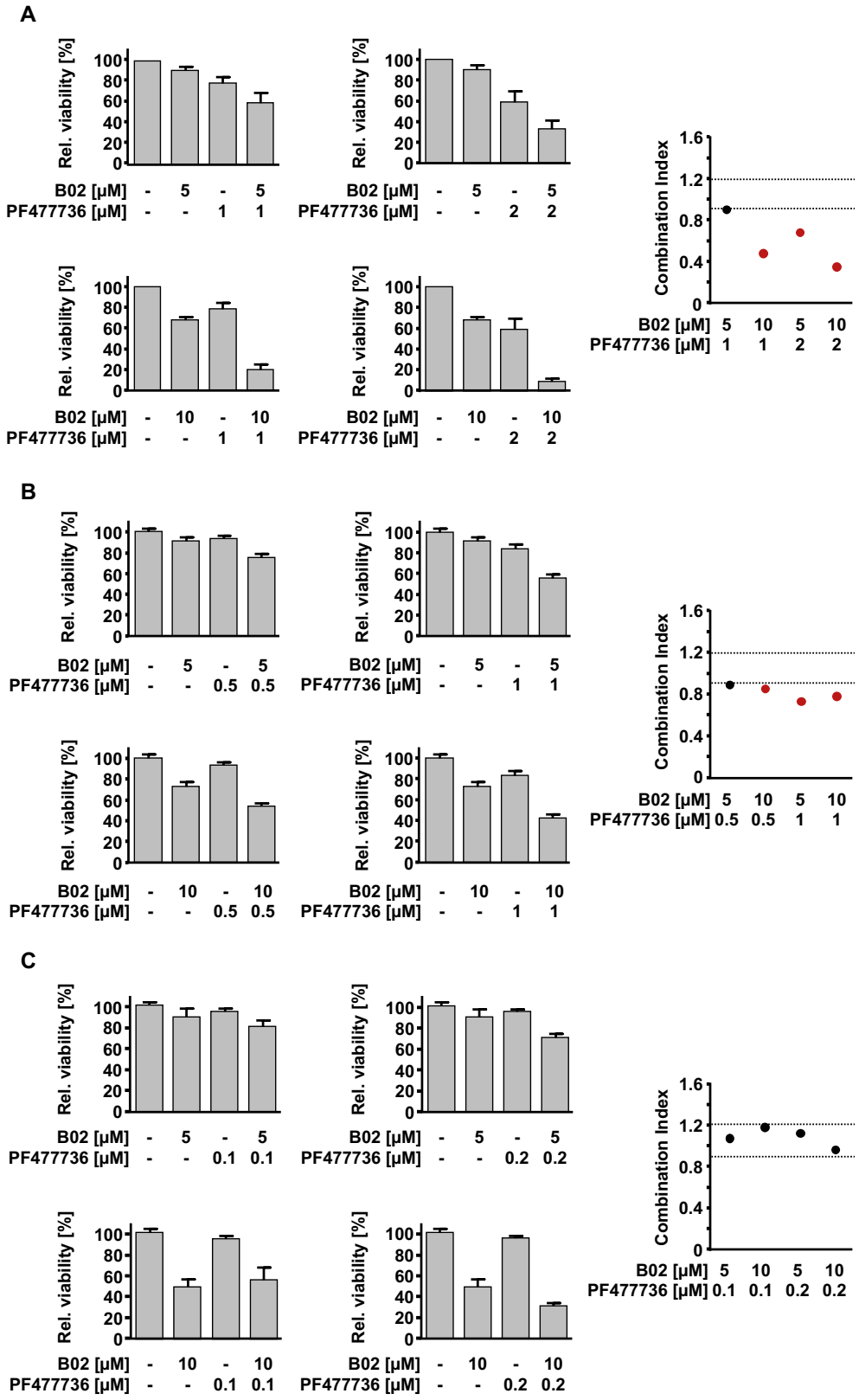

Figure 70: Viability of cisplatin resistant tumor cells of different tissue types after co-treatment with RAD51$_i$ B02 and CHK1$_i$ PF477736

SH-SY5Y^{CisPt} neuroblastoma cells (A), A549^{CisPt} lung cancer cells (B) or A2780^{CisPt} ovarian cancer cells (C) cells were treated with different low to moderate cytotoxic concentrations of B02 or/and PF477736 for 72 h and viability was measured via the AlamarBlue assay. The viability of the untreated control for each cell variant was set at 100%, and all associated treatments were related to this value. Data presented are the mean + SD from one to three independent experiments, each performed in biological quadruplicates. The viability data were used to calculate combination indices (CI) with the use of the CompuSyn software (CI > 1.2 antagonistic; 0.9 ≤ CI ≤ 1.2 additive; CI < 0.9 synergistic).

These results raised the question of why this distinct reaction occurred. Therefore, the basal protein levels of RAD51, CHK1 and PrimPol were analyzed in the different cisplatin-resistant cell variants and their parental cell lines. This analysis revealed that CHK1 and RAD51 proteins were almost not detectable in A2780^{CisPt} cells, although A2780^{WT} cells still expressed both of them (Figure 71). A2780^{CisPt} also expressed slightly less PrimPol than their parental cells A2780^{WT}. Between the other cell pairs, there were no major differences in protein expression of all analyzed factors.

These findings indicate that the low protein expression of RAD51 and CHK1 may be a contributing factor to the comparatively weak response of A2780^{CisPt} cells to simultaneous inhibition of these two factors. In addition, the evidence suggests that the protein expression of PrimPol, a TLS polymerase, is not a determinant in this regard.

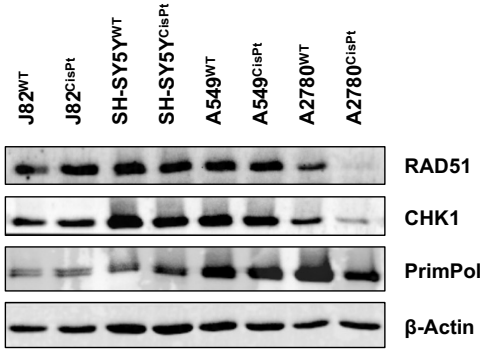

Figure 71: Protein expression of RAD51, CHK1 and PrimPol in tumor cell lines originating from different tissue types and their CisPt resistant counterparts under basal conditions
The protein expression of RAD51, CHK1 and PrimPol was measured in J82^{CisPt} bladder carcinoma cells, SH-SY5Y^{CisPt} neuroblastoma cells, A549^{CisPt} lung cancer cells and A2780^{CisPt} ovarian cancer cells and their parental counterparts. The protein expression of β-Actin was used as loading control.

3.6.2 Mechanistic studies in SH-SY5Y^{CisPt}

As described above (see chapter 3.6.1), synergistic cytotoxic effects were found in cisplatin-resistant SH-SY5Y cells with the combination of B02 and PF477736. To verify that the synergistic cytotoxicity in J82 and SH-SY5Y cell lines is triggered by the same molecular processes, further investigations were performed regarding key events of the molecular mechanism observed in J82^{CisPt} cells. One endpoint considered was the induction of an S-phase arrest after 24 h of treatment when measuring the cell cycle distribution in the flow cytometer. The untreated control of SH-SY5Y^{CisPt} cells showed, with only 8.1%, a not very pronounced S-phase. Treatment with the two inhibitors slightly increased the percentage of cells in S-phase, while the mono-treatments rather remained at control level (Figure 72A). The phosphorylation of RPA32 as an indicator of replication stress and γH2AX as a sign of DNA damage were selected as further key events of the mechanism. Protein expression of the two markers was detected after

the PF477736 mono-treatment and the combination treatment with B02, but more prominently with the combination treatment at the 24 h time point (Figure 72B) (Western Blot analysis of pRPA32 (S4, S8) was conducted by Lena Abbey (Institute of Toxicology, Heinrich Heine University, Düsseldorf)). Given that the key events selected from the molecular mechanism of B02 + PF477736 treatment in J82^{CisPt} cells also occur in SH-SY5Y^{CisPt} cells, it can be postulated that comparable molecular processes are responsible for the triggering of synergistic cytotoxicity in these two cell lines.

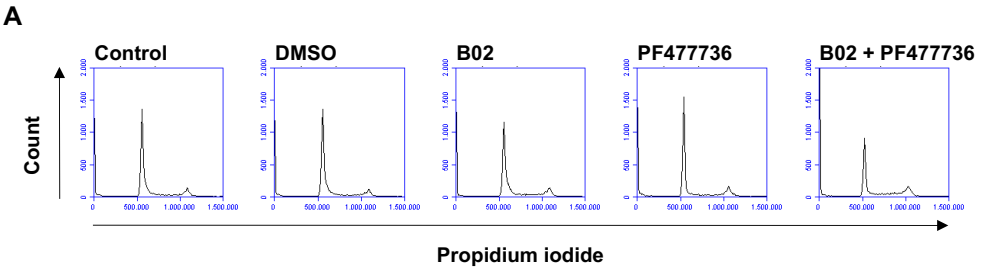

	Control	DMSO	B02	PF477736	B02 + PF477736
S-phase [%]	8.1	7.5	9.5	7.2	13.7

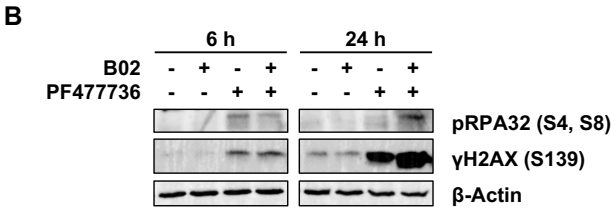

Figure 72: Reaction of SH-SY5Y^{CisPt} to co-treatment with RAD51$_i$ B02 and CHK1$_i$ PF477736
A: Following 24 h treatment with 1 µM PF477737, 10 µM B02 or a combination of both, propidium iodide-based cell cycle analysis was performed by flow cytometric measurement with emphasis on the proportion of cells in S-phase. 0.11% DMSO was included in the study as solvent control. Displayed representative histograms and gating of the flow cytometric analyses were generated using BD Accuri C6 software. A total of 10000 counts per sample were measured for quantification.
B: Induction of pRPA32 (S4, S8) and γH2AX was examined via Western blot analyses with protein extracts of SH-SY5Y^{CisPt} cells treated for 6 h or 24 h with the combination of 1 µM PF477736 + 10 µM B02 or the corresponding mono-treatments. The protein expression of β-Actin was used as loading control. Western Blot analysis of pRPA32 (S4, S8) was conducted by Lena Abbey (Institute of Toxicology, Heinrich Heine University Düsseldorf).

3.6.3 Combinations of other RAD51 and CHK1 modulators in J82^{CisPt}

In addition to PF477736, two other CHK1 inhibitors, SB218078 and LY2603618, and the pan-CHK inhibitor AZD7762 were tested in combination with RAD51$_i$ B02.

SB218078, just like PF477736, is described as selective and ATP-competitive CHK1 inhibitor (Jackson *et al.*, 2000). However, the results of the viability measurement after combining B02 with two different concentrations of SB218078 in J82^{CisPt} cells revealed additive cytotoxicity rather than synergistic cytotoxicity (Figure 73).

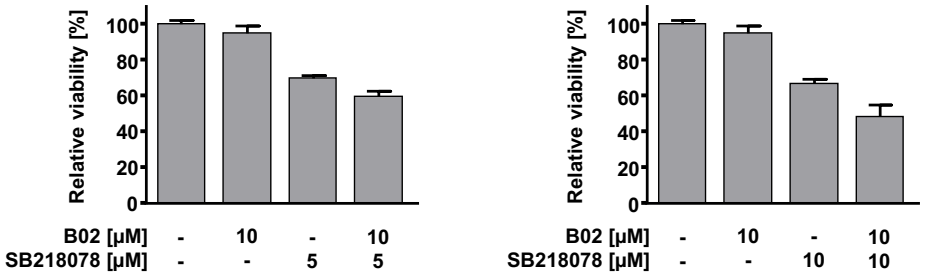

Figure 73: Viability of J82^{CisPt} after co-treatment with RAD51$_i$ B02 and CHK1$_i$ SB218078
J82^{CisPt} cells were subjected to treatment with different low to moderate cytotoxic concentrations of B02 or/and SB218078 for 72 h and cell viability was determined through the AlamarBlue assay. The untreated control was set to 100% viability and all other groups were related to this. Data presented are the mean + SD from biological quadruplicates.

LY2603618 is another well-known selective CHK1 inhibitor (King *et al.*, 2014). Combining B02 with LY2603618 evoked cytotoxicity in additive to synergistic manner in J82^{CisPt} cells (Figure 74A). Evaluating the key events of the molecular mechanism, this combination of compounds induced S-phase arrest after 24 h as well as phosphorylation of RPA32 and H2AX after 6 h already (Figure 74B, C). While the S-phase arrest was clearly stronger than following mono-treatment with LY2603618, the signals of pRPA32 and γH2AX were of similar intensity in both treatment groups.

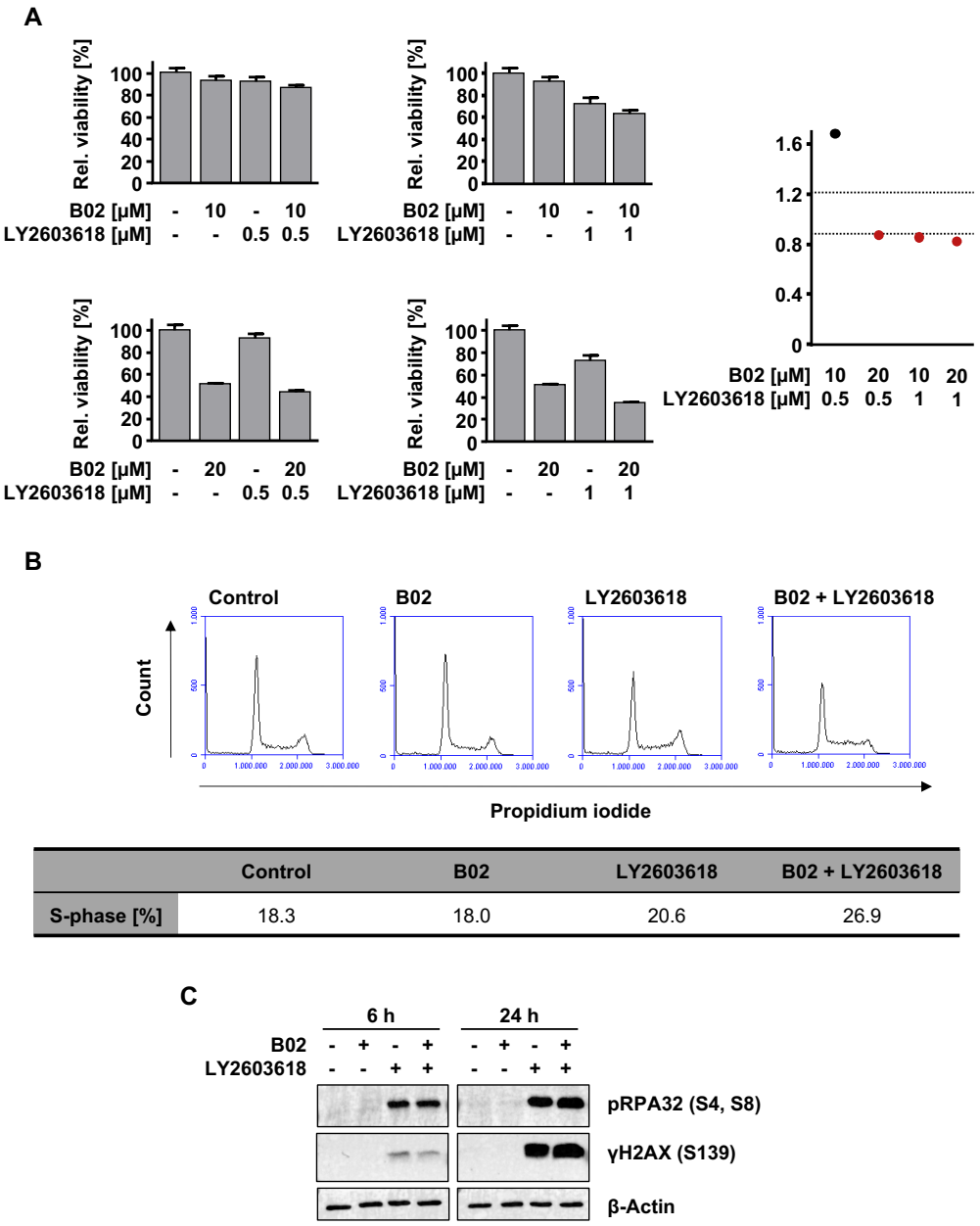

	Control	B02	LY2603618	B02 + LY2603618
S-phase [%]	18.3	18.0	20.6	26.9

Figure 74: Reaction of J82^{CisPt} to co-treatment with RAD51$_i$ B02 and CHK1$_i$ LY2603618
A: J82^{CisPt} cells were treated with the indicated concentrations of B02 or/and LY2603618 over a 72-hour period and cell viability was subsequently measured using the AlamarBlue assay. The untreated control was set to 100% viability and all other groups were related to this. Data presented are the mean + SD from three independent experiments, each performed in biological quadruplicates. From the obtained viability data, combination indices (CI) were calculated using CompuSyn software (CI > 1.2 antagonistic; $0.9 \leq CI \leq 1.2$ additive; CI < 0.9 synergistic).
B: Following 24 h treatment with 10 µM B02, 1 µM LY2603618 or a combination of both, propidium iodide-based cell cycle analysis was performed by flow cytometric measurement with emphasis on the proportion of cells in S-phase. Displayed representative histograms and gating of the flow cytometric analyses were generated using BD Accuri C6 software. A total of 10000 counts per sample were measured for quantification.
C: Induction of pRPA32 (S4, S8) and γH2AX was examined via Western blot analyses with protein extracts of J82^{CisPt} cells treated for 6 h or 24 h with the combination of 10 µM B02 + 1 µM LY2603618 or the corresponding mono-treatments. The protein expression of β-Actin was used as loading control.

The inhibitor AZD7762 also acts in a reversible and ATP-competitive manner, but unlike PF477736, AZD7762 is equally potent for both checkpoint kinases CHK1 and CHK2 (Zabludoff *et al.*, 2008). Analyzing the viability of a combination of B02 with AZD7762 revealed a greater reduction in viability than would be expected from the cytotoxicity caused by the individual substances, pointing to synergistic effects (Figure 75).

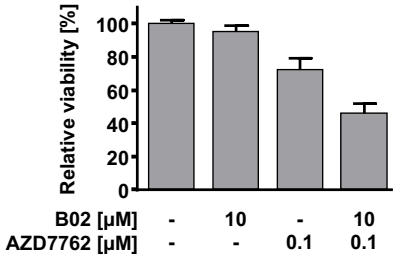

Figure 75: Viability of J82^{CisPt} after co-treatment with RAD51$_i$ B02 and pan-CHK$_i$ AZD7762
J82^{CisPt} cells were treated with different low to moderate cytotoxic concentrations of B02 or/and AZD7762 for 72 h and viability was assessed through the AlamarBlue assay. The viability of the untreated control was set at 100%, and all treatments were related to this value. Data presented are the mean + SD from biological quadruplicates.

Besides B02, two other RAD51 inhibitors, RI-1 and RI(dI)2, and the RAD51 stimulator RS-1 were evaluated in combination with CHK1$_i$ PF477736.

RI-1 covalently binds to RAD51 and thereby irreversibly destabilizes a protein-protein interface that is essential for RAD51 oligomerization into filaments on DNA (Budke *et al.*, 2012). The analysis of cytotoxicity of a combination of CHK1 inhibitor PF477736 with RI-1 resulted in rather additive to possibly slightly synergistic effects, as a mean viability of 64% was measured after combination of both agents and 77% and 94% following corresponding mono-treatments (Figure 76).

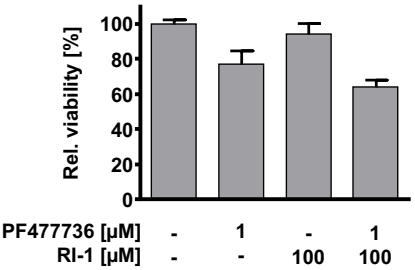

Figure 76: Viability of J82^{CisPt} after co-treatment with CHK1$_i$ PF477736 and RAD51$_i$ RI-1
J82^{CisPt} cells were treated with the indicated concentrations of PF477736 or/and RI-1 over a 72-hour period and viability was measured employing the AlamarBlue assay. The untreated control was set to 100% viability and all other groups were related to this. Data presented are the mean + SD from biological quadruplicates.

RI(dl)2 is a RAD51 inhibitor that still allows binding of RAD51 to ssDNA, but specifically inhibits D-loop formation (Lv *et al.*, 2016). Combining CHK1$_i$ PF477736 with two different concentrations of RI(dl)2 resulted in strong synergistic reduction in viability after 72 h treatment (Figure 77A). Further studies looking at some key aspects of the molecular mechanism detected with B02 + PF477736 were conducted to investigate whether the same events are initiated with RI(dl)2. Cell cycle analysis revealed a prominent S-phase arrest after 24 h treatment with the combination of both inhibitors, stronger than with PF477736 alone (Figure 77B). Also, protein expression of pRPA32 and γH2AX was induced synergistically by RI(dl)2 + PF477736 after 6 h already (Figure 77C).

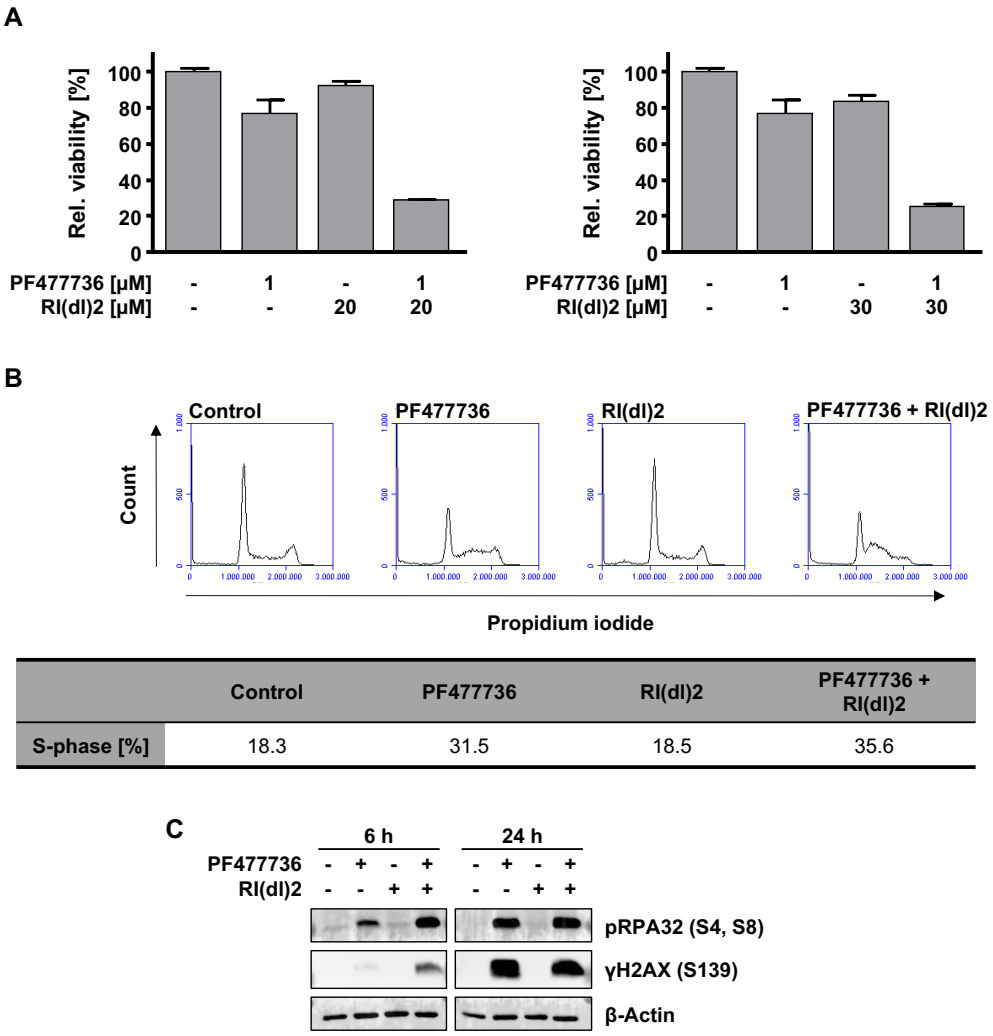

	Control	PF477736	RI(dl)2	PF477736 + RI(dl)2
S-phase [%]	18.3	31.5	18.5	35.6

Figure 77: Reaction of J82^{CisPt} to co-treatment with CHK1$_i$ PF477736 and RAD51$_i$ RI(dl)2
A: J82^{CisPt} cells were treated with the indicated concentrations of PF477736 or/and RI(dl)2 for 72 h and viability was subsequently assessed via the AlamarBlue assay. The viability of the untreated control was set at 100%, and all other groups were related to this. Data presented are the mean + SD from biological quadruplicates.
B: Following 24 h treatment with 1 µM PF477737, 30 µM RI(dl)2 or a combination of both, propidium iodide-based cell cycle analysis was performed by flow cytometric measurement with emphasis on the proportion of cells in S-phase. A total of 10000 counts per sample were measured for quantification.
C: Induction of pRPA32 (S4, S8) and γH2AX was examined via Western blot analyses with protein extracts of J82^{CisPt} cells treated for 6 h or 24 h with the combination of 1 µM PF477736 + 30 µM RI(dl)2 or the corresponding mono-treatments. The protein expression of β-Actin was used as loading control.

RS-1 is a RAD51 stimulatory compound, that enhances DNA binding of RAD51, filament stability and D-loop formation (Jayathilaka *et al.*, 2008). J82^{CisPt} cells were treated with a combination of PF477736 and RS-1 to see if RS-1, through its RAD51 stimulatory properties, can revert the cytotoxic effect mediated by the CHK1 inhibitor. However, the combination of PF477736 + RS-1 resulted in a synergistic reduction in viability to a similar extent as the combination of PF477736 with RAD51$_i$ B02 (Figure 78). Treatment of the cells with all three modulators (PF477736, B02 and RS-1) also led to a similar cytotoxic effect as with the other two combinations.

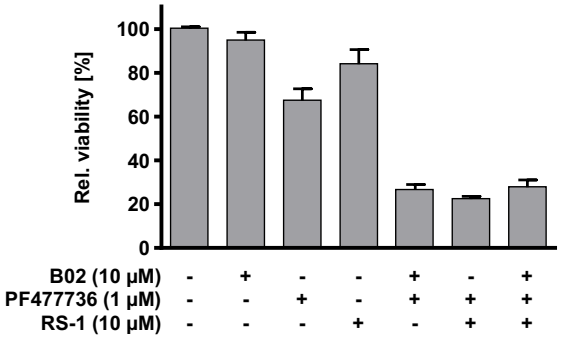

Figure 78: Viability of J82^{CisPt} after co-treatment with RAD51$_i$ B02, CHK1$_i$ PF477736 and RAD51 stimulator RS-1
J82^{CisPt} cells were treated with the indicated concentrations of B02, PF477736 or/and RS-1 for 72 h and cell viability was measured using the AlamarBlue assay. The untreated control was set to 100% viability and all other groups were related to this. Data presented are the mean + SD from biological quadruplicates.

In summary, the synergistic cytotoxicity of B02 + PF477736 is not cell line-specific to J82^{CisPt} since the combination is also effective in cisplatin-resistant tumor cells of other entities as well as in non-resistant tumor cells. Furthermore, the synergism of B02 + PF477736 is not a compound-specific effect since similar results were obtained when the inhibitors were substituted by some other members of the corresponding substance classes.

3.7 Cytotoxicity of B02 + PF477736 in normal tissue cells *in vitro*

In order to gain a first insight into the intensity of potential adverse effects of the concurrent treatment with B02 and PF477736, cytotoxicity experiments were performed with two different types of normal tissue cell models: human induced pluripotent stem cells (hiPSCs) representing replicative normal cells such as stem cells/progenitor cells of the hematopoietic system and primary fibroblasts as model of terminally differentiated cells. Since the molecular mechanism of the substances tested aims at the replication of cells, these two differently proliferating cell models were chosen to compare responses of highly proliferative and low-proliferative normal tissues.

3.7.1 Cytotoxicity of B02 + PF477736 in human induced pluripotent stem cells (hiPSCs)

Stem cells are naturally occurring, highly proliferative cells, that are capable of differentiating into different types of tissues and renewing cells with a short lifespan. They are often affected by CATs as undesirable side effects due to the characteristic of cytostatics to attack highly proliferative tissue. Likewise, it was speculated that also the combination of B02 + PF477736 affects the viability of stem cells. In collaboration with Isaac Musong Mboni Johnston (Institute of Toxicology, Heinrich Heine University, Düsseldorf), the AlamarBlue assay was used to determine the effect of B02 and PF477736 on the viability of F-4 hiPSCs after 72 hours of treatment. First, 10 µM B02 and 1 µM PF477736 were tested, as these were the concentrations that did not yet induce strong cytotoxicity in the tumor cells in mono-treatment but showed a synergistic effect in combination. It was found that treatment of F-4 hiPSCs with these concentrations was highly cytotoxic in mono-treatments already (40% viability with B02, 3% viability with PF477736) (Figure 79A). The low viability of especially the PF477736 mono-treatment did not allow any conclusions to be drawn about the combinatory effect of both substances. Therefore, in a second experimental run, the concentrations of both inhibitors were reduced to 7 µM for B02 and 0.1 µM for PF477736 in order to be able to determine the combinatory effect of treatment with both substances in hiPSCs (Figure 79B). This time, the mono treatments showed moderate cytotoxicity, namely 52% viability with B02 and 68% viability with PF477736. For the combination of both inhibitors a viability of 12% was measured, indicating that there is an additive to synergistic toxicity in hiPSCs with the concentrations tested.

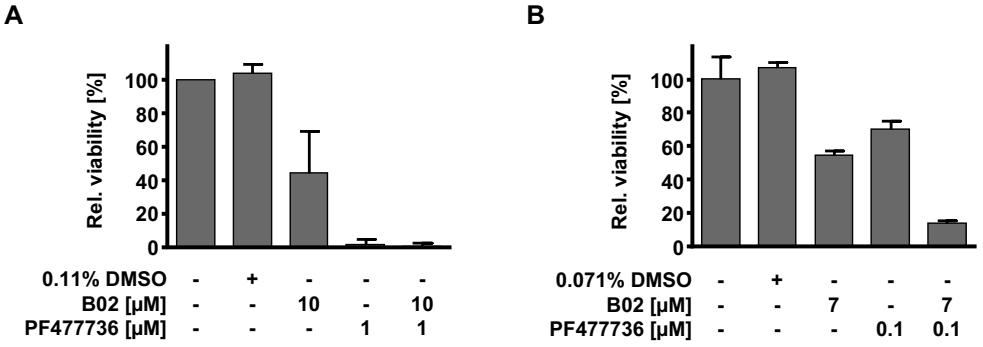

Figure 79: Viability of Foreskin-4 human induced pluripotent stem cells (F-4 hiPSCs) after co-treatment with RAD51$_i$ B02 and CHK1$_i$ PF477736
F-4 hiPSCs were treated with different concentrations of B02 or/and PF477736 over a 72-hour period and viability was measured using the AlamarBlue assay. The untreated control was set to 100% viability and all other groups were related to this. DMSO was included in the study as solvent control. Data presented are the mean + SD from two independent experiments. Experiments were conducted in collaboration with Isaac Musong Mboni Johnston (Institute of Toxicology, Heinrich Heine University, Düsseldorf).

3.7.2 Cytotoxicity of B02 + PF477736 in human primary fibroblasts

In contrast to hiPSCs, the majority of cells in the human body have little to no proliferative capacity. Representative for this tissue type, normal human dermal fibroblasts (NHDF) were analyzed with regard to their cytotoxicity response by Lena Abbey (Institute of Toxicology, Heinrich Heine University, Düsseldorf). Due to their relatively low proliferation activity, it was expected that the combination treatment of B02 + PF477736 would not affect the viability of these cells as much as tumor cells or stem cells. Just like the hiPSCs, the NHDF cells reacted more sensitive to the inhibitors than J82^{CisPt} cells (Figure 80). Yet, if one compares the measured viability of the combination treatments with those of the corresponding mono-treatments, it can be seen that the dual inhibition of RAD51 and CHK1 elicits rather antagonistic to additive effects in these cells.

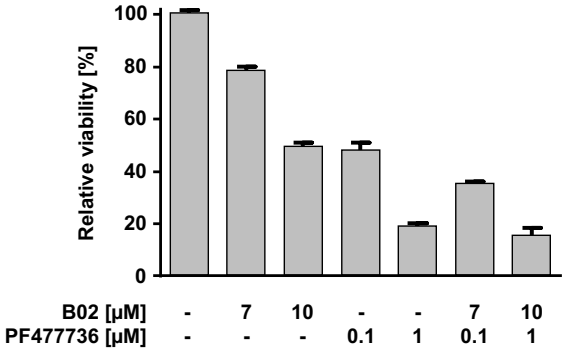

Figure 80: Viability of normal human dermal fibroblasts (NHDF) after co-treatment with RAD51$_i$ B02 and CHK1$_i$ PF477736
NHDF cells were treated with different concentrations of B02 or/and PF477736 for 72 h and cell viability was determined through the AlamarBlue assay. The untreated control was set to 100% viability and all other groups were related to this. Data presented are the mean + SD from biological quadruplicates. The experiment was conducted by Lena Abbey (Institute of Toxicology, Heinrich Heine University, Düsseldorf).

In conclusion, the distinct outcomes observed in hiPSCs and NHDF indicate that the combined treatment of CHK1$_i$ + RAD51$_i$ predominantly targets highly proliferative cells.

3.8 Xenograft animal experiment with B02 + PF477736

A xenograft experiment in NSG-(K^bD^b)^{null} mice (see chapter 2.1.7.2) was conducted to assess the anti-tumor efficacy as well as adverse side effects of the combination treatment with RAD51 inhibitor B02 and CHK1 inhibitor PF477736 *in vivo*.

3.8.1 Pre-tests for the determination of the cell number for injection

As no empirical data on a suitable cell number for the injection of J82^{CisPt} in a xenograft mouse model was yet available, the number of J82^{CisPt} cells for injection in the main experiment should be determined in a pre-experiment with two animals.

For this first experiment, the cell numbers tested were oriented to published xenograft data with $J82^{WT}$ cells ranging from $2x10^6$ to $1x10^7$ cells (McCormack *et al.*, 2013; Li *et al.*, 2015; Zhang *et al.*, 2017; Tsai *et al.*, 2019; Wu *et al.*, 2020). Two different cell numbers, $1x10^6$ and $3x10^6$ $J82^{CisPt}$ cells per flank of the animals, were tested for their tumor forming capacity (Figure 81). The tumor growth was observed over 53 days after cell injection and tumor volumes were calculated from size measurements with a caliper. With both cell numbers, measurable tumors were detected not before 37 days after cell injection and after that, tumors showed a very flat growth curve. The tumors growing from the lower cell number after 53 days reached a mean volume of 81 mm^3, while the higher cell number at the same time resulted in tumors with a mean volume of 159 mm^3. Since, in the main experiment, it was aimed to reach a tumor volume between 150 – 200 mm^3 after around two weeks, and the cell numbers tested in the pre-experiment were clearly under this threshold, but the higher tested cell number showed a slightly stronger tumor forming ability, it was decided to increase the cell number for the main experiment to $5x10^6$ cells.

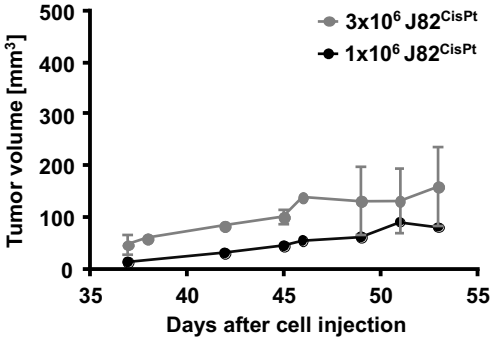

Figure 81: Tumor growth of different cell numbers of $J82^{CisPt}$ cells in a xenograft experiment
$1x10^6$ or $3x10^6$ $J82^{CisPt}$ cells were injected into the flanks of NSG-$(K^bD^b)^{null}$ mice. Tumor size measurements with a caliper were performed regularly from day 37 until day 53 after inoculation. From the measured values, tumor volumes were calculated and displayed here over the time course. Data are shown as mean (± SD if applicable) of one or two tumors.

3.8.2 Tumor growth in the main experiment with B02 + PF477736 treatment

In the main experiment, we aimed to compare the tumor volume between the different treatment groups in order to demonstrate an antitumorigenic effect of the combination treatment of B02 + PF477736. The size measurements for calculating the volume of the tumors could not be started before day 27 after the cell injection. At earlier time points small bumps were visible in the area of the injection in almost all mice, but these were not large enough to ensure a reliable size measurement. At the end of the experiment, almost all mice had measurable but very small tumors at both injection sites. Looking at the average tumor volumes in the groups over time, the tumors in the control group seemed to grow faster than in the treatment groups

(Figure 82A). No difference existed between the mono-treatments and the combination treatment. However, even for the period examined from day 27 to 47, no very strong tumor growth was observed in any of the experimental groups, considering that the maximum permitted tumor volume in European xenograft studies is 1000 mm^3 and the mean group values at termination in this experiment were about 50 – 100 mm^3.

Looking at the individual values of the tumor volumes, it can be seen that the increased mean value in the control group is attributable solely to two tumors from two different mice, which grew much more than the other tumors in the group (Figure 82B). The other tumors in the control group had similar volumes to those in the treatment groups. In conclusion, the limited tumor growth observed in all treatment groups precludes any definitive assessment of the antitumor efficacy of B02 + PF477736 based on the obtained data.

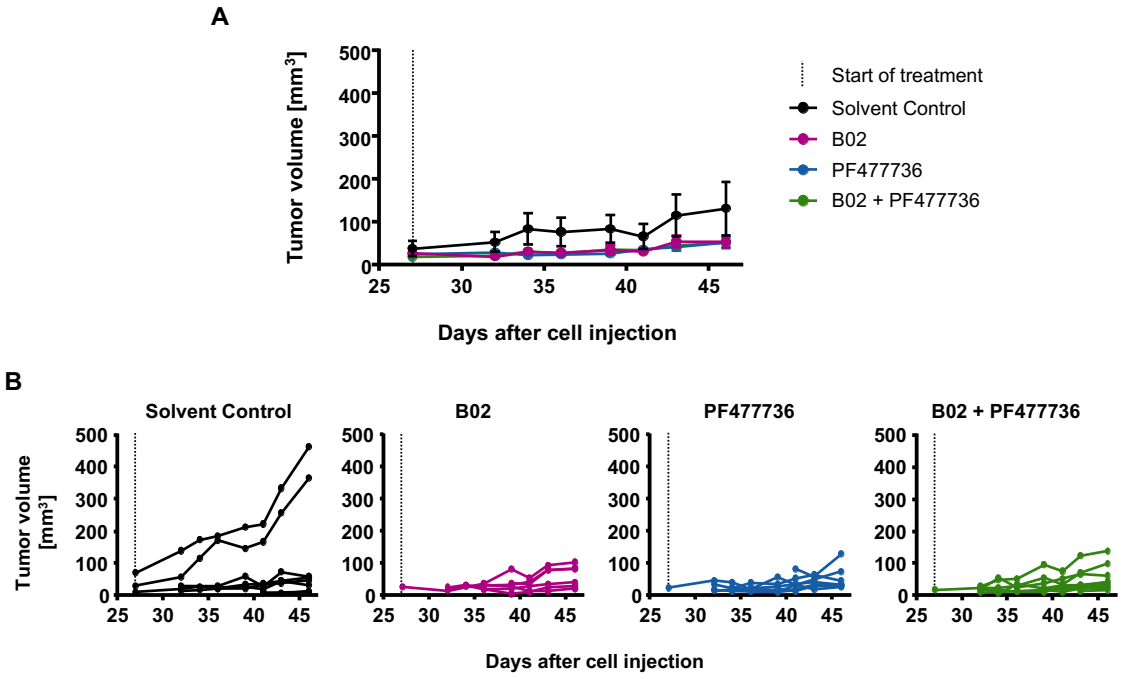

Figure 82: Influence of B02 or/and PF477736 treatment on tumor growth in a xenograft experiment with J82^{CisPt} cells

5x10^6 J82^{CisPt} cells were injected into the flanks of NSG-(K^bD^b)^{null} mice (day 0). Tumor size measurements with a caliper were performed regularly from day 27 until day 47 after inoculation. Treatment with 10 mg/kg B02 or/and 10 mg/kg PF477736 was started on day 27 after inoculation. Corn oil was included in the study as solvent control. From the measured values, tumor volumes were calculated and displayed here over the time course. Data are shown as mean ± SEM of treatment groups (A) and individually for the 8 – 10 tumors per treatment group (B).

3.8.3 Animal weights over the course of the experiment with B02 + PF477736 treatment

The animal weights were regularly checked since weight loss can be connected to the animals' suffering from the tumor burden or toxicity of the applied treatment. Apart from slight daily fluctuations, the mean relative weights of the animals compared to their start weights generally increased steadily in all treatment groups after the injection of the tumor cells and also after the start of the different treatments. The relative weight gain also did not differ significantly between the individual experimental groups (Figure 83). The fact that no decrease in body weight was observed in the mice treated with the inhibitors indicates that the compounds were in general well tolerated.

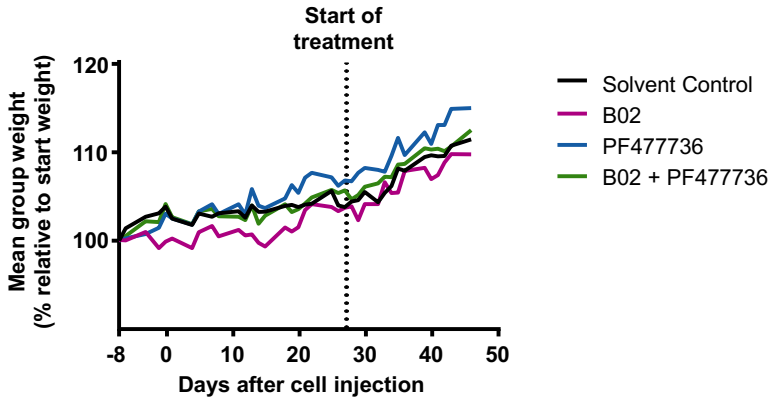

Figure 83: Monitoring of animal weight in the xenograft experiment with B02 or/and PF477736 treatment
$5x10^6$ $J82^{CisPt}$ cells were injected into the flanks of NSG-$(K^bD^b)^{null}$ mice (day 0). Animals were weighted regularly from 8 days before tumor cell injection until day 47 after inoculation. Treatment with 10 mg/kg B02 or/and 10 mg/kg PF477736 was started on day 27 after tumor inoculation. Corn oil was included in the study as solvent control. Animal weights were normalized to their respective start weights and are displayed here over the time course. Data are shown as mean of each treatment group.

3.8.4 Organ weights

At the end of the experiment, a variety of organs (brain, lung, heart, liver and kidneys) were extracted from the animals to compare their weights between the treatment groups. A reduction in the weight of an organ may indicate that cells in this tissue have died to an unphysiological extent, for example due to organ toxicity caused by the applied inhibitors. An increase in the weight of an organ, on the other hand, can represent an attempt by this organ to adapt to an increased need for functional performance.

Since the absolute weights of the organs depend on the size and body weight of the mice, the length of the tibia bone was used to normalize the values. Apart from the liver, the values determined only varied slightly between the individual animals in the respective group. For all organs considered, the relative organ weights did not differ

significantly between the different treatment groups (Figure 84) suggesting that no notable organ toxicity was triggered by B02, PF477736 or the combination of both.

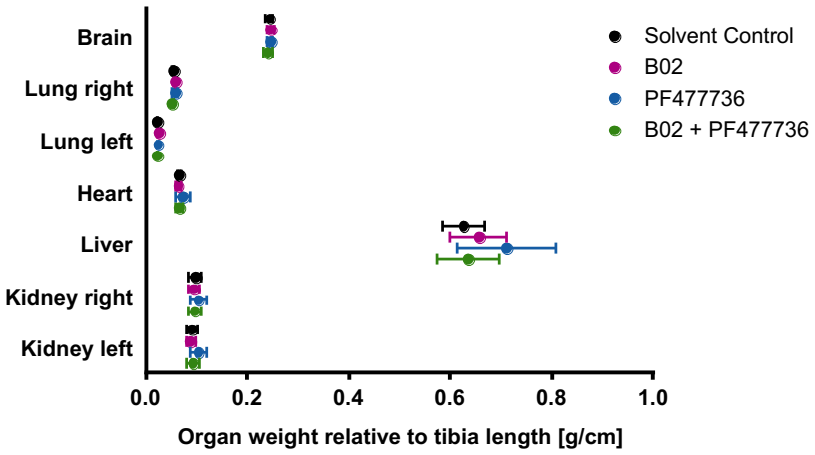

Figure 84: Organ weights in the xenograft experiment with B02 or/and PF477736 treatment
$5x10^6$ $J82^{CisPt}$ cells were injected into the flanks of NSG-$(K^bD^b)^{null}$ mice (day 0). Mice were treated with six doses of 10 mg/kg B02 or/and 10 mg/kg PF477736 over three weeks. Corn oil was included in the study as solvent control. The organs of the mice were harvested on day 47/48 after tumor inoculation. Organ weights were normalized using the tibia length of the respective animal. Data are shown as mean ± SEM of each treatment group.

3.8.5 EDTA blood parameters

The analysis of the number and percentage of the different types of blood cells can provide information about inflammations and infections or anemia i.e. disturbance in red blood cells.

Inflammations or infections can be detected by increased levels of immune cells in the blood, the leukocytes, which are composed of lymphocytes, neutrophils and monocytes. In the case of the mice used for the experiment, the blood parameters differ from those of wildtype mice in that the basal number of leukocytes is naturally lower due to their immunosuppressed condition. The blood parameter values measured at the beginning of the experiment were in line with published data for the used mouse strain (Layssol-Lamour *et al.*, 2021) (Supplementary Figure 4). The number of leukocytes at the end of the experiment was significantly increased in the solvent control and the PF477736 treatment compared to the beginning of the experiment (Figure 85A). In the case of the PF477736 treatment, this increase was due to the increased number of neutrophils. In the solvent control, lymphocytes, monocytes and neutrophils were equally increased. Nevertheless, none of the white blood cell counts showed a significant difference between the different treatment groups.

The number of erythrocytes, the hemoglobin content and the hematocrit are used to calculate values such as the mean corpuscular volume (MCV), mean corpuscular hemoglobin (MCH, MCHC) and red blood cell distribution width (RDWc, RDWs), which are used to diagnose anemia. Anemia can for example be caused by reduced generation of erythrocytes e.g. caused by bone marrow aplasia, increased degradation of erythrocytes or chronic bleeding e.g. due to ulcers. None of the analyzed values showed a difference between the time points or between the treatment groups (Figure 85B, Supplementary Figure 5).

An altered platelet count can indicate a coagulation disorder, as these cells are essential for blood clotting. The platelet counts as well as the plateletcrit were not significantly changed between treatment groups after the experiment, and also compared to the beginning of the experiment (Figure 85C). Thereof calculated values, namely mean platelet volume (MPV) and platelet distribution width (PDWc, PDWs) were also not different between start and end of experiment and treatment groups (Supplementary Figure 5).

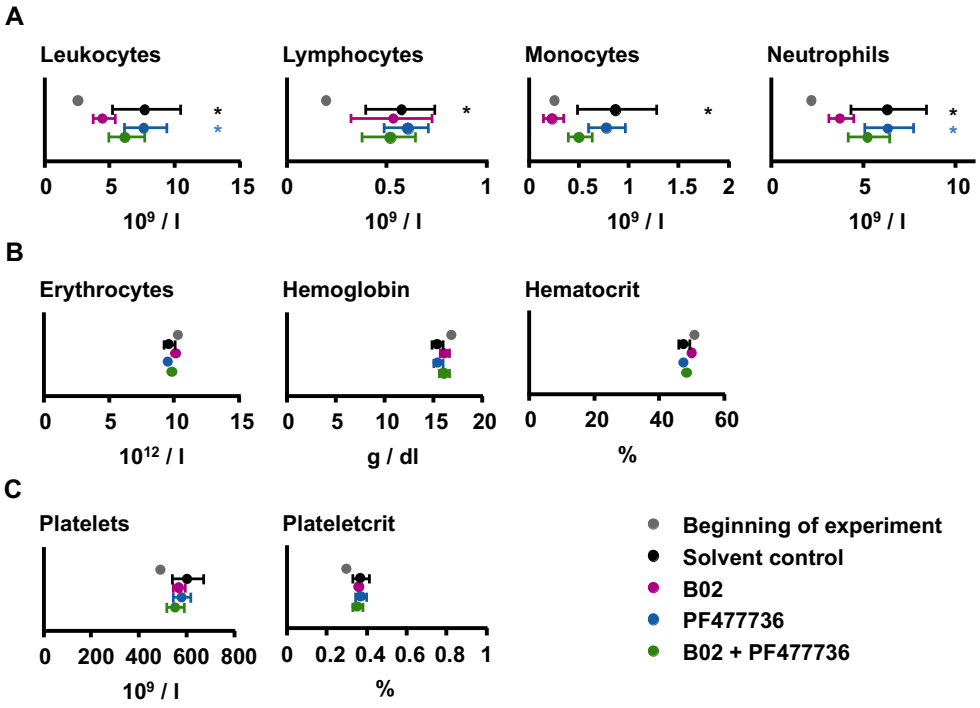

Figure 85: Blood parameters in the xenograft experiment with B02 or/and PF477736 treatment
$5x10^6$ $J82^{CisPt}$ cells were injected into the flanks of NSG-$(K^bD^b)^{null}$ mice (day 0). For basal values of blood parameters, blood was taken from the mice one day before tumor cell injection (Beginning of experiment). Mice were treated with six doses of 10 mg/kg B02 or/and 10 mg/kg PF477736 over three weeks. Corn oil was included in the study as solvent control. Blood of the mice was again taken on day 47/48 after tumor inoculation. Data are shown as mean ± SEM of each treatment group (n = 3 – 5). For the beginning of the experiment the mean of all 18 mice was formed. *p ≤ 0.05; significant compared to beginning of experiment.

In summary, the white blood cell counts exhibited a slight increase in the solvent control and the PF477736 mono-treatment at the termination of the experiment, when compared with the initial readings. The comparison of the different treatment groups at the end of the experiment revealed no detectable differences, indicating that the applied inhibitory treatment had no notable impact on the blood composition.

3.8.6 Bone marrow RNA analysis of mice treated with B02 + PF477736

As described, the blood analyses showed no abnormalities. The cells contained in the blood are renewed at regular intervals. The stem cells and progenitor cells required for this are found in the bone marrow. As these are highly proliferative cell types, it is assumed that they could be most affected as a side effect of the treatment used. Even if no changes have been detected at the blood level, it is possible that the precursor cells in the bone marrow have been damaged by the treatment. This should be investigated based on RT-qPCR for factors related to transport, detoxification, cell cycle and cell death. The bone marrow RNA of the animals that received the combination treatment of B02 and PF477736 was compared with the RNA of the solvent control animals (Figure 86). The mRNA expression of transporter Bcrp was very weak, yet similar, in both treatment groups. mRNA for the transporter Oct2 was also very low in the B02 + PF477736 treatment, while it was not detected at all in the control group. Besides this, only the mRNA of the mitochondrial damage response marker Pgc1a was upregulated in the animals treated with the combination therapy compared to the control, and this with a very large standard deviation. All other factors considered were not differently expressed on the mRNA level. These results demonstrate that the treatment did not induce any severe adverse effects on the hematological stem cells of the bone marrow.

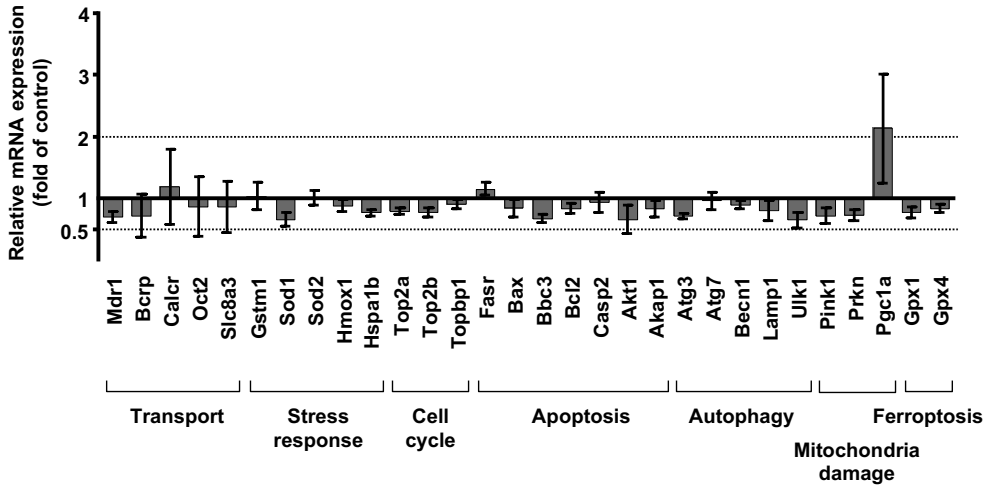

Figure 86: mRNA expression of transport, stress and cell death factors in bone marrow of NSG-(K^bD^b)^{null} mice after treatment with RAD51$_i$ B02 and CHK1$_i$ PF477736
Mice were treated two times per week for three weeks with B02 + PF477736 before mRNA expression analysis of selected factors by RT-qPCR. RNA from bone marrow of all five animals in a treatment group was pooled before cDNA synthesis. The solvent control (corn oil) was set to 1.0 and the B02 + PF477736 treatment group was related to this. Thresholds for increased/decreased mRNA expression were set at 2-fold difference between treated vs. solvent control (dotted lines). Data presented are the mean ± SD from technical triplicates.

Summarizing the results of the *in vivo* analyses, it is unclear whether B02 + PF477736 treatment can effectively reduce tumor growth, considering the generally low tumor formation capacity of J82^{CisPt} cells. Furthermore, the application of the inhibitors did not result in any detectable effects on the normal cells and tissues which were subjected to investigation.

4 Discussion

4.1 Potential underlying mechanisms for CisPt resistance in J82 cells

The modification of a plethora of different factors has been described as potentially contributing to the development of cisplatin resistance. These include a reduced intracellular drug accumulation or an increased scavenging of cisplatin by GSH or metallothioneins as pre-target factors, an altered recognition of the induced damage or an increased repair capacity as on-target factors and defects in the execution of cell death mechanisms as post-target factors (Galluzzi *et al.*, 2012). The observed cross-resistance of $J82^{CisPt}$ to other platinating compounds, carboplatin and oxaliplatin (Figure 13), suggested that the mechanism of cisplatin resistance in $J82^{CisPt}$ may be linked to alterations in Platinum-DNA adduct formation. Indeed, short-term and long-term cisplatin treatment showed attenuated CisPt-DNA adduct formation in $J82^{CisPt}$ cells compared to $J82^{WT}$ (Figure 22, Figure 23) (Höhn *et al.*, 2016).

Factors that can lead to reduced adduct formation include reduced cisplatin import into the cell or increased cisplatin export from the cell. The cisplatin-exporting transporter ATP7A was upregulated on the mRNA level in $J82^{CisPt}$, while the mRNA of other exporters such as ATP7B and MATE1 was downregulated (Figure 18) (Ciarimboli, 2012). The mRNA of BCRP, a known exporter of various drugs like 5-FU and doxorubicin, was upregulated in $J82^{CisPt}$ cells, but cisplatin is in fact not described as substrate of this transporter (Yuan *et al.*, 2009). The transporters CTR1 and OCT2 are known to import cisplatin into cells (Ciarimboli, 2012). The downregulation of the mRNA of importer OCT2 would therefore indicate a reduced import of cisplatin into $J82^{CisPt}$ cells. However, if the mechanism of cisplatin resistance is based on this transporter, cross-resistance of $J82^{CisPt}$ to doxorubicin would have been expected, as doxorubicin is also a substrate of OCT2 (Otter *et al.*, 2021). So, overall, examination of the expression of various known drug exporters at the RNA level revealed a rather inconsistent pattern. In addition, on protein level no transporters were found differentially expressed in $J82^{WT}$ and $J82^{CisPt}$ (Figure 20).

Enhanced detoxification before cisplatin reaches the DNA could also be a reason for reduced DNA adduct formation. The cross-resistance to oxidants suggested that radical scavenger proteins that bind to both reactive oxygen species (ROS) and cisplatin might be upregulated in $J82^{CisPt}$ (Figure 15). An upregulation of anti-oxidative proteins heme oxygenase 1 (HMOX1) and glutathione S-transferase 1 (GSTM1) in $J82^{CisPt}$ was already shown on the mRNA level (Höhn *et al.*, 2016). Additionally, $J82^{CisPt}$ demonstrated elevated levels of glutathione S-transferase 3 (GSTM3) at the protein level following cisplatin administration (Figure 21). Increased levels of heme oxygenases and

glutathione S-transferases have been reported to be associated with cisplatin resistance (Lewis *et al.*, 1988; Goto *et al.*, 1995; Peng *et al.*, 2020) and GSTM1-impaired mice were found to be more prone to cisplatin induced ototoxicity (Li *et al.*, 2022), suggesting detoxifying roles for cisplatin.

An increased DNA content of the cells and thus a "dilution" of the cisplatin-induced DNA damage could also be an explanation for the weaker adduct formation in $J82^{CisPt}$. Aneuploidy, a condition of an altered chromosome number, is an extremely common characteristic of tumor cells (Weaver and Cleveland, 2006) and the parental $J82^{WT}$ cells were already described as triploid when they were first characterized (O'Toole *et al.*, 1978), which suggests that they have a tendency towards inconsistency in the number of chromosomes. Also it has been shown that gains in the chromosome number can lead to resistance against cisplatin (Vitale *et al.*, 2007; Replogle *et al.*, 2020). An indication of aneuploidy in $J82^{CisPt}$ cells was provided by flow cytometric studies, in which $J82^{CisPt}$ cells constantly showed a stronger propidium iodide signal, corresponding to the DNA content, than $J82^{WT}$ (Figure 29). Furthermore, it has been described that elevated RAD51B expression facilitates the development of aneuploidy and that the expression of IL-6 and IL-8 is upregulated in response to aneuploidy (Stingele *et al.*, 2012). Interestingly, basal expression of all three mentioned factors was found to be upregulated on the RNA level in $J82^{CisPt}$ (Figure 18).

Since long-term treatment (24 h), where a steady state between adduct formation and repair is established, still showed fewer Pt(GpG) adducts in $J82^{CisPt}$ than in $J82^{WT}$ (Figure 23A, B), a faster processing of CisPt-DNA adducts in $J82^{CisPt}$ might also contribute to the reduced adduct number. This is countered, however, by the fact that there is a good correlation between the number of adducts and the reduction in viability (Figure 23C), which indicates that processes downstream of DNA adduct formation do not play a major role in the CisPt resistance mechanism. It can also be concluded from this correlation that the Pt(GpG) adducts measured in the Southwestern blot play a major role in cytotoxicity and that other types of DNA intrastrand crosslinks and the less occurring but potentially more toxic DNA interstrand crosslinks are rather negligible.

Other conceivable influences on the formation of adducts, such as reduced DNA accessibility or a time delay in the conversion of monoadducts to CisPt-DNA crosslinks, were not explored further in this study. It would be necessary to conduct investigations on the chromatin state or detailed time kinetic experiments, respectively, for clarification of the impact of these two molecular modifications.

In summary, it can be said that altered cisplatin transport across the cell membrane might be contributing to decreased CisPt-DNA adduct formation in CisPt resistant J82 cells but

is unlikely to be exclusively responsible for the pronounced difference in the number of CisPt-DNA adducts observed in $J82^{WT}$ and $J82^{CisPt}$. It is reasonable to assume that an increased detoxification capacity and an increased DNA content are additionally decisive for this observation. On the other hand, an increased repair capacity of CisPt-induced DNA damage does not appear to be involved in the molecular mechanism of acquired CisPt resistance in $J82^{CisPt}$ cells.

As already mentioned above, various endpoints indicated an increased chromosome number in $J82^{CisPt}$. Aneuploidy is often a consequence of chromosomal instability (CIN) (Thompson and Compton, 2008). CIN is widely spread among cancers and is even stated as one of the hallmarks of cancer (Hanahan, 2022). $J82^{CisPt}$ cells indeed showed characteristics of CIN with deformed nuclei and chromatin bridges, as well as a high number of abnormalities in mitosis (Figure 24, Figure 25) (Bhatia and Kumar, 2014). In addition, the proteome analysis revealed significant upregulation of centrosomal protein of 55 kDa (CEP55) in $J82^{CisPt}$, a protein required for successful cytokinesis (Supplementary Table 2) (Zhao *et al.*, 2006). CEP55 overexpression has been shown to promote chromosomal instability (Sinha *et al.*, 2020). CIN, in fact, is a double-edged sword. It is reported to be beneficial for tumor cell survival and to contribute to the development of multidrug resistances (Lee *et al.*, 2011). Conversely, evidence suggests that CIN can induce a range of cellular stresses, including metabolic stress, replication stress, and proteotoxic stress (Shaukat *et al.*, 2015; Khan *et al.*, 2018; Wilhelm *et al.*, 2020; Hosea *et al.*, 2024). $J82^{CisPt}$ indeed showed enhanced sensitivity to replication stress-inducing substances such as 5-FU and OH-Urea (Figure 14). This might be based on the cells' endeavor to compensate for their elevated DNA content by increased DNA replication speed, as they have a higher expression of parts of replicative polymerases (DNA polymerase α catalytic subunit (POLA1) and DNA polymerase δ subunit 3 (POLD3)) (Supplementary Table 2). The POLD3 gene is in fact frequently found amplified in human tumors and POLD3 is also a subunit of the translesion synthesis (TLS) polymerase ζ (Pol ζ), which in cooperation with TLS polymerase Pol η allows the bypassing of cisplatin-induced GpG adducts (Fuchs *et al.*, 2021). Still, increased replication speed is coupled with greater nucleotide consumption, which could in turn be the reason for the higher susceptibility of $J82^{CisPt}$ to nucleotide depletion by replication stress-inducing substances. Aneuploid cells were also described as particularly sensitive to CHK1 inhibitors (Vitale *et al.*, 2007) and $J82^{CisPt}$ were found to be sensitive to CHK1 inhibition before (Höhn *et al.*, 2016).

Based on the results found in J82^{CisPt} cells, which point in different directions, it becomes evident that it is not trivial to identify a single causal reason for cisplatin resistance and it is presumably rather an interplay of multiple influencing factors that cause drug resistance. The CisPt resistance mechanism in J82^{CisPt} probably involves CIN and aneuploidy-related features, detoxification mechanisms, and possibly transport processes, which together lead to reduced CisPt-DNA adduct formation.

4.2 Comparison of different CisPt resistant cell variants

When examining the RNA expression patterns of the different cisplatin-resistant cell lines J82^{CisPt}, SH-SY5Y^{CisPt} and A549^{CisPt}, there were only a few overlaps detectable (Supplementary Figure 2). In J82^{CisPt} and A549^{CisPt} MATE1, and in J82^{CisPt} and SH-SY5Y^{CisPt} OCT2 and MDR1 mRNA were downregulated compared to the respective parental cells. After cisplatin treatment, RAD51B mRNA was downregulated in both J82 cell variants as well as both A549 variants. In contrast, there was no overlap in basal or cisplatin-induced changes in the factors analyzed between cisplatin-resistant A549 and SH-SY5Y cells. Overall, the mRNA analysis of the cisplatin-resistant cell variants originating from different tumor entities showed rather different pictures, indicating that distinct molecular mechanisms underlie their cisplatin responses and resistances to cisplatin.

One question that needs to be asked is, if it is even likely that the same mechanisms lead to CAT resistance in different tumor entities. Mechanisms for tumorigenesis are often similar, e.g. BRCAness, which refers to HR defects phenocopying BRCA1/2 mutations, has been observed in a wide variety of tumor entities (Lord and Ashworth, 2016). In principle, it can therefore be assumed that mechanisms for the development of resistance can also overlap. Nevertheless, there are many different factors that can influence the development of resistance (Galluzzi *et al.*, 2012) and in a heterogeneous cell population various factors can even come together, therefore it can not necessarily be expected that the same characteristic changes leading to cisplatin resistance are triggered in heterogeneous cell populations of different tumor cell entities, even when the same selection protocol is applied. However, it must also be said that the mRNA analysis of pre-selected factors should be considered as an initial screening step for a first superficial impression on the tumor cell characteristics of A549^{CisPt} and SH-SY5Y^{CisPt}. More in-depth studies on the potential mechanisms of cisplatin resistance in A549 cells and SH-SY5Y cells, such as analyses of CisPt-DNA adduct formation, would be necessary to make a conclusive statement regarding the similarity of the different cell lines.

4.3 Distinct responses of J82^{WT} and J82^{CisPt} to RAD51 inhibition

Treatment of J82^{WT} and J82^{CisPt} cells with the RAD51 inhibitor B02 showed less cytotoxicity in J82^{CisPt} (Figure 16, Figure 17). This effect was observed over a treatment period of one to four days, ruling out time point specificity (Supplementary Figure 1). The most straightforward explanation for the observed cross-resistance to B02 would be an increased expression of RAD51 in J82^{CisPt}, as in this case, with the same inhibitor concentration in J82^{WT} and J82^{CisPt}, a greater quantity of functional RAD51 would remain available for DNA protection processes in J82^{CisPt}. Elevated expression of RAD51 has already been described for various cancer types and has been associated with drug resistance and poor patient survival (Slupianek *et al.*, 2001; Raderschall *et al.*, 2002; Fan *et al.*, 2004; Qiao *et al.*, 2005; Sarwar *et al.*, 2017; Morrison *et al.*, 2021; Wu and Zhao, 2021; Tsai *et al.*, 2023). In J82^{CisPt}, however, no altered expression of RAD51 was found at either mRNA or protein level as compared with J82^{WT} (Figure 18, Figure 71). The influence of transport processes across the cell membrane can probably be neglected, as computer-based modeling performed by Pablo Cea-Medina (Gohlke working group, Institute of Pharmaceutical and Medicinal Chemistry, Heinrich Heine University, Düsseldorf) indicated that B02 very likely can enter the cell by diffusion. Moreover, reduced target binding of the inhibitor in J82^{CisPt}, e.g. due to mutation-induced structural changes of RAD51, can be excluded, since the same concentrations of B02 showed an inhibition of RAD51 foci formation after irradiation to a similar extent in J82^{WT} cells and J82^{CisPt} cells (Figure 26).

It is noticeable that the SubG1 fraction analyzed by flow cytometry did not reflect the measured cytotoxicity difference (Figure 29). Therefore, it can be assumed that not only cell death-related mechanisms are involved in the cells' response. Others have reported enhanced mitochondrial ROS formation after RAD51 inhibition (Jin and Kim, 2017; Xu *et al.*, 2020). In addition, the increase in mRNA expression of mitochondrial damage response factors following B02 treatment in J82^{WT} cells, but not in J82^{CisPt} cells (Figure 28), suggests that mitochondrial damage might be specifically induced in the parental cell variant and may explain its higher sensitivity to B02. Nevertheless, the difference in cytotoxicity was found both when employing the AlamarBlue assay and the Neutral Red assay (Figure 16, Figure 17). These two viability assays have different read-outs; the AlamarBlue assay is based on metabolic activity i.e. mitochondrial functionality, while the Neutral Red assay uses lysosomal membrane integrity as a measure of viability (O'Brien *et al.*, 2000; Repetto *et al.*, 2008). It can therefore be concluded that the different response of the two cell variants to B02 treatment is not solely based on metabolic effects.

If the reduction in viability is not solely due to the induction of cell death or metabolic deficits, senescence could be another decisive factor. Triggering of senescence presumably through impairment of RAD51, and thereby inhibition of the HR pathway, has previously been shown with a variety of compounds (Feringa *et al.*, 2018; Lindemann *et al.*, 2021; Chen *et al.*, 2024). Similar effects could therefore also be expected from the inhibition of RAD51 itself. The mRNA expression analysis of a selection of senescence markers after B02 treatment showed an upregulation of HMGB1 to a similar extent in $J82^{WT}$ and $J82^{CisPt}$ (Figure 28). The process of senescence is understood to be associated with the release of HMGB1 from the nucleus and its subsequent secretion by the cells (Sofiadis *et al.*, 2021). Therefore, it is difficult to make a statement about senescence induction from the upregulated mRNA expression of this marker alone. In addition, the similar increase in mRNA expression in both cell variants suggests that this factor is not responsible for the differing B02 sensitivities in $J82^{WT}$ and $J82^{CisPt}$. In contrast, p21 is more strongly upregulated in $J82^{WT}$ than in $J82^{CisPt}$ after B02 administration (Figure 28). However, p21 is not a specific marker for senescence, but is also involved in processes of cell cycle arrest regulation (Christmann *et al.*, 2003). Particularly at the rather early timepoint of analysis (24 h) and with missing upregulation of further senescence-related factors, its role in the regulation of cell cycle arrest is presumably more relevant than senescence-related functions in this context. Hence, the mRNA expression analyses performed do not provide any evidence for senescence being involved in the response to RAD51 inhibition in both J82 variants. However, for a final assessment of whether senescence occurs after B02 treatment, a β-galactosidase staining needs to be conducted.

RAD51 plays a central role not only in the repair of DNA double-strand breaks by HR, but also in the replication stress response and in mitotic DNA synthesis, which is a coping strategy for cells that enter mitosis with under-replicated DNA (Bhowmick *et al.*, 2023). Since no cross-resistance to other substances such as doxorubicin or radiation, which require HR as the main repair pathway for processing DNA damage, was observed (Figure 14), it is unlikely that the improved survival rate of $J82^{CisPt}$ is due to an increased HR capacity. An improved replication stress response can also be ruled out due to the cross-sensitivity of $J82^{CisPt}$ to OH-Urea and 5-FU (Figure 14). In this case, therefore, the involvement of RAD51 in mitotic processes appears to contribute to the different response of $J82^{WT}$ and $J82^{CisPt}$ and the results of several evaluated endpoints emphasize this. While $J82^{WT}$ showed a pronounced G2/M population following B02 treatment, $J82^{CisPt}$ under the same conditions did not (Figure 29). The flow cytometric measurement cannot discriminate whether the cells are in the G2-phase or mitosis. However, it is well-known that DNA damage often inhibits transition of cells from G2-phase to mitosis

in order to carry out DNA repair beforehand. To induce G2/M arrest, the kinase CHK1 is activated and phosphorylates the phosphatase CDC25c. CDC25c is then degraded and can no longer exert its activating, dephosphorylating function on the CyclinB1/ cyclin-dependent kinase 1 (CDK1) complex, which would be required for the transition from G2 to mitosis (DiPaola, 2002). p21 can also induce a G2/M arrest by inhibiting CyclinB1/CDK1 directly, or via activation of the CHK1-CDC25c pathway (Lossaint *et al.*, 2011). Interestingly, CHK1, CDC25c and p21 were all upregulated after B02 treatment specifically in $J82^{WT}$ (Figure 28). As CDC25c is degraded during cell cycle arrest, its mRNA upregulation might be a cellular attempt to rebuild the CDC25c protein pool. A G2/M arrest may be reflected by a reduction in the signal of the mitotic marker pH3, as the transition to mitosis is blocked. Contradictory to that an increase in pH3 signal was found with higher B02 concentrations and this effect was in the mean stronger in $J82^{WT}$ than in $J82^{CisPt}$ cells (Figure 30, Figure 31). Interestingly, an increase in pH3 with B02 has been observed in HCT-116 colon cancer cells earlier (Schürmann *et al.*, 2021). Histones are DNA-binding proteins found in the chromatin of eukaryotic cells, responsible for the protection and packaging of DNA. Histones and their post-translational modifications also play a central role in cellular processes like transcription regulation, DNA repair, DNA replication and chromosomal stability. The phosphorylation of histone H3 at Serine 10 is considered to be a crucial event for the onset of mitosis, as it initiates restructuring of the chromatin from relaxed to condensed form necessary for mitosis, and this signal sustains until H3 dephosphorylation occurs in anaphase (Hendzel *et al.*, 1997; Crosio *et al.*, 2002). After B02 treatment, histone H3 is still phosphorylated at Serine 10 exclusively in cells with doubled chromosome content (Figure 31). Firstly, this result rules out a mitosis-unspecific phosphorylation of histone H3. Secondly, it argues against premature entry into mitosis of cells with under-replicated DNA. Still, results obtained from staining of mitotic spindle apparatus markers indicated that cells have strongly malformed spindle apparatuses, resulting in disability to successfully complete mitosis (Figure 32). In line with our findings, others have reported metaphase arrest and spindle defects with RAD51 inhibition before (Jin and Kim, 2017). The increase in the percentage of pH3 positive J82 cells following B02 treatment is probably due to the fact that pH3 is a marker for the initial phases of mitosis and most cells stagnate at a mitotic stage before H3 dephosphorylation takes place. While no mitotic cells at stages later than prometaphase were detected in $J82^{WT}$, a small number of $J82^{CisPt}$ cells still completed the transition to meta- or even anaphase. This could explain the less pronounced increase in pH3 signal in B02-treated $J82^{CisPt}$ as compared to $J82^{WT}$. Nevertheless, $J82^{CisPt}$ cells in late mitotic phases did not show

correctly formed spindles either and no cells were found in telophase or cytokinesis. This suggests that mitotic progression of J82^{CisPt} is also severely restricted by the inhibition of RAD51. It is therefore feasible that on molecular level the same effects occur in J82^{CisPt} as in J82^{WT}, only with a slight time delay, resulting in the appearance of reduced sensitivity. It is possible that this time delay is a result of J82^{CisPt} cells being adapted to mitotic irregularities due to their CIN and having developed strategies to deal with them up to a certain point. The increased expression of the polymerase α and δ subunits in J82^{CisPt} may have a positive impact here (Supplementary Table 2), as it has already been shown that inhibition of these polymerases by aphidicolin in combination with B02 treatment leads to a pronounced delay in anaphase onset (Wassing *et al.*, 2021).

It was noticeable that many of the effects observed with B02 were only seen upon treatment with a concentration of 20 µM. It therefore appears as if there is some kind of threshold at this point. For this reason, it should be checked whether the effects described with B02 are truly attributable to the targeting of RAD51 or whether the inhibitor may trigger RAD51 non-specific effects in the cells when applied in high concentrations. Especially RAD51 paralogs (RAD51B, RAD51C, RAD51D, XRCC2, XRCC3) would be feasible targets of B02, because they share high protein sequence similarity (Lin *et al.*, 2006). In addition, the mRNA expression of some RAD51 paralogs was found basally upregulated in J82^{CisPt} when compared to J82^{WT} (Figure 18). Under the assumption that these paralogs are also targeted by B02, their upregulation could be part of the explanation for the reduced sensitivity of J82^{CisPt} to B02. To exclude this possibility, experiments on selected endpoints were repeated upon RAD51 knockdown by siRNA-based approach. It cannot be ruled out completely that siRNA causes off-target effects too, since short stretches of sequence homology can exist among RNA molecules encoding structurally different classes of proteins, but in general siRNA is considered a very specific method for knocking down a target protein (Weiss *et al.*, 2007). It could be demonstrated at the RNA level that this is very likely also the case for the RAD51 siRNA used in this study, as the siRNA decreased the mRNA content of RAD51 itself, but not its paralogs (Figure 34).

The endpoints selected for comparative analysis of B02 and siRNA were viability (after 72 h), cell cycle distribution (after 24 and 72 h), and pH3 staining (after 24 h incubation), as differences in the response of J82^{WT} and J82^{CisPt} to B02 were seen at these timepoints. With RAD51 siRNA, both viability measurement and pH3 staining not only showed no difference between the reaction of J82^{WT} and J82^{CisPt}, but also no decrease in viability or increase in pH3 signal was observed at all (Figure 35, Figure 37). Cell cycle

analyses after 72 h incubation with RAD51 siRNA showed a slight G2/M-phase arrest in $J82^{WT}$ and no changes in the cell cycle of $J82^{CisPt}$ (Figure 36). These different responses were already visible after 24 h with B02 treatment, so it is conceivable that the effects evoked by siRNA occur with a time delay and, therefore, the time points of analysis chosen for the other endpoints (cytotoxicity and phosphorylation of H3) were too early. This assumption is supported by the observation that the knockdown efficiency at protein level was not yet strongly pronounced after 24 h incubation with RAD51 siRNA and only manifested itself after an extended incubation period (Figure 33).

However, even if the results generated with B02 cannot be reproduced by RAD51 knockdown using siRNA, this does not necessarily mean that RAD51-independent mechanisms play a role in the B02-mediated effects. The difference between these two approaches is that when a protein is inhibited by a pharmacological compound, the protein itself remains present, with only a specific activity being blocked. In contrast, with siRNA, the mRNA of the target protein is already degraded by the siRNA, preventing the translation of the whole protein. As the lifespan of already synthesized proteins is finite, the use of siRNA will eventually result in a deficit of the affected protein. In many cases, the findings reported from pharmacological inhibition and siRNA coincide, but exceptions have also been described in which siRNA knockdown triggers different mechanisms in cells than a specific small molecule inhibitor (Weiss *et al.*, 2007). Of note, such difference between protein inhibition and depletion has been observed before also for RAD51. RAD51 depletion via siRNA caused defects in replication fork reversal, while RAD51 inhibition by B02 rather destabilized reversed forks (Zellweger *et al.*, 2015; Taglialatela *et al.*, 2017). Also, it has, in fact, already been shown in U2OS cells that targeting RAD51 with siRNA rather led to a reduction in the mitotic population (Wassing *et al.*, 2021) and not an increase as it was shown here upon use of B02. For a final assessment of the RAD51 specificity of the effects induced by B02, it could be additionally tested whether vector-based overexpression of RAD51 can reverse the effects induced by B02.

4.4 Molecular mechanism of combination treatment with B02 + PF477736 in $J82^{CisPt}$

Combining low to moderate toxic concentrations of $RAD51_i$ B02 with $CHK1_i$ PF477736 evoked additive to synergistic cytotoxicity in $J82^{CisPt}$ (Figure 49). Similar effects have already been described in non-resistant cancer cells for combinatorial inhibition of other factors of the replication stress response, e.g. RAD51 + Wee1 (Lindemann *et al.*, 2021) or ATR + CHK1 (Sanjiv *et al.*, 2016). Even though an altered replication stress response does not seem to be a major mechanism of cisplatin resistance of $J82^{CisPt}$,

its targeting is still a promising approach for overcoming acquired drug resistance. Since rapid proliferation and associated increased replication stress is a common feature of all tumor cells, we hypothesized that reinforcement of replication stress by simultaneous targeting to two replication fork stabilizing factors might be a promising strategy to deal with acquired drug resistance. Targeting superordinate control mechanisms of DNA replication is even anticipated to be a more promising approach than attacking one specific resistance mechanism, as it cannot be assumed that identical resistance mechanisms are induced in each cell of a heterogenous cell population. Effectiveness of co-treatment with PF477736 + B02 has indeed been proven not only in $J82^{CisPt}$, but also in cisplatin resistant cells of other tumor entities, as well as $J82^{WT}$ cells (Figure 69, Figure 70). In addition, synergistic cytotoxicity induction in $J82^{CisPt}$ was also obtained with other combinations of $RAD51_i$ + $CHK1_i$ (B02 + LY2603618 or RI(dl)2 + PF477736) (Figure 74, Figure 77). This finding suggests that the triggering of synergistic cytotoxicity is not confined to B02 and PF477736 but rather is a group-specific effect of chemically different types of $RAD51_i$ and $CHK1_i$.

Although no mRNA regulations promoting apoptosis could be detected in $J82^{CisPt}$, the synergism of B02 and PF477736 was nicely reflected in Western blot analyses for the apoptotic markers cleaved caspase 7 and cleaved PARP (Figure 50, Figure 52). Consistent with this, the pan-caspase inhibitor QVD reduced the induction of the SubG1 fraction, representing dead cells, after combined treatment with B02 and PF477736 (Figure 53). These findings demonstrate that the synergistic cell death induced by co-treatment with $RAD51_i$ plus $CHK1_i$ is at least partially apoptosis-dependent.

To elucidate the underlying molecular mechanisms of the synergistic cell death induction caused by combined treatment with B02 and PF477736, proliferation- and cell cycle-related endpoints were examined. Here, possible effects caused by B02 as discussed in chapter 4.3 are likely not of relevance because the concentration selected for the combination treatment did not yet elicit them. While monotherapy with PF477736 and combined treatment (B02 + PF477736) induced an S-phase arrest to the same extent, in the co-treatment this was accompanied by a stronger accumulation of dead cells (Figure 55). This finding well reflects the synergistic cytotoxic effect of the inhibitor combination and indicates that under conditions of CHK1 inhibition alone, cells may be able to recover from S-phase arrest, while the likelihood of executing cell death is higher upon additional inhibition of RAD51. Additionally, $J82^{CisPt}$ cells treated with the combination of B02 and PF477736 showed reduced replication activity measured by EdU incorporation after 24 h treatment (Figure 57). Since there were

more cells in S-phase with the combination treatment, but less replication activity, this led to the assumption that cells remain in S-phase for a longer period of time than usual due to hampered replication.

Having a closer look at the effects on replication fork level, cells co-treated with B02 and PF477736 for 6 h showed a decelerated replication fork progression, indicated by shorter CldU/IdU double-labelled DNA fibers as compared to the untreated control and the mono-treatments (Figure 58A). Slowed rates of fork progression can be a consequence of increased origin firing (Zhong *et al.*, 2013). Also, it is described that the ATR-CHK1 axis negatively regulates global origin firing and its inhibition can lead to excessive origin firing (Syljuåsen *et al.*, 2005; Moiseeva *et al.*, 2017). However, under the considered conditions this is likely not the case in J82^{CisPt}, since the percentages of origins varied only slightly between the treatment conditions (Figure 58B). This is in line with other publications stating that CHK1 inhibition can evoke replication fork slow-down independent of origin firing by creating replication barriers (González Besteiro *et al.*, 2019). Furthermore, when evaluating the asymmetries at tri-colored replication origins, we found a statistically significant increase after co-treatment compared to the other groups (Figure 58C). This indicates pronounced replication fork stalling, as the sister forks emanating from the same origin should normally travel with similar speed. To conclude, B02 + PF77736 treatment in J82^{CisPt} cells leads to a severe disruption of DNA replication dynamics due to stalling of replication forks, which is not seen upon mono-treatments. Of note, this did not cause transcriptional upregulation of various replicative and non-replicative polymerases in an attempt to cope with stalled replication by subsequently increasing DNA synthesis or bypassing of replication impairments (Figure 59). Unfortunately, TLS polymerase η, which is described as being recruited to CHK1$_i$-induced replication barriers (González Besteiro *et al.*, 2019), was not included in this study.

Errors that occur during replication can either be so drastic that they lead directly to cell death in S-phase, or they can be carried over into mitosis and interfere with proper cell separation. In fact, premature entry into mitosis with under-replicated DNA has been reported when cancer cells are treated with the CHK1 inhibitor prexasertib in combination with B02 (Mattiello *et al.*, 2021). Under-replicated DNA must be replenished by mitotic DNA synthesis. However, since RAD51 is an important factor in this pathway (Wassing *et al.*, 2021), it can be assumed that inhibition of RAD51 promotes mitotic catastrophe, which can lead to cell death (Vakifahmetoglu *et al.*, 2008). Indeed, there was a small number of J82^{CisPt} cells that showed premature entry into mitosis with under-replicated DNA after B02 + PF477736 treatment (Figure 62) and morphological features of mitotic catastrophe were observed in the nuclei of some

co-treated cells (Figure 63). However, as this phenomenon cannot sufficiently explain the strong cytotoxic and pro-apoptotic effect evoked by the combined treatment, it is considered to be a minor finding in J82^{CisPt} cells. Supposing that mitotic effects are unlikely to play a major role in the synergistic toxicity of RAD51$_i$ + CHK1$_i$ co-treatment, we rather speculated that treatment with CHK1$_i$ + RAD51$_i$ represents a “final hit”, so that J82^{CisPt} cells no longer enter mitosis, but instead die directly in S-phase.

On stalled replication forks, excessive DNA unwinding occurs as a result of uncoupling of the MCM helicase from the polymerase, producing high levels of ssDNA (Byun *et al.*, 2005). To protect ssDNA from degradation, it is coated with RPA. The number of nuclear RPA foci was indeed increased after a 24 h treatment with CHK1$_i$, but even more and at an earlier stage after a combined treatment with B02 + PF477736 (Figure 60). Concurringly, after 24 h monotherapy with CHK1$_i$ and after 6 h of combination treatment with RAD51$_i$, a high abundance of Ser33-phosphorylated RPA subunit RPA32, catalyzed by ATR, and Ser4/Ser8-phosphorylated RPA32, mediated by DNA-PK and ATM, were detected (Figure 61). These RPA phosphorylations are elicited by the mentioned ATM/ATR kinases in response to replication stress in order to increase RPA affinity for ssDNA and switch from replicative to reparative DNA synthesis (Shi *et al.*, 2010; Liu *et al.*, 2012; Liao *et al.*, 2018). Increased levels of other targets of ATM/ATR kinases, i.e. pKAP1 (Ser824), pCHK1 (Ser345) and pp53 (Ser15), were detected both after PF477736 mono-treatment and co-treatment with B02 (Figure 61, Figure 65). This suggests that CHK1$_i$ treatment is capable to trigger ATM/ATR signaling towards various phosphorylation substrates. By contrast, for the rapid phosphorylation and chromatin association of RPA, a co-treatment with RAD51$_i$ is necessary. This highlights the synergistic effects of CHK1$_i$ and RAD51$_i$ particularly on DNA replication structures. Notably, the synergism at an early time point is not linked to altered expression of the compounds’ target proteins, as CHK1 and RAD51 protein levels remained unaffected by inhibitor treatment and the combination treatment also did not lead to compensatory mechanisms in RAD51 and CHK1 at the mRNA expression level (Figure 59, Figure 61, Figure 64, Figure 65).

RPA is thought to protect ssDNA at stalled replication forks only temporarily, and this function is then taken over by RAD51 filaments (Liao *et al.*, 2018). The RAD51 inhibitor B02 blocks RAD51 binding to ssDNA (Huang *et al.*, 2012), as demonstrated by the absence of RAD51 foci induction after IR exposure (Figure 26) (Wassing *et al.*, 2021). In doing so, B02 disrupts both the ssDNA-protective function of RAD51 at stalled replication forks and its role in DNA strand exchange during homologous recombination. Consequently, the exchange of RPA by RAD51 and thus the long-term protection of nascent DNA is abolished by the RAD51 inhibitor B02. When the presence of ssDNA

exceeds the amount of RPA available in the cell, DNA strand breaks have been shown to occur (Toledo *et al.*, 2013). This threshold is likely to be reached more rapidly with $RAD51_i$ treatment because under these conditions RPA is retained on ssDNA rather than being replaced by RAD51, resulting in a depletion of the free RPA pool. Indeed, synergistic induction of phosphorylated histone 2AX at Ser139 (γH2AX), known as a marker for DNA damage as well as replication fork collapse (Alexander and Orr-Weaver, 2016), and DNA strand breaks were observed after dual treatment with B02 and PF477736 (Figure 65, Figure 66). This DNA damage signaling was generated mainly in S-phase cells and also originated from cells that showed high levels of ssDNA (Figure 67, Figure 68).

Once the cause of replication fork stalling has been removed, a restart of the replication fork can theoretically take place. Homologous recombination, and RAD51 as a key protein for mediating DNA strand exchange, is a crucial element in restarting arrested replication forks (Petermann *et al.*, 2010; Mason *et al.*, 2019). As a result, RAD51-deficient cells are presumably less efficient at replication fork restart than control cells and are more likely to experience prolonged fork stalling, which can lead to replication fork collapse and one-ended DSBs (Zeman and Cimprich, 2014). The strong synergistic effects observed with the combination of $CHK1_i$ PF477736 with $RAD51_i$ RI(dl)2, which specifically inhibits D-loop formation (Budke *et al.*, 2016; Lv *et al.*, 2016), i.e. strand exchange necessary for HR and HR-mediated replication fork restart, suggest that in particular the deficiency to restart stalled replication forks triggers the strong cytotoxic effect of the $RAD51_i$ + $CHK1_i$ combination (Figure 77). Considering that PARP stabilizes replication forks in their regressed state by limiting their restart (Berti *et al.*, 2013), it is reasonable to assume that PARP inhibition promotes the restart of regressed forks. Therefore, antagonistic effects were expected for a combination treatment with the $CHK1_i$ PF477736 + $PARP_i$ Niraparib, as one compound induces replication fork stalling and the other promotes fork restart. Indeed, antagonistic effects were observed with this combination, as measured by decreased cytotoxicity and S-phase arrest (Figure 48, Supplementary Figure 3). This finding indirectly supports the idea that the inability to restart stalled replication forks by inhibiting RAD51 with B02 plays a decisive role in triggering cytotoxicity.

In conclusion, the synergistic toxicity induced by the dual inhibition of RAD51 and CHK1 is likely due to the interruption of multiple mechanisms that allow the bypassing of DNA replication barriers created by CHK1 inhibition (Berti *et al.*, 2020) (Figure 87). On the one hand, $RAD51_i$ B02 prevents RAD51-dependent fork protection, as well as recombination-mediated template switching, which allows replication fork restart.

Simultaneously, with CHK1 inhibited by PF477736, repriming is not as efficient as under normal conditions since CHK1 is a regulator of the DNA primase PrimPol (Mehta *et al.*, 2022). Taken together, concurrent disruption of these two replication fork protectors results in persistent replication fork stalling without proper protection of accumulating ssDNA by RPA, as a lack of exchange by RAD51 eventually exploits the RPA pool. The hypothesis is that this ultimately leads to the collapse of replication forks accompanied by accumulation of DNA strand breaks that provoke cell death in S-phase.

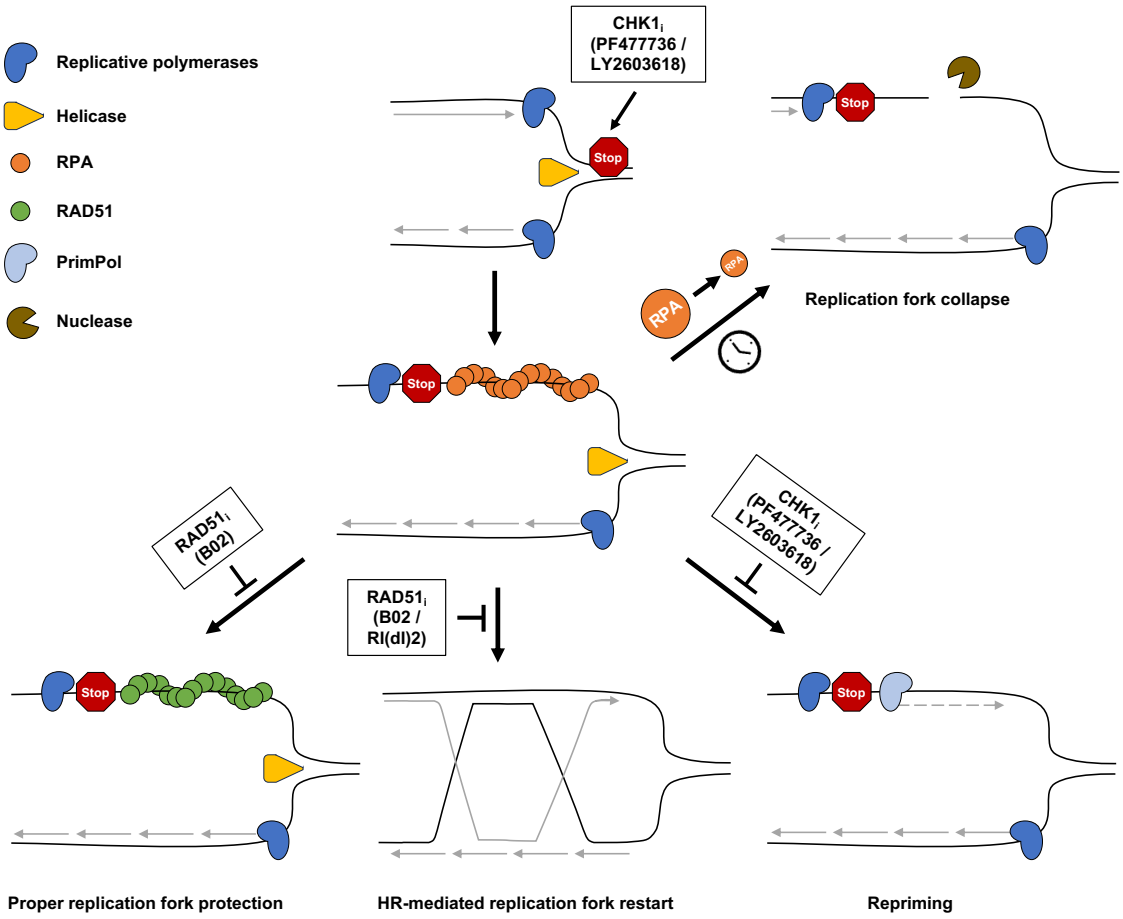

Figure 87: Model of synergistic toxicity evoked by combined inhibition of CHK1 and RAD51 in cisplatin-resistant tumor cells
CHK1 inhibition by PF477736 or LY2603618 causes replication fork stalling, leading to increased levels of ssDNA, which are initially covered by RPA. Due to inhibition of RAD51 by B02 or RI(dl)2 ssDNA-protection and, potentially more important, replication fork restart processes involving RAD51 are restricted. Additionally, repriming by PrimPol is not efficient when CHK1 is inhibited. Altogether this leads to long-lasting replication fork stalling without adequate protection of accumulating ssDNA, eventually depleting the RPA pool. This results in replication fork collapse, triggering cell death in S-phase.

4.5 Anti-tumor efficacy of B02 + PF477736 *in vivo*

The simultaneous treatment with B02 and PF477736 showed promising results with its synergistic cytotoxic effect observed in tumor cells of different entities in *in vitro* experiments. Therefore, a xenograft experiment with $J82^{CisPt}$ cells in NSG-$(K^bD^b)^{null}$ mice was performed to verify the anti-tumor efficiency *in vivo*. Unfortunately, the anti-tumor efficacy was not analyzable properly from the performed xenograft experiment due to extremely weak tumor forming capacity of $J82^{CisPt}$ cells *in vivo*. The subcutaneous injections of the cells appear to have worked in principle, as small bumps were visible immediately after the injections and all animals had developed at least one tumor, albeit a small one, by the end of the study. The tumor growth of $J82^{CisPt}$ cells in the employed immunodeficient mouse model simply seemed to proceed very slowly. This data is in line with publications reporting that tumor growth of $J82^{WT}$ cells is also rather slow as injection of $2x10^6$ cells only resulted in a tumor volume around 0.3 cm^3 after four weeks (Zhang *et al.*, 2017) or high cell numbers up to $1x10^7$ were used for xenograft formation (Li *et al.*, 2015; Wu *et al.*, 2020). Factors that were altered by selection in the cisplatin-resistant cells may have enhanced this poor engrafting property. This could include, for example, the differences found in the protein expression of cell adhesion molecules or cytoskeleton-associated factors (Figure 20, Supplementary Table 2, Supplementary Table 3), as cytoskeleton defects have been shown before to impair tumor growth in an orthotopic mouse model (McGarry *et al.*, 2021). The aneuploidy apparently present in $J82^{CisPt}$ (see chapter 4.1) could also have negative effects on the cells capacity to form tumors *in vivo*, as already described by others (Sheltzer *et al.*, 2017). In any case, the injected cell number had no major influence on the tumor formation capacity, as the tumors formed upon injection of $5x10^6$ cells in the main experiment did not grow faster than the tumors with $3x10^6$ cells in the pre-experiment (Figure 81, Figure 82).

Even though the mice used in the xenograft experiment are characterized by strong immunosuppression, they still have a small proportion of an intact innate immune system. It is possible that the $J82^{CisPt}$ cells have acquired a property that makes them vulnerable to the residual innate immune system and thus their number has already been strongly diminished before tumor growth can commence. A strategy that is often used to circumvent this is whole body irradiation of the mice before implanting the tumor cells in order to eliminate the last remnants of the immune system (Miers *et al.*, 2005; Tokalov *et al.*, 2010). One disadvantage of this approach, however, is that the mice already get stressed by the pre-irradiation before the actual experiment starts.

Due to the limited tumor growth, the original plan to start treatment with B02 and PF477736 when the average tumor volume reached 0.15 – 0.2 cm^3 and to analyze reduction in tumor size with the treatment had to be discarded. Instead, treatment with the inhibitors was commenced after a waiting period of 27 days and the new strategy was to see if there was slowed-down tumor growth following treatment with $RAD51_i$ + $CHK1_i$. When comparing the mean tumor volumes of the different treatment groups, it actually looks as if the control group had a stronger tumor growth than the treated groups and that there was no difference in tumor growth between the mono-treatments and the combination treatment with the inhibitors (Figure 82). This difference is in fact only based on two tumors grown in two different animals in the control group that grew much faster than the rest, but the majority of tumors in the control group grew at a similar slow rate as the tumors in the inhibitor-treated groups. Overall, a reliable statement about the *in vivo* anti-tumor efficacy of the tested treatment with B02 and PF477736 is not possible, as the tumors grew far too slowly to reliably detect marked differences between the different treatments.

There are no other studies available combining $CHK1_i$ + $RAD51_i$ *in vivo*, but CHK1 inhibitors as well as RAD51 inhibitors (also PF477736 and B02) have often been proven to effectively reduce tumor sizes in combination with cytostatics in xenograft experiments (Blasina *et al.*, 2008; Zhang *et al.*, 2009; Huang and Mazin, 2014; Barnard *et al.*, 2016; Aubry *et al.*, 2020). Combining inhibition of RAD51 with inhibition of Wee1, a checkpoint kinase important for G2-M transition, also acted synergistic in an orthotopic mouse model using head and neck squamous cell carcinoma cells (Lindemann *et al.*, 2021), showing that disrupting cell cycle processes while inhibiting RAD51 is an effective strategy for tumor cell killing. Based on these data, one can be optimistic that in a xenograft model with cisplatin resistant cells showing better tumor formation than $J82^{CisPt}$, the synergistic effect of PF477736 and B02 observed *in vitro* can be reproduced.

4.6 Effect of the combination treatment of B02 + PF477736 on non-malignant cells

A second aspect of the xenograft experiment was to investigate the general tolerability of the treatment with B02 and PF477736 and the analysis of adverse effects on selected normal tissues. As stated above, no other animal studies applying a combination treatment of $CHK1_i$ and $RAD51_i$ are available but there are several studies that use B02 or PF477736 as a single treatment or in combination with other inhibitors or cytostatic drugs. In these reports, the inhibitors were often administered to the mice in higher total doses (up to 200 mg/kg for B02, up to 160 mg/kg for PF477736) than in the study described here (60 mg/kg respectively) and were well tolerated in terms of weight loss (Zhang *et al.*, 2009; Carrassa *et al.*, 2012; Huang and Mazin, 2014; Iacobucci *et al.*, 2015; Lindemann *et al.*, 2021). In the study presented here, the mice also seemed to tolerate the single- and combi-treatment with the two compounds very well, as they showed no signs of abnormal weight loss or other stress symptoms such as scruffy fur or aggressive behavior (Figure 83). The organ weights of the animals treated with the inhibitors also showed no significant changes compared to the solvent control (Figure 84).

The replication stress response as a target is generally expected to have a wide therapeutic window, as it affects highly proliferative tissues only and there is much less proliferation in most normal tissues than in tumors. Normal tissue cells which have a high proliferation rate include cells of the hematopoietic system. Based on this, the focus in the investigation of adverse effects in the animal experiment was placed on blood cells and their progenitors in the bone marrow. Contrary to expectations, neither the analysis of the RNA expression of stress or cell death markers in the bone marrow cells nor the blood parameters revealed any changes that would indicate an adverse effect of the B02 + PF477736 co-treatment (Figure 85, Figure 86). Only Peroxisome proliferator-activated receptor gamma coactivator 1α (Pgc1a), a regulator of mitochondrial biogenesis, showed an upregulation in mRNA expression with treatment, albeit with large standard deviation. Higher levels of Pgc1a are described as being associated with rapid post-stress proliferation of hematopoietic stem cells for faster recovery from mild hypoxic stress (Basu *et al.*, 2013). Therefore, we assume that the simultaneous inhibition of RAD51 and CHK1 may have likewise evoked mild stress in the mitochondria of the bone marrow cells, which in turn has led to the upregulation of Pgc1a mRNA as a compensatory mechanism indicative of cellular recovery and proliferation.

In contrast to the absence of cytotoxic effects in the hematopoietic stem cells *in vivo*, the combination of B02 + PF477736 evoked pronounced cytotoxicity in a synergistic

manner in an *in vitro* cytotoxicity assay with human induced pluripotent stem cells (Figure 79). Conversely, only a rather additive effect was observed in NHDF cells, representing low proliferative normal cells (Figure 80). This supports the assumption that especially highly proliferating tissues are affected by the targeting of RAD51 and CHK1. Nevertheless, the reason why the hematopoietic stem cells *in vivo* did not react in a manner similar to that of the hiPSCS *in vitro* represents an unresolved question.

The observation that there are no marked differences between the treatment groups in the *in vivo* experiment raises the question of whether the time point of analysis, i.e. one week after the three-week treatment scheme with the inhibitors, is either too early or too late to observe a stress response in the bone marrow or the blood parameters. The turnover rates of blood cells in mice are 15 – 90 days for T-lymphocytes, 1 – 2 days for monocytes, 0.75 days for neutrophils, 41 days for erythrocytes and 4 days for platelets (Van Putten and Croon, 1958; Schmitt *et al.*, 2001; De Boer and Perelson, 2013; Patel *et al.*, 2021). Supposing that negative effects on the hematopoietic cells had already occurred at the beginning of the three-week treatment period with the compounds, it can be assumed that these would already be visible on the level of the blood parameters as a decline in the number of one or more types of blood cells at the time of analysis. Even if cytotoxic effects on the blood cell precursors only occurred after repeated treatment, effects should at least be visible for monocytes, neutrophils and platelets, as these have a particularly short regeneration time. Besides a generally reduced generation of fully differentiated cells, the treatment might also trigger a change in blood cell composition. However, no changes were visible in the blood composition. Stem cell differentiation markers indicative of distinct hematopoietic lineages e.g. IL-3Rα (CD123) for common myeloid progenitors (Testa *et al.*, 2014) or IL-7Rα (CD127) for common lymphoid progenitors in mice (Kondo *et al.*, 1997) were not included in the performed mRNA analysis and should be examined in forthcoming studies. These markers may reveal a shift in hematopoiesis towards a particular blood cell lineage that is not yet detectable as a change in the blood composition.

Another point that needs to be considered is whether the inhibitors were able to reach the bone marrow to trigger an adverse effect there. Unfortunately, no pharmacokinetic data from *in vivo* studies, where the distribution into bones has been proven, are available for either B02 or PF477736 or other $RAD51_i$ or $CHK1_i$. Another question is what the bioavailability of the applied substances was. A basic pharmacokinetics study found that PF477736 was dose-dependently absorbed after intraperitoneal injection and was moderately distributed into different body tissues after intravenous administration (Blasina *et al.*, 2008). However, the solvent used can have a very large influence on

the bioavailability. Unfortunately, both substances are very poorly soluble in water, hence dissolution in isotonic NaCl solution was not an option. In the aforementioned study PF477736 was dissolved in 50 nM sodium acetate buffer and 4% dextrose (Blasina *et al.*, 2008). In a study with B02, 20% DMSO was used to dissolve the compound (Huang and Mazin, 2014). Such high concentrations of DMSO are not permitted for animal testing in Europe, so a different approach had to be taken. Since both inhibitors showed acceptable fat solubility, corn oil was used as a solvent in the study presented here. When organs were removed at the end of the experiment, a strong accumulation of corn oil was found in the intraperitoneal space of the animals. It therefore appears that the amount of oil injected into the animals exceeded their capacity to eliminate it. Whether the oil still contained residual amounts of the inhibitors or whether they were completely absorbed is unclear. To investigate the drugs' bioavailability and distribution, it would have been necessary to identify the applied substances in blood samples and different tissue types of the mice by chemical analyses.

Due to the unclear uptake of the substances, the animal study carried out does not allow a meaningful statement about possible side effects of B02 and PF477736. Unfortunately, the aforementioned animal studies with either B02 or PF477736 did not include a detailed assessment of side effects to enable reliable comparison with the obtained results. Furthermore, no clinical studies have been conducted with RAD51 inhibitors so far, but several studies with CHK1 inhibitors have already been completed or are ongoing. The $CHK1_i$ PF477736 was tested in a phase 1 clinical trial in combination with gemcitabine for the treatment of advanced solid tumors back in 2011 (ClinicalTrials.gov ID NCT00437203). However, unfortunately, the study was terminated prematurely due to business reasons and was therefore not fully analyzed. A phase 1 study with another $CHK1_i$ (i.e. MK-8776) showed that monotherapy with this inhibitor was generally well tolerated by patients (Daud *et al.*, 2015). The most common side effects of the treatment were QTc prolongation, nausea, fatigue, and constipation. In combination with gemcitabine, adverse effects on blood cells also occurred, but these were not reported upon MK-8776 monotherapy. A monotherapy of $CHK1_i$ prexasertib was even tested in a phase 2 clinical trial on a group of patients suffering from platinum-resistant recurrent ovarian cancer (Konstantinopoulos *et al.*, 2022). In this setting, the overall therapeutic response rate was limited, but among the responding tumors, the slowing of tumor growth persisted for several months. The authors propose CCNE1 amplification and thereto relating cyclin E1 overexpression as biomarker for a favorable response. Concerning adverse effects, the patients showed hematologic abnormalities, as already described in other studies with prexasertib (Hong

et al., 2018; Byers *et al.*, 2021). Still, these were well manageable by administering the peptide hormone granulocyte-colony stimulating factor (G-CSF), which causes hematopoietic stem cells to be flushed out of the bone marrow into the blood and is frequently used to prevent chemotherapy-induced neutropenia.

These data suggest that treatment with $CHK1_i$ is generally well tolerated in humans and that occasionally occurring hematologic side effects are reversible and manageable. It can therefore be assumed that the same also applies to PF477736. Whether this is also the case for $RAD51_i$, i.e. B02, is difficult to assess, but the generally good tolerability in animal studies provides supportive evidence for this hypothesis. Even if both inhibitors are well tolerated individually, the combination of them may evoke stronger side effects. This can only be investigated in detail in further *in vivo* studies in which B02 and PF477736 are administered together. Nevertheless, this would necessitate the assurance of the bioavailability of both compounds through the implementation of a more absorbable formulation than dissolution in corn oil.

5 Conclusion

The mechanism of acquired cisplatin resistance in $J82^{CisPt}$ is probably related to aneuploidy, enhanced detoxifying capacity and drug transport processes. Some of the properties going along with resistance, presumably enhanced chromosomal instability and aneuploidy, are hypothesized to make the cells highly sensitive to replication stress inducing compounds. This characteristic can be exploited for overcoming resistance by inhibition of factors of the replication stress response. The combinatorial inhibition of CHK1 and RAD51 was found particularly promising for overcoming resistance, not only in $J82^{CisPt}$, but also in drug-resistant malignant cells of other origin. $CHK1_i$ + $RAD51_i$ trigger their synergistic cytotoxicity via replication fork arrest, which eventually leads to replication fork collapse due to the simultaneous restriction in replication fork protection, replication fork restart and repriming-associated mechanisms. Whether the tumor-killing effectiveness is reflected *in vivo* and what adverse effects result from the treatment can unfortunately not be conclusively assessed from the animal study carried out and requires further investigation. As concluded from the mechanism of action and *in vitro* cytotoxicity tests in normal tissue cells, it can be assumed that highly proliferative tissues, e.g. hematopoietic stem cells, are also primarily affected by the treatment with $CHK1_i$ + $RAD51_i$. It is worth noting that these normal cells are also attacked by conventional cytostatic drugs and there are already coping strategies, e.g. G-CSF, in use. It is therefore worth pursuing the therapeutic strategy employing $CHK1_i$ + $RAD51_i$ or inhibitors of factors regulating the replication stress response in general in order to overcome acquired CAT resistance.

6 Outlook

In this work it was shown that the cisplatin-resistant J82^{CisPt} cells are cross-resistant to the RAD51 inhibitor B02. The question of what causes this cross-resistance could not be conclusively answered in this study. The results suggested that dissimilar responses of J82^{WT} cells and J82^{CisPt} cells to B02-mediated mitotic disruption might play a role in this context. To further elucidate this hypothesis, it would be interesting to investigate whether the mitotic abnormalities observed after B02 treatment actually have their origin in mitosis or whether RAD51 inhibition evokes effects in the S-phase, which in turn cause malformations of the mitotic spindles. To investigate this, one could use a cyclin-dependent kinase 1 (CDK1) inhibitor, e.g. RO3306, to force a G2 arrest in the cells and thus synchronize the cell population in this cell cycle phase. When the cells are released from the arrest, a pulse treatment with B02 could then be performed so that mitotic cells are specifically challenged. This experimental setup would be useful to ascertain whether subsequent investigations into the mechanism of cross-resistance exhibited by J82^{CisPt} to B02 should rather focus on replicative processes or mitotic events.

In addition, since the effects observed with B02 could not be reproduced with RAD51 siRNA, it remains unclear whether B02-mediated effects are RAD51 specific. To further elucidate this question, a potential alternative approach would be to knock out the RAD51 gene via the use of CRISPR/Cas9 technology, followed by a comparative analysis of relevant endpoints e.g. pH3 staining with those observed after B02 treatment. It can be hypothesized that if the B02-mediated cellular dysfunctions are due to RAD51 inhibition, RAD51 knock out should induce similar impairments. Additionally, B02 treatment could be conducted simultaneously with transient overexpression of RAD51, which is achieved through the transfection of an expression vector. If B02 exerts its effects through RAD51 inhibition, these effects should be diminished by the concurrent vector-based RAD51 expression.

The studies on the molecular mechanism of the synergistic cytotoxicity evoked by B02 + PF477736 treatment in J82^{CisPt} cells revealed that the combination of the two agents arrests replication forks, accumulates ssDNA and causes DNA damage. The precise processes by which simultaneous RAD51 and CHK1 inhibition lead to the generation of DNA damage following ssDNA formation can only be assumed from the known roles of the two proteins in the replication stress response. The utilization of the iPOND technique may facilitate a more precise clarification on which proteins e.g. TLS polymerase Pol η, fork protector BRCA2 or nuclease MRE11 are recruited to the stalled replication forks and are possibly involved in the described

cell response. iPOND stands for isolation of proteins on nascent DNA and is essentially a reverse chromatin immunoprecipitation that involves purifying newly replicated DNA, along with its associated proteins, and analyzing them through either immunoblotting or mass spectrometry (Dungrawala and Cortez, 2015). The method of C-Trap® Optical Tweezers, whereby an isolated DNA strand is fixated and can be manipulated by addition of inhibitors or specific proteins, even allows the real-time visualization of protein binding kinetics on DNA by fluorescence imaging and could therefore assist to decipher the underlying biomolecular mechanisms of DNA damage induction by B02 + PF477736.

It was proven that the synergistic induction of cell death by B02 + PF477736 is at least partly mediated by apoptosis. Besides the involvement of apoptosis, the conducted mRNA expression analyses and an initial Western blot analysis for LC3 suggested that autophagy-related processes may also play a role in triggering the cytotoxicity. To further unravel the role of autophagy in this context, autophagosome biogenesis could be detected through co-localization analysis of the two markers WD repeat domain phosphoinositide-interacting protein 2 (WIPI2) and LC3 in an immunofluorescence staining. WIPI2 is recruited to the autophagosome membrane, where it mediates the conjugation of LC3 with phosphatidylethanolamine (Yamamoto *et al.*, 2023). Thus, the co-localization of both proteins serves as marker of autophagosome formation during the early stage of autophagy. Moreover, different modulators of early- and late-stage autophagy e.g. autophagy enhancer rapamycin or autophagy inhibitor chloroquine could be combined with the treatment of B02 and PF477736 for an evaluation of whether they exert an additive or antagonistic influence on the cytotoxicity induced by the two DDR inhibitors. This would provide insights into the involvement of autophagic processes in the cell death induction by inhibition of RAD51 and CHK1.

In order to provide a clearer assessment of the possible uses of the proposed treatment with B02 + PF477736, it would be beneficial to investigate in more detail which tumor cell characteristics, in addition to RAD51 and CHK1 protein expression, might serve as biomarkers of $RAD51_i$ + $CHK1_i$ antitumor effectiveness in CisPt resistant tumor cells. In this context, it would be particularly interesting to inspect whether the CIN-/aneuploidy-associated phenotype, as observed in $J82^{CisPt}$, is also found in other cell models (i.e. $A549^{CisPt}$ cells and $SH\text{-}SY5Y^{CisPt}$ cells) responding synergistically to combination treatment with B02 + PF477736 and whether this might be an explanation for their synergistic response. Chromosomal instability may be identified through the staining of the mitotic spindle apparatus, as has been previously demonstrated in J82 cells. The most reliable method for the detection of aneuploidy is through the staining of the cells' chromosomes in metaphase, which enables the analysis

of their karyotype. The metaphase staining could be combined with fluorescent in situ hybridization (FISH) analysis to gain a more detailed understanding of which chromosomes exactly are amplified.

The *in vivo* xenograft experiment carried out in the course of this work did not provide reliable information on the anti-tumor efficacy of treatment with B02 + PF477736 due to the poor tumor-forming ability of the CisPt resistant bladder carcinoma cells $J82^{CisPt}$. For clarification, the combination treatment should be tested in xenograft models employing other CisPt resistant tumor cell lines that show better tumor forming ability *in vivo*. The two cell lines $A549^{CisPt}$ (lung carcinoma cells) and SH-$SY5Y^{CisPt}$ (neuroblastoma cells), like $J82^{CisPt}$, showed synergistic cytotoxicity after B02 + PF477736 treatment *in vitro* and would therefore be suitable candidates for the *in vivo* experiment. However, these cells have never been used in a xenograft experiment before and it would therefore be necessary to test whether they are capable of properly forming tumors *in vivo*. As an alternative to the subcutaneous xenograft mouse model, it would also be feasible to utilize an orthotopic mouse model for the study. Orthotopic mouse models are defined by the fact that the tumors under investigation develop in the same organ from which the grafted cells were originally derived. This approach has the advantage of better mimicking the native tumor microenvironment, which could potentially enhance the tumor growth rate in comparison to the subcutaneous xenograft model. However, this methodology precludes the convenient monitoring of tumor growth using a caliper. Instead, tumors must be visualized using e.g. ultrasound to ascertain their dimensions. With access to biopsy samples from patients suffering from cisplatin-resistant tumors, it would even be possible to generate patient derived xenografts (PDX) or patient derived tumor organoids (PDTO) and evaluate the tumor-killing effectiveness of the treatment strategy with $RAD51_i$ + $CHK1_i$. These patient-derived cell samples might even reflect the clinically occurring characteristics of CisPt resistant malignant cells more accurately than the resistant cells selected from established cell lines in a laboratory setting. Nevertheless, in contrast to animal experiments, it is not possible to assess the potential side effects of the treatment in PDTO, as these reflect only the tumor tissue and not an entire organism.
Another aspect of the conducted animal study that may require improvement is the solvent of the applied inhibitors. Since the administration in corn oil led to oil residues in the intraperitoneal space of the mice, a different formulation using solubility enhancers (e.g. polysorbate 80 or polyethylene glycol 300) might be useful to prevent these accumulations and ensure complete absorption of the substances.

7 Summary

Despite the fact that cisplatin has been a key chemotherapeutic agent in the treatment of various cancer types for decades, acquired drug resistance of malignant cells is still a major clinical obstacle. The primary mechanism of action of cisplatin is to induce replication stress by forming crosslinks in genomic DNA. This results in the activation of the DNA damage response (DDR), a complex network that regulates cell cycle arrest, DNA repair and cell death. Deregulations in these pathways may be contributing factors in the acquirement of cisplatin resistance. From this we hypothesize that pharmacological modulation of factors involved in the DDR or DNA repair represents a potential strategy for overcoming acquired resistance of tumor cells to cisplatin. The aim of this work therefore was to identify pharmacological inhibitors of DDR or DNA repair mechanisms that are able to re-sensitize cisplatin-resistant cells to cisplatin treatment or, in combination with a second DDR inhibitor, circumvent acquired cisplatin resistance.

To this end, cisplatin-resistant bladder carcinoma cells J82^{CisPt} were treated with combinations of inhibitors of DDR- and DNA repair-related factors to identify additive or synergistic cytotoxic effects. To ascertain the universal significance of the findings, the selected combination treatment was examined for its cytotoxicity in cisplatin-resistant tumor cell lines originating from different tumor entities. The underlying molecular mechanisms of the synergism of a combination treatment that was identified as a potentially efficacious therapeutic strategy was then examined in more detail. For this purpose, investigations concerning cell cycle alterations, proliferation effects, DNA damage induction and DDR activation were performed. In addition, the cytotoxicity of the selected compound combination was examined in normal tissue cells *in vitro* to obtain an initial impression of potential adverse effects. Finally, combined treatment with the selected agents was tested in a xenograft mouse model to determine the antitumor efficacy and possible adverse effects *in vivo*.

We found that the combination of a CHK1- (PF477736) and a RAD51-inhibitor (B02) synergistically induced cell death not only in J82^{CisPt}, but also in cisplatin-resistant tumor cells of other origin (A549^{CisPt} lung carcinoma cells and SH-SY5Y^{CisPt} neuroblastoma cells). Initial experiments suggest that cisplatin resistance in the different cell lines is based on distinct molecular mechanisms and that the effectiveness of treatment with CHK1$_i$ + RAD51$_i$ positively correlates with protein expression of the two factors.

J82^{CisPt} treated with PF477736 and B02 showed S-phase arrest and reduced EdU incorporation. DNA Fiber Spreading assay revealed shorter tracks at ongoing replication forks and asymmetric replication origins, suggesting replication barriers. At the same time, the number of RPA foci as a marker for ssDNA was increased. Furthermore, DNA strand breaks were detected by comet assay and the DNA double strand break marker γH2AX was specifically increased in S-phase cells. Based on these findings, we propose that the synergistic toxicity of PF477736 and B02 in J82^{CisPt} is mediated by disrupting S-phase progression. This is associated with the stalling of replication forks and the excessive formation of ssDNA. The inability to properly protect or restart the replication fork if RAD51 and CHK1 are simultaneously inhibited leads to replication fork collapse and eventually cell death. Noteworthy, selected key endpoints could be reproduced in SH-SY5Y^{CisPt}, so it can be assumed that the described mechanism is universally valid.

In addition to studies examining the molecular mechanism of CHK1$_i$ + RAD51$_i$, the cytotoxic effect of the combination treatment was analyzed in non-malignant human cells to make an initial assessment of possible adverse effects of the drug combination. For this purpose, the viability of human induced pluripotent stem cells (hIPSCs), as model for highly proliferative cells e.g. hematopoietic stem cells, and Normal Human Dermal Fibroblasts (NHDF), which reflect low-proliferative cells, was analyzed after treatment with B02 + PF477736. Viability measurements revealed synergistic cytotoxicity in high-proliferative hIPSCs, but rather additive effects in low-proliferative NHDF. This finding underlines the fact that highly replicative cell types are particularly affected by the co-treatment.

Moreover, a xenograft model in mice was employed to assess the anticancer efficacy, as well as adverse effects of B02 + PF477736 as combination and mono treatments *in vivo*. Due to poor tumor formation of the J82^{CisPt} cells *in vivo*, the performed experiment unfortunately did not provide unequivocal results on the antitumor efficacy of the treatment. At the same time, no adverse effects of the applied inhibitors were observed in the mice.

In conclusion, the present work could demonstrate that simultaneously inhibiting CHK1 and RAD51 as factors involved in the regulation of the replicative stress response is a promising approach to overcome acquired cisplatin resistance.

8 Zusammenfassung

Cisplatin (CisPt) wird seit vielen Jahren als Chemotherapeutikum zur Behandlung verschiedener Krebsarten eingesetzt. Die erworbene Resistenz maligner Zellen gegen das Medikament stellt jedoch nach wie vor eine klinische Herausforderung dar. Der primäre Wirkmechanismus von CisPt besteht in der Induktion von Replikationsstress durch die Bildung von Quervernetzungen in der genomischen DNA. Dies führt zur Aktivierung der DNA-Schadensantwort (DDR); einem komplexen Netzwerk, das die Auslösung von Zellzyklusarrest, DNA-Reparatur und Zelltod reguliert. Deregulationen in diesen Signalwegen können zu einer Resistenzentwicklung gegen CisPt beitragen. Wir stellen die Hypothese auf, dass die pharmakologische Modulation von DDR- oder DNA-Reparatur-Faktoren eine potentielle Strategie zur Überwindung der erworbenen CisPt-Resistenz von Tumorzellen darstellt. Ziel dieser Arbeit war es daher DDR-/DNA-Reparatur-Inhibitoren zu identifizieren, die CisPt-resistente Zellen für eine Behandlung mit CisPt resensibilisieren oder in Kombination mit einem zweiten DDR-Inhibitor eine erworbene CisPt-Resistenz umgehen können.

Zu diesem Zweck wurden die CisPt-resistenten Blasenkarzinomzellen J82^{CisPt} mit Kombinationen aus Inhibitoren von DDR- und DNA-Reparatur-Faktoren behandelt, um additive oder synergistische zytotoxische Effekte zu ermitteln. Im Anschluss wurde der molekulare Mechanismus des Synergismus einer Kombinationsbehandlung, die als potenziell wirksame therapeutische Strategie identifiziert worden war, näher untersucht. Dabei wurden Veränderungen des Zellzyklus, Auswirkungen auf die Proliferation, die Induktion von DNA-Schäden sowie die Aktivierung der DDR analysiert. Außerdem wurde die ausgewählte Kombinationsbehandlung *in vitro* hinsichtlich ihrer Toxizität in CisPt-resistenten Tumorzelllinien aus diversen Tumorentitäten sowie in nicht-malignen Zellen untersucht. Schließlich wurde die ausgewählte Inhibitor-Kombination in einem Xenograft-Mausmodell getestet, um die antitumorale Wirksamkeit *in vivo* zu bestimmen.

In der vorliegenden Studie wurde festgestellt, dass die Kombination eines RAD51- (B02) und eines CHK1-Inhibitors (PF477736) sowohl in J82^{CisPt}, als auch in CisPt-resistenten Tumorzellen anderer Entitäten (A549^{CisPt} Lungenkarzinomzellen und SH-SY5Y^{CisPt} Neuroblastomzellen) synergistisch Zelltod auslöste. Erste Versuchsergebnisse deuten darauf hin, dass die CisPt-Resistenz der verschiedenen Zelllinien auf unterschiedlichen Mechanismen beruht und dass die Effektivität der CHK1$_i$ + RAD51$_i$ Behandlung positiv mit der Proteinexpression der beiden angegriffenen Faktoren korreliert.
Die Behandlung von J82^{CisPt} Zellen mit PF477736 und B02 führte zu einem Zellzyklusarrest in der S-Phase und einer Verringerung des EdU-Einbaus.

Die Ergebnisse des *DNA Fiber Spreading assay* wiesen kürzere Stränge neusynthetisierter DNA an aktiven Replikationsgabeln, sowie asymmetrische Replikationsursprünge auf, was auf Replikationsbarrieren hindeutet. Gleichzeitig nahm die Anzahl an RPA Foci zu, die als Marker für einzelsträngige DNA dienen. Darüber hinaus wurden mittels *Comet assay* DNA-Strangbrüche nachgewiesen, und der Marker für DNA-Doppelstrangbrüche, γH2AX, war spezifisch in Zellen der S-Phase erhöht. Diese Ergebnisse legen nahe, dass die synergistische Toxizität von PF477736 und B02 in $J82^{CisPt}$ durch eine Störung der Progression der S-Phase vermittelt wird. Dies steht in Zusammenhang mit der Blockierung von Replikationsgabeln und der daraus resultierenden exzessiven Bildung von einzelsträngiger DNA. Die blockierten Replikationsgabeln können bei inhibiertem RAD51 und CHK1 weder angemessen geschützt noch neu gestartet werden, was zum Kollaps der Replikationsgabeln und letztendlich zum Zelltod führt. Es ist hervorzuheben, dass ausgewählte zentrale Befunde in $SH\text{-}SY5Y^{CisPt}$ reproduziert werden konnten, was darauf hinweist, dass es sich um einen Zelllinien-übergreifenden Wirkmechanismus handelt.

Zusätzlich zu Studien, welche den molekularen Mechanismus von $CHK1_i$ + $RAD51_i$ untersuchten, sollte die zytotoxische Wirkung der Kombinationsbehandlung auf Normalgewebszellen analysiert werden, um eine erste Einschätzung möglicher Nebenwirkungen vorzunehmen. Zu diesem Zweck wurde die Zellviabilität humaner induzierter pluripotenter Stammzellen (hIPSCs), als Modell für hochproliferative Zellen z. B. hämatopoetische Stammzellen, und humaner Fibroblasten der Haut (NHDF), die schwach proliferierende Zellen darstellen, nach Behandlung mit B02 + PF477736 analysiert. Die Viabilitätsmessungen ergaben eine synergistische Zytotoxizität in hIPSCs, während in NHDF lediglich additive Effekte beobachtet wurden. Dies bestätigt die Annahme, dass insbesondere hochreplikative Zelltypen von der Behandlung betroffen sind.

Des Weiteren wurde ein Xenograft Experiment in Mäusen durchgeführt, um die tumorwachstumshemmende Wirkung sowie adverse Effekte von B02 und PF477736 als Kombinations- und Monobehandlung *in vivo* zu untersuchen. Aufgrund der schwachen Tumorbildung der $J82^{CisPt}$-Zellen im Tiermodell konnte die antitumorale Wirksamkeit der Behandlung nicht eindeutig nachgewiesen werden. Gleichzeitig wurden bei den Versuchstieren keine adversen Effekte der applizierten Inhibitoren festgestellt.

Zusammenfassend konnte die vorliegende Arbeit zeigen, dass die gleichzeitige Hemmung von CHK1 und RAD51 als Faktoren, die an der Regulierung der replikativen Stressantwort beteiligt sind, ein vielversprechender Ansatz zur Überwindung erworbener Cisplatin-Resistenz ist.

9 List of references

Aguilera, A, and Gómez-González, B (2008). Genome instability: a mechanistic view of its causes and consequences. Nat Rev Genet 9, 204–217.

Alexander, JL, and Orr-Weaver, TL (2016). Replication fork instability and the consequences of fork collisions from rereplication. Genes Dev 30, 2241–2252.

Anand, U, Dey, A, Chandel, AKS, Sanyal, R, Mishra, A, Pandey, DK, De Falco, V, Upadhyay, A, Kandimalla, R, Chaudhary, A, *et al.* (2023). Cancer chemotherapy and beyond: Current status, drug candidates, associated risks and progress in targeted therapeutics. Genes Dis 10, 1367–1401.

Aubry, A, Pearson, JD, Huang, K, Livne-bar, I, Ahmad, M, Jagadeesan, M, Khetan, V, Ketela, T, Brown, KR, Yu, T, *et al.* (2020). Functional genomics identifies new synergistic therapies for retinoblastoma. Oncogene 39, 5338–5357.

Bagnardi, V, Rota, M, Botteri, E, Tramacere, I, Islami, F, Fedirko, V, Scotti, L, Jenab, M, Turati, F, Pasquali, E, *et al.* (2015). Alcohol consumption and site-specific cancer risk: a comprehensive dose–response meta-analysis. Br J Cancer 112, 580–593.

Baik, M-H, Friesner, RA, and Lippard, SJ (2003). Theoretical Study of Cisplatin Binding to Purine Bases: Why Does Cisplatin Prefer Guanine over Adenine? J Am Chem Soc 125, 14082–14092.

Bakkenist, CJ, and Kastan, MB (2003). DNA damage activates ATM through intermolecular autophosphorylation and dimer dissociation. Nature 421, 499–506.

Ball, HL, Myers, JS, and Cortez, D (2005). ATRIP Binding to Replication Protein A-Single-stranded DNA Promotes ATR–ATRIP Localization but Is Dispensable for Chk1 Phosphorylation. Mol Biol Cell 16, 2372–2381.

Barnard, D, Diaz, HB, Burke, T, Donoho, G, Beckmann, R, Jones, B, Barda, D, King, C, and Marshall, M (2016). LY2603618, a selective CHK1 inhibitor, enhances the anti-tumor effect of gemcitabine in xenograft tumor models. Invest New Drugs 34, 49–60.

Basu, S, Broxmeyer, HE, and Hangoc, G (2013). Peroxisome Proliferator-Activated-γ Coactivator-1α–Mediated Mitochondrial Biogenesis Is Important for Hematopoietic Recovery in Response to Stress. Stem Cells Dev 22, 1678–1692.

Baudoin, NC, and Cimini, D (2018). A guide to classifying mitotic stages and mitotic defects in fixed cells. Chromosoma 127, 215–227.

Baumann, P, and West, SC (1998). Role of the human RAD51 protein in homologous recombination and double-stranded-break repair. Trends Biochem Sci 23, 247–251.

Berenblum, I (1941). The Mechanism of Carcinogenesis. A Study of the Significance of Cocarcinogenic Action and Related Phenomena. Cancer Res 1, 807–814.

Bergmann, L, Lang, A, Bross, C, Altinoluk-Hambüchen, S, Fey, I, Overbeck, N, Stefanski, A, Wiek, C, Kefalas, A, Verhülsdonk, P, *et al.* (2020). Subcellular Localization and Mitotic Interactome Analyses Identify SIRT4 as a Centrosomally Localized and Microtubule Associated Protein. Cells 9, 1950.

Berti, M, Cortez, D, and Lopes, M (2020). The plasticity of DNA replication forks in response to clinically relevant genotoxic stress. Nat Rev Mol Cell Biol 21, 633–651.

Berti, M, Ray Chaudhuri, A, Thangavel, S, Gomathinayagam, S, Kenig, S, Vujanovic, M, Odreman, F, Glatter, T, Graziano, S, Mendoza-Maldonado, R, *et al.* (2013). Human RECQ1 promotes restart of replication forks reversed by DNA topoisomerase I inhibition. Nat Struct Mol Biol 20, 347–354.

Bhatia, A, and Kumar, Y (2014). Relevance of microscopic indicators of chromosomal instability in routine reporting of malignancies. Diagn Cytopathol 42, 181–188.

Bhowmick, R, Hickson, ID, and Liu, Y (2023). Completing genome replication outside of S phase. Mol Cell 83, 3596–3607.

Bian, J, Zhang, L, Han, Y, Wang, C, and Zhang, L (2015). Histone Deacetylase Inhibitors: Potent Anti-Leukemic Agents. Curr Med Chem 22, 2065–2074.

Bianchi, V, Pontis, E, and Reichard, P (1986). Changes of deoxyribonucleoside triphosphate pools induced by hydroxyurea and their relation to DNA synthesis. J Biol Chem 261, 16037–16042.

Biber, S, and Wiesmüller, L (2021). Analysis of Replication Dynamics Using the Single-Molecule DNA Fiber Spreading Assay. In: Cell Cycle Checkpoints, ed. JJ Manfredi, New York, NY: Springer US, 57–71.

Blasina, A, Hallin, J, Chen, E, Arango, ME, Kraynov, E, Register, J, Grant, S, Ninkovic, S, Chen, P, Nichols, T, *et al.* (2008). Breaching the DNA damage checkpoint via PF-00477736, a novel small-molecule inhibitor of checkpoint kinase 1. Mol Cancer Ther 7, 2394–2404.

Block, G, Patterson, B, and Subar, A (1992). Fruit, vegetables, and cancer prevention: A review of the epidemiological evidence. Nutr Cancer 18, 1–29.

Bos, JL (1989). ras oncogenes in human cancer: a review. Cancer Res 49, 4682–4689.

Bryant, HE, Schultz, N, Thomas, HD, Parker, KM, Flower, D, Lopez, E, Kyle, S, Meuth, M, Curtin, NJ, and Helleday, T (2005). Specific killing of BRCA2-deficient tumours with inhibitors of poly(ADP-ribose) polymerase. Nature 434, 913–917.

Budke, B, Logan, HL, Kalin, JH, Zelivianskaia, AS, Cameron McGuire, W, Miller, LL, Stark, JM, Kozikowski, AP, Bishop, DK, and Connell, PP (2012). RI-1: a chemical inhibitor of RAD51 that disrupts homologous recombination in human cells. Nucleic Acids Res 40, 7347–7357.

Budke, B, Lv, W, Kozikowski, AP, and Connell, PP (2016). Recent Developments Using Small Molecules to Target RAD51: How to Best Modulate RAD51 for Anticancer Therapy? ChemMedChem 11, 2468–2473.

Byers, LA, Navarro, A, Schaefer, E, Johnson, M, Özgüroğlu, M, Han, J-Y, Bondarenko, I, Cicin, I, Dragnev, KH, Abel, A, *et al.* (2021). A Phase II Trial of Prexasertib (LY2606368) in Patients With Extensive-Stage Small-Cell Lung Cancer. Clin Lung Cancer 22, 531–540.

Byun, TS, Pacek, M, Yee, M, Walter, JC, and Cimprich, KA (2005). Functional uncoupling of MCM helicase and DNA polymerase activities activates the ATR-dependent checkpoint. Genes Dev 19, 1040–1052.

Cann, KL, and Dellaire, G (2011). Heterochromatin and the DNA damage response: the need to relax. Biochem Cell Biol 89, 45–60.

Carrassa, L, Chilà, R, Lupi, M, Ricci, F, Celenza, C, Mazzoletti, M, Broggini, M, and Damia, G (2012). Combined inhibition of Chk1 and Wee1: In vitro synergistic effect translates to tumor growth inhibition in vivo. Cell Cycle 11, 2507–2517.

Chatterjee, N, and Walker, GC (2017). Mechanisms of DNA damage, repair, and mutagenesis. Environ Mol Mutagen 58, 235–263.

Chen, F, Zhao, W, Du, C, Chen, Z, Du, J, and Zhou, M (2024). Bleomycin induces senescence and repression of DNA repair via downregulation of Rad51. Mol Med 30, 54.

Chou, T-C (2010). Drug Combination Studies and Their Synergy Quantification Using the Chou-Talalay Method. Cancer Res 70, 440–446.

Christmann, M, Tomicic, MT, Roos, WP, and Kaina, B (2003). Mechanisms of human DNA repair: an update. Toxicology 193, 3–34.

Ciarimboli, G (2012). Membrane Transporters as Mediators of Cisplatin Effects and Side Effects. Scientifica 2012, 1–18.

Ciarimboli, G, Deuster, D, Knief, A, Sperling, M, Holtkamp, M, Edemir, B, Pavenstädt, H, Lanvers-Kaminsky, C, Am Zehnhoff-Dinnesen, A, Schinkel, AH, *et al.* (2010). Organic Cation Transporter 2 Mediates Cisplatin-Induced Oto- and Nephrotoxicity and Is a Target for Protective Interventions. Am J Pathol 176, 1169–1180.

Ciarimboli, G, Ludwig, T, Lang, D, Pavenstädt, H, Koepsell, H, Piechota, H-J, Haier, J, Jaehde, U, Zisowsky, J, and Schlatter, E (2005). Cisplatin Nephrotoxicity Is Critically Mediated via the Human Organic Cation Transporter 2. Am J Pathol 167, 1477–1484.

Ciccia, A, and Elledge, SJ (2010). The DNA Damage Response: Making It Safe to Play with Knives. Mol Cell 40, 179–204.

Cohen, GM (1997). Caspases: the executioners of apoptosis. Biochem J 326, 1–16.

Conti, BA, and Smogorzewska, A (2020). Mechanisms of direct replication restart at stressed replisomes. DNA Repair 95, 102947.

Cortez, D, Guntuku, S, Qin, J, and Elledge, SJ (2001). ATR and ATRIP: Partners in Checkpoint Signaling. Science 294, 1713–1716.

Cory, S, and Adams, JM (2002). The Bcl2 family: regulators of the cellular life-or-death switch. Nat Rev Cancer 2, 647–656.

Crosio, C, Fimia, GM, Loury, R, Kimura, M, Okano, Y, Zhou, H, Sen, S, Allis, CD, and Sassone-Corsi, P (2002). Mitotic Phosphorylation of Histone H3: Spatio-Temporal Regulation by Mammalian Aurora Kinases. Mol Cell Biol 22, 874–885.

Cui, Y, König, J, Buchholz, JK, Spring, H, Leier, I, and Keppler, D (1999). Drug resistance and ATP-dependent conjugate transport mediated by the apical multidrug resistance protein, MRP2, permanently expressed in human and canine cells. Mol Pharmacol 55, 929–937.

D'Arcy, MS (2019). Cell death: a review of the major forms of apoptosis, necrosis and autophagy. Cell Biol Int 43, 582–592.

Daud, AI, Ashworth, MT, Strosberg, J, Goldman, JW, Mendelson, D, Springett, G, Venook, AP, Loechner, S, Rosen, LS, Shanahan, F, *et al.* (2015). Phase I Dose-Escalation Trial of Checkpoint Kinase 1 Inhibitor MK-8776 As Monotherapy and in Combination With Gemcitabine in Patients With Advanced Solid Tumors. J Clin Oncol 33, 1060–1066.

Davis, AJ, Chen, BPC, and Chen, DJ (2014). DNA-PK: A dynamic enzyme in a versatile DSB repair pathway. DNA Repair 17, 21–29.

De Boer, RJ, and Perelson, AS (2013). Quantifying T lymphocyte turnover. J Theor Biol 327, 45–87.

el-Deiry, WS, Harper, JW, O'Connor, PM, Velculescu, VE, Canman, CE, Jackman, J, Pietenpol, JA, Burrell, M, Hill, DE, and Wang, Y (1994). WAF1/CIP1 is induced in p53-mediated G1 arrest and apoptosis. Cancer Res 54, 1169–1174.

DiPaola, RS (2002). To arrest or not to G(2)-M Cell-cycle arrest : commentary re: A. K. Tyagi et al., Silibinin strongly synergizes human prostate carcinoma DU145 cells to doxorubicin-induced growth inhibition, G(2)-M arrest, and apoptosis. Clin. cancer res., 8: 3512-3519, 2002. Clin Cancer Res Off J Am Assoc Cancer Res 8, 3311–3314.

Donahue, BA, Yin, S, Taylor, JS, Reines, D, and Hanawalt, PC (1994). Transcript cleavage by RNA polymerase II arrested by a cyclobutane pyrimidine dimer in the DNA template. Proc Natl Acad Sci 91, 8502–8506.

Duan, M, Speer, RM, Ulibarri, J, Liu, KJ, and Mao, P (2021). Transcription-coupled nucleotide excision repair: New insights revealed by genomic approaches. DNA Repair 103, 103126.

Dungrawala, H, and Cortez, D (2015). Purification of Proteins on Newly Synthesized DNA Using iPOND. In: The Nucleus, ed. R Hancock, New York, NY: Springer New York, 123–131.

Eastman, A (1983). Characterization of the adducts produced in DNA by cis-diamminedichloroplatinum(II) and cis-dichloro(ethylenediamine)platinum(II). Biochemistry 22, 3927–3933.

Elmore, S (2007). Apoptosis: A Review of Programmed Cell Death. Toxicol Pathol 35, 495–516.

Fagbemi, AF, Orelli, B, and Schärer, OD (2011). Regulation of endonuclease activity in human nucleotide excision repair. DNA Repair 10, 722–729.

Fan, R, Kumaravel, TS, Jalali, F, Marrano, P, Squire, JA, and Bristow, RG (2004). Defective DNA Strand Break Repair after DNA Damage in Prostate Cancer Cells. Cancer Res 64, 8526–8533.

Feringa, FM, Raaijmakers, JA, Hadders, MA, Vaarting, C, Macurek, L, Heitink, L, Krenning, L, and Medema, RH (2018). Persistent repair intermediates induce senescence. Nat Commun 9, 3923.

Fichtinger-Schepman, AM, van Oosterom, AT, Lohman, PH, and Berends, F (1987). cis-Diamminedichloroplatinum(II)-induced DNA adducts in peripheral leukocytes from seven cancer patients: quantitative immunochemical detection of the adduct induction and removal after a single dose of cis-diamminedichloroplatinum(II). Cancer Res 47, 3000–3004.

Fragkos, M, Choleza, M, and Papadopoulou, P (2023). The Role of γH2AX in Replication Stress-induced Carcinogenesis: Possible Links and Recent Developments. Cancer Diagn Progn 3, 639–648.

Fuchs, J, Cheblal, A, and Gasser, SM (2021). Underappreciated Roles of DNA Polymerase δ in Replication Stress Survival. Trends Genet 37, 476–487.

Galluzzi, L, Senovilla, L, Vitale, I, Michels, J, Martins, I, Kepp, O, Castedo, M, and Kroemer, G (2012). Molecular mechanisms of cisplatin resistance. Oncogene 31, 1869–1883.

Genschel, J, Bazemore, LR, and Modrich, P (2002). Human Exonuclease I Is Required for 5′ and 3′ Mismatch Repair. J Biol Chem 277, 13302–13311.

González Besteiro, MA, Calzetta, NL, Loureiro, SM, Habif, M, Bétous, R, Pillaire, M, Maffia, A, Sabbioneda, S, Hoffmann, J, and Gottifredi, V (2019). Chk1 loss creates replication barriers that compromise cell survival independently of excess origin firing. EMBO J 38, e101284.

Goto, S, Yoshida, K, Morikawa, T, Urata, Y, Suzuki, K, and Kondo, T (1995). Augmentation of transport for cisplatin-glutathione adduct in cisplatin-resistant cancer cells. Cancer Res 55, 4297–4301.

Grimm, S, Stanger, BZ, and Leder, P (1996). RIP and FADD: two “death domain”-containing proteins can induce apoptosis by convergent, but dissociable, pathways. Proc Natl Acad Sci 93, 10923–10927.

Groselj, B, Sharma, NL, Hamdy, FC, Kerr, M, and Kiltie, AE (2013). Histone deacetylase inhibitors as radiosensitisers: effects on DNA damage signalling and repair. Br J Cancer 108, 748–754.

Guo, Z, Kumagai, A, Wang, SX, and Dunphy, WG (2000). Requirement for Atr in phosphorylation of Chk1 and cell cycle regulation in response to DNA replication blocks and UV-damaged DNA in *Xenopus* egg extracts. Genes Dev 14, 2745–2756.

Gutierrez, R, and O’Connor, TR (2021). DNA direct reversal repair and alkylating agent drug resistance. Cancer Drug Resist.

Haaf, T, Golub, EI, Reddy, G, Radding, CM, and Ward, DC (1995). Nuclear foci of mammalian Rad51 recombination protein in somatic cells after DNA damage and its localization in synaptonemal complexes. Proc Natl Acad Sci 92, 2298–2302.

Hanahan, D (2022). Hallmarks of Cancer: New Dimensions. Cancer Discov 12, 31–46.

Helleday, T (2011). The underlying mechanism for the PARP and BRCA synthetic lethality: Clearing up the misunderstandings. Mol Oncol 5, 387–393.

Hendzel, MJ, Wei, Y, Mancini, MA, Van Hooser, A, Ranalli, T, Brinkley, BR, Bazett-Jones, DP, and Allis, CD (1997). Mitosis-specific phosphorylation of histone H3 initiates primarily within pericentromeric heterochromatin during G2 and spreads in an ordered fashion coincident with mitotic chromosome condensation. Chromosoma 106, 348–360.

Hill, MM, Adrain, C, Duriez, PJ, Creagh, EM, and Martin, SJ (2004). Analysis of the composition, assembly kinetics and activity of native Apaf-1 apoptosomes. EMBO J 23, 2134–2145.

Hoeijmakers, JHJ (2001). Genome maintenance mechanisms for preventing cancer. Nature 411, 366–374.

Höhn, A, Krüger, K, Skowron, MA, Bormann, S, Schumacher, L, Schulz, WA, Hoffmann, MJ, Niegisch, G, and Fritz, G (2016). Distinct mechanisms contribute to acquired cisplatin resistance of urothelial carcinoma cells. Oncotarget 7, 41320–41335.

Hong, DS, Moore, K, Patel, M, Grant, SC, Burris, HA, William, WN, Jones, S, Meric-Bernstam, F, Infante, J, Golden, L, *et al.* (2018). Evaluation of Prexasertib, a Checkpoint Kinase 1 Inhibitor, in a Phase Ib Study of Patients with Squamous Cell Carcinoma. Clin Cancer Res 24, 3263–3272.

Hosea, R, Hillary, S, Naqvi, S, Wu, S, and Kasim, V (2024). The two sides of chromosomal instability: drivers and brakes in cancer. Signal Transduct Target Ther 9, 75.

Huang, F, and Mazin, AV (2014). A Small Molecule Inhibitor of Human RAD51 Potentiates Breast Cancer Cell Killing by Therapeutic Agents in Mouse Xenografts. PLoS ONE 9, e100993.

Huang, F, Mazina, OM, Zentner, IJ, Cocklin, S, and Mazin, AV (2012). Inhibition of Homologous Recombination in Human Cells by Targeting RAD51 Recombinase. J Med Chem 55, 3011–3020.

Iacobucci, I, Di Rorà, AGL, Falzacappa, MVV, Agostinelli, C, Derenzini, E, Ferrari, A, Papayannidis, C, Lonetti, A, Righi, S, Imbrogno, E, *et al.* (2015). In vitro and in vivo single-agent efficacy of checkpoint kinase inhibition in acute lymphoblastic leukemia. J Hematol OncolJ Hematol Oncol 8, 125.

Ishida, S, Lee, J, Thiele, DJ, and Herskowitz, I (2002). Uptake of the anticancer drug cisplatin mediated by the copper transporter Ctr1 in yeast and mammals. Proc Natl Acad Sci 99, 14298–14302.

Jackson, JR, Gilmartin, A, Imburgia, C, Winkler, JD, Marshall, LA, and Roshak, A (2000). An indolocarbazole inhibitor of human checkpoint kinase (Chk1) abrogates cell cycle arrest caused by DNA damage. Cancer Res 60, 566–572.

Jamieson, ER, and Lippard, SJ (1999). Structure, Recognition, and Processing of Cisplatin−DNA Adducts. Chem Rev 99, 2467–2498.

Jayathilaka, K, Sheridan, SD, Bold, TD, Bochenska, K, Logan, HL, Weichselbaum, RR, Bishop, DK, and Connell, PP (2008). A chemical compound that stimulates the human homologous recombination protein RAD51. Proc Natl Acad Sci 105, 15848–15853.

Jin, Z-L, and Kim, N-H (2017). RAD51 maintains chromosome integrity and mitochondrial distribution during porcine oocyte maturation *in vitro*. J Reprod Dev 63, 489–496.

Kadyrov, FA, Dzantiev, L, Constantin, N, and Modrich, P (2006). Endonucleolytic Function of MutLα in Human Mismatch Repair. Cell 126, 297–308.

Khan, M, Shaukat, Z, Saint, R, and Gregory, SL (2018). Chromosomal instability causes sensitivity to protein folding stress and ATP depletion. Biol Open 7, bio038000.

Kim, C, Paulus, BF, and Wold, MS (1994). Interactions of human replication protein A with oligonucleotides. Biochemistry 33, 14197–14206.

King, C, Diaz, H, Barnard, D, Barda, D, Clawson, D, Blosser, W, Cox, K, Guo, S, and Marshall, M (2014). Characterization and preclinical development of LY2603618: a selective and potent Chk1 inhibitor. Invest New Drugs 32, 213–226.

Kischkel, FC, Hellbardt, S, Behrmann, I, Germer, M, Pawlita, M, Krammer, PH, and Peter, ME (1995). Cytotoxicity-dependent APO-1 (Fas/CD95)-associated proteins form a death-inducing signaling complex (DISC) with the receptor. EMBO J 14, 5579–5588.

Klungland, A (1997). Second pathway for completion of human DNA base excision-repair: reconstitution with purified proteins and requirement for DNase IV (FEN1). EMBO J 16, 3341–3348.

Kondo, M, Weissman, IL, and Akashi, K (1997). Identification of Clonogenic Common Lymphoid Progenitors in Mouse Bone Marrow. Cell 91, 661–672.

Kong, M, Ditsworth, D, Lindsten, T, and Thompson, CB (2009). α4 Is an Essential Regulator of PP2A Phosphatase Activity. Mol Cell 36, 51–60.

Konstantinopoulos, PA, Lee, J, Gao, B, Miller, R, Lee, J-Y, Colombo, N, Vergote, I, Credille, KM, Young, SR, McNeely, S, *et al.* (2022). A Phase 2 study of prexasertib (LY2606368) in platinum resistant or refractory recurrent ovarian cancer. Gynecol Oncol 167, 213–225.

Kubota, Y, Nash, RA, Klungland, A, Schär, P, Barnes, DE, and Lindahl, T (1996). Reconstitution of DNA base excision-repair with purified human proteins: interaction between DNA polymerase beta and the XRCC1 protein. EMBO J 15, 6662–6670.

Lai, Y, Zhu, M, Wu, W, Rokutanda, N, Togashi, Y, Liang, W, and Ohta, T (2019). HERC2 regulates RPA2 by mediating ATR-induced Ser33 phosphorylation and ubiquitin-dependent degradation. Sci Rep 9, 14257.

Lainé, J-P, and Egly, J-M (2006). Initiation of DNA repair mediated by a stalled RNA polymerase IIO. EMBO J 25, 387–397.

Lambert, PF, Kashanchi, F, Radonovich, MF, Shiekhattar, R, and Brady, JN (1998). Phosphorylation of p53 Serine 15 Increases Interaction with CBP. J Biol Chem 273, 33048–33053.

Larson, CA, Blair, BG, Safaei, R, and Howell, SB (2009). The Role of the Mammalian Copper Transporter 1 in the Cellular Accumulation of Platinum-Based Drugs. Mol Pharmacol 75, 324–330.

Layssol-Lamour, CJ, Sarry, J-E, Braun, J-PD, Trumel, C, and Bourgès-Abella, NH (2021). Reference Values for Hematology, Plasma Biochemistry, Bone Marrow Cytology and Bone Histology of NOD *Cg-Prkdc* ^{scid} *Il2rg*^{tm1Wjl}/SzJ Immunodeficient Mice. J Am Assoc Lab Anim Sci 60, 4–17.

Lee, AJX, Endesfelder, D, Rowan, AJ, Walther, A, Birkbak, NJ, Futreal, PA, Downward, J, Szallasi, Z, Tomlinson, IPM, Howell, M, *et al.* (2011). Chromosomal Instability Confers Intrinsic Multidrug Resistance. Cancer Res 71, 1858–1870.

Lee, J-H, and Paull, TT (2005). ATM Activation by DNA Double-Strand Breaks Through the Mre11-Rad50-Nbs1 Complex. Science 308, 551–554.

Leung-Pineda, V, Ryan, CE, and Piwnica-Worms, H (2006). Phosphorylation of Chk1 by ATR Is Antagonized by a Chk1-Regulated Protein Phosphatase 2A Circuit. Mol Cell Biol 26, 7529–7538.

Lewis, AD, Hayes, JD, and Wolf, CR (1988). Glutathione and glutathione-dependent enzymes in ovarian adenocarcinoma cell lines derived from a patient before and after the onset of drug resistance: intrinsic differences and cell cycle effects. Carcinogenesis 9, 1283–1287.

Li, C-F, Wu, W-J, Wu, W-R, Liao, Y-J, Chen, L-R, Huang, C-N, Li, C-C, Li, W-M, Huang, H-Y, Chen, Y-L, *et al.* (2015). The cAMP responsive element binding protein 1 transactivates epithelial membrane protein 2, a potential tumor suppressor in the urinary bladder urothelial carcinoma. Oncotarget 6, 9220–9239.

Li, G-M (2008). Mechanisms and functions of DNA mismatch repair. Cell Res 18, 85–98.

Li, P, Liu, Z, Wang, J, Bi, X, Xiao, Y, Qiao, R, Zhou, X, Guo, S, Wan, P, Chang, M, *et al.* (2022). Gstm1/Gstt1 is essential for reducing cisplatin ototoxicity in CBA/CaJ mice. FASEB J 36.

Liao, H, Ji, F, Helleday, T, and Ying, S (2018). Mechanisms for stalled replication fork stabilization: new targets for synthetic lethality strategies in cancer treatments. EMBO Rep 19, e46263.

Lieber, MR (2008). The Mechanism of Human Nonhomologous DNA End Joining. J Biol Chem 283, 1–5.

Lin, Z, Kong, H, Nei, M, and Ma, H (2006). Origins and evolution of the *recA* / *RAD51* gene family: Evidence for ancient gene duplication and endosymbiotic gene transfer. Proc Natl Acad Sci 103, 10328–10333.

Lindemann, A, Patel, AA, Tang, L, Tanaka, N, Gleber-Netto, FO, Bartels, MD, Wang, L, McGrail, DJ, Lin, S-Y, Frank, SJ, *et al.* (2021). Combined Inhibition of Rad51 and Wee1 Enhances Cell Killing in HNSCC Through Induction of Apoptosis Associated With Excessive DNA Damage and Replication Stress. Mol Cancer Ther 20, 1257–1269.

Liu, Q, Guntuku, S, Cui, XS, Matsuoka, S, Cortez, D, Tamai, K, Luo, G, Carattini-Rivera, S, DeMayo, F, Bradley, A, *et al.* (2000). Chk1 is an essential kinase that is regulated by Atr and required for the G(2)/M DNA damage checkpoint. Genes Dev 14, 1448–1459.

Liu, S, Opiyo, SO, Manthey, K, Glanzer, JG, Ashley, AK, Amerin, C, Troksa, K, Shrivastav, M, Nickoloff, JA, and Oakley, GG (2012). Distinct roles for DNA-PK, ATM and ATR in RPA phosphorylation and checkpoint activation in response to replication stress. Nucleic Acids Res 40, 10780–10794.

Longley, DB, Harkin, DP, and Johnston, PG (2003). 5-Fluorouracil: mechanisms of action and clinical strategies. Nat Rev Cancer 3, 330–338.

Longley, MJ, Pierce, AJ, and Modrich, P (1997). DNA Polymerase δ Is Required for Human Mismatch Repair in Vitro. J Biol Chem 272, 10917–10921.

Lord, CJ, and Ashworth, A (2016). BRCAness revisited. Nat Rev Cancer 16, 110–120.

Lossaint, G, Besnard, E, Fisher, D, Piette, J, and Dulić, V (2011). Chk1 is dispensable for G2 arrest in response to sustained DNA damage when the ATM/p53/p21 pathway is functional. Oncogene 30, 4261–4274.

Lv, W, Budke, B, Pawlowski, M, Connell, PP, and Kozikowski, AP (2016). Development of Small Molecules that Specifically Inhibit the D-loop Activity of RAD51. J Med Chem 59, 4511–4525.

Ma, Y, Pannicke, U, Schwarz, K, and Lieber, MR (2002). Hairpin Opening and Overhang Processing by an Artemis/DNA-Dependent Protein Kinase Complex in Nonhomologous End Joining and V(D)J Recombination. Cell 108, 781–794.

Mah, L-J, El-Osta, A, and Karagiannis, TC (2010). γH2AX: a sensitive molecular marker of DNA damage and repair. Leukemia 24, 679–686.

Mansy, S, Chu, GYH, Duncan, RE, and Tobias, RS (1978). Heavy metal nucleotide interactions. 12. Competitive reactions in systems of four nucleotides with cis- or trans-diammineplatinum(II). Raman difference spectrophotometry of the relative nucleophilicity of guanosine, cytidine, adenosine, and uridine monophosphates and analogous DNA bases. J Am Chem Soc 100, 607–616.

Marteijn, JA, Lans, H, Vermeulen, W, and Hoeijmakers, JHJ (2014). Understanding nucleotide excision repair and its roles in cancer and ageing. Nat Rev Mol Cell Biol 15, 465–481.

Mason, JM, Chan, Y-L, Weichselbaum, RW, and Bishop, DK (2019). Non-enzymatic roles of human RAD51 at stalled replication forks. Nat Commun 10, 4410.

Matsuoka, S (1998). Linkage of ATM to Cell Cycle Regulation by the Chk2 Protein Kinase. Science 282, 1893–1897.

Matsuoka, S, Rotman, G, Ogawa, A, Shiloh, Y, Tamai, K, and Elledge, SJ (2000). Ataxia telangiectasia-mutated phosphorylates Chk2 *in vivo* and *in vitro*. Proc Natl Acad Sci 97, 10389–10394.

Mattiello, L, Soliman Abdel Rehim, S, Musella, M, Sistigu, A, Guarracino, A, Vitale, S, Corradi, F, Galassi, C, Sperati, F, Manic, G, *et al.* (2021). The Targeting of MRE11 or RAD51 Sensitizes Colorectal Cancer Stem Cells to CHK1 Inhibition. Cancers 13, 1957.

Mboni-Johnston, IM, Kouidrat, NMZ, Hirsch, C, Weber, AG, Meißner, A, Adjaye, J, and Schupp, N (2023). Sensitivity of Human Induced Pluripotent Stem Cells and Thereof Differentiated Kidney Proximal Tubular Cells towards Selected Nephrotoxins. Int J Mol Sci 25, 81.

McCabe, N, Turner, NC, Lord, CJ, Kluzek, K, Białkowska, A, Swift, S, Giavara, S, O'Connor, MJ, Tutt, AN, Zdzienicka, MZ, *et al.* (2006). Deficiency in the Repair of DNA Damage by Homologous Recombination and Sensitivity to Poly(ADP-Ribose) Polymerase Inhibition. Cancer Res 66, 8109–8115.

McCormack, E, Adams, KJ, Hassan, NJ, Kotian, A, Lissin, NM, Sami, M, Mujić, M, Osdal, T, Gjertsen, BT, Baker, D, *et al.* (2013). Bi-specific TCR-anti CD3 redirected T-cell targeting of NY-ESO-1- and LAGE-1-positive tumors. Cancer Immunol Immunother 62, 773–785.

McGarry, DJ, Armstrong, G, Castino, G, Mason, S, Clark, W, Shaw, R, McGarry, L, Blyth, K, and Olson, MF (2021). MICAL1 regulates actin cytoskeleton organization, directional cell migration and the growth of human breast cancer cells as orthotopic xenograft tumours. Cancer Lett 519, 226–236.

Mehta, KPM, Thada, V, Zhao, R, Krishnamoorthy, A, Leser, M, Lindsey Rose, K, and Cortez, D (2022). CHK1 phosphorylates PRIMPOL to promote replication stress tolerance. Sci Adv 8, eabm0314.

Mello, JA, Lippard, SJ, and Essigmann, JM (1995). DNA Adducts of cis-Diamminedichloroplatinum(II) and Its Trans Isomer Inhibit RNA Polymerase II Differentially in Vivo. Biochemistry 34, 14783–14791.

Miers, L, DeNardo, SJ, Lamborn, K, and DeNardo, GL (2005). Implantation of Different Malignant Human Cell Lines in an Athymic Mouse Does Not Alter Success and Growth Rates of Either Xenograft. Cancer Biother Radiopharm 20, 614–619.

Moiseeva, T, Hood, B, Schamus, S, O'Connor, MJ, Conrads, TP, and Bakkenist, CJ (2017). ATR kinase inhibition induces unscheduled origin firing through a Cdc7-dependent association between GINS and And-1. Nat Commun 8, 1392.

Morrison, C, Weterings, E, Mahadevan, D, Sanan, A, Weinand, M, and Stea, B (2021). Expression Levels of RAD51 Inversely Correlate with Survival of Glioblastoma Patients. Cancers 13, 5358.

Mourón, S, Rodriguez-Acebes, S, Martínez-Jiménez, MI, García-Gómez, S, Chocrón, S, Blanco, L, and Méndez, J (2013). Repriming of DNA synthesis at stalled replication forks by human PrimPol. Nat Struct Mol Biol 20, 1383–1389.

Moynahan, ME, Chiu, JW, Koller, BH, and Jasin, M (1999). Brca1 Controls Homology-Directed DNA Repair. Mol Cell 4, 511–518.

Mu, D, Park, C-H, Matsunaga, T, Hsu, DS, Reardon, JT, and Sancar, A (1995). Reconstitution of Human DNA Repair Excision Nuclease in a Highly Defined System. J Biol Chem 270, 2415–2418.

Murai, J, and Pommier, Y (2023). BRCAness, Homologous Recombination Deficiencies, and Synthetic Lethality. Cancer Res 83, 1173–1174.

Musiałek, MW, and Rybaczek, D (2021). Hydroxyurea—The Good, the Bad and the Ugly.

Nigro, JM, Baker, SJ, Preisinger, AC, Jessup, JM, Hosteller, R, Cleary, K, Signer, SH, Davidson, N, Baylin, S, Devilee, P, *et al.* (1989). Mutations in the p53 gene occur in diverse human tumour types. Nature 342, 705–708.

Norbury, CJ, and Zhivotovsky, B (2004). DNA damage-induced apoptosis. Oncogene 23, 2797–2808.

O'Brien, J, Wilson, I, Orton, T, and Pognan, F (2000). Investigation of the Alamar Blue (resazurin) fluorescent dye for the assessment of mammalian cell cytotoxicity. Eur J Biochem 267, 5421–5426.

Oda, K, Arakawa, H, Tanaka, T, Matsuda, K, Tanikawa, C, Mori, T, Nishimori, H, Tamai, K, Tokino, T, Nakamura, Y, *et al.* (2000). p53AIP1, a Potential Mediator of p53-Dependent Apoptosis, and Its Regulation by Ser-46-Phosphorylated p53. Cell 102, 849–862.

Olive, PL, and Banáth, JP (2006). The comet assay: a method to measure DNA damage in individual cells. Nat Protoc 1, 23–29.

Olive, PL, and Banáth, JP (2009). Kinetics of H2AX phosphorylation after exposure to cisplatin. Cytometry B Clin Cytom 76B, 79–90.

O'Toole, C, Price, ZH, Ohnuki, Y, and Unsgaard, B (1978). Ultrastructure, karyology and immunology of a cell line originated from a human transitional-cell carcinoma. Br J Cancer 38, 64–76.

Otter, M, Csader, S, Keiser, M, and Oswald, S (2021). Expression and Functional Contribution of Different Organic Cation Transporters to the Cellular Uptake of Doxorubicin into Human Breast Cancer and Cardiac Tissue. Int J Mol Sci 23, 255.

Paalman, SR, Sung, C, and Clarke, ND (1997). Specificity of DNA Repair Methyltransferases Determined by Competitive Inactivation with Oligonucleotide Substrates: Evidence That *Escherichia coli* Ada Repairs O^6 -Methylguanine and O^4 -Methylthymine with Similar Efficiency. Biochemistry 36, 11118–11124.

Pannunzio, NR, Watanabe, G, and Lieber, MR (2018). Nonhomologous DNA end-joining for repair of DNA double-strand breaks. J Biol Chem 293, 10512–10523.

Pasero, P, and Vindigni, A (2017). Nucleases Acting at Stalled Forks: How to Reboot the Replication Program with a Few Shortcuts. Annu Rev Genet 51, 477–499.

Patel, AA, Ginhoux, F, and Yona, S (2021). Monocytes, macrophages, dendritic cells and neutrophils: an update on lifespan kinetics in health and disease. Immunology 163, 250–261.

Peng, Y, Chen, Y, Chen, S, Wang, J, Jiang, C, Hou, W, and Xu, C (2020). JUND-dependent up-regulation of HMOX1 is associated with cisplatin resistance in muscle-invasive bladder cancer. J Biochem (Tokyo) 168, 73–82.

Perrino, M, Cooke-Barber, J, Dasgupta, R, and Geller, JI (2019). Genetic predisposition to cancer: Surveillance and intervention. Semin Pediatr Surg 28, 150858.

Petermann, E, Orta, ML, Issaeva, N, Schultz, N, and Helleday, T (2010). Hydroxyurea-Stalled Replication Forks Become Progressively Inactivated and Require Two Different RAD51-Mediated Pathways for Restart and Repair. Mol Cell 37, 492–502.

Pinto, AL, and Lippard, SJ (1985). Binding of the antitumor drug cis-diamminedichloroplatinum(II) (cisplatin) to DNA. Biochim Biophys Acta BBA - Rev Cancer 780, 167–180.

Podlutsky, AJa, Dianova, II, Podust, VN, Bohr, VA, and Dianov, GL (2001). Human DNA polymerase β initiates DNA synthesis during long-patch repair of reduced AP sites in DNA. EMBO J 20, 1477–1482.

Powers, KT, and Washington, MT (2018). Eukaryotic translesion synthesis: Choosing the right tool for the job. DNA Repair 71, 127–134.

Qiao, G-B, Wu, Y-L, Yang, X-N, Zhong, W-Z, Xie, D, Guan, X-Y, Fischer, D, Kolberg, H-C, Kruger, S, and Stuerzbecher, H-W (2005). High-level expression of Rad51 is an independent prognostic marker of survival in non-small-cell lung cancer patients. Br J Cancer 93, 137–143.

Raderschall, E, Stout, K, Freier, S, Suckow, V, Schweiger, S, and Haaf, T (2002). Elevated levels of Rad51 recombination protein in tumor cells. Cancer Res 62, 219–225.

Repetto, G, Del Peso, A, and Zurita, JL (2008). Neutral red uptake assay for the estimation of cell viability/cytotoxicity. Nat Protoc 3, 1125–1131.

Replogle, JM, Zhou, W, Amaro, AE, McFarland, JM, Villalobos-Ortiz, M, Ryan, J, Letai, A, Yilmaz, O, Sheltzer, J, Lippard, SJ, *et al.* (2020). Aneuploidy increases resistance to chemotherapeutics by antagonizing cell division. Proc Natl Acad Sci 117, 30566–30576.

Rickman, K, and Smogorzewska, A (2019). Advances in understanding DNA processing and protection at stalled replication forks. J Cell Biol 218, 1096–1107.

Robertson, AB, Klungland, A, Rognes, T, and Leiros, I (2009). DNA Repair in Mammalian Cells: Base excision repair: the long and short of it. Cell Mol Life Sci 66, 981–993.

Rocha, CRR, Silva, MM, Quinet, A, Cabral-Neto, JB, and Menck, CFM (2018). DNA repair pathways and cisplatin resistance: an intimate relationship. Clinics 73, e478s.

Rock, KL, and Kono, H (2008). The Inflammatory Response to Cell Death. Annu Rev Pathol Mech Dis 3, 99–126.

Rogakou, EP, Pilch, DR, Orr, AH, Ivanova, VS, and Bonner, WM (1998). DNA Double-stranded Breaks Induce Histone H2AX Phosphorylation on Serine 139. J Biol Chem 273, 5858–5868.

Roos, WP, and Kaina, B (2013). DNA damage-induced cell death: From specific DNA lesions to the DNA damage response and apoptosis. Cancer Lett 332, 237–248.

Roos, WP, and Krumm, A (2016). The multifaceted influence of histone deacetylases on DNA damage signalling and DNA repair. Nucleic Acids Res, gkw922.

Roos, WP, Thomas, AD, and Kaina, B (2016). DNA damage and the balance between survival and death in cancer biology. Nat Rev Cancer 16, 20–33.

Saelens, X, Festjens, N, Walle, LV, Gurp, MV, Loo, GV, and Vandenabeele, P (2004). Toxic proteins released from mitochondria in cell death. Oncogene 23, 2861–2874.

Sak, A, Stueben, G, Groneberg, M, Böcker, W, and Stuschke, M (2005). Targeting of Rad51-dependent homologous recombination: implications for the radiation sensitivity of human lung cancer cell lines. Br J Cancer 92, 1089–1097.

Sakahira, H, Enari, M, and Nagata, S (1998). Cleavage of CAD inhibitor in CAD activation and DNA degradation during apoptosis. Nature 391, 96–99.

Saldivar, JC, Cortez, D, and Cimprich, KA (2017). The essential kinase ATR: ensuring faithful duplication of a challenging genome. Nat Rev Mol Cell Biol 18, 622–636.

Sanjiv, K, Hagenkort, A, Calderón-Montaño, JM, Koolmeister, T, Reaper, PM, Mortusewicz, O, Jacques, SA, Kuiper, RV, Schultz, N, Scobie, M, *et al.* (2016). Cancer-Specific Synthetic Lethality between ATR and CHK1 Kinase Activities. Cell Rep 14, 298–309.

Sarwar, R, Sheikh, AK, Mahjabeen, I, Bashir, K, Saeed, S, and Kayani, MA (2017). Upregulation of RAD51 expression is associated with progression of thyroid carcinoma. Exp Mol Pathol 102, 446–454.

Sasco, AJ, Secretan, MB, and Straif, K (2004). Tobacco smoking and cancer: a brief review of recent epidemiological evidence. Lung Cancer 45, S3–S9.

Sazonova, EV, Petrichuk, SV, Kopeina, GS, and Zhivotovsky, B (2021). A link between mitotic defects and mitotic catastrophe: detection and cell fate. Biol Direct 16, 25.

Schmitt, A, Guichard, J, Massé, J-M, Debili, N, and Cramer, EM (2001). Of mice and men. Exp Hematol 29, 1295–1302.

Schulz, WA (2023). Molecular Biology of Human Cancers, Cham: Springer International Publishing.

Schürmann, L, Schumacher, L, Roquette, K, Brozovic, A, and Fritz, G (2021). Inhibition of the DSB repair protein RAD51 potentiates the cytotoxic efficacy of doxorubicin via promoting apoptosis-related death pathways. Cancer Lett 520, 361–373.

Shaukat, Z, Liu, D, Choo, A, Hussain, R, O'Keefe, L, Richards, R, Saint, R, and Gregory, SL (2015). Chromosomal instability causes sensitivity to metabolic stress. Oncogene 34, 4044–4055.

Sheltzer, JM, Ko, JH, Replogle, JM, Habibe Burgos, NC, Chung, ES, Meehl, CM, Sayles, NM, Passerini, V, Storchova, Z, and Amon, A (2017). Single-chromosome Gains Commonly Function as Tumor Suppressors. Cancer Cell 31, 240–255.

Shen, Z (2011). Genomic instability and cancer: an introduction. J Mol Cell Biol 3, 1–3.

Shi, W, Feng, Z, Zhang, J, Gonzalez-Suarez, I, Vanderwaal, RP, Wu, X, Powell, SN, Roti Roti, JL, Gonzalo, S, and Zhang, J (2010). The role of RPA2 phosphorylation in homologous recombination in response to replication arrest. Carcinogenesis 31, 994–1002.

Shieh, S-Y, Ikeda, M, Taya, Y, and Prives, C (1997). DNA Damage-Induced Phosphorylation of p53 Alleviates Inhibition by MDM2. Cell 91, 325–334.

Sinha, D, Nag, P, Nanayakkara, D, Duijf, PHG, Burgess, A, Raninga, P, Smits, VAJ, Bain, AL, Subramanian, G, Wall, M, *et al.* (2020). Cep55 overexpression promotes genomic instability and tumorigenesis in mice. Commun Biol 3, 593.

Slupianek, A, Schmutte, C, Tombline, G, Nieborowska-Skorska, M, Hoser, G, Nowicki, MO, Pierce, AJ, Fishel, R, and Skorski, T (2001). BCR/ABL Regulates Mammalian RecA Homologs, Resulting in Drug Resistance. Mol Cell 8, 795–806.

Sofiadis, K, Josipovic, N, Nikolic, M, Kargapolova, Y, Übelmesser, N, Varamogianni-Mamatsi, V, Zirkel, A, Papadionysiou, I, Loughran, G, Keane, J, *et al.* (2021). HMGB1 coordinates SASP-related chromatin folding and RNA homeostasis on the path to senescence. Mol Syst Biol 17, e9760.

Stanevich, V, Jiang, L, Satyshur, KA, Li, Y, Jeffrey, PD, Li, Z, Menden, P, Semmelhack, MF, and Xing, Y (2011). The Structural Basis for Tight Control of PP2A Methylation and Function by LCMT-1. Mol Cell 41, 331–342.

Stanton, RA, Gernert, KM, Nettles, JH, and Aneja, R (2011). Drugs that target dynamic microtubules: A new molecular perspective. Med Res Rev 31, 443–481.

Stiff, T, O'Driscoll, M, Rief, N, Iwabuchi, K, Löbrich, M, and Jeggo, PA (2004). ATM and DNA-PK Function Redundantly to Phosphorylate H2AX after Exposure to Ionizing Radiation. Cancer Res 64, 2390–2396.

Stingele, S, Stoehr, G, Peplowska, K, Cox, J, Mann, M, and Storchova, Z (2012). Global analysis of genome, transcriptome and proteome reveals the response to aneuploidy in human cells. Mol Syst Biol 8, 608.

Stucki, M, Pascucci, B, Parlanti, E, Fortini, P, Wilson, SH, Hübscher, U, and Dogliotti, E (1998). Mammalian base excision repair by DNA polymerases δ and ε. Oncogene 17, 835–843.

Sugasawa, K, Ng, JMY, Masutani, C, Iwai, S, Van Der Spek, PJ, Eker, APM, Hanaoka, F, Bootsma, D, and Hoeijmakers, JHJ (1998). Xeroderma Pigmentosum Group C Protein Complex Is the Initiator of Global Genome Nucleotide Excision Repair. Mol Cell 2, 223–232.

Sung, H, Ferlay, J, Siegel, RL, Laversanne, M, Soerjomataram, I, Jemal, A, and Bray, F (2021). Global Cancer Statistics 2020: GLOBOCAN Estimates of Incidence and Mortality Worldwide for 36 Cancers in 185 Countries. CA Cancer J Clin 71, 209–249.

Syljuåsen, RG, Sørensen, CS, Hansen, LT, Fugger, K, Lundin, C, Johansson, F, Helleday, T, Sehested, M, Lukas, J, and Bartek, J (2005). Inhibition of Human Chk1 Causes Increased Initiation of DNA Replication, Phosphorylation of ATR Targets, and DNA Breakage. Mol Cell Biol 25, 3553–3562.

Taglialatela, A, Alvarez, S, Leuzzi, G, Sannino, V, Ranjha, L, Huang, J-W, Madubata, C, Anand, R, Levy, B, Rabadan, R, *et al.* (2017). Restoration of Replication Fork Stability in BRCA1- and BRCA2-Deficient Cells by Inactivation of SNF2-Family Fork Remodelers. Mol Cell 68, 414-430.e8.

Taglialatela, A, Leuzzi, G, Sannino, V, Cuella-Martin, R, Huang, J-W, Wu-Baer, F, Baer, R, Costanzo, V, and Ciccia, A (2021). REV1-Polζ maintains the viability of homologous recombination-deficient cancer cells through mutagenic repair of PRIMPOL-dependent ssDNA gaps. Mol Cell 81, 4008-4025.e7.

Tanida, I, Ueno, T, and Kominami, E (2008). LC3 and Autophagy. In: Autophagosome and Phagosome, ed. V Deretic, Totowa, NJ: Humana Press, 77–88.

Testa, U, Pelosi, E, and Frankel, A (2014). CD 123 is a membrane biomarker and a therapeutic target in hematologic malignancies. Biomark Res 2, 4.

Thompson, LH, and Schild, D (2001). Homologous recombinational repair of DNA ensures mammalian chromosome stability. Mutat Res Mol Mech Mutagen 477, 131–153.

Thompson, SL, and Compton, DA (2008). Examining the link between chromosomal instability and aneuploidy in human cells. J Cell Biol 180, 665–672.

Tirman, S, Cybulla, E, Quinet, A, Meroni, A, and Vindigni, A (2021a). PRIMPOL ready, set, reprime! Crit Rev Biochem Mol Biol 56, 17–30.

Tirman, S, Quinet, A, Wood, M, Meroni, A, Cybulla, E, Jackson, J, Pegoraro, S, Simoneau, A, Zou, L, and Vindigni, A (2021b). Temporally distinct post-replicative repair mechanisms fill PRIMPOL-dependent ssDNA gaps in human cells. Mol Cell 81, 4026-4040.e8.

Tokalov, SV, Enghardt, W, and Abolmaali, N (2010). Improvement of Radiation-Mediated Immunosuppression of Human NSCLC Tumour Xenografts in a Nude Rat Model. J Biomed Biotechnol 2010, 1–4.

Toledo, LI, Altmeyer, M, Rask, M-B, Lukas, C, Larsen, DH, Povlsen, LK, Bekker-Jensen, S, Mailand, N, Bartek, J, and Lukas, J (2013). ATR Prohibits Replication Catastrophe by Preventing Global Exhaustion of RPA. Cell 155, 1088–1103.

Tong, Y, Ying, H, Liu, R, Li, L, Bergholz, J, and Xiao, Z-X (2015). Pin1 inhibits PP2A-mediated Rb dephosphorylation in regulation of cell cycle and S-phase DNA damage. Cell Death Dis 6, e1640–e1640.

Trujillo, KM, Yuan, S-SF, Lee, EY-HP, and Sung, P (1998). Nuclease Activities in a Complex of Human Recombination and DNA Repair Factors Rad50, Mre11, and p95. J Biol Chem 273, 21447–21450.

Tsai, Y, Jou, Y, Tsai, H, Shiau, A, Wu, C, and Tzai, T (2019). Prothymosin-α enhances phosphatase and tensin homolog expression and binds with tripartite motif-containing protein 21 to regulate Kelch-like ECH-associated protein 1/nuclear factor erythroid 2-related factor 2 signaling in human bladder cancer. Cancer Sci 110, 1208–1219.

Tsai, Y-F, Chan, L-P, Chen, Y-K, Su, C-W, Hsu, C-W, Wang, Y-Y, and Yuan, S-SF (2023). RAD51 is a poor prognostic marker and a potential therapeutic target for oral squamous cell carcinoma. Cancer Cell Int 23, 231.

Vakifahmetoglu, H, Olsson, M, and Zhivotovsky, B (2008). Death through a tragedy: mitotic catastrophe. Cell Death Differ 15, 1153–1162.

Van Der Weegen, Y, Golan-Berman, H, Mevissen, TET, Apelt, K, González-Prieto, R, Goedhart, J, Heilbrun, EE, Vertegaal, ACO, Van Den Heuvel, D, Walter, JC, *et al.* (2020). The cooperative action of CSB, CSA, and UVSSA target TFIIH to DNA damage-stalled RNA polymerase II. Nat Commun 11, 2104.

Van Putten, LM, and Croon, F (1958). The Life Span of Red Cells in the Rat and the Mouse as Determined by Labeling with DFP32 in Vivo. Blood 13, 789–794.

Vitale, I, Galluzzi, L, Vivet, S, Nanty, L, Dessen, P, Senovilla, L, Olaussen, KA, Lazar, V, Prudhomme, M, Golsteyn, RM, *et al.* (2007). Inhibition of Chk1 Kills Tetraploid Tumor Cells through a p53-Dependent Pathway. PLoS ONE 2, e1337.

Wagner, JM, and Karnitz, LM (2009). Cisplatin-Induced DNA Damage Activates Replication Checkpoint Signaling Components that Differentially Affect Tumor Cell Survival. Mol Pharmacol 76, 208–214.

Wajant, H (2002). The Fas Signaling Pathway: More Than a Paradigm. Science 296, 1635–1636.

Ward, IM, and Chen, J (2001). Histone H2AX Is Phosphorylated in an ATR-dependent Manner in Response to Replicational Stress. J Biol Chem 276, 47759–47762.

Wassing, IE, Graham, E, Saayman, X, Rampazzo, L, Ralf, C, Bassett, A, and Esashi, F (2021). The RAD51 recombinase protects mitotic chromatin in human cells. Nat Commun 12, 5380.

Weaver, BA, and Cleveland, DW (2006). Does aneuploidy cause cancer? Curr Opin Cell Biol 18, 658–667.

Weinstock, MA (1995). Overview of ultraviolet radiation and cancer: what is the link? How are we doing? Environ Health Perspect 103, 251–254.

Weiss, WA, Taylor, SS, and Shokat, KM (2007). Recognizing and exploiting differences between RNAi and small-molecule inhibitors. Nat Chem Biol 3, 739–744.

West, AC, and Johnstone, RW (2014). New and emerging HDAC inhibitors for cancer treatment. J Clin Invest 124, 30–39.

Weterings, E (2003). The role of DNA dependent protein kinase in synapsis of DNA ends. Nucleic Acids Res 31, 7238–7246.

Wilhelm, T, Said, M, and Naim, V (2020). DNA Replication Stress and Chromosomal Instability: Dangerous Liaisons. Genes 11, 642.

Wu, W-R, Lin, J-T, Pan, C-T, Chan, T-C, Liu, C-L, Wu, W-J, Sheu, JJ-C, Yeh, B-W, Huang, SK, Jhung, J-Y, *et al.* (2020). Amplification-driven BCL6-suppressed cytostasis is mediated by transrepression of FOXO3 and post-translational modifications of FOXO3 in urinary bladder urothelial carcinoma. Theranostics 10, 707–724.

Wu, Y, and Zhao, H (2021). CTBP1 strengthens the cisplatin resistance of gastric cancer cells by upregulating RAD51 expression. Oncol Lett 22, 810.

Xiao, Z, Chen, Z, Gunasekera, AH, Sowin, TJ, Rosenberg, SH, Fesik, S, and Zhang, H (2003). Chk1 Mediates S and G2 Arrests through Cdc25A Degradation in Response to DNA-damaging Agents. J Biol Chem 278, 21767–21773.

Xu, L, Wu, T, Lu, S, Hao, X, Qin, J, Wang, J, Zhang, X, Liu, Q, Kong, B, Gong, Y, *et al.* (2020). Mitochondrial superoxide contributes to oxidative stress exacerbated by DNA damage response in RAD51-depleted ovarian cancer cells. Redox Biol 36, 101604.

Yamamoto, H, Zhang, S, and Mizushima, N (2023). Autophagy genes in biology and disease. Nat Rev Genet 24, 382–400.

Yonezawa, A, Masuda, S, Nishihara, K, Yano, I, Katsura, T, and Inui, K (2005). Association between tubular toxicity of cisplatin and expression of organic cation transporter rOCT2 (Slc22a2) in the rat. Biochem Pharmacol 70, 1823–1831.

Yuan, J, Lv, H, Peng, B, Wang, C, Yu, Y, and He, Z (2009). Role of BCRP as a biomarker for predicting resistance to 5-fluorouracil in breast cancer. Cancer Chemother Pharmacol 63, 1103–1110.

Zabludoff, SD, Deng, C, Grondine, MR, Sheehy, AM, Ashwell, S, Caleb, BL, Green, S, Haye, HR, Horn, CL, Janetka, JW, *et al.* (2008). AZD7762, a novel checkpoint kinase inhibitor, drives checkpoint abrogation and potentiates DNA-targeted therapies. Mol Cancer Ther 7, 2955–2966.

Zelensky, A, Kanaar, R, and Wyman, C (2014). Mediators of Homologous DNA Pairing. Cold Spring Harb Perspect Biol 6, a016451–a016451.

Zellweger, R, Dalcher, D, Mutreja, K, Berti, M, Schmid, JA, Herrador, R, Vindigni, A, and Lopes, M (2015). Rad51-mediated replication fork reversal is a global response to genotoxic treatments in human cells. J Cell Biol 208, 563–579.

Zeman, MK, and Cimprich, KA (2014). Causes and consequences of replication stress. Nat Cell Biol 16, 2–9.

Zhang, C, Yan, Z, Painter, CL, Zhang, Q, Chen, E, Arango, ME, Kuszpit, K, Zasadny, K, Hallin, M, Hallin, J, *et al.* (2009). PF-00477736 Mediates Checkpoint Kinase 1 Signaling Pathway and Potentiates Docetaxel-Induced Efficacy in Xenografts. Clin Cancer Res 15, 4630–4640.

Zhang, H, Liu, L, Liu, C, Pan, J, Lu, G, Zhou, Z, Chen, Z, and Qian, C (2017). Notch3 overexpression enhances progression and chemoresistance of urothelial carcinoma. Oncotarget 8, 34362–34373.

Zhang, Y, Yuan, F, Presnell, SR, Tian, K, Gao, Y, Tomkinson, AE, Gu, L, and Li, G-M (2005). Reconstitution of 5′-Directed Human Mismatch Repair in a Purified System. Cell 122, 693–705.

Zhao, H, and Piwnica-Worms, H (2001). ATR-Mediated Checkpoint Pathways Regulate Phosphorylation and Activation of Human Chk1. Mol Cell Biol 21, 4129–4139.

Zhao, W, Seki, A, and Fang, G (2006). Cep55, a Microtubule-bundling Protein, Associates with Centralspindlin to Control the Midbody Integrity and Cell Abscission during Cytokinesis. Mol Biol Cell 17, 3881–3896.

Zhong, Y, Nellimoottil, T, Peace, JM, Knott, SRV, Villwock, SK, Yee, JM, Jancuska, JM, Rege, S, Tecklenburg, M, Sclafani, RA, *et al.* (2013). The level of origin firing inversely affects the rate of replication fork progression. J Cell Biol 201, 373–383.

Ziv, Y, Bielopolski, D, Galanty, Y, Lukas, C, Taya, Y, Schultz, DC, Lukas, J, Bekker-Jensen, S, Bartek, J, and Shiloh, Y (2006). Chromatin relaxation in response to DNA double-strand breaks is modulated by a novel ATM- and KAP-1 dependent pathway. Nat Cell Biol 8, 870–876.

Zou, H, Li, Y, Liu, X, and Wang, X (1999). An APAF-1·Cytochrome c Multimeric Complex Is a Functional Apoptosome That Activates Procaspase-9. J Biol Chem 274, 11549–11556.

Zou, L, and Elledge, SJ (2003). Sensing DNA Damage Through ATRIP Recognition of RPA-ssDNA Complexes. Science 300, 1542–1548.

10 Appendix

10.1 Supplementary material

10.1.1 Supplementary figures

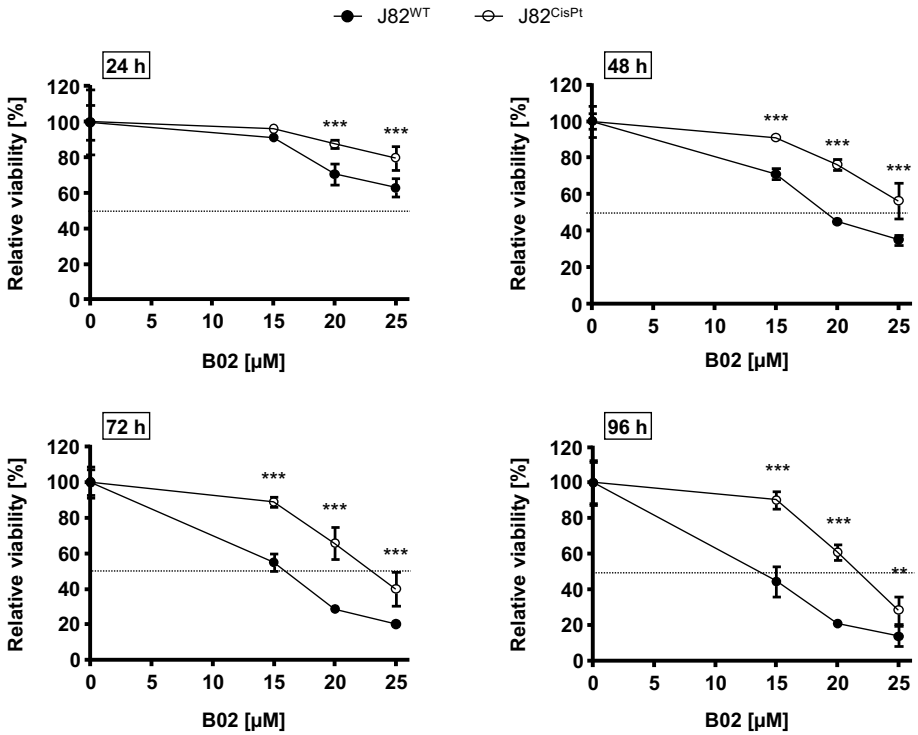

Supplementary Figure 1: Comparison of cytotoxicity in J82^{WT} and J82^{CisPt} with RAD51 inhibitor B02 after different treatment durations
J82^{WT} and J82^{CisPt} cells were treated with different concentrations of RAD51 inhibitor B02 for 24 h, 48 h, 72 h or 96 h and viability was measured via AlamarBlue assay. The untreated control of each cell variant was set to 100% viability and all associated treatments were related to this. Data presented are the mean ± SD from three independent experiments, each performed in quadruplicate. **p ≤ 0.01; ***p ≤ 0.001; significant compared to J82^{WT}.

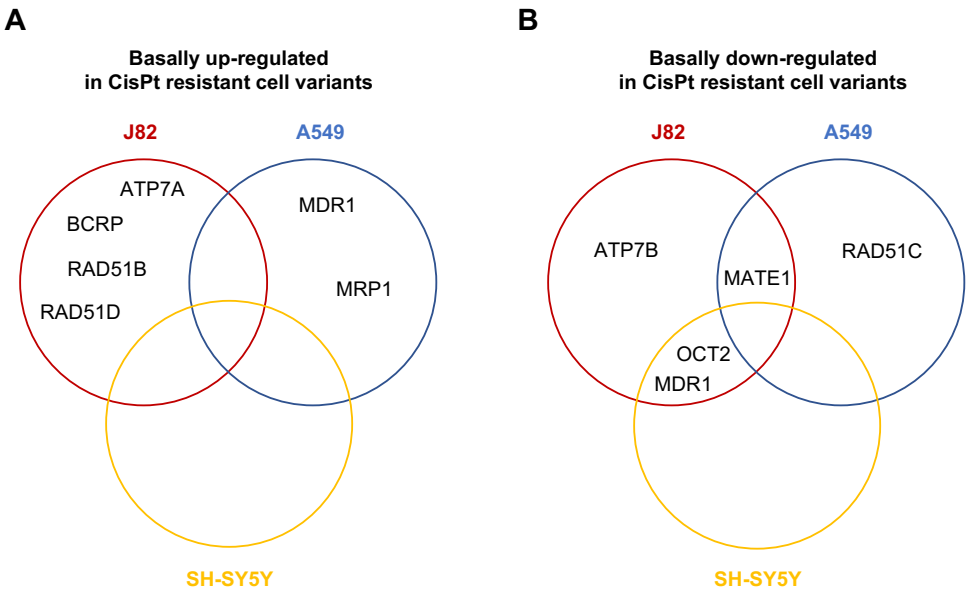

C

After 24 h CisPt treatment

	WT		CisPt resistant	
	Up-regulated	**Down-regulated**	**Up-regulated**	**Down-regulated**
J82	CTR2 XRCC2 XRCC3 CHK1 CDC25c IGBP1 PPP2CA	ATP7A ATP7B MRP1 RAD51B	RAD51	RAD51B
A549	ATP7A CTR2 RAD52	FANCD2 RAD51 RAD51B XRCC2 (XRCC3)	CTR2 RAD51C	RAD51B
SH-SY5Y	-	OCT2	-	-

Supplementary Figure 2: Comparative overview of the mRNA changes observed in different cisplatin resistant cell lines under basal conditions and after cisplatin administration
Overview of factors found basally up-regulated (A) or basally down-regulated (B) in their mRNA expression in bladder carcinoma cells J82^{CisPt}, lung carcinoma cells A549^{CisPt} and neuroblastoma cells SH-SY5Y^{CisPt} related to their respective parental cells. C: Tabular list of up- or downregulated factors compared between the cisplatin-resistant cell lines mentioned and their parental cells after 24 h cisplatin administration.

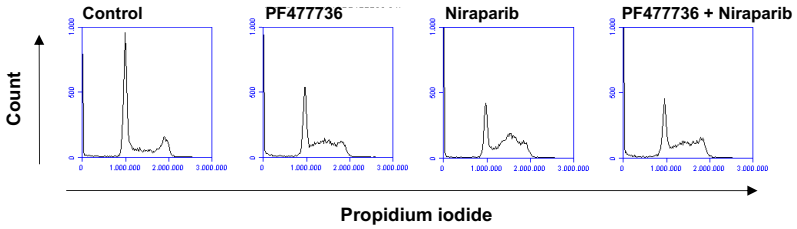

	Control	PF477736	Niraparib	PF477736 + Niraparib
S-phase [%]	15.9	33.4	40.1	30.6

Supplementary Figure 3: Analysis of S-phase arrest induction after combination treatment with CHK1 + PARP inhibition in J82^{CisPt}
J82^{CisPt} cells were treated with 1 µM CHK1$_i$ PF477736 or/and 5 µM PARP$_i$ Niraparib. Following 24 h treatment, propidium iodide-based cell cycle analysis was performed by flow cytometric measurement with emphasis on the percentage of cells in S-phase. A total of 10000 counts were measured for quantification.

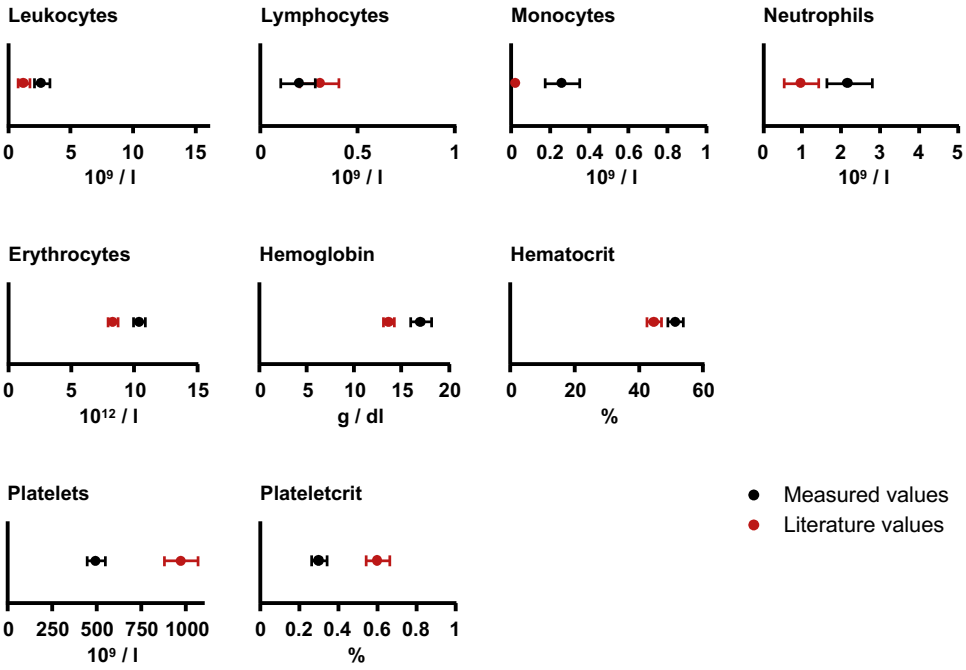

Supplementary Figure 4: Comparison of the blood values measured basally in the xenograft experiment with literature values
For basal values of blood parameters, blood was taken from the NSG-(K^{b}D^b)^{null} mice one day before tumor cell injection. Data are shown as mean ± SD of all 18 mice in the experiment (indicated in black). Literature values ± SD (indicated in red) were taken from Layssol-Lamour *et al.*, 2021.

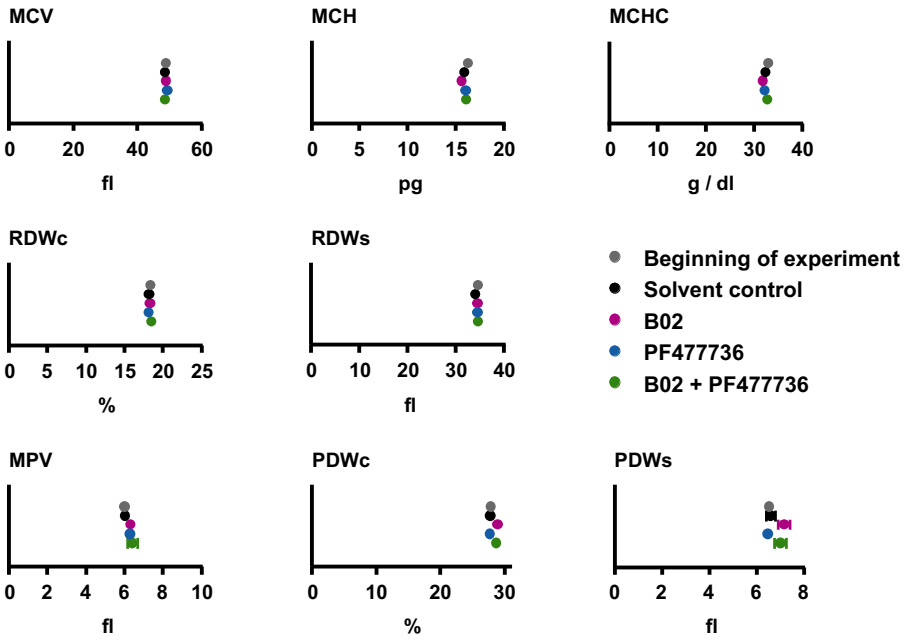

Supplementary Figure 5: Additional blood parameters in the xenograft experiment with B02 or/and PF477736 treatment

$5x10^6$ $J82^{CisPt}$ cells were injected into the flanks of NSG-$(K^bD^b)^{null}$ mice (day 0). For basal values of blood parameters, blood was taken from the mice one day before tumor cell injection (Beginning of experiment). Mice were treated with six doses of 10 mg/kg B02 or/and 10 mg/kg PF477736 over three weeks. Corn oil was included in the study as solvent control. Blood of the mice was again taken on day 47/48 after tumor inoculation. Data are shown as mean ± SEM of each treatment group (n = 3 – 5). For beginning of experiment the mean values of all 18 mice was formed. (Abbreviations: MCV, mean corpuscular volume; MCH, mean corpuscular hemoglobin; MCHC, mean corpuscular hemoglobin concentration; RDWc/RDWs, red cell distribution width; MPV, mean platelet volume; PDWc/PDWs, platelet distribution width)

10.1.2 Supplementary tables

Supplementary Table 1: Summary of cross-resistance analyses of J82^{CisPt} to various conventional anticancer therapeutics and DDR modifiers
J82^{WT} and J82^{CisPt} cells were treated with the indicated substances for 72 h and viability was measured using the AlamarBlue assay. Described responses (resistant; similar; sensitive) are based on statistical differences ($p \leq 0.05$) in the cytotoxicity data (IC_{50}) comparing J82^{WT} and J82^{CisPt} cells. Basis for statistical calculations were data obtained from at least three independent experiments each performed in quadruplicate.

Substance	Substance group	IC_{50} (µM)		J82^{CisPt} response
		J82^{WT}	J82^{CisPt}	
Cisplatin	Platinating agents	4	16	Resistant
Carboplatin		31	71	Resistant
Oxaliplatin		14	27	Resistant
Doxorubicin	Topoisomerase II inhibitors	0.8	0.8	Similar
Ionizing radiation	-	19	19	Similar
TBOOH	Oxidants	16	> 40	Resistant
H_2O_2		41	> 100	Resistant
OH-Urea	Ribonucleotide reductase inhibitors	550	170	Sensitive
5-Fluorouracil	Antimetabolites	5	0.9	Sensitive
Mirin	MRE11 inhibitors	66	70	Similar
B02	RAD51 inhibitors	16	23	Resistant
Niraparib	PARP inhibitors	41	48	Similar
PF477736	CHK1 inhibitors	3	4	Similar
Entinostat	HDAC inhibitors	8	6	Sensitive
Vorinostat		9	5	Sensitive

Supplementary Table 2: List of proteins found upregulated in J82^{CisPt} when compared to J82^{WT} under basal conditions in the proteome analysis
Threshold for increased expression was set at 2-fold difference between J82^{CisPt} vs. J82^{WT} and statistical significance ($p \leq 0.05$). Significantly differentially regulated proteins were clustered into KEGG pathways and pathways with at least two representatives are listed. The list also contains proteins not assigned to a KEGG pathway and proteins upregulated 2-fold, but not statistically significant. Proteome data was generated from triplicate.

KEGG pathway	Proteins
Endocytosis	ADP ribosylation factor guanine nucleotide exchange factor 1; RAB11 family interacting protein 5; ADP ribosylation factor GTPase activating protein 3; amphiphysin; major histocompatibility complex, class I, E; SMAD family member 3
Pathways in cancer	SMAD family member 3; nuclear factor kappa B subunit 2; platelet derived growth factor receptor beta; Rac family small GTPase 2
Focal adhesion	Myosin light chain kinase; platelet derived growth factor receptor beta; Rac family small GTPase 2; thrombospondin 1
Metabolic pathways	Fumarylacetoacetate hydrolase; acyl-CoA synthetase long chain family member 5; lysophosphatidylcholine acyltransferase 2; glycerol-3-phosphate acyltransferase 3
Rap1 signaling pathway	Platelet derived growth factor receptor beta; Rac family small GTPase 2; thrombospondin 1
Human T-cell leukemia virus 1 infection	Major histocompatibility complex, class I, E; SMAD family member 3; nuclear factor kappa B subunit 2
Shigellosis	Calcium binding and coiled-coil domain 2; septin 8; PYD and CARD domain containing
Cell adhesion molecules	Cell adhesion molecule 1; major histocompatibility complex, class I, E; syndecan 1
Regulation of actin cytoskeleton	Myosin light chain kinase; platelet derived growth factor receptor beta; Rac family small GTPase 2
MAPK signaling pathway	Nuclear factor kappa B subunit 2; platelet derived growth factor receptor beta; Rac family small GTPase 2
Calcium signaling pathway	Glutamate ionotropic receptor NMDA type subunit 2D; myosin light chain kinase; platelet derived growth factor receptor beta

KEGG pathway	Proteins
Human papillomavirus infection	Major histocompatibility complex, class I, E; platelet derived growth factor receptor beta; thrombospondin 1
Epstein-Barr virus infection	Major histocompatibility complex, class I, E; nuclear factor kappa B subunit 2; NFKB inhibitor epsilon
Natural killer cell mediated cytotoxicity	Major histocompatibility complex, class I, E; Rac family small GTPase 2
Adipocytokine signaling pathway	NFKB inhibitor epsilon; acyl-CoA synthetase long chain family member 5
Phagosome	Major histocompatibility complex, class I, E; thrombospondin 1
Viral myocarditis	Major histocompatibility complex, class I, E; Rac family small GTPase 2
Pancreatic cancer	SMAD family member 3; Rac family small GTPase 2
Malaria	Syndecan 1; thrombospondin 1
Human immunodeficiency virus 1 infection	Major histocompatibility complex, class I, E; Rac family small GTPase 2
Viral carcinogenesis	Major histocompatibility complex, class I, E; nuclear factor kappa B subunit 2
Human cytomegalovirus infection	Major histocompatibility complex, class I, E; Rac family small GTPase 2
C-type lectin receptor signaling pathway	PYD and CARD domain containing; nuclear factor kappa B subunit 2
MicroRNAs in cancer	Platelet derived growth factor receptor beta; thrombospondin 1
Yersinia infection	PYD and CARD domain containing; Rac family small GTPase 2
Glycerophospholipid metabolism	Lysophosphatidylcholine acyltransferase 2; glycerol-3-phosphate acyltransferase 3
PI3K-Akt signaling pathway	Platelet derived growth factor receptor beta; thrombospondin 1
ECM-receptor interaction	Syndecan 1; thrombospondin 1
Necroptosis	PYD and CARD domain containing; macroH2A.2 histone
Th17 cell differentiation	SMAD family member 3; NFKB inhibitor epsilon

KEGG pathway	Proteins
Alcoholism	Glutamate ionotropic receptor NMDA type subunit 2D; macroH2A.2 histone
Salmonella infection	Sorting nexin 18; PYD and CARD domain containing
Influenza A	Calcium binding and coiled-coil domain 2; PYD and CARD domain containing
Diabetic cardiomyopathy	SMAD family member 3; Rac family small GTPase 2
TGF-beta signaling pathway	SMAD family member 3; thrombospondin 1
Cellular senescence	Major histocompatibility complex, class I, E; SMAD family member 3
Proteoglycans in cancer	Syndecan 1; thrombospondin 1
Thermogenesis	Acyl-CoA synthetase long chain family member 5; NADH:ubiquinone oxidoreductase complex assembly factor 7
Adherens junction	SMAD family member 3; Rac family small GTPase 2
Neurotrophin signaling pathway	Rho GDP dissociation inhibitor beta; NFKB inhibitor epsilon
Choline metabolism in cancer	Platelet derived growth factor receptor beta; Rac family small GTPase 2
Colorectal cancer	SMAD family member 3; Rac family small GTPase 2
B cell receptor signaling pathway	NFKB inhibitor epsilon; Rac family small GTPase 2
cAMP signaling pathway	Glutamate ionotropic receptor NMDA type subunit 2D; Rac family small GTPase 2
Wnt signaling pathway	SMAD family member 3; Rac family small GTPase 2
Apelin signaling pathway	SMAD family member 3; myosin light chain kinase
Ras signaling pathway	Platelet derived growth factor receptor beta; Rac family small GTPase 2
Fc gamma R-mediated phagocytosis	Amphiphysin; Rac family small GTPase 2
Prion disease	Glutamate ionotropic receptor NMDA type subunit 2D; Rac family small GTPase 2
Legionellosis	PYD and CARD domain containing; nuclear factor kappa B subunit 2
Fluid shear stress and atherosclerosis	Rac family small GTPase 2; syndecan 1

KEGG pathway	Proteins
NOD-like receptor signaling pathway	PYD and CARD domain containing; thyroid hormone receptor interactor 6
Neutrophil extracellular trap formation	MacroH2A.2 histone; Rac family small GTPase 2
Not assigned to a pathway	Active breakpoint cluster region-related protein; Raftlin; Amphoterin-induced protein 2; Calcium-transporting ATPase type 2C member 1; SH3 domain-binding protein 4; Apolipoprotein L2; Tripartite motif-containing protein 16; Serine beta-lactamase-like protein LACTB, mitochondrial; Interferon regulatory factor 2-binding protein 2; Dihydropyrimidinase-related protein 3; StAR-related lipid transfer protein 13; Synaptogyrin-1; OCIA domain-containing protein 2; Lymphoid-specific helicase; Mitochondrial peptide methionine sulfoxide reductase; Protein EVI2B; DnaJ homolog subfamily C member 2; Annexin A8; Vesicle transport through interaction with t-SNAREs homolog 1A; Nucleoplasmin-3; Golgi integral membrane protein 4; Microtubule-associated protein RP/EB family member 2; Forkhead box protein L2; Probable E3 ubiquitin-protein ligase HERC4; Palladin; Nucleoredoxin; DNA polymerase alpha catalytic subunit; Discoidin, CUB and LCCL domain-containing protein 2; EH domain-binding protein 1-like protein 1; Matrix metalloproteinase-14; Centrosomal protein of 55 kDa; Synaptotagmin-15; Carboxypeptidase D; E3 ubiquitin-protein ligase TRIM47; Uveal autoantigen with coiled-coil domains and ankyrin repeats; Wolframin; Supervillin; Prolyl 3-hydroxylase 2; Smoothelin; Latexin; 55 kDa erythrocyte membrane protein; Testin; Protein NOXP20; Ubiquitin carboxyl-terminal hydrolase isozyme L3; LisH domain-containing protein ARMC9; Formin-like protein 1; TraB domain-containing protein; Synaptopodin

KEGG pathway	Proteins
Not significant	Coiled-coil domain-containing protein 9; DNA polymerase delta subunit 3; Ras GTPase-activating-like protein IQGAP3; Cytoplasmic protein NCK1; WW domain-containing adapter protein with coiled-coil; Brefeldin A-inhibited guanine nucleotide-exchange protein 3; Solute carrier family 12 member 7; Rab-like protein 3; Metalloreductase STEAP3; Normal mucosa of esophagus-specific gene 1 protein; N-acetylgalactosaminyltransferase 7; Partitioning defective 3 homolog; Replication protein A 14 kDa subunit; histone H1t; Sperm-associated antigen 5; Ankyrin repeat and MYND domain-containing protein 2; Interferon-induced protein with tetratricopeptide repeats 3; Cyclic GMP-AMP synthase; gamma-adducin; Leucine-rich repeat-containing protein 7

Supplementary Table 3: List of proteins found down-regulated in $J82^{CisPt}$ when compared to $J82^{WT}$ under basal conditions in the proteome analysis
Threshold for decreased expression was set at 2-fold difference between $J82^{CisPt}$ vs. $J82^{WT}$ and statistical significance ($p \leq 0.05$). Significantly differentially regulated proteins were clustered into KEGG pathways and pathways with at least two representatives are listed. The list also contains proteins not assigned to a KEGG pathway and proteins down-regulated 2-fold, but not statistically significant. Proteome data was generated from triplicate.

KEGG pathway	Proteins
Metabolic pathways	Aldehyde dehydrogenase 1 family member L1; 5'-aminolevulinate synthase 1; ferrochelatase; quinolinate phosphoribosyltransferase; glutaryl-CoA dehydrogenase; monoamine oxidase A; aldehyde dehydrogenase 6 family member A1; asparagine synthetase; dehydrogenase E1 and transketolase domain containing 1; aldehyde dehydrogenase 5 family member A1; L-2-hydroxyglutarate dehydrogenase; acetylserotonin O-methyltransferase like; nicotinate phosphoribosyltransferase; palmitoyl-protein thioesterase 2; serine palmitoyltransferase long chain base subunit 2

KEGG pathway	Proteins
Biosynthesis of cofactors	5'-aminolevulinate synthase 1; ferrochelatase; quinolinate phosphoribosyltransferase; gamma-glutamyl hydrolase; nicotinate phosphoribosyltransferase
Tryptophan metabolism	Glutaryl-CoA dehydrogenase; monoamine oxidase A; dehydrogenase E1 and transketolase domain containing 1
Pathways in cancer	Fibroblast growth factor 2; laminin subunit beta 2; transforming growth factor beta 2
Lysosome	Sulfatase modifying factor 1; adaptor related protein complex 1 subunit sigma 2; palmitoyl-protein thioesterase 2
Tuberculosis	Regulatory factor X5; transforming growth factor beta 2
Malaria	LDL receptor related protein 1; transforming growth factor beta 2
Tight junctions	Occludin; tight junction protein 2
Amoebiasis	Laminin subunit beta 2; transforming growth factor beta 2
Cell adhesion molecules	Occludin; PVR cell adhesion molecule
PI3K-Akt signaling pathway	Fibroblast growth factor 2; laminin subunit beta 2
Glycine, serine and threonine metabolism	5'-aminolevulinate synthase 1; monoamine oxidase A
Estrogen signaling pathway	Keratin 17; keratin 19
Butanoate metabolism	Aldehyde dehydrogenase 5 family member A1; L-2-hydroxyglutarate dehydrogenase
Toxoplasmosis	Laminin subunit beta 2; transforming growth factor beta 2
Leishmaniasis	MARCKS like 1; transforming growth factor beta 2
Alanine, aspartate and glutamate metabolism	Asparagine synthetase (glutamine-hydrolyzing); aldehyde dehydrogenase 5 family member A1
MAPK signaling pathway	Fibroblast growth factor 2; transforming growth factor beta 2
Staphylococcus aureus infection	Keratin 17; keratin 19

KEGG pathway	Proteins
Gastric cancer	Fibroblast growth factor 2; transforming growth factor beta 2
Porphyrin metabolism	5'-aminolevulinate synthase 1; ferrochelatase
Proteoglycans in cancer	Fibroblast growth factor 2; transforming growth factor beta 2
Nicotinate and nicotinamide metabolism	Quinolinate phosphoribosyltransferase; nicotinate phosphoribosyltransferase
Lysine degradation	Glutaryl-CoA dehydrogenase; dehydrogenase E1 and transketolase domain containing 1
Hepatocellular carcinoma	SWI/SNF related, matrix associated, actin dependent regulator of chromatin, subfamily d, member 1; transforming growth factor beta 2
Not assigned to a pathway	Coiled-coil domain-containing protein 43; Paladin; Pregnancy-specific beta-1-glycoprotein 9; Uncharacterized protein C1orf198; Protein 4.1; Extracellular sulfatase Sulf-1; Polypyrimidine tract-binding protein 2; Protein PAXX; Interferon-induced transmembrane protein 3; Peroxisome proliferator-activated receptor gamma coactivator 1α (Pgc1a), proliferator-activated receptor gamma coactivator-related protein 1; Teneurin-3; Chloride intracellular channel protein 3; Transgelin; Metallo-beta-lactamase domain-containing protein 2; Protein spinster homolog 1; CD9 antigen; Putative GTP-binding protein 6; Protein MGARP; Torsin-1A; Annexin A3; CXXC motif containing zinc binding protein; Crooked neck-like protein 1; Follistatin-related protein 1; Fermitin family homolog 2; Protein phosphatase methylesterase 1; Aflatoxin B1 aldehyde reductase member 2; Pregnancy-specific beta-1-glycoprotein 2; Plakophilin-2; ELAV-like protein 2; Nuclear factor of activated T-cells 5; WD repeat-containing protein 26; Disabled homolog 2; Succinate dehydrogenase assembly factor 2, mitochondrial; Sodium-coupled neutral amino acid transporter 2; Synaptogyrin-3; Keratin, type II

KEGG pathway	Proteins
	cytoskeletal 8; Extracellular matrix protein 1; Syntaxin-binding protein 6; Mesoderm-specific transcript homolog protein; Tyrosine-protein phosphatase non-receptor type 2; Divergent protein kinase domain 2A; Transmembrane protein 201; General transcription factor 3C polypeptide 4; Phospholipid scramblase 4; GRAM domain-containing protein 2B; Pregnancy-specific beta-1-glycoprotein 1; UPF0489 protein C5orf22
Not significant	Interferon-induced GTP-binding protein Mx1; ER lumen protein-retaining receptor 1; Cytochrome B reductase 1; vacuolar fusion protein CCZ1 homolog B; A-kinase anchor protein 12; dCTP pyrophosphatase 1; septin 6; syntaxin-3; cytochrome c-type heme lyase; Armadillo repeat-containing protein 1; frataxin, mitochondrial; peptide deformylase, mitochondrial; 60S ribosomal protein L26-like 1; surfeit locus protein 1; NPC intracellular cholesterol transporter 2; E3 ubiquitin-protein ligase RNF5; Beta-centractin; Beta-actin-like protein 2; perilipin-2; transmembrane protein 192; cystathionine gamma-lyase; peptidyl-prolyl cis-trans isomerase C; syntaxin 6; histone H3.2; prefoldin subunit 5; ubiquitin-conjugating enzyme E2 T; glycine cleavage system H protein, mitochondrial; protein THEM6; palmitoyltransferase ZDHHC13; enoyl-[acyl-carrier-protein] reductase, mitochondrial; embryonal Fyn-associated substrate; transportin-2; ubiquinone biosynthesis protein COQ9, mitochondrial; E3 ubiquitin-protein ligase Itchy homolog; ADP-ribose glycohydrolase MACROD1; transcription factor AP-2-beta

Supplementary Table 4: Outcomes of combination treatments with various anticancer therapeutics and inhibitors of replicative stress response in J82^{CisPt}
J82^{CisPt} cells were treated for 72 h with different concentration combinations of the indicated substances and viability was measured using the AlamarBlue assay. From viability data (one to three independent experiments in quadruplicate) the combination indices (CI) were calculated and summarized in this table (CI < 0.9 synergistic; 0.9 ≤ CI ≤ 1.2 additive; CI > 1.2 antagonistic).

Substance 1	Substance 2	Effect in J82^{CisPt}
Cisplatin	**B02**	Additive
OH-Urea	**B02**	Antagonistic
OH-Urea	**PF477736**	Synergistic
5-Fluorouracil	**B02**	Antagonistic
5-Fluorouracil	**PF477736**	Synergistic
Niraparib	**B02**	Antagonistic
LY2603618	**B02**	Additive / Synergistic
PF477736	**B02**	Additive / Synergistic
RI(dI)2	**PF477736**	Synergistic

10.2 Publications & congress participations

For reasons of priority, parts of this work have already been published.

10.2.1 List of publications

Mann J, Niedermayer K, Krautstrunk J, Abbey L, Wiesmüller L, Piekorz R and Fritz G (2025) Combined inhibition of RAD51 and CHK1 causes synergistic toxicity in cisplatin resistant cancer cells by triggering replication fork collapse. Int J Cancer 156(2): 389-402. (DOI: 10.1002/ijc.35164)

10.2.2 List of congress participations

10.2.2.1 Poster presentations

„Targeting mechanisms of the DNA damage response (DDR) to overcome acquired resistance to conventional anticancer therapeutics (CATs)"
6th German Pharm Tox Summit
Mar 2021, online

„Targeting RAD51 and Chk1 in a combination therapy to overcome acquired cisplatin resistance in tumor cells"
DGDR-KRUPP symposium on DNA Repair and Human Disease
Apr 2022, Jena, Germany

„Targeting RAD51 and Chk1 in a combination therapy to overcome acquired cisplatin resistance in bladder carcinoma cells"
21st International AEK Cancer Congress
Feb 2023, Kassel, Germany

„Combination therapy with CHK1- and RAD51-inhibitor to overcome acquired cisplatin resistance in bladder carcinoma cells"
3rd Chromosomal Instability as a Driver of Human Disease Conference
Oct 2023, Dubrovnik, Croatia

„Combination therapy with CHK1- and RAD51-inhibitor to overcome acquired cisplatin resistance in bladder carcinoma cells"
Symposium of the Research Training Group 2578
Oct 2023, Düsseldorf, Germany

10.2.2.2 Talks

„Targeting mechanisms of the DNA damage response to overcome cisplatin resistance”
5th AEK Autumn School - Replication stress in Cancer
Nov 2020, online

“Targeting mechanisms of the DNA damage response (DDR) to overcome cisplatin resistance”
Update of the Düsseldorf School of Oncology
May 2021, online

„Targeting mechanisms of the DNA damage response to overcome cisplatin resistance”
Symposium of the Research Training Group 2578
Feb 2022, online
Best talk award

„Targeting RAD51 and Chk1 in a combination therapy to overcome acquired cisplatin resistance in tumor cells”
DGDR-KRUPP symposium DNA Repair and Human Disease
Apr 2022, Jena, Germany

“Targeting RAD51 and Chk1 in a combination therapy to overcome acquired cisplatin resistance in tumor cells”
Retreat of the Düsseldorf School of Oncology
May 2022, Düsseldorf, Germany

„Targeting RAD51 and Chk1 in a combination therapy to overcome acquired cisplatin resistance in tumor cells”
Retreat of the Research Training Group 2578
Nov 2022, Radevormwald, Germany

„Combination therapy with CHK1- and RAD51-inhibitor to overcome acquired cisplatin resistance in bladder carcinoma cells”
Symposium of the Research Training Group 2578
Oct 2023, Düsseldorf, Germany

11 Acknowledgements

For data protection reasons, the acknowledgements are not included in this version.

12 Eidesstattliche Erklärung

Ich versichere an Eides Statt, dass die hier vorliegende Dissertation von mir selbständig und ohne unzulässige fremde Hilfe unter Beachtung der „Grundsätze zur Sicherung guter wissenschaftlicher Praxis an der Heinrich-Heine-Universität Düsseldorf“ erstellt worden ist. Diese Dissertation wurde in der vorgelegten oder in ähnlicher Form, abgesehen von der angegebenen Publikation, noch bei keiner anderen Institution eingereicht oder veröffentlicht. Ich habe bisher keine anderen Promotionsversuche unternommen.

Düsseldorf, den 24.10.2024

_____

Julia Mann